DEVELOPMENT OF TOOLS FOR UNDERSTANDING BIOLOGICAL SULFUR CHEMISTRY

by

THOMAS SPENCER BAILEY

A DISSERTATION

Presented to the Department of Chemistry and Biochemistry
and the Graduate School of the University of Oregon
in partial fulfillment of the requirements
for the degree of
Doctor of Philosophy

June 2016

DISSERTATION APPROVAL PAGE

Student: Thomas Spencer Bailey

Title: Development of Tools for Understanding Biological Sulfur Chemistry

This dissertation has been accepted and approved in partial fulfillment of the requirements for the Doctor of Philosophy degree in the Department of Chemistry and Biochemistry by:

Darren Johnson	Chairperson
Michael Pluth	Advisor
Michael Haley	Core Member
Bruce Branchaud	Core Member
Ilya Bindeman	Institutional Representative

and

Scott L. Pratt	Dean of Graduate School

Original approval signatures are on file with the University of Oregon Graduate School.

Degree awarded June 2016

DISSERTATION ABSTRACT

Thomas Spencer Bailey

Doctor of Philosophy

Department of Chemistry and Biochemistry

June 2016

Title: Development of Tools for Understanding Biological Sulfur Chemistry

Hydrogen sulfide (H_2S) is an important biomolecule for its role in mediating redox homeostasis and signaling biological processes. The study of biological sulfide is currently impeded by a lack of tools available that adequately address the questions currently facing the field. The most pressing of these questions are: how does H_2S signal biological processes. To produce tools for studying H_2S, chemiluminescent scaffolds were designed to study both H_2S producing enzymes and directly measure free H_2S. Additionally, small molecule organic persulfides were synthesized and characterized in order to study the properties and reactivity of H_2S signaling species. By creating methods to directly measure biological H_2S and creating model systems to investigate the active signaling species, the biological reactivity of H_2S can be better understood.

The luminescent methods for detecting H_2S were developed in order to avoid photodecomposition inherent with fluorescent methods while still providing a spectroscopic readout for performing measurements in cells. D-cysteine concentrations can be measured using luciferin bioluminescence, and utilized to back out the H_2S producing activity of DAO. Free H_2S was measured using luminol derived chemiluminescence. The luminol scaffolds were studied in depth to determine what makes an H_2S probe selective for H_2S in order to inform the design of future H_2S probes.

Sulfide signaling processes were investigated using organic persulfide model systems. We found that under reducing conditions persulfides liberate free H_2S, and that under basic conditions they decompose. The decomposition pathway is governed by substituition at the α-carbon, which dictates the steric accessability of the inner sulfur atom to act as an electrophile. Persulifdes do not react with acids, and are easily tagged by electrophiles to form disulfides. Persulfides are sufficiently reducing to generate NO from nitrite, facilitating cross-talk between multiple signaling species. This cross talk is mediated by formation of perthionitrite, which may function as an independent signaling species.

This dissertation contains previously published co-authored material.

CURRICULUM VITAE

NAME OF AUTHOR: Thomas Spencer Bailey

GRADUATE AND UNDERGRADUATE SCHOOLS ATTENDED:

University of Oregon, Eugene, OR
Rochester Institute of Technology, Rochester, NY

DEGREES AWARDED:

Doctor of Philosophy, Chemistry, 2016, University of Oregon
Bachelor of Science, Chemistry, 2011, Rochester Institute of Technology

PUBLICATIONS

Pluth, M.D.; Bailey, T.S.; Hammers, M.D.; Hartle, M.D.; Henthorn, H.A.; Steiger, A.K. "Natural Products Containing Hydrogen Sulfide Releasing Moieties." *Synlett* **2015**, *26*, 2633-2643

Bailey, T.S.; Pluth, M.D. "Reactions of Isolated Persulfides Provide Insights into the Interplay Between H_2S and Persulfide Reactivity." *Free Radic. Biol. Med.* **2015**, *89*, 662-667

Bailey, T.S.; Pluth, M.D. "Chemiluminescent Detection of Enzymatically Produced H_2S." *Methods Enzymol.* **2015**, *554*, 81-99

Bailey, T.S.; Donor, M.T.; Naughton, S.P.; Pluth, M.D. "A Simple Bioluminescent Method for Measuring D-Amino Acid Oxidase Activity." *Chem. Commun.* **2015**, *51*, 5425-5428

Bailey, T.S.; Zakharov, L.N.; Pluth, M.D. "Understanding Hydrogen Sulfide Storage: Probing Conditions for Sulfide Release from Hydrodisulfides" *J. Am. Chem. Soc.* **2014**, *136* (30), 10573-10576

Bailey, T.S.; Pluth, M.D. "Chemiluminescent Detection of Enzymatically-Produced Hydrogen Sulfide: Substrate Hydrogen Bonding Influences Selectivity for H_2S over Biological Thiols" *J. Am. Chem. Soc.* **2013**, *135* (44), 16697-16704

Pluth, M.D; Bailey, T.S.; Hammers, M.D.; Montoya, L.A. "Chemical Tools for Studying Biological Hydrogen Sulfide" in *Biochalcogen Chemistry: The Biological Chemistry of Sulfur, Selenium, and Tellurium*; **2013**, 15-32

ACKNOWLEDGEMENTS

I would like to thank Dr. Letecia Montoya for assistance with cell culture and Dr. Milton Jackson Jr. for sharing his expertise with Raman Spectroscopy. Sean Naughton and Micah Donor performed the majority of the experimental work developing the bioluminescent assay for DAO.

Dr. Mike Strain gets his own section. Without his tireless efforts maintaining the NMR instruments, much of the work presented in this thesis would not have been possible. I would like to offer him additional thanks for the long conversations about the theory of NMR spectroscopy, helping to design some of the more complex experiments, and for giving me the basis to tackle the challenges of getting Topspin to do what you want it to do.

Mike, without you none of this ever would have been possible. I appreciate how easy it was to meet with you, and that talking to you always felt like a conversation, even when it probably shouldn't have been. Your boundless energy as a teacher, and as a scientist, set a high standard for what it means to be a professor, and I look forward to reading about all your cool new ideas for decades to come. I feel safe saying that my graduate school experience would have been much different without you, and that you are a huge part of why I have this opportunity to defend this thesis in the first place.

I would like to thank Dr. Alex Kendall and Dr. Alec Brown. Your passion for science, and eagerness to share it with anyone you met inspired me. You set me on the path to succeed as a graduate student, both because of your desire to ask the hard questions about the science you were doing, and your confidence to try new things in the lab. We'll summit the mountain again someday.

I would like to thank the members of the Pluth lab I have had the pleasure of getting to know during my graduate career. Dr. Jackie McGrath for being positive, welcoming, and always seeing things through to the end. Matt Hartle for reciprocating my enthusiasm for convoluted NMR experiments, and for keeping border disputes civil. Hillary Henthorn for understanding, and for being a helpful collaborator. Andrea for always telling it how it is, and for making the best of awkward situations. Alder for being patient with me as I learn how to be a mentor. To the people who I saw, but never truly

got to know. And Matt Hammers, you were the best hood mate I could ever hope for. You always went first, you were always there when you needed to be, and you always drove too fast. The Pluth Defense cannot be stopped!

I want to thank my friends for helping me keep things light. Lowren and Jes, for always having a couch to sleep on and never ceasing to amaze me. And Dr. Gabe Rudebusch, for helping me wear out the cushions on every barstool in town.

Last, I would like to thank my family. I'm sorry that I missed so many of the gatherings while I've been working on this, and I know I can never make up the time. You've done so much for me through the years that nothing I write here will possibly do you justice, and your enthusiasm to do more helps make any day better.

TABLE OF CONTENTS

LIST OF FIGURES

Figure Page

LIST OF SCHEMES

CHAPTER I

OVERCOMING THE INHERENT CHALLENGES IN STUDYING BIOLOGICAL HYDROGEN SULFIDE

The Biological Impact of H_2S

Hydrogen sulfide (H_2S) is a simple gaseous molecule, long recognized to have a significant influence on biological systems. Historically recognized for its toxicity, the earliest recorded instances of the impact of H_2S on life are several mass extinction events, including the Permian-Triassic extinction event some 250 million years ago where up to 98 % of all marine species and 70% of terrestrial vertebrate species becoming extinct during this time.[1,2] In current times, OSHA safety standards place an upper limit of 10 ppm as the permissible exposure level (PEL) for an 8 hour work shift in high sulfide environments, because larger exposure levels result in injury or death.[3]

Although exposure to large concentration of exogenous sulfide is toxic to vertebrate species, H_2S is important for sustaining most forms of life on earth. In addition to a large number of sulfur metabolizing bacteria, which are an important part of the sulfur cycle and rely on H_2S production to propagate their metabolism, multicellular organisms, including humans, require H_2S to function.[4] Produced primarily from cysteine or homocysteine, mammals employ a host of enzymes for the biogenesis of H_2S. The PLP dependant enzymes cystathionine-β-synthase (CBS) and cystathionine-γ-lyase (CSE) directly convert L-cysteine and homocysteine to H_2S, while L-cysteineaminotransferase (CAT) and D-aminoacidoxidase (DAO) work in tandem with 3-mercaptopyruvatesulfurtranferase (3-MST) to produce H_2S via 3-mercaptopyruvate

from L- or D-cysteine respectively (Figure 1.1).[5,6] Originally thought to be present in high micromolar concentrations,[7] revision in H_2S quantification methods has established that these enzymes maintain nanomolar intracellular H_2S levels.[8]

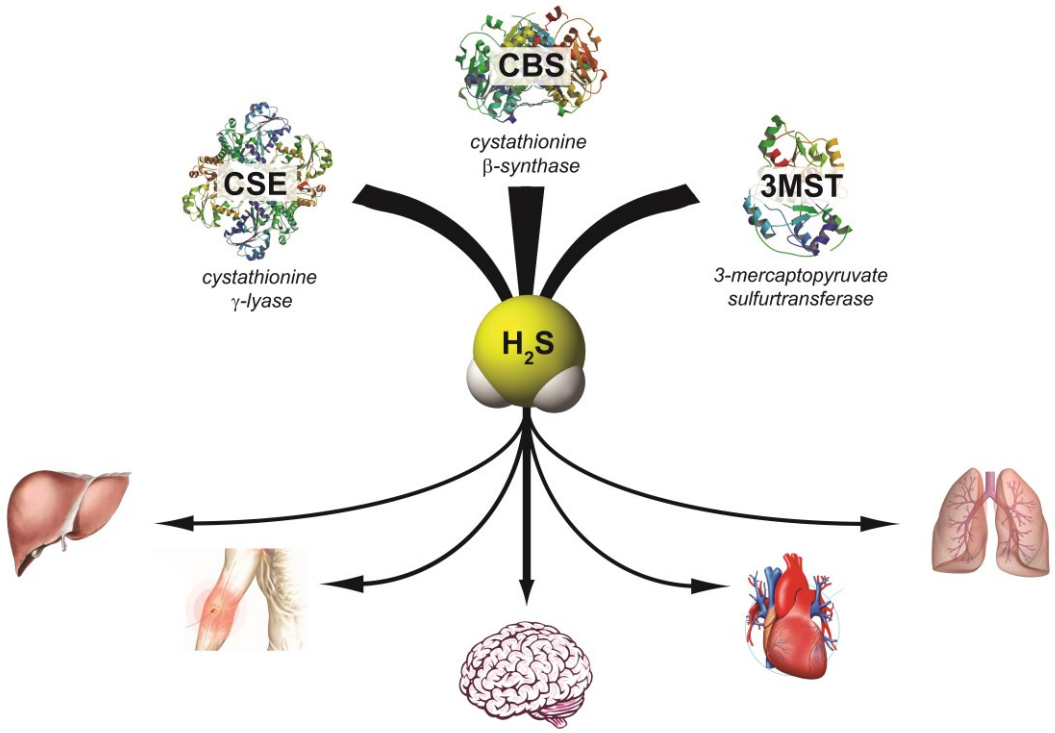

Figure 1.1. Enzymatic production of H_2S in mammals. Biosynthesized H_2S has wide ranging physiological implications, including regulatory roles in the digestive, central nervous, and pulmonary systems and signaling roles in the vascular and immune systems.

In higher order organisms biosynthesized H_2S performs regulatory functions and can act as a relay for triggering cellular processes.[4] In mammals, H_2S is primarily linked with functions including interactions with ion channels[9] and maintaining intracellular redox balance, however it also reacts with small molecules to alter their function.[10,11] Because of the ubiquity of these functions, and because H_2S producing enzymes are commonplace in a large variety of cellular environments, H_2S signaling is thought to occur across all major mammalian systems, including the cardiovascular, respiratory, gastrointestinal, immune, and nervous systems. As a result, the biological functions

attributed to H_2S include preserving long term potentiation in neurons, triggering vasorelaxation in the heart, and controlling inflammatory processes in tissues and organs. Misregulation of these functions, usually as a result of over- or under expression of H_2S producing enzymes, is known to result in a multitude of disease phenotypes, including neurodegenerative diseases, respiratory dysfunction, and diabetes.

Although a comprehensive understanding of H_2S biochemistry remains elusive, the functions attributed to H_2S are the result of a diverse pool of sulfur containing compounds. Biological sulfide can be divided into three categories: free sulfide, acid labile sulfide, and the reductant labile sulfane sulfur pool.[12] Free sulfide is comprised of H_2S in each of its three different protonation states. Under physiological conditions, free sulfide is comprised of ~80% HS^-, ~19% H_2S, and <<1% S^{2-}. These differences in protonation states impart diverse functionality on free sulfide, for example HS^- is a highly reactive nucleophile whereas H_2S is capable of diffusing through cell membranes. Acid labile sulfide is primarily made up of metal sulfide salts and is primarily found in iron/sulfur clusters, which are primarily employed biologically to facilitate electron transport. The sulfane sulfur pool is composed of a diverse array of partially oxidized sulfur compounds, consisting of persulfides (RSSH) and polysulfides (RSS_nSR), and is responsible for intracellular sulfur trafficking as well as regulating protein functionality.

Biological H_2S Sensing

A shortfall of investigating the biochemistry of H_2S is that many of the methods applied to determining not only the amount of H_2S, but whether or not H_2S and the enzymes that produce it are actually present, are not compatible with living organisms.

Expression of H_2S producing enzymes is typically determined by western blot, a chromatographic method which precludes measurement in a living organism. Studies determining the role of H_2S producing enzymes in physiological processes typically rely on knockout organisms or enzyme inhibitors, where the disease phenotypes or failure mode observed in the knockouts describe the enzyme's function.

Studies investigating the physiology of free H_2S are somewhat more advanced. Quantification of H_2S has been traditionally achieved either colorimetrically using the methylene blue assay (MB, Figure 1.2)[13] or by head space GC analysis. Although many studies quantify biological H_2S levels using the MB assay, it has recently been shown to have poor selectivity for sulfide, and is capable of extracting sulfur from many of the different sulfur pools.[7,14] Based on the poor accuracy and unfavorable detection limits of the previously described methods, a new method using monobromobimane was developed in order to accurately quantify free sulfide,[15] however none of the methods listed above can be used in living organisms.

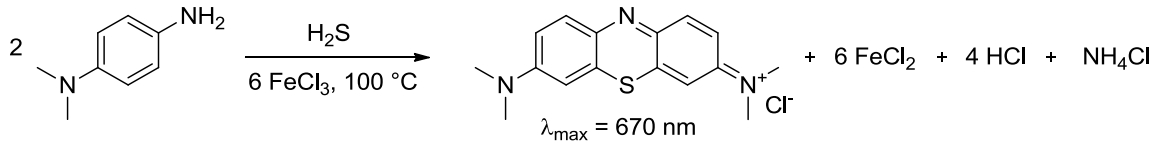

Figure 1.2 Quantification of H_2S by the methylene blue assay

Recently, new methods using small molecule fluorescent probes have been developed based on the unique reactive properties, such as its ability to effectively reduce azides, react twice as a nucleophile, and form metal sulfide salts (Figure 1.3).[16-18] Although fluorescent probes can effectively detect H_2S, accurate quantification of intracellular H_2S by these methods has not yet been achieved. Both the molecular probes,

and the methods employing them, are still an area of active development in order to overcome limitations such as insufficient detection limits, irreversible reaction with the analyte, and false positive results. For example, although the azide moiety generally shows high selectivity for H_2S over thiols, the H_2S/thiol selectivity is empirical, with some azide based probes displaying high selectivity for H_2S while similar probes do not.[19] Additionally, although azides sufficiently quench the fluorescence in the probes reported, they are susceptible to photodegredation when exposed to high intensity light, such as the excitation necessary for standard confocal microscopy experiments.[20] Most descriptions of H_2S biochemistry utilize a combination of enzyme knockouts, H_2S donor studies, and spectroscopic H_2S analysis to establish correlation between H_2S availability and the proposed functionality.[21-23]

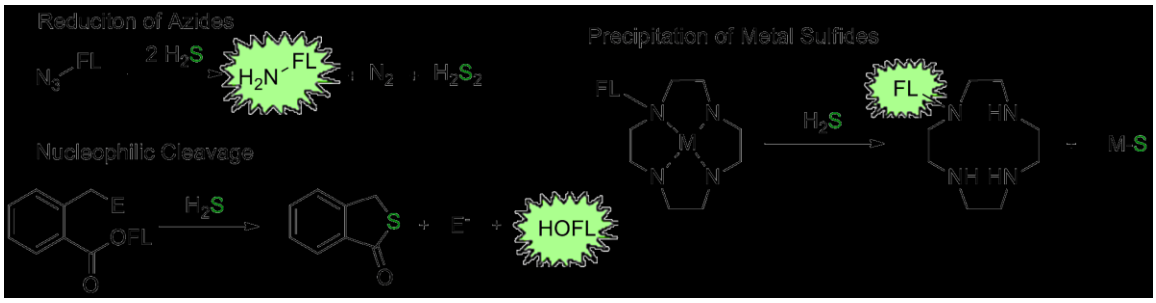

Figure 1.3. Reaction based approaches for fluorescent detection of H_2S.

The Sulfane Sulfur Pool

Analysis of the sulfane sulfur pool is even further in its infancy. Recently, the endogenous concentration of H_2S was revised based on the inaccuracy of the MB assay (*vide supra*), and new studies revealed the presence of sulfane sulfur compounds at concentrations previously attributed to H_2S.[24] Compared with H_2S, sulfur in the 2^- oxidation state, sulfane sulfur is partially oxidized (in the 1^- or 0 oxidation state) sulfur

that is not bound to carbon (Figure 1.4). It should come as no surprise then that, in addition to biogenesis pathways governed by the cysteine/cystine redox couple,[25] sulfane sulfur is typically though of as the oxidation by-product of H_2S signaling.

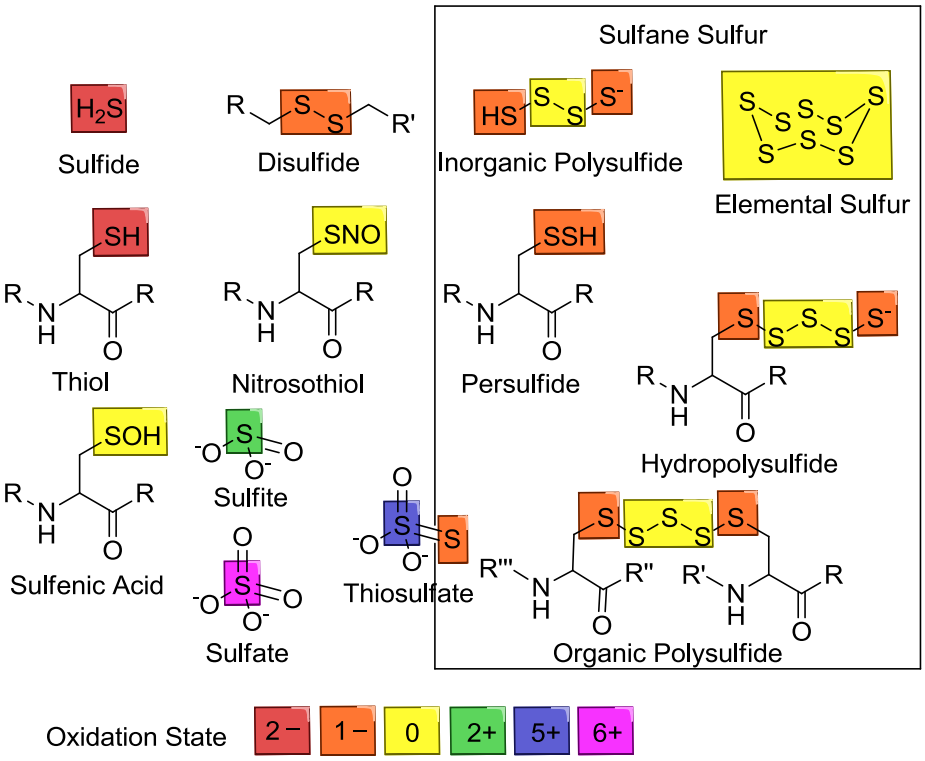

Figure 1.4. Oxidation States of Biologically Relevant Sulfur Compounds

Investigations into sulfane sulfur are accomplished using mass spectroscopic methods,[26] although fluorescent assays are under development,[16] and thus far have simply shown that sulfane sulfur is present biologically, however descriptions of sulfane sulfur bioactivity are limited. These species allow for sulfur transport in solution, and can alter protein functions through redox neutral post translational protein modification.[27,28] Additionally, persulfides are hypothesized to be effective antioxidants than thiols or free sulfide, based on the increased stability of the perthiyl radical ($HSS^{\bullet}$) when compared to thiyl radicals ($HS^{\bullet}$). However, because isolation of many sulfane sulfur compounds,

specifically the small molecule persulfides responsible for transulfuration, has remained elusive, further probing the involvement of persulfides in sulfide signaling remains a challenge. Current methods for studying sulfane sulfur rely on *in situ* generation of active compounds using a combination of oxidized sulfur precursors and H_2S (Scheme 1.1),[29] making disentangling the importance one species has toward any observed physiological function from the others difficult.

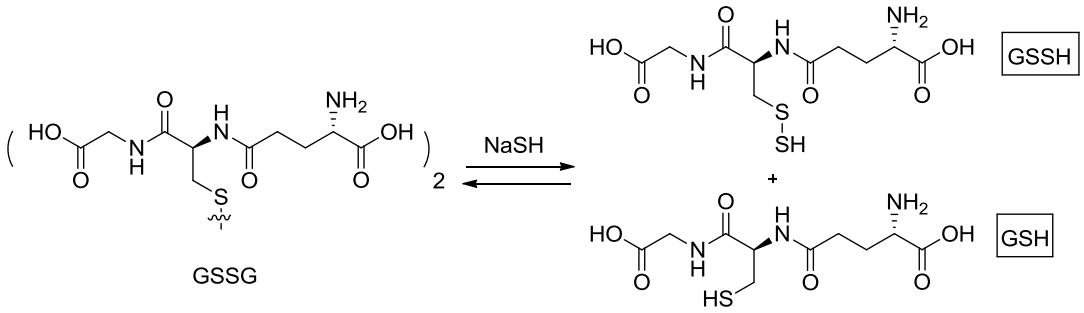

Scheme 1.1. *In situ* generation of persulfides for studying sulfane sulfur.

With these considerations in mind, a series of projects were undertaken in order to overcome the challenges currently facing the H_2S community. We investigated chemi- and bioluminescent methods for the biological detection of both free H_2S and the machinery that produces it. Luminol and luciferin scaffolds were employed to generate a spectroscopic response without the requirement of incident light. The luminol based chemiluminescent probes were employed for the detection and quantification of H_2S, and investigated using NMR methods to further elucidate the otherwise empirical selectivity of azides for H_2S over thiols. The luciferin based bioluminescent methods were probed for both the detection and activity of DAO. In addition to developing spectroscopic methods, a working model system for describing the chemistry of the sulfane sulfur pool was developed. The reactivity of persulfides was elucidated using isolated small molecule

organic model systems in aprotic media. The proposed reactivity model was used to probe the interaction of persulfides with nitrite, a biologically significant by-product of $NO_{(g)}$ signaling, which is shown to regenerate NO, possibly describing an additional basis for H_2S/NO cross-talk.

Co-author Information

Chapter II contains work co-authored by Thomas Spencer Bailey, Micah T. Donor, Sean P. Naughton, and Michael D. Pluth.

Chapter III contains work co-authored by Thomas Spencer Bailey, Lev N. Zakharov, and Michael D. Pluth.

Chapter IV contains work co-authored by Thomas Spencer Bailey and Michael D. Pluth.

Chapter V contains work co-authored by Thomas Spencer Bailey, Hillary A. Henthorn, and Michael D. Pluth

CHAPTER II

A SIMPLE BIOLUMINESCENT METHOD FOR MEASURING D-AMINO ACID OXIDASE ACTIVITY

The work on bioluminescent DAO detection was previously published (*Chem. Commun.* **2015**, 51, 5425-5428). Thomas Spencer Bailey designed the experiments performed herein and analyzed all of the data collected. Micah T. Donor performed and optimized the bioluminescent assay. Sean P. Naughton performed the NMR experiments that describe the selectivity of the method and the UV-Vis studies that describe the reaction rate. Michael D. Pluth was the principal investigator for this work.

Preface

D-amino acid oxidase (DAO) plays important roles in regulating D-amino acid neurotransmitters and was recently identified as a key enzyme integral to hydrogen sulfide production from D-Cys. We report here the development of a simple biocompatible, bioluminescent method for measuring DAO activity based on the highly selective condensation of D-Cys with 6-hydroxy-2-cyanobenzothiazole (CBT-OH) to form D-luciferin.

Introduction

Sulfur-containing compounds constitute a diverse palette of biologically-important molecules that play central roles in signaling and homeostasis. Among these species, hydrogen sulfide (H_2S) has emerged as an

important biological transmitter contributing to signaling processes supporting physiological functions ranging from long term potentiation in the central nervous system to vasorelaxation in the cardiovascular system.[30] Most prevalent as HS^- at physiological pH, sulfide can also be stored in acid-labile and reductant-labile pools.[31] Emerging evidence suggests that reductant-labile sulfane sulfur, which includes persulfides (RSSH) and polysulfides ($RS(S)_nSR$), is an important post-translational modification of Cys residues involved in altered protein function, cellular signaling,[32,33] and sulfide storage.[31,34-37] Most biosynthetic H_2S is produced enzymatically from Cys and Hcy by the pyridoxal-5-phosphate (PLP) dependent enzymes cystathionine-β-synthase (CBS) and cystathionine-γ-lyase (CSE) as well as L-cysteine aminotransferase (CAT) working together with the PLP-independent enzyme 3-mercaptopyruvate sulfurtransferase (3-MST).[30] Recent reports now suggests that a fourth enzymatic pathway, primarily active in the cerebellum and kidneys, generates H_2S from D-Cys.[6] These findings are supported by the observation that treatment of neuronal tissues with D-Cys results in faster and more efficient H_2S production than treatment with L-Cys. H_2S production from D-Cys relies on D-amino acid oxidase (DAO), which oxidatively deaminates D-amino acids to their corresponding α-keto acids.[38] Typically involved in neurochemical regulation of D-amino acid neurotransmitters in the brain, DAO metabolizes D-Cys to form 3-mercaptopyruvate (3-MP), which is a substrate for 3-MST (Scheme 2.1), thus connecting DAO with H_2S synthesis. Importantly, administration of D-Cys has been shown to elevate sulfane sulfur levels more effectively than L-Cys, suggesting a possible therapeutic potential of D-Cys

derived H_2S.[6] Despite the importance of DAO in neurochemical regulation and H_2S production, measuring DAO activity under non-invasive conditions remains a significant challenge.[39] For example, downstream detection of 3-MP or other α-oxy acids is not a specific assay for DAO activity because these α-oxy acids are also produced by other enzymes. To address this unmet need, we report here a simple bioluminescent method based on firefly luciferase for measuring D-Cys levels and DAO activity.

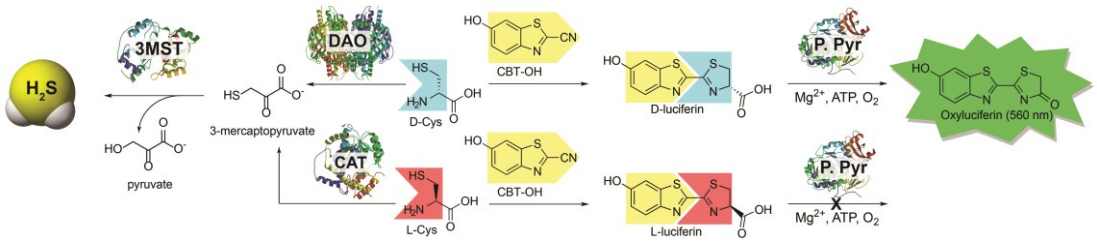

Scheme 2.1. Routes for H_2S synthesis from 3-MST and the associated strategy for using D-Cys to measure DAO activity using bioluminescence. DAO: D-amino acid oxidase; CAT: L-cysteine aminotransferase; 3-MST: 3-mercaptopyruvate sulfurtransferase; P. Pyr: Photinus Pyralis (firefly luciferase).

Because bioluminescence is a well-studied reporting method readily used for bioimaging with small molecule probes and quantitative measurements in ELISA assays,[40,41] we chose to use D-Cys as a substrate because it is metabolized by DAO and also reacts with 6-hydroxy-2-cyanobenzothiazole (CBT-OH) to form D-luciferin, which is substrate for firefly luciferase. Similar condensations of 1,2-aminothiols with 2-cyanobenzothioazoles have been previously applied as a template for polymer aggregation to monitor free Cys and homocysteine,[42] to monitor caspace activity in the presence of peroxide,[43] and to develop protein labeling strategies for genetically encoded 1,2-aminothiol residues in proteins[44,45] allowing for fluorescent and colorimetric imaging in live cell assays. Based on this

reactivity and because D-luciferin generates a bioluminescent signal when metabolized by firefly luciferase, we envisioned that treatment of DAO with a known concentration of D-Cys, followed by quenching of unreacted D-Cys with CBT-OH to generate D-luciferin, would provide a simple method for measuring DAO activity.

Results and Discussion

For this strategy to be biologically compatible, the reaction of CBT-OH with internal Cys residues in proteins or peptides must be reversible to ensure that CBT-OH is not scavenged by GSH or other cellular nucleophiles. Additionally, CBT-OH must react quickly and irreversibly with free D-Cys to generate the D-luciferin product. To establish this feasibility, we investigated the reversible addition of thiols to CBT-OH by ^{1}H NMR spectroscopy using N-acetyl cysteine (NAC) as a substrate. Because NAC lacks a free amine group, nucleophilic addition to the electrophilic CBT-OH generates an imidothioate that cannot cyclize to form the D-luciferin product. Treatment of CBT-OH with NAC resulted in complete consumption of the CBT-OH starting material and generation of new aromatic peaks in ^{1}H NMR spectrum, indicating complete reaction of CBT-OH with NAC (Figure 2.1b and 2.1c). Addition of one equivalent of Cys to the CBT-OH/NAC reaction mixture immediately generates new aromatic peaks as well as a characteristic peak at 5.4 ppm corresponding to luciferin (Figure 2.1d). Equilibration of the reaction mixture results in complete conversion of the NAC-adduct to the luciferin product, confirming the reversibility of NAC addition

(Figure 2.1e). Further treatment of the luciferin product with NAC failed to produce changes in the ^{1}H NMR spectrum, thus confirming that irreversibility of Cys addition. When GSH is used in place of NAC the conversion of CBT-OH to luciferin is slower, however, the luciferin product remains the primary reaction product (Figure A3). These results establish that internal thiols will not interfere in the detection of Cys by CBT-OH.

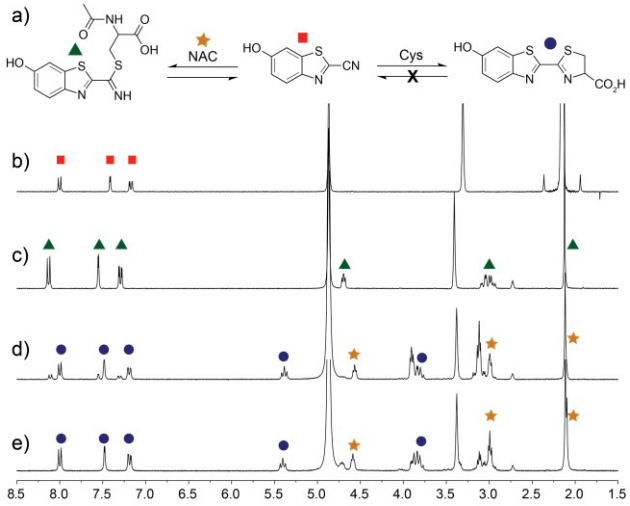

Figure 2.1. Selectivity of CBT-OH for Cys. (a) CBT-OH reacts reversibly with non-Cys thiols, but irreversibly with Cys. ^{1}H NMR spectra (500 MHz, d_6-DMSO/D_2O/CD_3OD mixture, room temperature) of (b) CBT-OH; (c) after equilibration with 1 equiv. of *N*-acetyl cysteine (NAC); (d) immediately after addition of Cys; and (e) after equilibration.

Having demonstrated that CBT-OH forms luciferin in the presence of multiple thiols, we next investigated whether the condensation rate of CBT-OH with Cys is fast enough to be a viable method of bioconjugation. To measure the rate of reaction of CBT-OH with Cys, we treated CBT-OH with different concentrations of excess Cys under pseudo first-order conditions and monitored the reaction by UV-vis spectroscopy (Figure A1). Based on these kinetic experiments, we determined that the reaction is first-order in Cys and determined

an overall second-order rate constant of 14.9 $M^{-1}s^{-1}$ for the reaction (Figure A2), which is similar to the previously reported value of 9.19 $M^{-1}s^{-1}$ for 1,2-aminothiol condensations with cyanbenzothiazoles.[44] This condensation is almost 200 times faster than the commonly-used azide/cycloalkyne click reaction (7.6 x 10^{-2} $M^{-1}s^{-1}$),[46] suggesting that the CBT-OH/Cys condensation reaction is kinetically viable for bioconjugation. Having investigated the reaction conditions under pseudo first order conditions, we further explored the suitability of the system for measuring D-Cys concentrations by treating 100 μM CBT-OH with sub-stoichiometric amounts of D-Cys and analyzing the resulting bioluminescent signal. Condensation of CBT-OH with D-cysteine enables us to detect changes in bioluminescent signal at resulting luciferin concentrations as low as 293 nM. After incubation for 1 hour to allow for conversion of CBT-OH to D-luciferin, introduction of luciferase resulted in a bioluminescent response that linearly correlated with D-Cys concentration (Figure 2.2b).

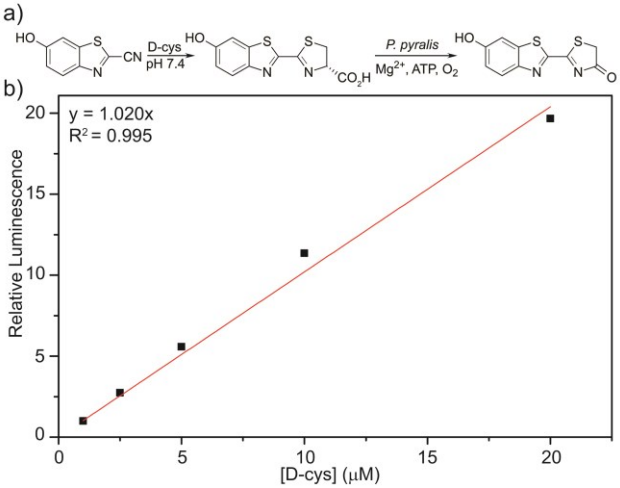

Figure 2.2. (a) Detection of D-Cys by condensation with CBT-OH followed by treatment with *P. pyralis* generates a bioluminescence response; (b) Bioluminescent response measured with varying concentrations of D-Cys incubated with 100 μM CBT-OH for 1 hr followed by addition of 0.1 mg/mL *P. pyralis*. The bioluminescence was integrated at 560 nm for 45 min in 10 mM Mg^{2+}, 2 mM ATP, pH 7.4 tris buffer (50 mM), 37 °C.

Based on the linear bioluminescence response with D-Cys concentration, we next used the CBT-OH system to measure DAO activity. Because DAO metabolizes D-Cys to 3-MP, introduction of an excess of CBT-OH at different time points in the reaction of DAO with D-Cys should convert any remaining, unreacted D-Cys to D-luciferin, which can then be measured by addition of luciferase. To test this design, 20 μM of D-Cys was incubated with 0.1 mg/mL DAO, and the reaction was quenched at different time points with an excess of CBT-OH. Addition of luciferase and measurement of the resultant bioluminescence from each sample revealed a rapid decrease in the observed bioluminescence signal, correlating with a decrease in D-Cys concentration upon metabolism by DAO (Figure 2.3a, black squares). By contrast, use of L- instead of D-Cys did not generate a bioluminescence response, confirming that the L-luciferin condensation product is not a bioluminescent substrate for luciferase. Similarly, if D-Cys is incubated with CBT-OH in the absence of DAO, the bioluminescence stays constant at each time point, confirming a constant concentration of D-Cys in the absence of DAO (Figure 2.3a, blue triangles). To further demonstrate that the developed method was reporting on DAO activity, we treated DAO with sodium benzoate, a competitive inhibitor of DAO, (K_i = 2.0 x 10^{-6} M)[38] in the presence of D-Cys and measured the bioluminescent response (Figure 2.3b). As expected, a significantly higher concentration of D-Cys remained during the assay, confirming that DAO activity was reduced. We also tested the developed assay to probe the affinity of other D-amino acids for DAO. For example, treatment of DAO with equimolar amounts of D-Cys and D-serine did not change the rate of D-Cys metabolism, suggesting that D-Cys is a better substrate for DAO than D-serine.

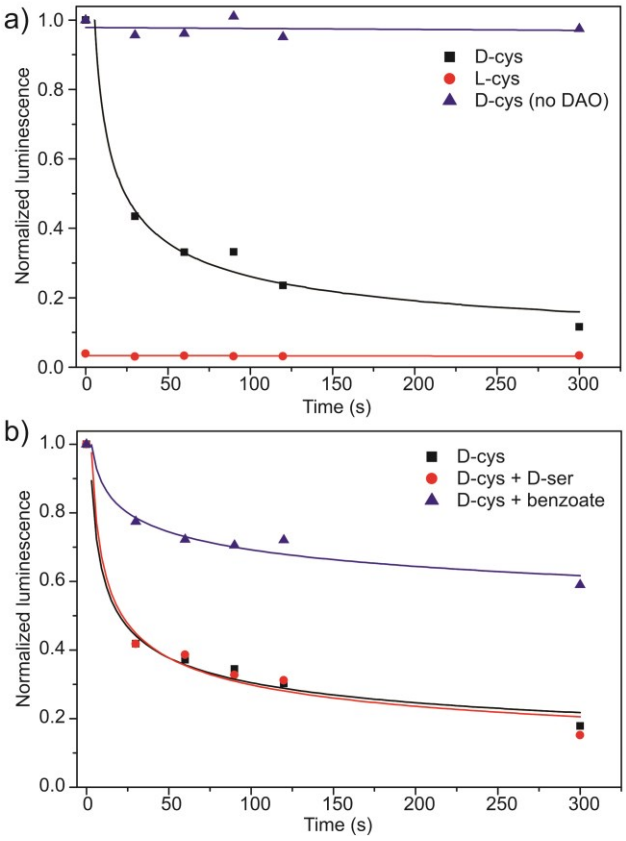

Figure 2.3. Bioluminescent response of (a) D/L-Cys with CBT-OH in the presence/absence of DAO and (b) D-Cys with the competitive inhibitor benzoate or potential substrate D-serine. Conditions: 20 μM Cys, 0.1 mg/mL DAO, 40 μM FAD. 50 mM pH 7.4 tris buffer, 37 °C. Competition experiments were performed with 2 μM sodium benzoate or 20 μM D-serine. After incubation, each sample was quenched with 100 μM CBT-OH and imaged with 0.1 mg/mL *P. pyralis*. at 560 nm for 45 min in 10 mM Mg^{2+}, and 2 mM ATP.

Conclusions

In conclusion, the condensation reaction of CBT-OH with Cys provides simple bioluminescent method for measuring D-Cys. We also demonstrated that this condensation reaction can also be used to monitor DAO activity by measuring unreacted D-Cys as a function of time and/or potential DAO inhibitors. Based on the availability of cell lines and animal models that express luciferase enzymes, we envision that this bioluminescent approach for investigating DAO activity and

function will provide a useful platform to inform on emerging the roles of DAO in neurochemistry and H_2S signaling.

Experimental Section

*Materials***.** 2-Cyano-6-hydroxybenzothiazole (CBT-OH), D-serine, D-cysteine•HCl, L-cysteine, N-acetyl cysteine (NAC), sodium beonzoate, adenosine triphosphate (ATP), flavin adenine dinucleotide disodium salt hydrate (FAD), and D-amino acid oxidase (DAO) from porcine kidneys were purchased form commercial sources. Quantilium recombinant lucfierase (*Photinus Pyralis*) was purchased from Promega. Deuterated solvents were purchased from Cambridge Isotope Laboratories and used as received. Tris(hydroxymethyl)aminomethane (tris, Aldrich) was used to make buffered solutions (50 mM tris, pH 7.4) with Millipore water.

*Instrumentation***.** NMR spectra were acquired on a Varian INOVA-500 spectrometer at 25.0 °C. Chemical shifts were measured in parts per million (δ) and were referenced to residual protic solvent resonances. UV-Vis spectroscopic measurements were obtained on a Cary 60, 100, or 300 spectrometer equipped with a Quantum Northwest temperature controller at 37.0 ± 0.05 °C. Bioluminescence measurements were recorded using a Tecan Safire^2 microplate reader at 37 °C.

*NMR Selectivity/Reversibility Experiments***.** 125 μL of a CBT-OH stock solution (40 mg/mL in d_6-DMSO) was added to 360 μL of an NAC solution (1.1 equiv. NAC, 14 mg/mL in CD_3OD) and allowed to equilibrate ([CBT-OH] = 59 mM, [NAC] = 64 mM). The changes in the NMR spectrum are observed after 15 minutes, and no further changes in the spectrum were observed after 6 hours. After equilibrium was

reached, 100 μL of L-cysteine (1 equiv., 34 mg/mL in D_2O) was added, and an NMR spectrum was taken immediately ([CBT-OH] = 49 mM, [NAC] = 53 mM, [L-Cys] = 49 mM). The mixture was allowed to equilibrate over a 24 hour period, and full conversion to L-luciferin observed. An additional 3 equiv. of NAC in CD_3OD were added back into the reaction mixture and no change in the NMR spectrum was observed over a 24 hour period ([CBT-OH] = 22 mM , [NAC] = 93 mM, [L-Cys] = 22 mM).

For the GSH experiments the experimental parameters had to be modified to ensure solubility. 125 μL of the CBT-OH stock solution were added to a mixture of 250 μL of d_6-DMSO and 360 μL of a GSH solution (1.1 equiv. GSH, 26.4 mg/mL in D_2O) and allowed to equilibrate ([CBT-OH] = 39 mM, [GSH] = 43 mM]). The changes in the NMR spectrum were observed after 15 minutes, and no further changes were observed after 1.5 hours as shown in spectrum (d, Figure A#). After equilibration, 100 mL of cysteine solution (1 equiv.) were added ([CBT-OH] = 34 mM, [GSH] = 38 mM, [cysteine] = 34 mM). After 7 hours no further change in the NMR spectrum were observed, presumably due to the complete oxidation of any remaining free thiols. This conclusion is supported by the disappearance of the triplet peak at 4.62 ppm in spectrum (d) and the new appearance of the quartet at 4.75 ppm in spectrum (e), which agrees with the literature value for GSSG. Addition of another 100 mL of cysteine solution and 200 mL of d_6-DMSO results in a simultaneous increase in the luciferin peaks with a corresponding decrease in remaining CBT-OH speaks as seen in spectrum (f) ([CBT-OH] = 25 mM, [GSH] = 28 mM, [cysteine] = 50 mM).

*UV-Vis Kinetic Measurements***.** A 10 mM stock solution of CBT-OH was prepared in DMSO, and a 100 mM solution of L-cysteine was prepared in tris buffer. The

CBT-OH solution was diluted to 25 μM in 3 mL of tris buffer. The desired amount of cysteine (250, 375, or 500 μM) was then added to the cuvette, and absorbance measurements were made at 366 nm every 0.05 s for up to 20 min. Each cysteine concentration was repeated in triplicate, and the data were fit directly to an exponential growth curve.

*Bioluminescence Detection***.** CBT-OH (100 μM) and D-cysteine (1-20 μM) were incubated for 1 hour in tris buffer. Luciferin formation was measured by adding 0.1 mg/mL luciferase in tris buffer with 10 mM $MgSO_4$, 2 mM ATP, 0.1 mM DAO, 40 μM FAD. The bioluminescent signal at 560 nm was integrated for 45 min.

*DAO Activity Assay***.** D-cysteine (20 μM) was added to 0.1 mg/mL DAO in Tris buffer with 40 μM FAD. At different time points (0, 30, 60, 90, 120, and 300 s) CBT-OH (100 μM) was added to the solution and the mixture was incubated at 37 °C for 1 hour. Luciferin formation was detected by adding 0.1 mg/mL luciferase in tris buffer (pH 7.4, 50 mM) with 10 mM $MgSO_4$, 2 mM ATP. Bioluminescent signal at 560 nm was integrated for 45 min. Negative controls followed the same method in the absence of DAO or using 20 μM L-cysteine instead of D-cysteine. Inhibition or competition experiments included the addition of either 2 μM sodium benzoate or 20 μM D-serine, respectively.

Supplementary Information is available in Appendix A.

CHAPTER III

CHEMILUMINESCENT DETECTION OF ENZYMATICALLY-PRODUCED HYDROGEN SULFIDE: SUBSTRATE HYDROGEN BONDING INFLUENCES SELECTIVITY FOR H_2S OVER BIOLOGICAL THIOLS

The work on chemiluminescent detection of enzymatically produced H_2S using luminol scaffolds was previously published (*J. Am. Chem. Soc.* **2013**, 135, 16697-16704). Thomas Spencer Bailey performed all chemical synthesis, purification, chemiluminescent measurements, and ^1H NMR titrations. The cell culture was performed by Leticia A. Montoya and the computational work was performed by Michael D. Pluth. Michael D. Pluth was the principle investigator for this work. The section on bioluminescent detection of H_2S using a luciferin based strategy did not appear in this publication and remains unpublished.

Preface

Hydrogen sulfide (H_2S) is now recognized as an important biological regulator and signaling agent that is active in many physiological processes and diseases. Understanding the important roles of this emerging signaling molecule has remained challenging, in part due to the limited methods available for detecting endogenous H_2S. Here we report two reaction-based ChemiLuminescent Sulfide Sensors, CLSS-1 and CLSS-2, with strong luminescence responses toward H_2S (128-, 48-fold, respectively) and H_2S detection limits (0.7 ± 0.3, 4.6 ± 2.0 μM, respectively) compatible with biological H_2S levels. CLSS-2 is highly selective for H_2S over other reactive sulfur, nitrogen, and oxygen species (RSONs) including GSH, Cys, Hcy, $S_2O_3^{2-}$, NO^{2-}, HNO,

$ONOO^-$, and NO. Despite its similar chemical structure, CLSS-1 displays lower selectivity toward amino acid-derived thiols than CLSS-2. The origin of this differential selectivity was investigated using both computational DFT studies and NMR experiments. Our results suggest a model in which amino acid binding to the hydrazide moiety of the luminol-derived probes provides differential access to the reactive azide in CLSS-1 and CLSS-2, thus eroding the selectivity of CLSS-1 for H_2S over Cys and GSH. Based on its high selectivity for H_2S, we used CLSS-2 to detect enzymatically-produced H_2S from isolated cystathionine γ-lyase (CSE) enzymes ($p < 0.001$) and also from C6 cells expressing CSE ($p < 0.001$). CLSS-2 can readily differentiate between H_2S production in active CSE and CSE inhibited with β-cyano alanine (BCA) in both isolated CSE enzymes ($p < 0.005$) and in C6 cells ($p < 0.005$). In addition to providing a highly sensitive and selective reaction-based tool for chemiluminescent H_2S detection and quantification, the insights into substrate-probe interactions controlling the selectivity for H_2S over biologically-relevant thiols may guide the design of other selective H_2S detection scaffolds.

Introduction

Hydrogen sulfide (H_2S), although generally known for its toxicity and characteristic odor, is now recognized as an important signaling molecule with diverse biological roles. Since the initial studies in 1996 showing that H_2S facilitates hippocampal long-term potentiation (LTP),[47] the discovered biological roles of H_2S have grown rapidly to range from roles in angiogenesis to wound healing.[30,48-50] In mammals, H_2S production is derived primarily from three enzymes: cystathionine-γ-lyase (CSE),

cystathionine-β-synthase (CBS), and 3-mercaptopyruvate sulfotransferase (3-MST).[30] The widespread but differential expression of these enzymes in different tissues suggests a broad importance and significance of H_2S in the cardiovascular, circulatory, respiratory, urinary, and nervous systems. Abnormal H_2S regulation, however, has been associated with hypertension,[51] diabetes,[52] as well as various diseases of mental deficiency including Down's syndrome[53] and Alzheimer's disease.[54] In addition to the pathophysiological conditions associated with H_2S misregulation, H_2S can also act on specific cellular targets, including heme proteins,[10] cysteine residues on K_{ATP} channels,[9] nitric oxide,[55] and other emerging targets.

As new biological functions of H_2S continue to emerge, new biocompatible tools to monitor H_2S are needed. Traditional methods of H_2S detection, including sulfide-selective electrodes, gas chromatography, or the methylene blue assay, are often limited by poor compatibility with live cells, limited temporal resolution, or extensive sample preparation requirements.[56-58] Recently, reaction-based methods of H_2S detection have emerged, which typically offer higher spatiotemporal resolution and greater live-cell compatibility than traditional detection methods. These reaction-based method have used H_2S as a nucleophile to attack activated electrophiles[14,59-62] or precipitate metal salts[63] or as a reductant to reduce azide or nitro groups on masked fluorophores.[64-67] Recent advances in H_2S detecting probes have focused probes localized to specific cellular locales in order to report H_2S in specific organelles,[68,69] proteins,[70] and cellular environments.[71] These recently-developed probes have expanded the toolbox available to scientists for studying the important and emerging roles of H_2S in biology.

A major challenge for all developed methodologies is effectively differentiating H_2S from the orders of magnitude larger concentrations of cellular GSH. Although azide-based H_2S probes generally show good selectivity for H_2S over other thiols,[72] this selectivity remains generally empirical with little understanding of the design principles required to modulate selectivity. For example, 7-azido coumarin exhibits excellent (~30-fold) selectivity for 100 μM H_2S over 1 mM cysteine or GSH,[73] whereas 3-azido coumarin exhibits only 2-fold selectivity for H_2S over 100 μM cysteine or GSH.[19] A second challenge, which complicates azide-based H_2S detection methods, is the inherent photosensitivity of aryl azides. This photosensitivity is generally not problematic for routine detection, but use of higher-powered excitation sources associated with confocal microscopy or HPLC detectors, or the extended excitation of azide-containing fluorophores, may complicate accurate detection. Although azide-based H_2S probes have been used in combination with epifluorescent or confocal microscopy, we have demonstrated that continuous exposure of prototypical azide-containing H_2S probes, such DNS-Az,[66] HSN2,[65] or C-7Az,[73] results in probe photoactivation within minutes (Figure 3.1).

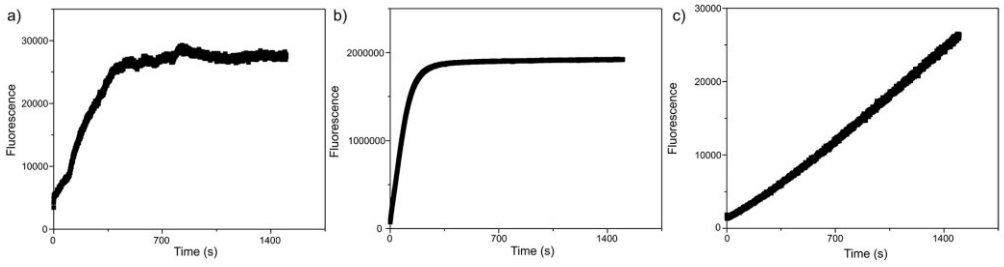

Figure 3.1. Photoactivation of (a) HSN2 (λ_{ex}= 435 nm, λ_{em}= 550 nm), (b) C-7Az (λ_{ex}= 340 nm, λ_{em}=445 nm), and (c) DNS-Az (λ_{ex}= 340 nm, λ_{em}= 510 nm). Measurements performed on 5 μM probe in pH 7.4 PIPES buffer (50 mM PIPES, 100 mM KCl, pH 7.4). Slits: excitation= 5 nm, emission= 1.4 nm.

One potential solution to this current limitation is to develop a chemiluminescent platform for H_2S detection. Because chemiluminescence does not require an excitation source, there is little chance for photodegredation of the sensing platform. Additionally, because biological materials typically do not spontaneously emit light, chemiluminescent detection methods offer high signal-to-noise ratios. Chemiluminescence is a well-studied analytical tool, capable of producing quantitative data used extensively in immunoassays[74,75] and in chromatography.[76-78] Although the preparation of new chemiluminescent or bioluminescent molecules is an active area of research,[79,80] chemiluminescent detection methods for small molecules remain greatly underexplored. Examples of reaction-based small-molecule chemiluminescent detection have primarily focused on the bioluminescent detection of reactive oxygen species such as H_2O_2.[81-83] Although chemiluminescent thiol detection methods have been reported, these methods typically have low selectivity for a specific thiol and measure the decrease in signal caused by reaction of the analyte with either the luminescent catalyst[84] or the oxidant.[78] Based on the opportunity to both expand the palette of chemiluminescent detection methods available for small-molecule biological analytes and overcome current limitations of H_2S-detection platforms, we report here the development of a chemiluminescent platform for H_2S detection. In addition to overcoming the excitation-derived photoactivation common for H_2S fluorescent probes, the developed manifold is used to also present insight, supported by experimental and theoretical underpinnings, into substrate-probe interactions dictating the selectivity for H_2S over other biologically-relevant thiols.

Results and Discussion

Probe Design and Response. We envisioned that a chemiluminescent H_2S reporter could be developed by combining H_2S-mediated azide reduction with a luminol-derived sensing platform (Scheme 3.1). Luminol chemiluminescence results from oxidation of the phthalhydrazide moiety, typically using H_2O_2 as an oxidant, horseradish peroxidase (HRP) as a catalyst to ensure high reproducibility, and an enhancer, such as *p*-iodophenol, to enhance the chemiluminescence brightness and lifetime.[85,86] Luminol oxidation proceeds through a transient singlet carbonyl species that decomposes to the phthalate product with concomitant N_2 extrusion and photon emission centered at 425 nm.[87] Because derivatizing the luminol amine group to contain electron withdrawing moieties, such as nitro[88] or acyl[89,90] group, significantly reduces chemiluminescence, we reasoned that replacement of the amine with an azide would result in a non-chemiluminescent compound. This azide-protected luminol scaffold could then be selectively unmasked by H_2S to generate free luminol and subsequently trigger a large increase in chemiluminescence. On the basis of these considerations, we designed two chemiluminescent sulfide sensors, CLSS-1 and CLSS-2, by converting the amine of luminol and isoluminol to the corresponding azide. CLSS-1 and CLSS-2 are rare examples of reaction-based chemiluminescent probes and, to the best of our knowledge, represent the first example of reaction-based chemiluminescent probes for H_2S.

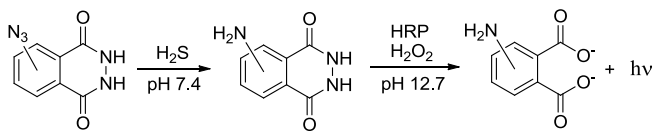

Scheme 3.1. Reduction of a luminol azide with H_2S generates the parent luminol amine. Subsequent reaction with H_2O_2/HRP (horseradish peroxidase) generates chemiluminescence.

Both luminol and isoluminol can be converted cleanly to their corresponding azides by treatment with tert-butyl nitrite (t-BuONO) and azidotrimethylsilane (TMS-N_3) in DMSO (Scheme 3.2). Monitoring the reaction of luminol azide (CLSS-1) or isoluminol azide (CLSS-2) with H_2S by ^1H NMR spectroscopy confirmed clean conversion of each azide to the corresponding amine (Figure B4, B5). In the absence of H_2S, treatment of CLSS-1 and CLSS-2 with HRP and H_2O_2 results did not generate a chemiluminescent response. By contrast, H_2S-mediated reduction of CLSS-1 or CLSS-2 followed by treatment with HRP and H_2O_2 generates a robust chemiluminescent response which, depending on the concentration, can be monitored spectroscopically or by the naked eye (Figure 3.2).

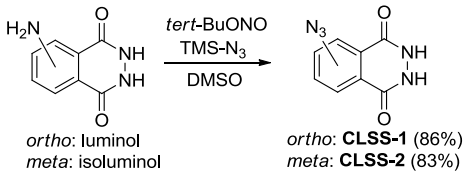

Scheme 3.2. Synthesis of CLSS-1 and CLSS-2.

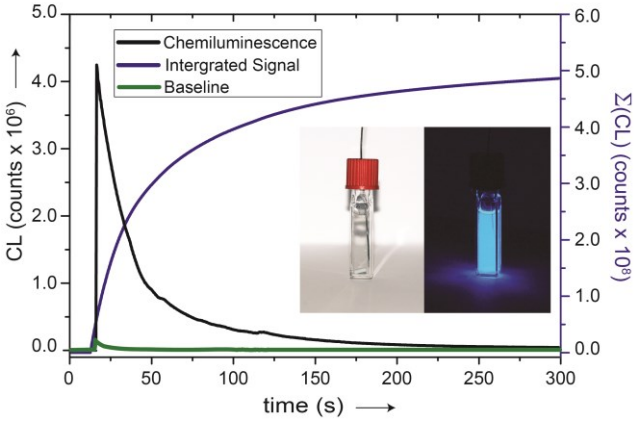

Figure 3.2. Chemiluminescent response of 50 μM CLSS-1 after incubation with 33 equiv of H_2S. Visual detection (inset) at 10x concentration, 5 s camera exposure. Samples were incubated for 60 min in pH 7.4 PIPES buffer at 37 ^oC prior to analysis.

Following the H_2S-derived chemiluminescent response of both CLSS-1 and CLSS-2, we determined the detection limit of each probe for H_2S. After incubating each probe for 1 h with different H_2S concentrations, we measured the chemiluminescent response after treatment with H_2O_2/HRP using *p*-iodophenol as an enhancer. A linear chemiluminescent response was observed for both CLSS-1 and CLSS-2 (Figure 3.3), thereby demonstrating the ability of each probe to quantify different H_2S concentrations. Based on the concentration-dependent H_2S response and the instrumental background measurements, we determined the H_2S detection limit (3σ) of CLSS-1 and CLSS-2 to be 0.7 ± 0.3 μM and 4.6 ± 2.0 μM, respectively. Although the total brightness of CLSS-2 is lower than that of CLSS-1, both of the detection limits are below the reported range of H_2S concentrations (20 μM – 100 μM) found in mammalian blood.[91-94] The effective concentration range where CLSS-1 and CLSS-2 have been shown to accurately detect H_2S (Figure 3.3) cover this entire range, highlighting the sensitivity and versatility of the developed sensing platform.

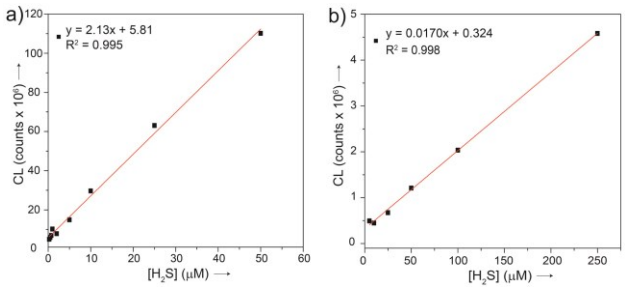

Figure 3.3. Concentration dependence of H_2S on the luminescence of a) CLSS-1 and b) CLSS-2. Values obtained are the background corrected integrated emission at λ_{em} = 425 nm and represent the average of at least 3 replicates. Samples were incubated for 60 min in pH 7.4 PIPES buffer at 37 ^{o}C prior to analysis.

Selectivity for H_2S. We next tested the response of CLSS-1 and CLSS-2 to biologically-relevant reactive sulfur, oxygen, and nitrogen species (RSONS). We first tested the selectivity of CLSS-1 for H_2S by addition of 33 equiv of cysteine (Cys), homocysteine (Hcy), *N*-acetylcysteine (NAC), reduced glutathione (GSH), thiosulfate ($S_2O_3^{2-}$), sulfate (SO_4^{2-}), nitric oxide (NO), nitroxyl (HNO), and nitrite (NO_2^-) (Figure 3.4). Based on previous reports using H_2S as a reductant for azides,[72] we expected that CLSS-1 would be highly selective for H_2S over RSONS including biologically-relevant thiols. Much to our surprise, although CLSS-1 showed a 128-fold turn on for H_2S and high selectivity for H_2S over oxygen and nitrogen reactive species, poor selectivity was observed with cysteine-derived reductants. Because CLSS-1 did not react with other reductants, such as HNO, we hypothesized that the observed chemiluminescent response from cysteine-derived thiols could be due to hydrogen bonding of the amino acid substrate to the luminol hydrazide moiety (Figure 3.6). Such hydrogen bonding would increase the effective thiol concentration near the azide of CLSS-1, orient the thiol toward attack on the azide (vide infra), and subsequently erode the selectivity for H_2S over thiols.[95] To test this theory experimentally, CLSS-1 was treated with *p*-toluenethiol (TolSH), which lacks an amino acid moiety to hydrogen bond with the luminol hydrazide. Consistent with our hypothesis, TolSH did not generate a chemiluminescent response from CLSS-1. Furthermore, CLSS-1 was also treated with 2-mercaptoethanol (2-ME), an alkyl thiol with a similar reduction potential (-0.26 V)[96] to that of cysteine (-0.22 V),[97] and no chemiluminescent response was observed (Figure 3.4). Based on these results, we expected that moving the azide from the *ortho* to *meta* ring position would increase the selectivity for H_2S over amino acid-derived thiols because of the

increased distance from the hydrazide moiety to the azide. Consistent with our hypothesis, CLSS-2 showed a 45-fold turn on for H_2S and high selectivity for H_2S over other RSONs (Figure 3.4b) including other reductants, such as TolSH, 2-ME, or HNO.[98] Similarly, treatment of CLSS-2 with 20 mM Cys does not result in a chemiluminescent response. These results demonstrate the efficacy as a selective chemiluminescent H_2S detector.

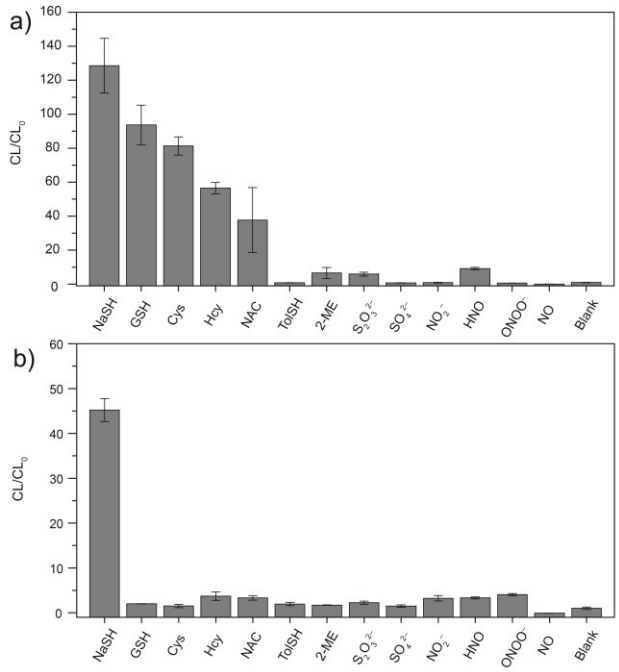

Figure 3.4. Selectivity of a) CLSS-1 and b) CLSS-2 with reactive oxygen, nitrogen, and sulfur species. Conditions: 50 μM probe, 33 equiv of RSONS, incubated 1 h at 37 ^{o}C. The reported intensities are background corrected, represent the integrated luminescence (λ_{em} = 425 nm), and are the average of at least 3 replicates. Error bars represent ± SE.

Understanding the Differential Reactivity of CLSS-1 and CLSS-2. To further understand the reactivity differences between CLSS-1 and CLSS-2, and to substantiate our hydrogen-bonding model, we performed DFT calculations at the B3LYP/6-311++G(d,p) level of theory using the IEPCM water solvation model for each probe as well as cysteine-coordinated adducts. We chose cysteine as a model amino acid

for these studies due to its differential reactivity toward CLSS-1 and CLSS-2 and also fewer available rotational and protonation states by comparison to GSH. To confirm that changes in the frontier orbital landscape of CLSS-1 and CLSS-2 were not responsible for the differential reactivity between the two probes, we calculated the HOMO and LUMO of CLSS-1 and CLSS-2. For both probes, the HOMO and LUMO are localized exclusively on the azide, suggesting that orbital differences or LUMO accessibility is not the source of the differential reactivity between CLSS-1 and CLSS-2 (Figure 3.5).

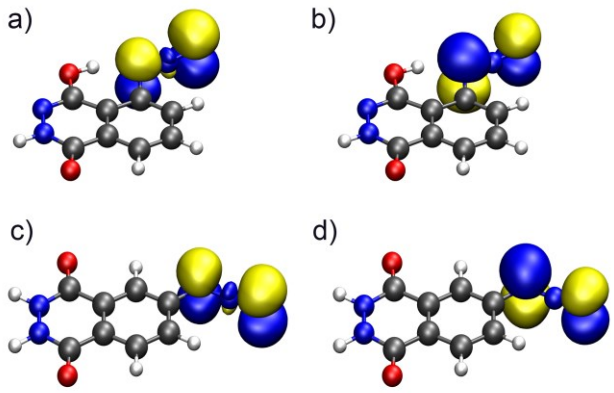

Figure 3.5. Frontier molecular orbitals of CLSS-1 and CLSS-2. (a) CLSS-1 HOMO, (b) CLSS-1 LUMO, (c) CLSS-2 HOMO, (d) CLSS-2 LUMO.

To investigate whether amino acid derived thiol interaction with the hydrazide moiety could contribute to the lower selectivity of CLSS-1, we optimized the geometry of the cysteine-bound adducts of both CLSS-1 and CLSS-2. In all cases, all luminol tautomers and cysteine protonation states were investigated to ensure that broad potential energy surface was surveyed during the optimizations. The optimized geometry of the CLSS-1/Cys adduct corresponded to a geometry in which the cysteine is hydrogen-bonded to the hydrazide moiety, and the cysteine thiol is situated 2.67 Å away from the azide nitrogen, suggesting the presence of a hydrogen bond between the –SH

and the azide group. This hydrogen bond distance is consistent with crystallographically-characterized hydrogen bonds between N-H and O-H groups to the terminal nitrogen of azides.[99-102] By contrast, the optimized geometry of the CLSS-2/Cys reveals that the thiol group from the cysteine is too far away from the azide to result in a favorable hydrogen bonding interaction. These structures corresponding to the energy minima of the CLSS-1/Cys and CLSS-2/Cys adducts are consistent with our hypothesis that amino acid hydrogen bonding to the luminol hydrazide dictates the observed selectivity differences for the two probes to thiol-containing amino acids.

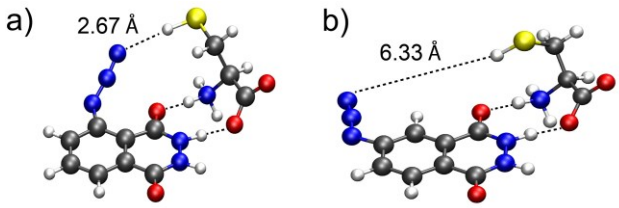

Figure 3.6. The calculated CLSS-1/Cys structure (a) is consistent with a weak hydrogen bond between the terminal nitrogen of the azide and the cysteine thiol. For CLSS-2/Cys (b), the distance between the azide and the cysteine thiol group is too large for a hydrogen bonding interaction. Geometries were optimized using Gaussian 09, B3LYP/6-311++G(d,p) using the IEPCM water solvation model.

To further understand the favorability of forming each adduct, we also compared the energies of the hydrogen-bonded adducts to other species likely present in solution. Because phthalhydrazides typically adopt a trimeric form in the solid state,[103] we also optimized the hydrogen-bonded trimer for both CLSS-1 and CLSS-2. For CLSS-1, the CLSS-1/Cys adduct in which the amino acid moiety was bound to the hydrazide and the thiol group was hydrogen bonded to the terminal nitrogen of the azide was the global energy minimum (Figure 3.7a). This conformation is 7.4 kcal/mol more stable than isolated CLSS-1 and cysteine, 1.5 kcal/mol more stable than the CLSS-1/Cys adduct

minimum without an SH/N_3 hydrogen bond, and 0.7 kcal/mol more stable than the CLSS-1 trimer. By contrast, the structure of CLSS-2 does not allow for SH/N_3 hydrogen bonding during cysteine coordination because of the large interatomic distance between the thiol and the azide (Figure 3.7b). In this case, the CLSS-2/Cys adduct is 0.5 kcal/mol less stable than the CLSS-2 trimer. Taken together, the results of the computational studies of CLSS-1 and CLSS-2 are consistent with the hypothesis that hydrogen bonding of cysteine to the hydrazide and azide erodes the selectivity of CLSS-1. Not only do these results help explain the observed selectivity, but they also provide valuable design strategies for developing future generations of highly-selective H_2S probes.

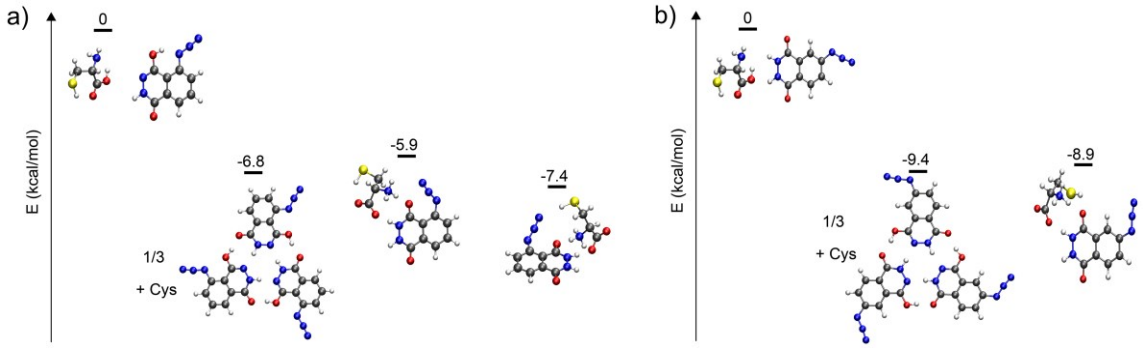

Figure 3.7. Energetic landscape of (a) CLSS-1 and (b) CLSS-2 binding to cysteine. For CLSS-1, the minimum energy state corresponds to the CLSS-1/Cys adduct with a N_3/SH hydrogen bond.

In addition to computational evidence for our hydrogen-bonding hypothesis, we also performed NMR titrations of CLSS-1 and CLSS-2 with different amino acids to further validate our model with solution data. We chose to use serine as a model amino acid because cysteine quickly reduces CLSS-1 under typical experimental conditions. Furthermore, the alcohol side chain of serine maintains a hydrogen bond donor but, unlike cysteine, is redox inactive. All ^{1}H NMR titrations were performed in DMSO to

ensure complete solubility of all components and to provide a hydrogen-bond disrupting environment similar to water. Similarly, to model the protonation state of the amino acids in water, and also to ensure complete solubility through the course of the titration, we prepared the tetrabutylammonium salts of each amino acid. By titrating tetrabutylammonium serine (TBA-Ser) into a solution of CLSS-1 and CLSS-2, striking changes in the aromatic region of the NMR spectra were observed, consistent with amino acid binding to the hydrazide moiety (Figure 3.8).

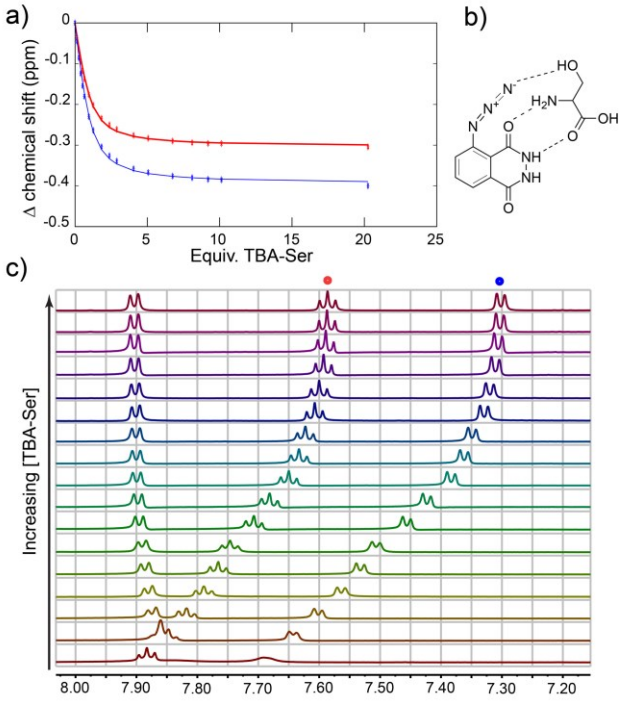

Figure 3.8. Representative titration data for TBA-Ser with CLSS-1. (a) Non-linear fitting of aromatic chemical shifts based on a 1:1 binding model; (b) proposed binding interaction; and (c) stacked ^{1}H NMR spectra showing the changes in the aromatic region of CLSS-1 during the course of the titration.

Control experiments to investigate dilution effects on CLSS-1 and CLSS-2, as well as self-association studies of TBA-Ser did not result in shifts in the aromatic region of the spectrum. These changes in the ^{1}H NMR shifts were fit to a 1:1 binding model

using the Thordarson fitting program[104] to afford binding affinities of 380 ± 80 M^{-1} and 260 ± 60 M^{-1} for CLSS-1/TBA-Ser and CLSS-2/TBA-Ser, respectively (Table 3.1). The slightly tighter binding of TBA-Ser to CLSS-1 over CLSS-2 is consistent with the computational studies and the proposed hydrogen bonding model.

We also performed ^1H NMR titrations with tetrabutylammonium valine (TBA-Val) as a second model system in which the side chain of the amino acid cannot hydrogen bond to the azide. As observed with TBA-Ser, TBA-Val binds to both CLSS-1 and CLSS-2 in a 1:1 stoichiometry with binding affinities of 3640 ± 270 M^{-1} and 3780 ± 370 M^{-1} for CLSS-1 and CLSS-2, respectively. The binding affinities measured for TBA-Val are larger than for TBA-Ser (Table 3.1), which is consistent with the reduced internal competition for intramolecular hydrogen bonding sites in valine. Based on these titration data, and the lower hydrogen bonding ability of thiols by comparison to alcohols, we expect the binding affinity of cysteine for CLSS-1 and CLSS-2 to be between the measured values for serine and valine. Under the general experimental conditions used to measure the selectivity date, a $10^3 – 10^4$ M^{-1} binding affinity between Cys/CLSS-1 would result in significant generation of the Cys/CLSS-1 adduct, which is consistent with the observed erosion in selectivity. In total, the NMR titration data are consistent with our model of amino acids binding to the luminol scaffold, which in turn, is consistent with the observed lower selectivity of CLSS-1 than CLSS-2 for H_2S over amino acid containing thiols.

Table 3.1: Binding affinities for CLSS-1 and CLSS-2 with model amino acids.[a]

	Binding Affinities (M^{-1})	
	CLSS-1	CLSS-2
TBA-Ser	380 ± 80	260 ± 60
TBA-Val	3640 ± 270	3780 ± 370

[a] Conditions: 10.0 mM probe, 0 – 200 mM amino acid, DMSO-d_6, 25.0 °C. Each value represents the average of three independent titrations.

Chemiluminescent Detection of Enzymatically-Produced H_2S. Having determined that CLSS-2 is highly selective for H_2S over other RSONS, we next demonstrated the ability of CLSS-2 to detect enzymatically-produced H_2S by using isolated and purified cystathionine γ-lyase (CSE). CSE is a PLP-dependent enzyme that converts Hcy or Cys to H_2S[105] and can be inhibited by β-cyano-L-alanine (BCA).[106] Control experiments measuring the response of CLSS-2 to Hcy, BCA, and the reaction by-products pyruvate (Pyr) and NH_3 all showed statistically significant lower ($p < 0.005$) chemiluminescent responses (Figure 3.9, white bars). Similarly, incubation of CLSS-2 with CSE in the absence of substrate showed no response. Introduction of the Hcy substrate to CSE, however, resulted in a robust response by comparison to CSE alone ($p < 0.001$) or CSE and Hcy inhibited with BCA ($p < 0.005$) (Figure 3.9, light grey bars). Furthermore, quantification of the H_2S produced from the CSE/Hcy system using the chemiluminescent response curve in Figure 3.3a is in agreement with the expected concentrations based on known CSE kinetic parameters.[107] Taken together, these results demonstrate the ability of CLSS-2 to detect and quantify enzymatically-produced H_2S from CSE and also differentiate between inhibited and uninhibited enzymes.

We next demonstrated the ability of CLSS-2 to detect and quantify endogenously-produced H_2S in C6 cells. C6 cells express CSE and produce H_2S endogenously,[108] thereby providing an ideal platform to demonstrate H_2S detection in the presence of other active biological processes. Incubation of CLSS-2 with C6 cell lysates lacking CSE substrates resulted in minimal luminescent response (Figure 3.9, dark grey), consistent with limited cellular H_2S production. This result confirmed that other biological species in the cellular milieu do not activate CLSS-2. By contrast, addition of Hcy as a CSE substrate significantly increased luminescence ($p < 0.001$) by comparison to lysates lacking substrate, signifying that CSE present in the cell lysates produced sufficient H_2S to be detected by CLSS-2. Furthermore, addition of Hcy and BCA abrogated the luminescent response ($p < 0.005$), which is consistent with CSE inhibition. These results build upon the isolated CSE experiments and demonstrate that CLSS-2 can detect endogenously-produced H_2S even in the presence of other biological species.

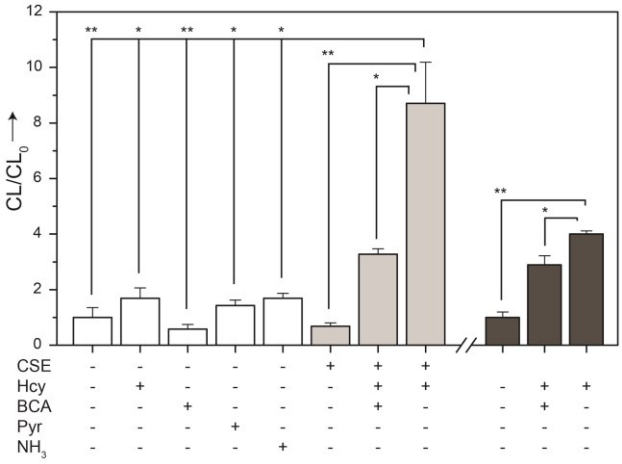

Figure 3.9. Detection of CSE-produced H_2S using CLSS-2. Conditions: Absence of enzyme (white), 10 μg CSE (light grey), 20 mM Hcy, 20 mM BCA, 25 μM pyruvate, 25 μM NH_3; incubated at in 3.0 mL buffer at 37 °C for 48 h prior to detection with 50 μM CLSS-2. Comparison with C6 cell lysates containing 2 x 10^6 cells (dark grey). Each data point represents the mean ± SE derived from at least 3 independent experiments; * indicates $p < 0.005$ and ** indicates $p < 0.001$.

Biocompatible Luminescent Sulfide Sensing. Although CLSS-2 is capable of detecting active CSE in C6 cell lysates, using a luminol based scaffold in live cells becomes problematic for a number of reasons. For example, the high pH and large concentration of H_2O_2 required for probe visualization are unlikely to be tolerated by live organisms and are difficult to introduce into live-cell environments. To leverage the benefits of a chemiluminescent sulfide probe without limiting experimental design space to *ex vivo* investigations, we designed CLSS-3 (Scheme 3.3), which is based on the luciferin scaffold, a class of bioluminescent molecules that liberates light through action of the firefly luciferase enzyme (*Photinus pyralis*). Luciferase converts luciferin to oxyluciferin with concomitant photon emission at an optimal pH of 7.8. Unlike the luminol system, the luciferase enzyme requires only ATP, Mg^{2+}, and O_2 to be active, all of which are abundant under normal biological conditions. Like luminol, luciferin scaffolds functionalized with electron withdrawing groups suffer from significantly diminished luminescence, and actually can act as luciferase enzyme inhibitors. Based on these considerations, we hypothesized that by appending an azide to aminoluciferin, we could leverage the selectivity and sensitivity of sulfide based azide reduction to generate a biocompatible method for chemiluminescent H_2S sensing.

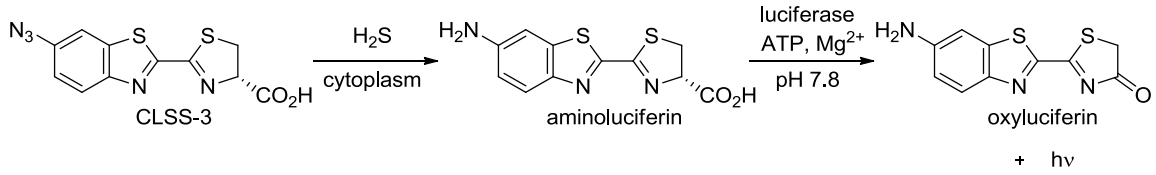

Scheme 3.3. Reduction of a luciferin azide with H_2S generates the parent aminoluciferin. Subsequent metabolism by luciferase (*P. pyralis*) generates chemiluminescence centered at 605 nm.

Azidoluciferin (CLSS-3) was synthesized from 2-chlorobenzothiazole in 5 steps (Scheme 3.4). Nitration of 2-chlorobenzothiazole, followed by reduction to the amine

yields 6-amino-2-chlorobenzothiazole. Displacement of the chloride by cyanide produces 6-amino-2-cyanobenzothiazole (CBT-NH_2). Condensation of the nitrile with D-cysteine affords aminoluciferin, which can be converted to CLSS-3 using a mixture of tert-butyl nitrite (t-BuONO) and azidotrimethylsilane (TMS-N_3) in MeCN. To determine whether the azide successfully quenched the luminescence of CLSS-3, we performed a comparative assay against aminoluciferin (Figure 3.10). Although aminoluciferin produces robust luminescence when treated with luciferin, the azide quenched CLSS-3 produces only background luminescence, making CLSS-3 a promising candidate for a reaction based sulfide probe.

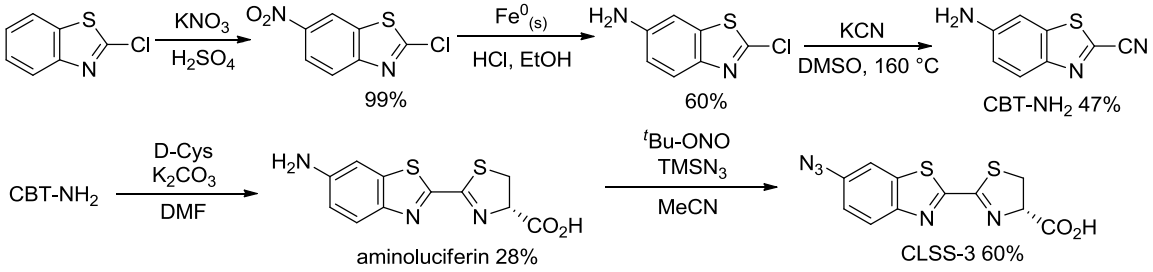

Scheme 3.4. Synthesis of CLSS-3.

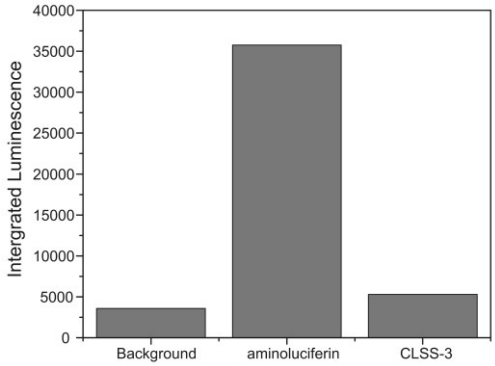

Figure 3.10. Detection of CSE-produced H_2S using CLSS-2. Conditions: Absence of enzyme (white), 10 μg CSE (light grey), 20 mM Hcy, 20 mM BCA, 25 μM pyruvate, 25 μM NH_3; incubated at in 3.0 mL buffer

Having shown the inactivity of CLSS-3 after treatment with luciferase, we next wanted investigated whether CLSS-3 could function as an H_2S sensor in the presence of

luciferase. Collaborative work with the Prescher lab at UC Irvine revealed that luciferase was capable of binding CLSS-3, and that CLSS-3 inhibits the enzymatic function of luciferase. Additionally, once bound to the enzyme CLSS-3 does not react with H_2S, strongly limiting the application of CLSS-3 for biologically compatible H_2S sensing. Overcoming these limitations would require a large H_2S flux at the injection site of CLSS-3, allowing reduction of the azide to form aminoluciferin, which can then be metabolized by luciferase to produce light.[109,110]

Conclusions

In conclusion, we have prepared two chemiluminescent probes for H_2S capable of detecting at physiologically-relevant levels of H_2S. Not only are these probes the first example of reaction-based chemiluminescent probes for H_2S, but they also offer insight into new strategies to separate the reactivity of H_2S from other biological thiols based on hydrogen bonding. In addition to detecting exogenous H_2S, we demonstrated that CLSS-2 can detect enzymatically-produced H_2S from both isolated CSE enzymes and also from C6 cell lysates and can also differentiate inhibited and native states of the enzyme. Although we designed CLSS-3 to overcome the biocompatability issues involved with using CLSS-2 for live cell imaging, we found that directly appending an azide to the luciferin scaffold produced a molecule that is not suitable for bioluminescent imaging. We anticipate that the chemical tools outlined here, as well as future scaffolds based on the design principles, will contribute to a greater understanding the multifaceted roles of biological H_2S.

Experimental Section

Materials and Methods. Synthetic precursors 3-aminophthalhydrazide and 4-aminophthalhydrazide were purchased from TCI and used as received. Tetrabutylammonium amino acid salts (TBA-Ser, TBA-Val),[111] HSN-2,[65] DsN_3,[66] and C-7Az[73] were prepared as described in the literature. Deuterated solvents were purchased from Cambridge Isotope Laboratories and used as received. Piperazine-N,N'-bis(2-ethansulfonic acid) (PIPES, Aldrich) and potassium chloride (99.999%, Aldrich) were used to make buffered solutions (50 mM PIPES, 100 mM KCl, pH 7.4) with Millipore water. Buffered solutions were degassed by vigorous sparging with N_2 and stored in an inert atmosphere glove box. Anhydrous sodium hydrogen sulfide (NaSH) was purchased from Strem Chemicals and handled under nitrogen. *S*-Nitroso-*N*-acetyl-DL-penicillamine (SNAP), sodium peroxynitrite (NaO_2NO), and Angeli's salt (NaN_2O_3) were purchased from Cayman Chemical and stored either at -30 or -80 ^oC prior to use. L-Cysteine, *N*-acetyl-L-cysteine, and DL-homocysteine were purchased from TCI. Reduced glutathione was purchased from Aldrich. Stock solutions of the reactive species were prepared in either buffer or DMSO under nitrogen immediately prior to use and were introduced into buffered solutions with a syringe. Note: Although CLSS-1 and CLSS-2 are not air-sensitive, some of the reactive sulfur, oxygen, and nitrogen species, including H_2S, are known to react with oxygen. To ensure accurate measurements and to prevent decomposition of potentially-reactive species, all experiments were performed under an inert atmosphere unless otherwise indicated. Both CLSS-1 and CLSS-2 react with H_2S under aerobic conditions to provide equivalent results as under anhydrous conditions. Stock solutions of the chemiluminescent probes

(10 mM) were prepared in DMSO and stored below -20 °C until immediately prior to use. In all spectroscopic experiments, the final concentration of DMSO was less than 0.5% of the total buffer volume.

Spectroscopic Methods. NMR spectra were acquired on a Brüker Avance-III-HD 600 MHz spectrometer with a Prodigy multinuclear broadband CryoProbe at 25.0 °C. Chemical shifts are reported in parts per million (δ) and are referenced to residual protic solvent resonances. The following abbreviations are used in describing NMR couplings: (s) singlet, (d) doublet, (b) broad, and (m) multiplet. IR spectra were measured on a Thermo Scientific Nicolet 6700 RT-IR using an ATR attachment. Chemiluminescence measurements were obtained on a Photon Technology International Quanta Master 40 spectrofluorimeter equipped with a Quantum Northwest TLC-50 temperature controller at 37.0 ± 0.05 °C. All chemiluminescent measurements were made under an inert atmosphere in septum-sealed cuvettes obtained from Starna Scientific and were repeated at least in triplicate. Bioluminescence measurements were made using a Tecan Safire^2 microplate reader at 37 °C without excluding O_2. High resolution mass spectrometry (HRMS) measurements were performed by the Biomolecular Mass Spectrometry Core of the Environmental Health Sciences Core Center at Oregon State University. Melting points were obtained using a Laboratory Devices Mel-Temp and are reported uncorrected.

General Procedure for NMR Titrations. A septum-sealed NMR tube was charged with either CLSS-1 or CLSS-2 (10 mM in 300 μL of DMSO-d_6) under N_2-atmosphere and aliquots of a DMSO-d_6 solution containing 200 mM amino acid mixed with 10 mM of the probe were added using a syringe. The chemical shifts of the

aromatic proton resonances were tracked and the data were fitted to a 1:1 binding model.[104]

Computational Details. Calculations were performed using the Gaussian 09 software package[112] with the GaussView graphical user interface.[113] Graphical representations were produced using VMD v1.9.[114] Geometry optimizations and unscaled frequency calculations were carried out at the B3LYP/6-311++G(d,p) level of theory using the IEF-PCM solvation model for water. Frequency calculations were performed on all converged structures to confirm that they corresponded to local minima. Calculated enthalpies are reported as zero-point corrected enthalpies. Initial structures for geometry optimizations were as follows: Each luminol tautomer was optimized starting with multiple azide orientations. For cysteine-luminol adducts, each luminol tautomer was optimized with the RCO_2H/RNH_2 and RCO_2^-/RNH_3^+ protonation states, multiple azide orientations, and multiple cysteine dihedral angles. In all cases, the lowest energy conformer/tautomer was used to compare the relative energetics of the calculated species.

General Procedure for Chemiluminescence Measurements. In a septum-sealed cuvette, a solution of the probe (50 μM) and the desired reactive species was incubated in 3.0 mL PIPES buffer (50 mM PIPES, 100 mM KCl, pH 7.4) for 60 min at 37.0 °C After incubation, 40 μL of 6 M NaOH was added to increase the pH to 12.7, an optimal level for luminol chemiluminescence, and also assures complete conversion of any remaining H_2S to sulfate upon addition of H_2O_2.[115] After pH adjustment, 10 μL of 10 U/mL Horseradish Peroxidase (HRP) with 0.2 μM p-iodophenol was added. A background reading was acquired for 60 s, after which 50 μL of H_2O_2 (35%) was added. The sample luminosity at 425 nm was integrated for 300 s after H_2O_2 addition. The data reported are

the average of at least three independent experiments. Errors are reported as ± SE, and *p*-values report the one-way ANOVA values.

General Procedure for Photoactivation Experiments. In a septum sealed cuvette, a 5 μM solution of each probe in PIPES buffer (50 mM PIPES, 100 mM KCl, pH 7.4) was excited at the absorption maximum of the corresponding amine product for 25 min at 37 °C. The samples were detected at the emission maximum for the unprotected fluorophore with excitation and emission slit widths set at 5 nm and 1.4 nm, respectively. The normalized data are presented in Figure 3.1.

General Procedure for Enzymatically Produced H_2S Luminescence Measurements. In a septum sealed cuvette, the desired reactive species were incubated in 3.0 mL PIPES buffer (50 mM PIPES, 100 mM KCl, pH 7.4) at 37.0 °C for 48 h. After initial incubation, 15 μL of 10 mM CLSS-2 in DMSO was added, and allowed to react for 60 min. After incubation, 40 μL of 6 M NaOH was added to increase the pH to 12.7, an optimal level for luminol chemiluminescence. After pH adjustment, 10 μL of 10 U/mL Horseradish Peroxidase (HRP) with 0.2 μM *p*-iodophenol was added. A background reading was acquired for 60 s, after which 50 μL of H_2O_2 (35%) was added. The sample luminosity at 425 nm was integrated for 40 s after H_2O_2 addition. The data reported are the average of at least three independent experiments.

Cell Culture and Lysing Procedure. C6 cells were obtained from ATCC and cultured in Dulbecco's Modified Eagle Medium (DMEM, Cellgro, MediaTek, Inc.) supplemented with 10% fetal bovine serum (FBS, HyClone), and 1% penicillin/streptomycin. Cells were passed and plated into T-75 flasks containing 10 mL of DMEM, and incubated at 37 °C with 5% CO_2. For luminescence studies, the cells

were washed with 1x phosphate buffered saline (PBS), trypsinized with 5 mL of Trypsin, and then centrifuged to form a cell pellet. The cell pellet was resuspended in 5 mL of 1x PBS and the cells were counted using a Bio RAD TC20 automated cell counter. Cells were centrifuged at 1,000 RPM for 5 min at room temperature, placed on ice and lysed using 100 μL of RIPA buffer (pH 7.5 10 mM Tris-HCl, 150 mM NaCl, 1.0% Nonidet P-40, 0.1% SDS, 0.1% sodium deoxycholate) containing protease inhibitor (PhosSTOP, Roche) for every $2x10^6$ cells in the pellet. Luminescence measurements on cell lysates were made using 100 μL of lysate solution ($2x10^6$ cells per experiment) under ambient atmosphere by following the general procedure for enzymatically produced H_2S outlined above.

Bioluminescence Detection. Aminoluciferin or CLSS-3 were incubated for 1 hr in tris buffer. Bioluminescence was produced by introduction of 0.1 mg/mL luciferase in tris buffer with 10 mM $MgSO_4$, 2 mM ATP, 0.1 mM DAO, 40 μM FAD. The bioluminescent signal at 605 nm was integrated for 45 min.

Syntheses

General procedure for luminol azidification. The appropriate aminophthalhydrazide (0.10 g, 0.56 mmol) was dissolved in 5 mL dry DMSO. At room temperature, 0.10 mL (0.85 mmol) of tert-butyl nitrite was added drop-wise. The reaction mixture was stirred for 1 h and then 0.95 mL (0.68 mmol) of trimethylsilyl azide (TMS-N_3) was added. The reaction mixture was stirred for an additional 1 h and the volatile components of the reaction mixture were then removed under vacuum without heating. The remaining DMSO solution was diluted with 50 mL of 5% dichloromethane in hexanes to yield a precipitate. The precipitate was collected and washed with

dichloromethane to afford the desired azide. The spectroscopic parameters of compounds CLSS-1 and CLSS-2, prepared by this method, are tabulated below.

3-Azidophthalhydrazide (CLSS-1). Yield: 95 mg (83%). ^{1}H NMR (600 MHz, DMSO-d_6) δ: 11.52 (b, 2H, NH), 7.87 (m, 2H, ArH), 7.68 (d, J = 7.7 Hz, 1H, ArH). ^{13}C{^{1}H} NMR (150 MHz, DMSO-d_6) δ: 156.0, 152.0, 139.3, 134.0, 128.8, 125.5, 122.2, 119.7. IR (cm^{-1}): 3167, 3013, 1896, 2617, 2191 [ν(N_3)], 2101 [ν(N_3)], 1650, 1611, 1597, 1487, 1454, 1357, 1326, 1290, 1206, 1193, 1180, 1164, 1121, 1067, 1003, 980, 902, 871, 769, 733, 697. Mp: 165 °C (dec.). HRMS-ESI (m/z): $[M+H]^+$ calcd for $[C_8H_6O_2N_5]^+$, 204.0521; found 204.0524.

4-Azidophthalhydrazide (CLSS-2). Yield: 100 mg (87%). ^{1}H NMR (600 MHz, DMSO-d_6) δ: 11.57 (s, br, 2H, NH), 8.07 (d, J = 8.5 Hz, 1H, ArH), 7.60 (s, 1H, ArH), 7.57 (dd, J = 8.5, 2.3 Hz, 1H, ArH). ^{13}C{^{1}H} NMR (150 MHz, DMSO-d_6) δ: 154.6, 154.4, 144.4, 133.0, 129.0, 128.1, 124.4, 114.5.; IR (cm^{-1}): 3417 3164, 3008, 2914, 2120 [ν(N_3)], 1662, 1603, 1554, 1496, 1458, 1435, 1405, 1367, 1344, 1290, 1252, 1218, 1172, 1108, 951, 819, 731, 646. Mp: 165 °C (dec). HRMS-EI (m/z): $[M]^+$ calcd for $[C_8H_5O_2N_5]^+$, 203.04433; found 203.04392.

CLSS-3 synthesis. Aminoluciferin was prepared from 2-chlorobenzothiazole according to literature precedent.[116]

6′-Azidoluciferin (CLSS-3). In the absence of water and oxygen, aminoluciferin (50.0 mg, 0.183 mmo) was suspended in anhydrous acetonitrile. This mixture was wrapped in aluminum foil to reduce exposure to light, and chilled to 0 °C in an ice bath. Tert-butyl nitrite (32.5 μL, 0.274 mmol) was added dropwise to the chilled solution, followed immediately by TMS-N_3 (28.6 μL, 0.219 mmol). The mixture was allowed to

warm to room temperature and stirred for 5 hr to produce a dark red solution. The volatile organics were evaporated under vacuum, and the resulting solid was tritrated with hexanes to produce CLSS-3 (33.5 mg, 60%) as a brown solid. ^{1}H NMR (600 MHz, DMSO-d_6) δ: 13.19 (s, br, COOH), 8.18 (d, J = 8.4 Hz, 1H, ArH), 8.06 (s, 1H, ArH), 7.34 (d, J = 8.4 Hz, 1H, ArH), 5.46 (t, J = 9 Hz, 1H, α-CH), 3.81 (t, J = 10.5 Hz, 1H), 3.72 (dd, J = 11.4, 8.4 Hz, 1H). ^{13}C{^{1}H} NMR (150 MHz, DMSO-d_6) δ: 171.5, 164.8, 160.8, 150.5, 139.5, 137.5, 125.7, 119.9, 113.2, 78.6, 35.3.; IR (cm^{-1}): 2920, 2115 [ν(N_3)], 1731, 1584, 1487, 1443, 1271, 1217, 1030, 910, 863, 809, 650

Associated Content

Tabulated selectivity data, titration data, photoactivation data, ^{1}H and ^{13}C{^{1}H} NMR spectra, mass spectra, optimized geometries for DFT calculations. This material can be found in Appendix B.

CHAPTER IV

REACTIONS OF ISOLATED PERSULFIDES PROVIDE INSIGHTS INTO THE INTERPLAY OF H_2S AND PERSULFIDE REACTIVITY

The work on fully characterizing tritylpersulfide and investigating its reactivity was published (*Journal of the American Chemical Society* **2014**, *136*, 10573-10576). Thomas Spencer Bailey performed all chemical synthesis, purification, NMR spectroscopy, IR spectroscopy, and UV-vis experiments. The Raman spectroscopy was performed by Milton Jackson Jr. and the X-Ray diffraction and structure refinement were performed by Lev. N. Zakharov. Michael D. Pluth was the principle investigator for this work. The follow up work on comparing persulfide reactivity under comparable conditions was published (*Free Radical Biology and Medicine* **2015**, *89*, 662-667). Spencer Bailey performed all chemical synthesis, purification, NMR spectroscopy, IR spectroscopy, and UV-vis experiments. Michael D. Pluth was the principle investigator for this work.

Preface

Hydrogen sulfide (H_2S) is an important biological signaling agent that exerts action on numerous (patho)physiological processes. Once generated, H_2S can be oxidized to generate reductant-labile sulfane sulfur pools, which include hydrodisulfides/persulfides (RSSH). Despite the importance of persulfides in H_2S storage and signaling, little is known about the physical properties or chemical reactivity of these compounds. We report here the synthesis, isolation, and characterization (NMR, IR, Raman, HRMS, X-ray) of small-molecule persulfides and highlight its reactivity with reductants, nucleophiles, electrophiles, acids, and bases. Our experimental results

establish that persulfides release H_2S upon reduction and using a combination of NMR and UV-Vis spectroscopy, we investigated the spectroscopic properties and reactivity of three isolated organic persulfides. We report a simple model for persulfide reactivity, which includes their roles as nucleophiles, electrophiles, and sulfide donors.

Introduction

Hydrogen sulfide (H_2S) continues to generate significant interest as an important biomolecule due to its role as a ubiquitous signaling molecule in diverse biological systems and processes.[30,117] Produced by both enzymatic[118] and non-enzymatic processes, H_2S plays important roles in maintaining immune, cardiovascular, neuronal, as well as other functions.[30,53] Although sulfide signaling mechanisms remain an active area of investigation, they also face significant challenges due to the inherent complexity of the chemical processes occurring during the course of such mechanisms. Cellular concentrations of free H_2S are now understood to be in the low to mid-nanomolar range,[119] which is significantly lower than the initial reports of physiologically-unreasonable micromolar levels of free sulfide.[120,121] This significant revision of endogenous sulfide levels is due in part to better tools for measuring and differentiating sulfide pools, and also reflects a broadened appreciation of the importance of reductant-labile forms of sulfide.[122] Contrasting acid-labile sulfide pools, which often consist of metal sulfides such as iron sulfur clusters,[12,123,124] the reductant-labile sulfane-sulfur pools are comprised primarily of oxidized thiols such as hydrodisulfides/persulfides (RSSH), hydropolysulfides (RSS_nSH), and both organic and inorganic polysulfides ($RS(S)_nSR$).[117,125-128] Although, Kevil and co-workers recently reported methods to separate the free, acid-labile, and reductant-labile sulfide pools,[129] there remains

controversy surrounding the basic reactivity of sulfane sulfur, specifically persulfides. For example, although some reports suggest that reductant-labile sulfane sulfur is also acid-labile,[130] it is more likely that acid-labile and reductant-labile sulfur form two chemically-distinct pools.[131]

The reductant-labile sulfane sulfur pool is hypothesized to play significant roles in the observed biological action associated with H_2S and also provides access to redox-neutral pathways for transsulfuration and transpersulfidation processes.[36,132] In addition to providing a significant source of redox-labile sulfide, proteins bearing persulfide modified cysteine residues show altered activity, such as increased nucleophilicity, by comparison to the parent thiols.[31,32,133-136] Persulfides may also play important roles in the observed antioxidant properties of H_2S, based on the higher stability of the persulfide radical ($RSS^{\bullet}$) compared with the thiyl radical ($RS^{\bullet}$).[137]

Despite the widespread importance of persulfides in biological processes, understanding the different reactivity of persulfides, thiols, and sulfide remains a significant challenge, in part due to the inherent complexity of the sulfane sulfur pool and in part due the difficulty of disentangling the innate chemistry of its constituents, because the chemistries of persulfides, thiols, and sulfide are largely intertwined. Further complicating our understanding of persulfide chemistry, many of the previous studies on persulfides have relied on persulfides generated *in situ* rather than purified compounds.[29,138-140] The difficulty in differentiating persulfide reactivity from other sulfhydryl-containing biomolecules has been reflected by the significant challenges in designing selective methods for labeling persulfides.[26,141,142] A more complete understanding of the inherent chemical properties and reactivity of persulfides would

allow for the development of more reliable persulfide detection methodologies and would also provide valuable insights into the roles of persulfides in biological signaling and regulation.

Determining the Properties of Organic Persulfides

To establish the spectroscopic and reactivity properties of persulfides, we chose to prepare tritylpersulfide (trityl = triphenylmethyl) due to stability of the *S*-nitrosothiol analogue, TrtSNO, and the crystallinity of the trityl group. Although there are various reports of persulfides in the literature, to the best of our knowledge, none of these have been characterized completely.[143-151] We viewed that isolation and characterization of molecules containing the –SSH functional group would allow for other researchers to better identify and characterize similar compounds in the future. Although the trityl group precludes water solubility, the investigation of persulfide reactivity in organic solution may provide insights into the chemistry of persulfides in hydrophobic environments in protein architectures, which are proposed to be involved in the activation of various enzymes. To prepare TrtSSH, we first treated TrtSH with AcSCl (**3**) in a benzene/Et_2O mixture to generate TrtSSAc (**4c**). Removal of the acetyl protecting group by acidic ethanolysis affords the desired persulfide product, TrtSSH. (Scheme 4.1).

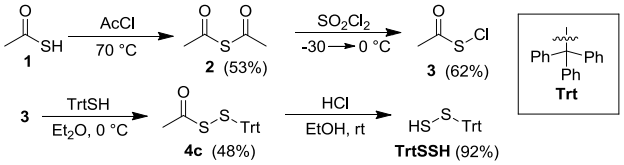

Scheme 4.1. Synthesis of TrtSSH.

With TrtSSH in hand, we fully characterized the compound and compared its chemical properties to those of TrtSH. Both the ^1H and $^{13}C\{^1H\}$ NMR spectra of TrtSSH are similar to those of TrtSH, but the ^1H NMR resonance of the sulfhydryl SSH is shifted

upfield to 2.7 ppm, by comparison to 3.1 ppm in TrtSH (Figure C8, C9). Much of the infrared and Raman spectra of TrtSSH and TrtSH are also similar due to their related structures; however, the S-H stretch shifts to a lower wavenumber by 65 cm^{-1} for TrtSSH when compared to TrtSH (Figure 4.1b). Comparison of the Raman spectrum of TrtSSH with that of S_8 showed similarities in the 200-500 cm^{-1} region corresponding sulfur-sulfur bond formation. HRMS analysis of TrtSSH confirmed its atomic composition, affording an m/z value of 307.0631 amu, which agrees well with the calculated value of 307.0621 amu for $TrtSS^-$. To further confirm the molecular structure of TrtSSH, single crystals suitable for X-ray diffraction were grown from toluene/Et_2O. TrtSSH crystallizes in $P2_12_12_1$ with an S-S bond length of 2.0396(12) Å and a CSSH dihedral angle of 82.2°, both of which are within the ranges common for disulfides (Figure 4.1a). The terminal –SSH hydrogen was located from the residual density map, and inspection of the packing diagram shows that it does not form hydrogen bonds with other atoms in the solid state (Figure C56).

Having confirmed the molecular identity of TrtSSH and established its spectroscopic properties, we next investigated the reactivity of TrtSSH to determine under which conditions sulfide, or other sulfur products, were released. We note that these investigations were performed in organic solution under anaerobic conditions to enable isolation of specific protonation states of both the persulfide and other reactants as well as to prevent unwanted oxidation chemistry. Although reports have suggested that H_2S can be released from persulfides upon protonation, reduction, and nucleophilic attack, we expected that only reduction would liberate sulfide because the sulfur oxidation state is higher in persulfides (either two S^{1-} or one S^0 and S^{2-}) than in H_2S (S^{2-}).

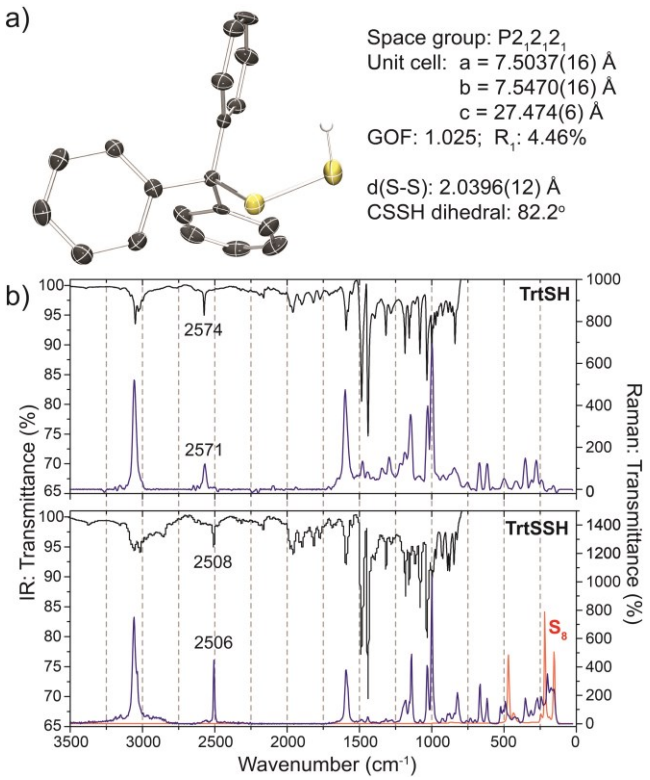

Figure 4.1. (a) X-ray crystal structure of TrtSSH. Thermal ellipsoids are drawn at the 50% probability level. Hydrogen atoms on the phenyl rings are omitted for clarity. Full crystallographic details are available in Appendix D. (b) Infrared (black) and Raman (blue) spectra of TrtSH (top) and TrtSSH (bottom). The Raman spectrum of S_8 (red) is shown for comparison.

As expected, treatment of TrtSSH with reductants, such as PPh_3 or $[NBu_4^+][BH_4^-]$ (Figure C10, C11) resulted in clean conversion of TrtSSH to TrtSH with concurrent liberation of sulfide.[152] These results confirm that persulfides are a source of reductant-labile sulfane sulfur (Table 4.1, entries 1-2). When TrtSSH was treated with sulfhydryl-containing species, such as TrtSH, BnSH, dithiopropane (DTP), or H_2S, however, sulfide release did not occur, suggesting that the thiols were either insufficiently reducing or that proton transfer is a mechanistically-important step (Table 4.1, entries 3-6). Treatment of TrtSSH with acid, either alone or in the presence of a thiol as a potential electron source, also failed to liberate sulfide (Table 4.1, entries 7-8). These results confirm that persulfides are a source of reductant-labile but not acid-labile sulfide.

Table 4.1. Reactivity of TrtSSH with different reactants including reductants, nucleophiles, bases, and acids.[a]

Entry	Reactant	Completion	Products
1	PPh_3	< 2 min	Ph_3PS, TrtSH
2	$[NBu_4^+][BH_4^-]$	< 2 min	TrtSH, BH_3, SH^-
3	DTP	n.r.	–
4	TrtSH	n.r.	–
5	BnSH	n.r.	–
6	H_2S	n.r.	–
7	AcOH	n.r.	–
8	AcOH + TrtSH	n.r.	–
9	$[Na^+][TrtS^-]$	< 2 min	TrtSH, S_8
10	$[NBu_4^+][CN^-]$	< 2 min	TrtSH, S_8
11	$[NBu_4^+][Cl^-]$	1 hr	TrtSH, S_8
12	$[NBu_4^+][Br^-]$	24 hr	TrtSH, S_8
13	$[NBu_4^+][I^-]$	> 48 hr	TrtSH, S_8
14	$[NBu_4^+][OAc^-]$	< 2 min	TrtSH, S_8
15	$[NBu_4^+][TFA^-]$	30 min	TrtSH, S_8
16	NEt_3	< 2 min	TrtSH, S_8
17	10% NEt_3	< 2 min	TrtSH, S_8
18	DMEDA	< 2 min	TrtSH, S_8
19	DMAP	< 2 min	TrtSH, S_8
20	Pyridine	> 48 hr	TrtSH, S_8
21	NEM[b]	24 hr	TrtSS-NEM

[a] Experiments were performed in CD_2Cl_2 at room temperature with 18 mM TrtSSH and reactant. All products were confirmed by ^1H or $^{31}P\{^1H\}$ NMR spectroscopy. BH_3 formation was identified by trapping with THF and characterization by ^{11}B NMR spectroscopy. S_8 formation was confirmed and quantified by titration with PPh_3 at the end of the reaction. [b] Reaction was incomplete due to slower reactivity of protonated TrtSSH, however addition of NEt_3 increased the reaction rate. Abbreviations: DTP: dithiopropane; DMEDA: *N*,*N*'-dimethylethylenediamine; DMAP: dimethylaminopyridine; NEM: *N*-ethyl-maleimide.

To further understand the reactivity of thiols toward TrtSSH, we treated TrtSSH with $TrtS^-$. Monitoring the reaction by ^1H NMR spectroscopy revealed clean conversion to TrtSH and the formation of S^0 (*vide infra*) (Table 4.1, entry 9). To clarify this

reactivity, we investigated whether the $TrtS^-$ was acting as a nucleophile or as a base by treating TrtSSH with different nucleophiles (CN^-, I^-, Br^-, Cl^-, TFA^-, and AcO^-) and bases (NEt_3, DMEDA, pyridine, and DMAP). Monitoring these reactions by ^1H NMR spectroscopy (Table 4.1, entries 10-20) revealed that the rate of conversion of TrtSSH to TrtSH and S^0 correlated with the basicity ($CN^- > AcO^- > TFA^- > Cl^- > Br^- > I^-$) rather than with anion nucleophilicity (Figure C19-C24). The same trends for reaction rate were maintained with amine bases: NEt_3 ~ DMEDA > DMAP > pyridine (Figure C25, C27-C29). Introduction of catalytic NEt_3 (entry 17, Figure C26) results in the same reactivity, thus supporting a base-mediated disproportionation mechanism. We also wanted to verify the multitude of reports highlighting the nucleophilicity of persulfides. Treatment of TrtSSH with *N*-ethylmaleimide (NEM), a common thiol labeling agent, resulted in slow conversion to the NEM-labeled disulfide (Figure C30). The slow reaction rate is consistent with proton transfer being important to observe reactivity. Adding a small amount of NEt_3 to the reaction drastically increases the reaction rate, mimicking the observed reactivity of persulfides with electrophiles in water.

Having determined that deprotonation results in disproportionation of TrtSSH to TrtSH and S^0, we wanted to further investigate the mechanistic details involved in this reaction. Monitoring the formation of TrtSH from the reaction between TrtSSH and different nucleophiles by ^1H NMR spectroscopy resulted in clean conversion to the TrtSH product without the formation of any NMR-active intermediates (Figure 4.2a). After the completion of each reaction, titration with PPh_3 and monitoring the formation of Ph_3PS, which is generated by reaction of PPh_3 with S^0, by $^{31}P\{^1H\}$ NMR spectroscopy established that 1 equiv. of S^0 was formed for each equiv of TrtSSH (Figure 4.2b).

Following the reaction of TrtSSH with [NBu_4^+][CN^-] by UV-Vis spectroscopy, however, showed the formation of a transient intermediate with λ_{max} = 340 nm (Figure C55), which we attribute to $TrtSS^-$. Disappearance of this band is accompanied by the appearance of a broad absorption band centered at 300 nm consistent with S_8 formation. Taken together, these data suggest that TrtSSH deprotonation initially generates $TrtSS^-$, which subsequently disproportionates into $TrtS^-$ and S^0, thus providing a mechanism for transsulfuration in the sulfane sulfur pool without disruption of redox homeostasis.

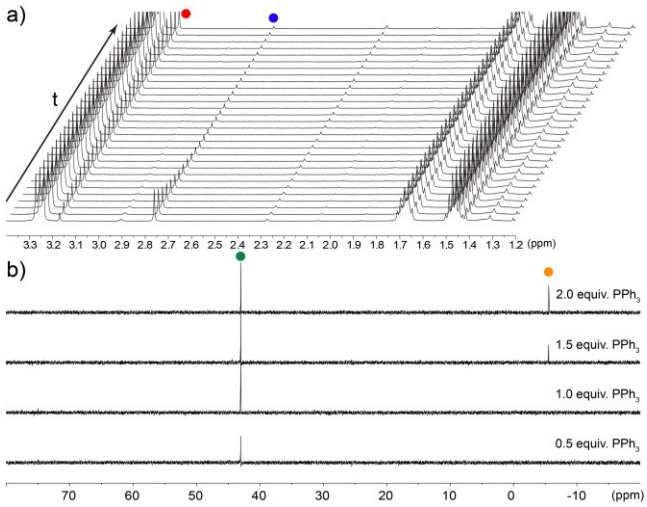

Figure 4.2. (a) ^{1}H NMR spectra of the conversion of 18 mM TrtSSH (●) to TrtSH (●) with 1 equiv of [NBu_4^+][TFA^-] recorded every 60 s. (b) Addition of PPh_3 (●) in 0.5 equiv. increments at the end of the reaction shows the clean formation of Ph_3PS (●).

Establishing a Model for Persulfide Reactivity

By contrast to proposed persulfide reactivity with thiols in water,[153] we did not observe H_2S release upon treatment of TrtSSH with thiols. We surmised that this difference could be due to steric constraints of the trityl group, differences in proton transfer in organic versus aqueous solution, or changes in persulfide electronics due to the stability of the trityl cation. For example, the trityl group is partially electron donating

due to the high stability of the trityl cation, thus reducing the electrophilicity of the α-sulfur of the persulfide by polarizing C-S bond, which should reduce its reactivity toward thiol nucleophiles. To investigate the reactivity difference between organic and aqueous persulfides, and produce a general model for persulfides, we have prepared and isolated two additional organic persulfides, benzyl persulfide (BnSSH) and adamantyl persulfide (AdSSH) (Figure 4.3), both of which are known in the literature and have significantly different physicochemical properties than TrtSSH.

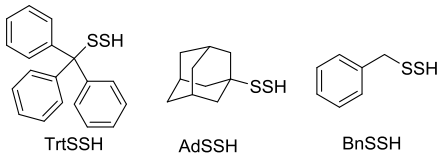

Figure 4.3. Chemical structure of the prepared persulfides: trityl persulfide (TrtSSH), adamantyl persulfide (AdSSH), and benzyl persulfide (BnSSH).

Although isolated persulfides have appeared sporadically in the literature and have been the focus of previous studies,[28] little work has been done to systematically characterize the reactivity of different persulfides under controlled and comparable conditions. We viewed that the TrtSSH, AdSSH, and BnSSH afforded this opportunity. AdSSH is similar to TrtSSH in that both are tertiary persulfides. Unlike TrtSSH, however, AdSSH has an entirely aliphatic backbone that is conformationally locked, which significantly reduces the electron donating ability by contrast to TrtSSH. Additionally, AdSSH is significantly less sterically hindered than TrtSSH. To compare the reactivity differences between tertiary and primary persulfides, we also prepared benzyl persulfide (BnSSH), which provides a less sterically hindered persulfide than AdSSH or TrtSSH and also provides an accessible electrophilic α-carbon. If the observed reactivity of these three dissimilar persulfide models provide identical reactivity, then the

reactivity differences between biological persulfides and the synthetic persulfides are to be likely attributed to solvents and/or proton transfer chemistry. The described persulfides were synthesized using the same general method described above (Scheme 4.2). The thiol of the desired persulfide is treated with acetylsulfenyl chloride (**3**) to yield the corresponding acetyldisuflide (**4x**). Acidic methanolysis of the acetyldisulfide yields the desired persulfide.

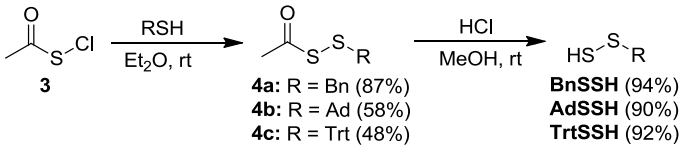

Scheme 4.2. General synthetic route to access organic persulfides.

With isolated persulfides in hand, we measured and compared their spectroscopic properties and compared these parameters to those of the parent thiols (Table 4.2). The sulfhydryl ^{1}H NMR resonance on each persulfide was measured in CD_2Cl_2 and was observed to be 3.02 ppm for BnSSH, 2.70 ppm for AdSSH, and 2.75 ppm for TrtSSH. For both BnSSH and AdSSH, the sulfhydryl proton shifts approximately 1.15 ppm downfield by comparison to the parent thiol, whereas for a 0.35 ppm upfield shift is observed for TrtSSH. Adding to the spectroscopic characterization, we also measured the S-H stretch of each compound using IR spectroscopy. All three of the persulfides show S-H stretches between 2490 and 2508 cm^{-1}, which in each case is about ~60 cm^{-1} lower in energy than the parent thiol. The combination of IR and ^{1}H NMR spectroscopic data provide general spectroscopic characteristics of persulfides when compared to their parent thiols, which should facilitate future characterization and identification of small molecule persulfides.

Table 4.2. Spectroscopic properties for the ^{1}H NMR resonance (δ) and IR stretching frequency (υ) of the S–H bond for AdSSH, BnSSH, and TrtSSH compared with their parent thiols.

	δ (ppm)		υ_{SH} (cm^{-1})	
R	RSSH	RSH	RSSH	RSH
Trt	2.75	3.10	2508	2574
Bn	3.02	1.86	2504	2560
Ad	2.70	1.57	2491	2567

Having characterized the spectroscopic properties of TrtSSH, AdSSH, and BnSSH, we next systematically investigated the chemical reactivity of the isolated persulfides with a variety of reductants, nucleophiles, bases, and gases (Table 4.3). Treatment of the persulfides, which contain sulfur atoms in the −1 oxidation state, with one equivalent of triphenylphosphine (PPh_3), a nucleophilic reductant, generates the parent thiol and triphenylphosphine sulfide (Ph_3PS). This reaction constitutes an overall 2-electron reduction and produces two sulfur atoms in the −2 oxidation state. Although TrtSSH and AdSSH react to cleanly afford Ph_3PS and the parent thiols as the only product, BnSSH also generates benzyltrisulfide (BnSSSBn, δ = 4.07 ppm) and H_2S (δ = 0.9 ppm, Figure C33). The ratio of BnSSSBn to BnSH is 3:4 by ^{1}H NMR spectroscopy and the $^{31}P\{^{1}H\}$ NMR spectrum of the reaction mixture shows unreacted PPh_3 in solution, suggesting that the trisulfide-generating reaction pathway does not consume PPh_3. One explanation for this difference in reactivity is that BnSSH may be sufficiently acidic (*vide infra*) such that deprotonation of the persulfide by PPh_3 becomes competitive with the rate of PPh_3-mediated reduction chemistry. Another interesting observation is that BnSSSBn is the only observed polysulfide formed during the reaction, and that higher order polysulfides, such as tetra- and pentasulfides, are not observed. This

selectivity is consistent with extraction of sulfur from trisulfides by PPh_3 in methylene chloride being slow[154] by comparison to either higher order polysulfides or persulfides.

Exposure of any of the isolated persulfides to other reducing agents, such as $H_2S_{(g)}$, $NO_{(g)}$, or dithiopropane (DTP) failed to produce any measurable reaction over a 48 hr period. The observed persulfide stability in the presence of DTP and $H_2S_{(g)}$ suggests that either these sulfhydryl-containing reductants are either not sufficiently reducing to release sulfide, or that proton transfer steps, which are not favorable in non polar solvents but should be facilitated by solvation in water, are important mechanistic components of the reduction process. To probe whether proton inventory was important to the reduction of persulfides by thiols, we treated AdSSH, TrtSSH, and BnSSH with $[Na^+][TrtS^-]$. We observed that instead of acting as a reducing agent and producing H_2S, treatment of the persulfides with $[Na^+][TrtS^-]$ produced TrtSH (δ = 3.1 ppm, Figures C37, C48), indicating that the thiolate was deprotonating the persulfides and generating a persulfide anion.

Table 4.3: Reactivity of persulfides in the presence of different reductants, nucleophiles, gases, and bases.

Reactant	TrtSSH		BnSSH		AdSSH	
	Products	**time**	**Products**	**time**	**Products**	**time**
PPh_3	TrtSH,	< 2	BnSH, BnSSSBn, H_2S,	16 hr	AdSH,	> 24
DTP	nr	–	nr	–	nr	–
$H_2S_{(g)}$	nr	–	nr	–	nr	–
$NO_{(g)}$	nr	–	nr	–	nr	–
$[Na^+][TrtS^-]$	TrtSH, S_8	< 2	Polysulfides	< 2	AdSH, S_8	< 2
$[NBu_4^+][HS^-]$	TrtSH, S_8,	> 24	H_2S, polysulfides	< 2	nr	–
$[NBu_4^+][CN^-]$	TrtSH, S_8	< 2	H_2S, BnSH,	< 2	AdSH, S_8	< 2
$[NBu_4^+][AcO^-$	TrtSH, S_8	< 2	Polysulfides	< 2	AdSH, S_8	< 2
$[NBu_4^+][Cl^-]$	TrtSH, S_8	1 hr	polysulfides	< 2	nr	–
$[NBu_4^+][I^-]$	nr	–	polysulfides	> 24	nr	–
NEt_3	TrtSH, S_8	< 2	polysulfides	< 2	AdSH, S_8	30

[a] Experiments were performed anhydrously and anaerobically in CD_2Cl_2 at room temperature with 18 mM persulfide and reactant. All reaction products were confirmed by ^1H or $^{31}P\{^1H\}$ NMR spectroscopy. S_8 formation was confirmed and quantified by titration with PPh_3 at the end of the reaction. Abbreviations: nr: no reaction, DTP: 1,3-dithiopropane. Reactions taking > 48 hours to occur are considered exhibit no reactivity.

To further explore the observed persulfide reactivity, we treated each persulfide with a variety of both anionic and neutral bases. For the series CN^-, AcO^-, Cl^-, and I^-, we observed that persulfides react with the anions at a rate increasing with anion basicity, which is consistent with a mechanism dependent on deprotonation. We observed a slower reaction rate for NEt_3 than with the charged bases, which we attribute to solvation effects. Because the experiments were conducted in CD_2Cl_2, charged species are solvated much more poorly than neutral species, and this property makes NEt_3 a weaker base by comparison to an anion such as acetate. The reaction of HS^- with BnSSH was fast, however no reaction was observed with either AdSSH or TrtSSH. If HS^- is acting as a base, it is unclear why the reactivity of HS^- with AdSSH and TrtSSH is so much lower than the other tested bases.

Upon treatment with each of the bases, BnSSH reacted the fastest, followed by TrtSSH, and then AdSSH. We theorize that the increase in reaction rate corresponds to a greater generation of the persulfide anion during the reaction, suggesting that BnSSH is most acidic, followed by TrtSSH, and then AdSSH. Additionally the products observed for the reaction of persulfide with base changed depending on the amount of steric hindrance surrounding the persulfide. AdSSH and TrtSSH are both tertiary persulfides, and in each case their reaction with base produced only the parent thiol and elemental sulfur. By contrast, for the primary persulfide BnSSH, we observed a variety of benzyl polysulfide products (n=2-6) in addition to the parent thiol (Table 4.3). When stronger bases were used, we observed H_2S generation from BnSSH during the reaction.

Table 4.3. Distribution of products observed in the reactions of benzyl persulfide as measured by integration of the peaks present in the product spectra.

Reactant	BnSH	BnSSBn	BnS_3Bn	BnS_5Bn	BnS_6Bn
PPh_3	0.54	0.07	0.39	-	-
$[Na^+][TrtS^-]$	0.41	-	0.30	0.22	0.07
$[NBu_4^+][HS^-]$	-	-	0.58	0.33	0.09
$[NBu_4^+][CN^-]$	0.28	0.15	0.37	0.14	0.06
$[NBu_4^+][AcO^-]$	0.26	0.08	0.48	0.18	-
$[NBu_4^+][Cl^-]$	-	-	0.61	0.28	0.11
$[NBu_4^+][I^-]$	-	-	0.5	0.35	0.15
NEt_3	0.28	0.03	0.39	0.21	0.09

[a] The polysulfides were identified using their reported chemical shifts.[155]

To verify that the persulfide anion was present over the course of the reaction, we monitored the reaction of the persulfides with base by UV-Vis spectroscopy (Figure 4.4). Previous work in aqueous buffers above pH 8.0 has shown a peak attributed to the cysteine persulfide anion appears between 335 – 350 nm with a molar absorptivity of ~400 $M^{-1}cm^{-1}$, although analytical standards for such compounds remain unavailable.[133,156] Upon treatment of BnSSH with AcO^-, we initially only observed a minimal change in the large shoulder sweeping down from the UV range. After a short incubation period, however, a peak centered near 340 nm appeared, which we attribute to the persulifde anion, which reaches a maximum intensity of 0.065 AU after 30 min. The solution was monitored for a total of 4 hr, after which the intensity of the peak centered near 340 nm returned to background levels, consistent with complete reaction of the persulfide anion. Further supporting the assignment of the 340 nm absorbance band as a persulfide anion, addition of anhydrous HCl in Et_2O to the reaction mixture immediately abolishes the 340 nm absorbance, which is consistent with protonation of the persulfide anion to generate the parent persulfide. We also observed that the UV-vis reactions

proceeded at a significantly slower rate than the NMR experiments, which is consistent with our proposed bimolecular persulfide decomposition reaction because the UV-Vis experiments were conducted at a significantly lower concentration.

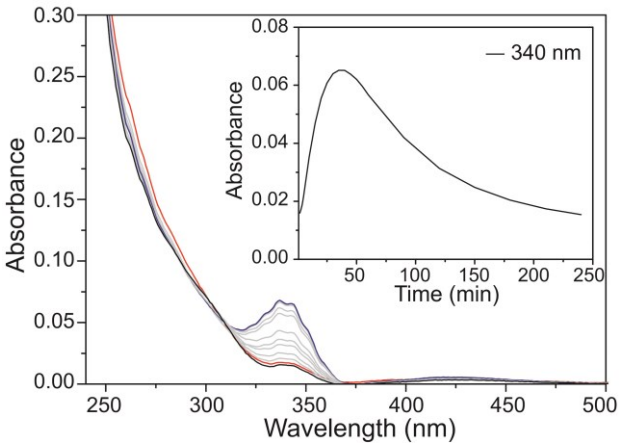

Figure 4.4. UV-Vis spectrum of 100 μM BnSSH reacting with 10 mM [NBu_4^+][AcO^-] in dichloromethane. Immediately after addition of base (black), the intensity of the peak centered around 340 nm increases for 30 min (blue), before returning to background levels (red). Inset: Intensity of persulfide anion (340 nm) with respect to time.

On the basis of the observed reactivity of the three persulfides investigated here, we propose a general mechanism for the observed base-mediated decomposition (Figure 4.5). For the reaction between two persulfides under basic conditions (**5**), if R is sufficiently sterically hindered or is a tertiary center, such as for AdSSH and TrtSSH, only the terminal sulfur atom of the persulfide is accessible for nucleophilic attack by other persulfides. This reaction results in formation of one equivalent of hydropolysulfide anion (**6**) and one equivalent of thiol. The resultant hydropolysulfide anions (**6**) can then react with additional persulfides to further elongate the hydropolysulfide chain (**7**). Once the sulfur chain in the hydropolysulfide anion is of sufficient length, an intramolecular nucleophilic attack results in extrusion of elemental sulfur (such as S_8) and generates the parent thiol. By contrast, when the R-group is not sterically hindered or is primary center,

such as for BnSSH, the α-sulfur atom becomes accessible for nucleophilic attack. Attack on the α-sulfur by a persulfide anion or hydropolysulfide anion results in formation of a symmetrical organic polysulfide (**8**) and HS^-, thus terminating the chain.

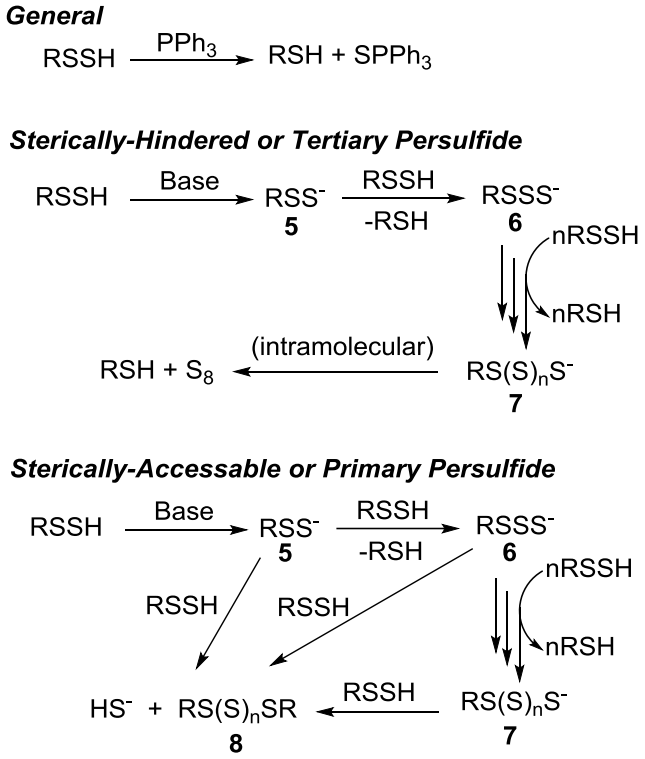

Figure 4.5. Proposed reaction mechanism for the reaction of persulfides (RSSH) with reductants and bases.

Conclusions

In summary we have prepared three organic persulfides, TrtSSH, AdSSH, and BnSSH, and investigated their reactivity in aprotic organic solvents using NMR and UV-vis spectroscopic to determine how differences in persulfide structure relate to differences in observed reactivity. The chemical reactivity data obtained from TrtSSH demonstrates that persulfides do not react with nucleophiles or acids, but rather release sulfide upon reduction and disproportionate to release S^0, likely as S_8 under physiological conditions, upon deprotonation (Figure 4.5). These results clarify the innate reactivity of

persulfides and confirm that persulfides are viable sources of reductant-labile sulfur. Although our experiments were performed in organic solution under anaerobic conditions, and thus may not directly represent the exact reactivity of organic persulfides in aerobic aqueous environments, we believe that the reaction profiles of these isolated persulfides contributes positively to unravelling the complex reactivity associated with biological persulfides. For example we observed that persulfide stability inversely correlates with persulfide acidity, with acidic persulfides decomposing more rapidly than less-acidic persulfides. This observation may help explain why although cysteine persulfides in enzyme active sites act as highly-reactive nucleophiles, less-acidic glutathione persulfide (GSSH) is present and stable in micromolar concentrations in the cytoplasm. Furthermore, differences in solvation and hydrogen bonding environments available to GSSH compared to the cysteine persulfides in enzyme pockets may also contribute to these differences in reactivity. In our model studies, we also observed that the steric bulk near the persulfide significantly impacts the reactivity, and this observation may have consequences in determining the relative electrophilicity and nucleophilicity of the sulfur atoms of the persulfide. This observation may also suggest that specific proteins or protein pockets may be sufficiently shielded to prevent the formation of longer-chain polysulfides, thus imparting selectivity on polysulfide chain length and associated changes in reactivity based on which hydropolysulfides can be generated. Additionally, we observed that persulfides can only release H_2S following reduction by another species, including another persulfide, which supports the general hypothesis that persulfides may play important roles for sulfide storage and transport, whereas free H_2S/HS^- is prone to reaction with other reactive biological species. Taken

together, these results provide new insights into persulfide reactivity gleaned from simple model compounds investigated under identical conditions.

Experimental Section

Materials and Methods. Benzylpersulfide (**BnSSH**)[157] adamantylpersulfide (**AdSSH**)[158] and triphenylmethylpersulfide (**TrtSSH**)[159] have been reported previously, but we report modified synthetic procedures and complete characterization data below. Thioacetic acid, acetyl chloride, sulfuryl chloride and the required thiols were purchased from commercial suppliers and used as received. Triphenylphosphine, $[NBu_4^+][BH_4^-]$, $[NBu_4^+][CN^-]$, $[NBu_4^+][Cl^-]$, $[NEt_4^+][Br^-]$, $[NBu_4^+][I^-]$, $[NBu_4^+][OAc^-]$, and DMAP were handled in an inert atmosphere glove box and used at received. $[NBu_4^+][SH^-]$ was prepared by reaction of NaSH with $[NBu_4^+][Cl^-]$ in MeCN in the absence of both water and air. Concentration of the solution under vacuum, followed by trituration of the resulting solid with Et_2O produces $[NBu_4^+][HS^-]$ as a white solid. Dithiopropane, acetic acid, and benzyl thiol were degassed using three freeze-pump-thaw cycles and stored under nitrogen. TEA, DMEDA, and pyridine were distilled under vacuum prior to use and stored under nitrogen. Trityl thiolate was generated by deprotonation of trityl thiol with sodium hydride. $[NBu_4^+][TFA^-]$ was prepared by reaction of trifluoroacetic acid with $[NBu_4^+][OH^-]$. $NO_{(g)}$ was prepared by the slow addition of H_2SO_4 to a concentrated aqueous solution of $NaNO_2$. The evolved gas was purified by passing through a column of NaOH pellets and low-boiling impurities were condensed by passage through a glass wool filled coil at −78 °C, and collected in a storage bulb. $H_2S_{(g)}$ was purchased from Sigma Aldrich and transferred through a custom-built stainless steel transfer line into a glass storage bulb prior to use. *Note*: Hydrogen sulfide and its salts are highly toxic and should be handled carefully to avoid exposure. Deuterated solvents were purchased from

Cambridge Isotope Laboratories, degassed using three freeze-pump-thaw cycles and stored under nitrogen over 4Å molecular sieves. Diethyl ether and toluene were degassed by sparging with argon followed by passage through a Pure Process Technologies solvent purification system. All air-free manipulations were performed using standard Schlenk techniques or by use of an Innovative Technology glove box.

Spectroscopic methods. NMR spectra were acquired on a Brüker Avance-III-HD 600 spectrometer with a Prodigy multinuclear broadband CryoProbe or a Varian INVOA-500 spectrometer at 25.0 °C. Chemical shifts are reported in parts per million (δ) and are referenced to residual protic solvent resonances. The following abbreviations are used in describing NMR couplings: (s) singlet, (d) doublet, (b) broad, and (m) multiplet. Persulfide reactivity was assessed by NMR using anhydrous and anaerobic CD_2Cl_2 at room temperature with 18 mM persulfide and reactant (Table 4.2, #). UV-vis spectroscopic measurements were performed on a Cary 60 spectrophotometer equipped with a Quantum Northwest cuvette temperature controller under anaerobic conditions in 1.0 cm path length septum-sealed cuvettes obtained from Starna Scientific. IR spectra were measured in the solid phase on a Thermo Scientific Nicolet 6700 RT-IR using an ATR attachment. Raman spectra were recorded in the solid phase on a WITEC alpha300 S scanning near-field optical microscope. High resolution mass spectrometry (HRMS) measurements were performed by the Biomolecular Mass Spectrometry Core of the Environmental Health Sciences Core Center at Oregon State University.

X-Ray Crystallography. Single crystals of TrtSSH suitable for X-ray diffraction were grown from a mixed toluene/Et_2O solution. Diffraction data were collected on a Bruker Smart Apex diffractometer at 150(2) K using Mo K_α radiation (λ = 0.71073 Å).

Data reduction was performed in SAINT, and absorption corrections were applied using SADABS. All refinements were performed using the SHELXTL software package.[160-162] All non-hydrogen atoms were refined anisotropically. Hydrogen atoms were found from the residual density map and were refined with isotropic thermal parameters. The terminal H atom in the SSH group was disordered over two positions, which were refined to a 60:40 ratio by iterative refinement of of different occupation factors. TrtSSH crystallized in the non-centrosymmetric space group $P2_12_12$ with an associated Flack parameter of 0.14(10).

Synthetic procedures

Diacetylsulfide (**2**): Acetyl chloride (12.15 mL, 170.3 mmol) was added dropwise to thioacetic acid (**1**, 6.0 mL, 85 mmol) under nitrogen. The reaction mixture was refluxed at 70 °C for 5 h, during which time the color changed from light yellow to deep red. After heating, the reaction mixture was allowed to cool to room temperature and vacuum distillation (40 °C bath temperature) afforded 5.31 g (53% yield) of **2** as a light pink to fuchsia liquid. Diacetylsulfide, **2**, can be stored at −20 °C without decomposition. ^{1}H NMR (600 MHz, $CDCl_3$) δ: 2.51 (s, 6H)

Acetyl sulfenylchloride (**3**). In rigorously dried glassware using anhydrous reagents, sulfuryl chloride (3.73 mL, 46.2 mmol) was added dropwise to diacetylsulfide (5.3 g, 45 mmol) at −30 °C in a dry ice/methanol bath under nitrogen. The reaction mixture was warmed from −30 °C to −5 °C over the course of 1 h, during which time the color of the solution changed from pale yellow to orange. The generated SO_2 was removed at −15 °C under vacuum at 20 torr. Vacuum distillation at 100 mtorr of the remaining mixture at 0 °C into a receiving flask at −40 °C produced 3.10 g (28.0 mmol,

62.3%) of a bright yellow liquid, with spectroscopic properties matching previous reports. This compound was used immediately. ^{1}H NMR (600 MHz, $CDCl_3$) δ: 2.41 (s, 3H). $^{13}C\{^{1}H\}$ NMR (150 MHz, $CDCl_3$) δ: 190.1, 26.5.

General procedure for preparation of acetyldisulfides*:* The desired thiol (1.82 mmol) was dissolved in 1.0 mL of dry Et_2O and was added dropwise at room temperature to acetylsulfenyl chloride (**2**, 221 mg, 2.00 mmol) dissolved in 1.0 mL of dry Et_2O under nitrogen. For best results, use freshly distilled **2**. The reaction mixture was allowed to stir for 1.5 h. The remaining volatiles were removed under vacuum to give the corresponding acetyl disulfide as a solid. These compounds are all generally stable on the bench top and appear to be stable indefinitely in the freezer.

Benzylacetyldisulfide (**4a**). The general procedure described above was modified in the following ways: the volatiles were removed at 0 °C instead of at rt. Benzylacetyldisulfide was isolated as a pale white solid in 86.5% yield (300 mg). ^{1}H NMR (600 MHz, $CDCl_3$) δ: 7.31 (m, 5H), 3.93 (s, 2H), 2.34 (s, 3H). $^{13}C\{^{1}H\}$ NMR (150 MHz, $CDCl_3$) δ: 195.2, 136.2, 129.6, 128.7, 127.9, 43.0, 28.8.

Adamantylacetyldisulfide (**4b**). The general procedure yields 287 mg (57.5%) of a loose white solid. ^{1}H NMR (600 MHz, $CDCl_3$) δ: 2.47 (s, 3H), 2.07 (bs, 3H), 1.83 (d, 6H, J = 2.4 Hz), 1.66 (q, 6H, J = 12 Hz). $^{13}C\{^{1}H\}$ NMR (150 MHz, $CDCl_3$) δ: 195.9, 50.5, 42.2, 36.0, 29.9, 28.9.

Tritylacetyldisulfide (**4c**): The general procedure described above was modified in the following ways: triphenylmethyl thiol was dissolved in 2 mL of 50:50 benzene/Et_2O. Recyrstalization of the resulting solid from MeOH 306.2 mg (48% yield) of **4c** as a white

crystalline solid. ^{1}H NMR (600 MHz, CD_2Cl_2) δ: 7.33 (m, 15H), 2.03 (s, 3H). $^{13}C\{^{1}H\}$ NMR (150 MHz, $CDCl_3$) δ: 194.2, 143.3, 130.2, 128.0, 127.4, 73.38, 28.3.

General procedure for preparation of persulfides*:* Methanolic HCl (5 N) was prepared by adding acetyl chloride to dry degassed methanol in an ice bath. The acetyldisulfide (100 mg,) was dissolved in 1.0 mL of methanol and cooled in an ice bath under nitrogen. Methanolic HCl (5 N, 342 μL) was added to the solution dropwise, and the resultant reaction mixture was allowed to stir overnight. It is important that no metals be in the reaction vessel at this time. The disulfide does not immediately dissolve fully, and takes up to 3 hr to fully dissolve. After stirring for 24 h, the solvents were removed under vacuum to yield the desired persulfide.

Benzylpersulfide (**BnSSH**). The general procedure yields 74.0 mg (94%) of a viscous liquid. This compound has a half-life of approximately 2 weeks when stored at −20 °C in the absence of both water and oxygen. ^{1}H NMR (600 MHz, CD_2Cl_2) δ: 7.32 (m, 5H), 3.91 (s, 2H), 2.96 (bs, 1H, SH). $^{13}C\{^{1}H\}$ NMR (150 MHz, CD_2Cl_2) δ: 137.5, 129.8, 129.0, 128.0, 43.4. IR (cm^{-1}): 3061, 3028, 2914, 2505, 1493, 1452, 1070, 763, 697, 665. HRMS-ESI (m/z): [M-H] calcd for [$C_7H_8S_2$] 156.0068; found 156.0060.

Adamantylpersulfide (**AdSSH**). The general procedure yields 74.4 mg (90%) of viscous oil that quickly solidifies on cooling. Adamantylpersulfide appears stable indefinitely when stored at −20 °C, and solution samples do not significantly degrade over the course of a few days. ^{1}H NMR (600 MHz, CD_2Cl_2) δ: 2.70 (s, 1H, SH), 2.13 (bs, 3H), 1.88 (d, 6H, J = 2.5 Hz), 1.73 (q, 6H, J = 12 Hz). $^{13}C\{^{1}H\}$ NMR (150 MHz, CD_2Cl_2) δ: 46.7, 41.5, 36.0, 30.0. IR (cm^{-1}): 2904, 2849, 2674, 2655, 2491, 1439, 1341, 1311,

1297, 1254, 1102, 1041, 977, 867, 686. HRMS-ESI (m/z): [M-H] calcd for [$C_{10}H_{16}S_2$] 200.0694; found 200.0695.

Tritylpersulfide (**TrtSSH**): The general procedure yields 80.9 mg (92% yield) as a white crystalline solid. Tritylpersulfide appears stable indefinitely when stored at −20 °C, and solution samples do not significantly degrade over the course of a few days. When handling be aware that dried tritylpersulfide is very staticky. ^{1}H NMR (600 MHz, CD_2Cl_2) δ: 7.30 (m, 15H), 2.72 (s, 1H, SH). ^{13}C{^{1}H} NMR (150 MHz, CD_2Cl_2) δ: 143.5, 129.9, 128.0, 127.1, 70.4. IR (cm^{-1}): 3016, 2058, 1959, 1592, 1488, 1439, 1317, 1181, 1157, 1080, 1033, 1000, 924, 877. HRMS-ESI (m/z): $[M-H]^-$ calcd for $[C_{19}H_{15}S_2]^-$ 307.0621; found 307.0631.

General procedure for NMR reactions. A septum-sealed NMR tube was charged with TrtSSH (2.0 mg in 350 μL of CD_2Cl_2) under an N_2-atmosphere in a glove box. After measuring an initial NMR spectrum, reactants (1 equiv. in 200 μL CD_2Cl_2) were added and the reaction progress was monitored by ^{1}H NMR spectroscopy until completion.

Associated Content

NMR spectra, UV-Vis data, crystallographic data. This material can be found in Appendix C

CHAPTER V

THE INTERSECTION OF NO AND H_2S: PERSULFIDES REACT WITH NITRITE TO PRODUCE NO

The work investigating the reaction of persulfides with nitrite has not yet been published; however, a manuscript is in preparation. Thomas Spencer Bailey performed all chemical synthesis, purification, NMR spectroscopy, and UV-vis experiments. The computational analysis of the energy landscape was performed by Hillary A. Henthorn. Michael D. Pluth was the principle investigator for this work.

Introduction

Reduced sulfur, specifically H_2S, is important for its roles in signaling biological processes and mediating redox homeostasis.[30,117] In mammalian species, H_2S has been linked with functions in the immune, cardiovascular, and central nervous systems, [30,53] and is produced endogenously by the action of multiple enzymatic and non-enzymatic pathways from cysteine feedstocks.[118] In addition to the fully reduced free sulfide state (S^{2-}), which consists of both free sulfide and acid labile sulfur pools, oxidation of H_2S to sulfane sulfur (S^0 oxidation state) produces compounds such as persulfides (RSSH) and polysulfides (RSS_nSR), contributing to the diversity of biological sulfur chemistry.[117,125-128] Among sulfane sulfur species, persulfides are of particular interest because they exist endogenously at physiological significant concentrations (50-100 μM) and provide a redox neutral pathway for transsulfuration and transpersulfidation.[31,32,133-136] Proteins bearing persulfide modified cysteine residues show altered activity, such as increased nucleophilicity, compared to the parent thiols.[31,32,133-136] Persulfides have also been

hypothesized to have a strong contribution to the observed redox properties produced by exogenous H_2S, based on the increased stability of the persulfide radical ($RSS^{\bullet}$) compared to the thiyl radical ($RS^{\bullet}$).[137]

One active area of research within the biological sulfur field is focused on investigating the overlap between H_2S and $NO_{(g)}$,[163] especially within the cardiovascular system.[164] Although $NO_{(g)}$ is well understood to be active in vasorelaxation processes, the emergence of H_2S as a vasodilator is recent.[165] For example H_2S opens ATP-sensitive potassium channels (K_{ATP}) by persulfidation of a disulfide in SUR1,[166] which induces vasorelaxation in endothelial cells.[167] Whether H_2S and $NO_{(g)}$ exhibit synergy in their vasorelaxation profiles is still the topic of some debate.[168] For example, although underexpression of H_2S producing enzymes results in the inhibition of $NO_{(g)}$ producing enzymes,[164] exogenous H_2S has been shown to decrease $NO_{(g)}$ production.[169] Likewise, ferrous hemes in H_2S producing enzymes are capable of reducing nitrite to $NO_{(g)}$, however these same enzymes are inactive while $NO_{(g)}$ is bound.[170] Additionally both H_2S and $NO_{(g)}$ independently function to regulate cGMP, a potent activator of both vasorelaxation and angiogenesis.[171] The cooperativity of H_2S and $NO_{(g)}$ is further complicated by the existence of S/N hybrid species, which form at the interface of H_2S and $NO_{(g)}$ chemistry.[172-174]

Based on the large body of evidence showing that the biochemistry of $NO_{(g)}$ and H_2S are highly intertwined, we were interested in investigating the contribution of persulfides to $NO_{(g)}/H_2S$ crosstalk. In our previous investigations into persulfide reactivity, we did not observe direction reaction between persulfides and $NO_{(g)}$. However, we did find that persulfides are both good nucleophiles and reductants, leading us to

investigate the reaction of persulfides with nitrite, the product of $NO_{(g)}$ oxidation. We hypothesized that based on the favorable RSSH→ RSS$^{\bullet}$ redox couple, that a persulfide may be a strong enough reductant to reduce nitrite back to $NO_{(g)}$. This reactivity would provide a pathway for propagation of $NO_{(g)}$ signaling processes by the sulfane sulfur pool, and contribute to the biological crosstalk between $NO_{(g)}$ and H_2S.

Results and Discussion

Upon treating adamantyl persulfide (AdSSH) with nitrite (Figure 5.1a) we immediately observe the appearance of new absorbance bands (Figure 5.1b) and the solution visibly changes from colorless to green-blue. The new band centered at 617 nm grows in steadily over the course of ~20 min before beginning to decay, at which time a new band centered at 446 nm begins to increase. The conversion of the 617 nm species to the 446 nm is clean, with an isosbestic point at 540 nm. The band at 446 nm reaches its maximum intensity after 150 min, at which time the band at 617 nm has completely disappeared, leaving an orange solution. In the absence of O_2 and with minimal exposure to light the orange color of the solution is maintained indefinitely, however in the spectrometer it slowly decays over a few hours to produce a colorless solution.

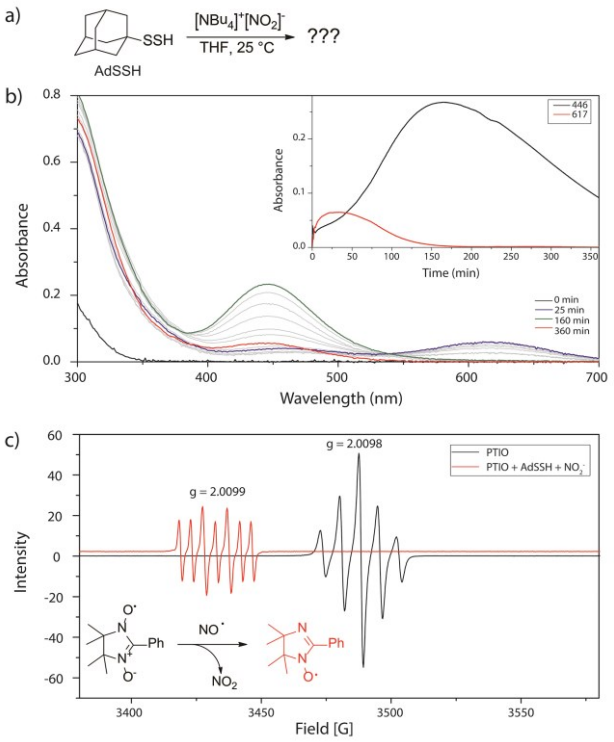

Figure 5.1. Reactivity of persulfides with nitrite. (a) Adamantyl persulfide (AdSSH) reacts with nitrite in THF at room temperature. (b) UV-Vis spectrum of the reaction (500 μM AdSSH with 500 μM NO_2^-) monitored over 6 hr. Inset: Intensity of the peaks at red: 617 nm and **black**: 446 nm with respect to time. (c) EPR spectrum of **black**: 5 mM PTIO in THF; red: with 2.5 mM reaction mixture with 1 mM PTIO injected.

To show that the reaction between persulfides and nitrite is general, and ensure that the observed reactivity is specifically between the persulfide and nitrite, we varied both the nitrite counter ion and the persulfide backbone (Figure D1-3). Neither replacement of the NBu_4^+ cation with PNP^+, nor changing the adamantyl functional group to either benzyl or triphenylmethyl changed the observed spectroscopic properties of the reaction mixture, only the rates of conversion between species. To test our hypothesis that persulfides react with nitrite to produce $NO_{(g)}$, we treated the reaction mixture with PTIO, a known EPR probe for $NO_{(g)}$. Based on the change in the EPR splitting pattern of PTIO after treatment with our persulfide/nitrite mixture (Figure 5.1c), we concluded that

persulfides do react with nitrite to produce $NO_{(g)}$. This result was independently confirmed by binding liberated NO to cobalt phthalocyanine (Figure D4).

Because persulfides react with nitrite to form $NO_{(g)}$, we wanted to investigate the mechanistic pathway for $NO_{(g)}$ formation. Our initial hypothesis that persulides would react with nitrite centered on the high stability of the persulfide radical. Considering that thiyl radicals typically absorb visible light around ~400 nm, we initially attributed the 446 nm absorbance in the UV-Vis spectrum to the perthiyl radical. Based on the previous investigations into the interactions between sulfide and nitrite,[175-178] we hypothesized that an S/N hybrid compound might be formed as an intermediate to $NO_{(g)}$ formation. Example of previous S/N hybrids are shown in Figure 5.2. Comparing the UV-Vis spectrum observed in our reaction to the spectral properties of known S/N hybrid compounds, we likened the blue green 617 nm absorbance to that of the ~600 nm green absorbance of a nitrosothiol (Table 5.1). Nitrosothiols are the product of the reaction of nitrite with thiols, however this reaction is typically catalyzed by acid under highly acidic conditions, or by direct reaction with $NO_{(g)}$ in the presence of O_2. Based on the likeness of the reaction UV-Vis spectrum to that of a nitrosothiol, and the increased nucleophilicity of persulfides compared to thiols, we hypothesized that a persulfide might react directly with nitrite resulting in a new S/N hybrid species: a nitrosopersulfide (RSSNO), which would then decompose to produce $NO_{(g)}$ and a perthiyl radical ($RSS^{\bullet}$).

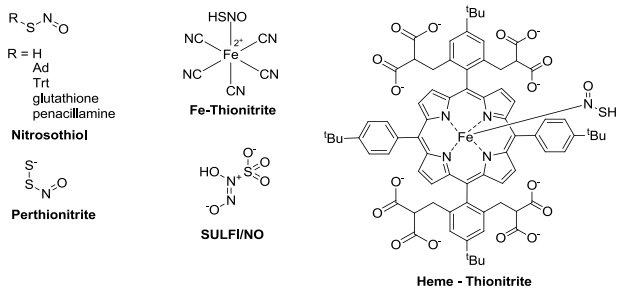

Figure 5.2. Structures of known S/N hybrid compounds

	UV Bands (nm)	^{15}N NMR Peaks (ppm)
Nirosothiol		
R- H_{aq}	340	322
GSH_{aq}	335, 545 (weak)	409
$SNAP_{aq}$	340, 590 (weak)	-
Ad_{THF}	345, 576 (weak)	460
Trt_{DCM}	348, 602 (weak)	-
Perthionitrite		
H_2O	412	-
Acetone	448	354
Fe-thionitrite	535	-
Heme-thionitrite	432	-
SULFI/NO	259	-

Table 5.1. Reported spectroscopic properties for known S/N hybrid compounds. Compounds with a '-' have not been characterized by the listed method. Perthionitrite has been characterized in both aqueous and organic media, with both properties tabulated above.

To verify the above hypothesis, we conducted DFT calculations on the energy coordinate of our proposed mechanism. Additionally, there are relatively few spectroscopic techniques for probing the local environment in reactive sulfur species. For example, naturally abundant sulfur nuclei are typically NMR inactive, and S-S bond vibrations are sufficiently low in energy that they are not easily observed by IR. However, because there are no previous reports for an organic nitrosopersulfide, the plausibility of a nitrosopersulfide as an observable intermediate was in question. The energy surface for the conversion of AdSSH to AdS_4Ad via AdSSNO and $AdSS^{\bullet}$ was investigated using M06, BMK, and B3LYP methods (Figure 5.3). Regardless of computational method, the conversion from persulfide to tertrasulfide with concurrent production of $NO_{(g)}$ is thermodynamically favorable, with minimal barriers to conversion between species. Interestingly, the proposed nitrosopersulfide intermediate was calculated to be lower in energy than the starting materials, with an S-N bond strength of only ~14 kcal/mol. Based on the long lifetime observed for the 617 nm species (Figure

5.1b inset), the weak bond strength, and thus instability, of a nitrosopersulfide makes it unlikely to be involved in the reaction.

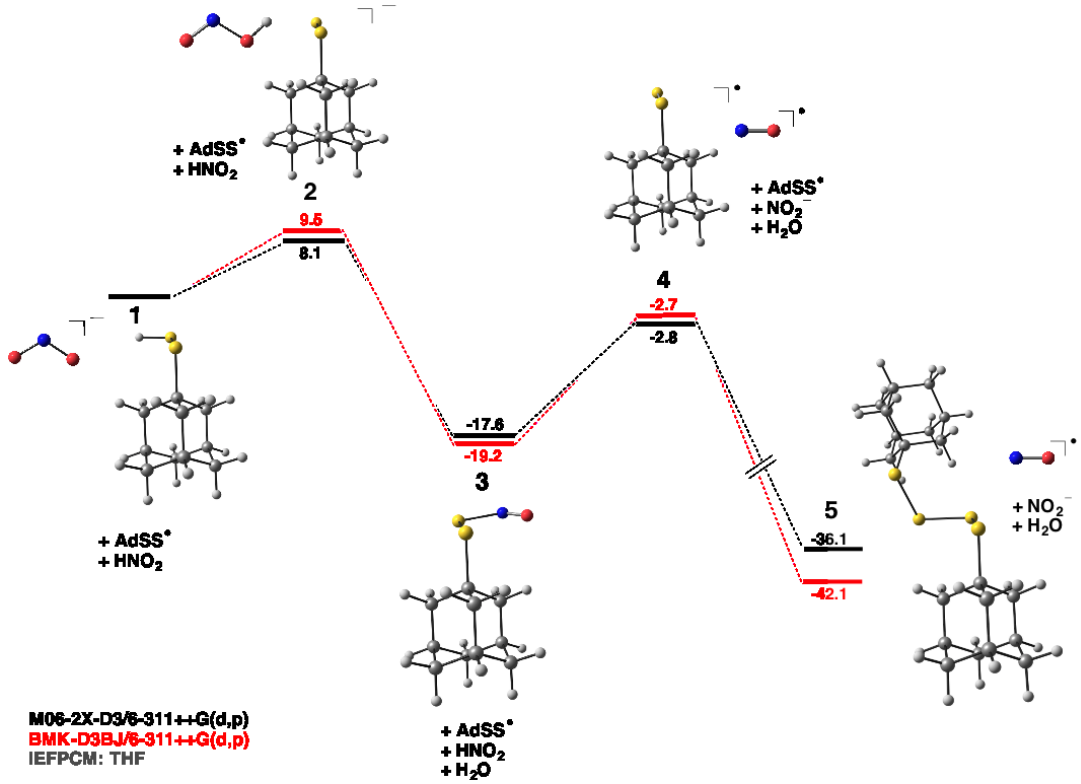

Figure 5.3. Calculated potential energy surfaces for the generation of NO• via AdSSNO at the M06-2X-D3/6-311++G(d,p) (black) and BMK-D3BJ/6-311++G(d,p) (red) levels of theory with IEFPCM solvation (THF). Energies are reported in kcal/mol.

	6-311++G(d,p)					
	B3LYP	BMK	M06-2X	B3LYP-D3BJ	BMK-D3BJ	M06-2X-D3
1	0	0	0	0	0	0
2	11.3	8.5	8.0	12.1	9.5	8.1
3	-17.3	-17.6	-17.5	-19.2	-19.2	-17.6
4	-4.6	-3.7	-2.9	-3.1	-2.7	-2.8
5	-27.5	-36.2	-35.5	-33.1	-42.1	-36.1
	Def2-TZVPPD					
	B3LYP	BMK	M06-2X	B3LYP-D3BJ	BMK-D3BJ	M06-2X-D3
1	0	0	0	0	0	0
2	11.9	8.5	9.0	12.7	9.4	9.1
3	-16.5	-16.2	-16.9	-18.3	-18.0	-17.0
4	-3.6	-1.8	-1.9	-2.1	-0.8	-1.8
5	---	---	-35.7	---	---	---

Table 5.2. Calculated energetics for the generation of NO• via AdSSNO at various levels of theory with IEFPCM solvation (THF)

Because the reaction mechanism is unlikely to proceed through a long lived nitrosopersulfide intermediate, we returned our attention to identifying the species responsible for the observed changes in the UV-Vis spectrum. Among known sulfur or nitrogen containing compounds, the trisulfur radical anion ($[S_3]^{\bullet-}$) was the only species with spectral characteristics matching those observed. However, $[S_3]^{\bullet-}$ had not been previously reported in THF, and typically requires elevated temperatures to form preferentially over longer chain polysulfide dianions. To clarify the discrepancy, we treated S_8 with $[NBu_4]^+[HS]^-$, and immediately observed a strong absorbance band at 617 nm (Figure 5.4a black trace). Similarly, the same 617 nm band was observed when AdSSH was treated with $[NBu_4]^+[OAc]^-$ (Figure D5), leading us to conclude that upon treatment of persulfides with base that $[S_3]^{\bullet-}$ is formed.

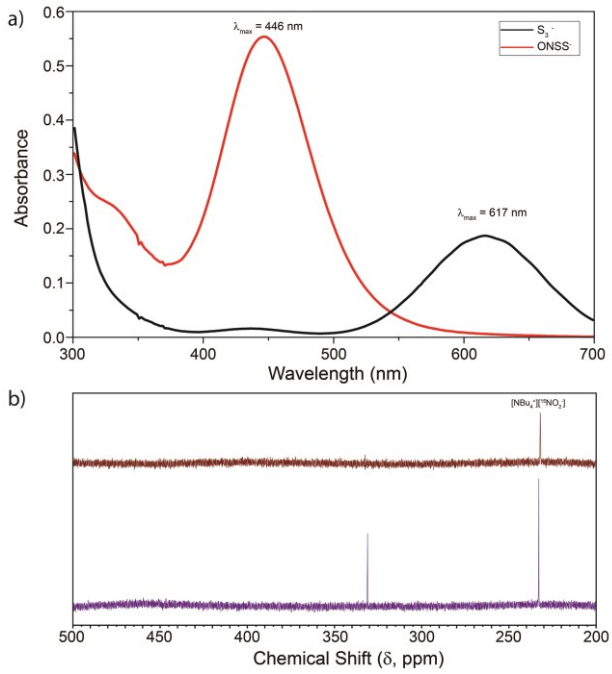

Figure 5.4. Spectroscopic identification of reaction intermediates. (a) red: $[NBu_4]^+[ONSS]^-$ λ_{max} = 446 nm and **black: $[S_3]^{\bullet-}$** λ_{max} = 617 nm. (b) ^{15}N NMR spectra (60.8 MHz, d_8-THF, room temperature) of top: $[NBu_4^+][^{15}NO_2^-]$ and bottom: $[NBu_4]^+[O^{15}NSS]^-$. These spectra use CH_3NO_2 as the $\delta = 0$ ppm reference standard.

Because $[S_3]^{\bullet-}$ is typically generated from S_8 in the presence of a nucleophilic base, such as *tert*-butoxide or ammonia, we concluded that S_8 must be produced as a first step during the reaction, and that nitrite must therefore be sufficiently basic in THF to facilitate base-mediated persulfide decomposition. In our previous work studying the reactions of persulfide with base, we did not observe $[S_3]^{\bullet-}$ formation. To confirm that the 617 nm absorbance belonged to $[S_3]^{\bullet-}$, we trapped the resulting anions with benzyl chloride (BnCl). Treatment of solutions of $[S_3]^{\bullet-}$ with BnCl immediately abated the band at 617 nm (Figure D6), and investigation of the reaction products by ^{1}H NMR spectroscopy show not only the formation of benzyl trisulfide, but also of longer chain benzylic polysulfides (Figure D10). These results not only show that there are multiple polysulfide species equilibrating in solution, but also describe why we were previously unable to observe $[S_3]^{\bullet-}$ formation: any $[S_3]^{\bullet-}$ produced was quenched by reaction with the solvent, because we were conducting our experiments in dichloromethane.

Upon identification that the 617 nm band likely corresponds to $[S_3]^{\bullet-}$, and that there were a mixture of polysulfides present in solution, the band at 446 nm was easily identified as perthionitrite ion ($[ONSS]^-$) (Figure 5.4a red trace). In polar aprotic solvents nitrite reacts with elemental sulfur to produce perthionitrite with a strong absorbance at 446 nm (Figure D7), and includes a small shoulder at 617 nm. To confirm that we were making perthionitrite, and that no other nitrogen containing species appear during the reaction coordinate, we monitored the reaction of $[NBu_4^+][^{15}NO_2^-]$ by ^{15}N NMR spectroscopy (Figure 4b). We did not observe any additional peaks in the ^{15}N spectrum during the course of the reaction (Figure D11), however we did observe small modulation in the difference between the nitrite and perthionitrite chemical shifts.

Having identified the intermediates observed during the reaction, and knowing that $NO_{(g)}$ is liberated during the reaction, we next investigated how changing the free $NO_{(g)}$ concentration impacted the solution equilibrium. Treatment of a solution of $[S_3]^{\bullet-}$ with authentic $NO_{(g)}$ quickly consumes $[S_3]^{\bullet-}$ and generates perthionitrite (Figure 5). Comparatively, when $[NBu_4]^+[HS]^-$ is treated with $NO_{(g)}$ no reaction is observed (Figure D8). This result confirms the previous suspicion that in order for H_2S and $NO_{(g)}$ to react an oxidant must be present.

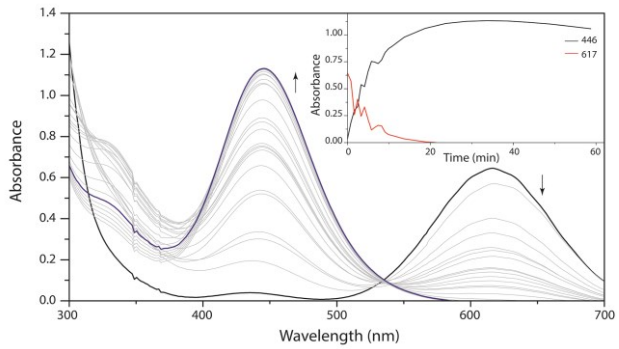

Figure 5.5. Reaction of $[S_3]^{\bullet-}$ black trace with $NO_{(g)}$ to produce $[NBu_4]^+[ONSS]^-$ (blue trace). Inset: Intensity of the peaks at **black**: 617 nm and red: 446 nm with respect to time

Conclusion

We have investigated the interaction between persulfides and nitrite, and found that the two react to produce $NO_{(g)}$. Although we originally hypothesized that this transformation would occur via a nitrosopersulfide intermediate, we performed calculations that showed such an intermediate would be unstable and likely short lived. As a result, nitrosopersulfides are likely not biologically important for proliferating signaling activities. Instead, we found that this conversion first requires the decomposition of the persulfides to form polysulfides or elemental sulfur, followed by reaction with nitrite to form perthionitrite. Although these results show that persulfides are not directly involved in the production of $NO_{(g)}$, they highlight the overall importance

of sulfane sulfur for carrying out signaling processes. In this case, persulfies do not act as signaling species, but rather provide a mechanism for sulfane sulfur transport. Because elemental sulfur typically is minimally soluble in solution, persulfides facilitate solvation of sulfane sulfur and propagate signaling processes in otherwise unfavorable environments.

There is some debate in the literature as to the biological significance of perthionitrite,[175,179] with the aqueous stability of perthionitrite being a primary area of concern. We have found that the addition of water, in the absence of oxygen, to perthionitrite generated in THF does not promote perthionitrite decomposition (Figure D9), but rather the perthionitrite absorbance displays solvatochromism with respect to aqueous solvation. Although this result does not prove that perthionitrite is biologically significant, it does support the idea that perthionitrite is stable in aqueous environments. Taken together, these results show the versatility of persulfides both as primary signaling species, and as transport agents for facilitating other processes. Thus, persulfides are an important part of the sulfane sulfur pool, which contributes to the sulfane sulfur pool's role in mediating NO/H_2S crosstalk.

Experimental Section

Materials and Methods. The preparation of benzylpersulfide (**BnSSH**) adamantylpersulfide (**AdSSH**) and triphenylmethylpersulfide (**TrtSSH**) is discussed in chapter 4. Cobalt (II) phthalocyanine, elemental sulfur and $[NBu_4^+][NO_2^-]$ were handled in an inert atmosphere glove box and used as received. $[NBu_4^+][SH^-]$ and $[NBu_4^+][^{15}NO_2^-]$ were prepared by reaction of the appropriate sodium salt with $[NBu_4^+][Cl^-]$ in MeCN in the absence of both water and air. Filtration to remove NaCl,

followed by concentration of the solution under vacuum and trituration of the resulting solid with Et_2O produces either $[NBu_4^+][HS^-]$ or $[NBu_4^+][^{15}NO_2^-]$ as a white solid. $NO_{(g)}$ was prepared by the slow addition of H_2SO_4 to a concentrated aqueous solution of $NaNO_2$. The evolved gas was purified by passing through a column of NaOH pellets and low-boiling impurities were condensed by passage through a glass wool filled coil at −78 °C, and collected in a storage bulb. Bis(triphenylphosphine)-iminium nitrite ($[PNP^+][NO_2^-]$) was prepared by the literature method.[180] Deuterated solvents were purchased from Cambridge Isotope Laboratories, degassed using three freeze-pump-thaw cycles and stored under nitrogen over 4Å molecular sieves. THF was degassed by sparging with argon followed by passage through a Pure Process Technologies solvent purification system. All air-free manipulations were performed using standard Schlenk techniques or by use of an Innovative Technology glove box.

Spectroscopic methods. NMR spectra were acquired on a Brüker Avance-III-HD 600 spectrometer with a Prodigy multinuclear broadband CryoProbe or a Varian INVOA-500 spectrometer at 25.0 °C. Chemical shifts are reported in parts per million (δ) and are referenced to residual protic solvent resonances. The following abbreviations are used in describing NMR couplings: (s) singlet, (d) doublet, (b) broad, and (m) multiplet. Persulfide reactivity with nitrite was assessed by UV-Vis using anhydrous and anaerobic THF at 25 °C using 500 μM persulfide and nitrite. ^{15}N NMR experiments were carried out with 50 mM reactants using anhydrous and anaerobic d_8-THF at 25 °C. UV-vis spectroscopic measurements were performed on a Cary 100 spectrophotometer equipped with a Quantum Northwest cuvette temperature controller under anaerobic conditions in 1.0 cm path length septum-sealed cuvettes obtained from Starna Scientific.

Associated Content

NMR spectra, and UV-Vis data. This material can be found in Appendix D

APPENDIX A

SUPPLEMENTAL INFORMATION: A SIMPLE BIOLUMINESCENT METHOD FOR MEASURING D-AMINO ACID OXIDASE ACTIVITY

UV-Vis Data

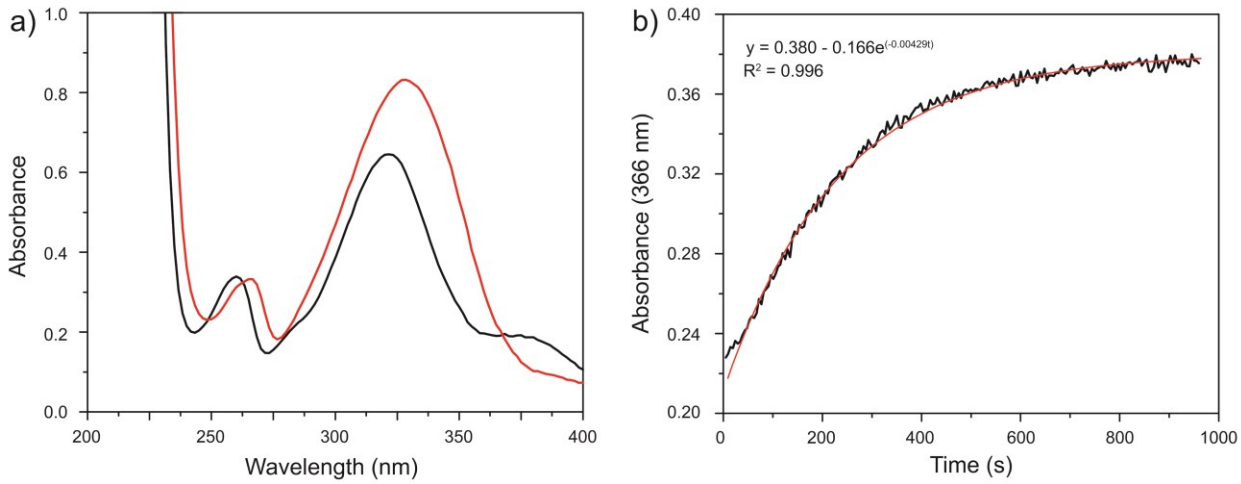

Figure A1. (a) The UV-vis absorbance spectra of 50 μM CBT-OH (black) and D-luciferin (red). (b) The reaction of 25 μM CBT-OH with 375 μM D-cysteine monitored at 366 nm for 15 min with data collected every 0.05 s. The data were fit directly to an exponential growth function to obtain the pseudo-first order rate constant.

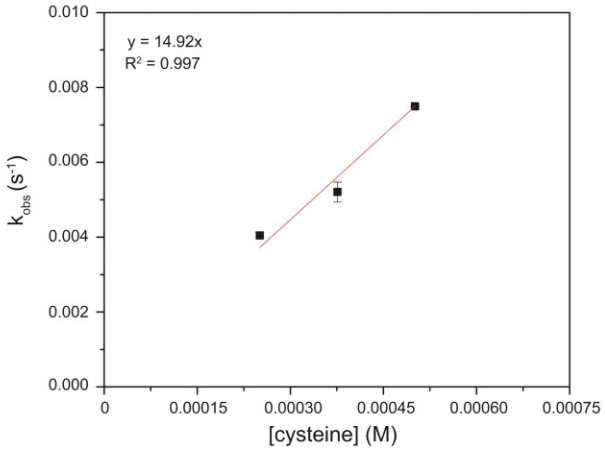

Figure A2. Plot of pseudo-first order rate constant (k_{obs}) with respect to cysteine concentration. Each point is the average of three independent runs. Error bars represent the standard deviation of the data. The slope of the line is the overall second order rate constant for the reaction.

NMR Selectivity Data

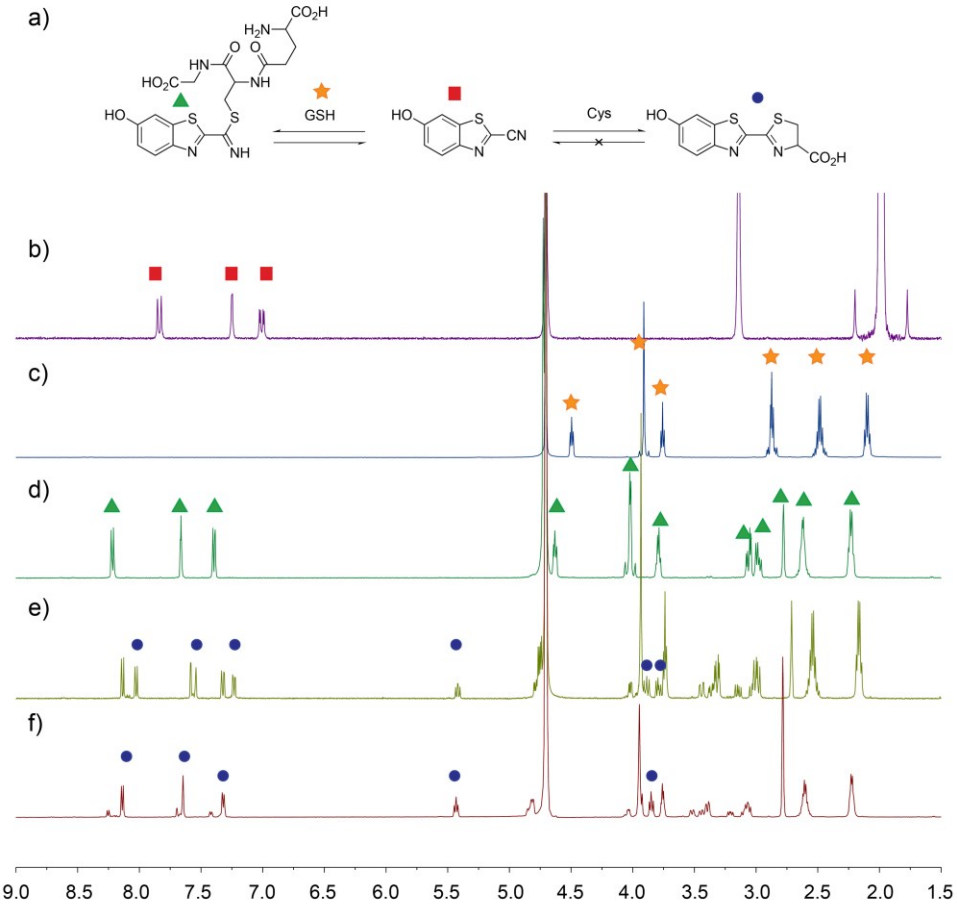

Figure A3. Selectivity of CBT-OH for Cys over GSH. (a) CBT-OH reacts reversibly with GSH and irreversibly with cysteine. ^{1}H NMR spectra (500 MHz, d_6-DMSO/D_2O mixture, room temperature) of (b) CBT-OH and (c) GSH; (d) after 1.5 hr; (e) after 7 hours with 1 equiv of cysteine; (f) after the addition of an additional equivalent of cysteine.

APPENDIX B:

SUPPORTING INFORMATION: CHEMILUMINESCENT DETECTION OF ENZYMATICALLY-PRODUCED HYDROGEN SULFIDE: SUBSTRATE HYDROGEN BONDING INFLUENCES SELECTIVITY FOR H_2S OVER BIOLOGICAL THIOLS

Selectivity Data

Table B1. Selectivity of CLSS-1 and CLSS-2 with 33 equiv. of selected biologically-relevant reactive sulfur, oxygen, and nitrogen species.

	Normalized Luminescence (CL/CL_0)	
Reactant	CLSS-1	CLSS-2
Blank	1.0 ± 0.1	1.0 ± 0.3
H_2S	128 ± 16	45 ± 3
Cys	81 ± 5	1.5 ± 0.03
GSH	94 ± 12	3.7 ± 0.9
Hcy	57 ± 3	3.3 ± 0.5
NAC	37 ± 19	3.3 ± 0.4
Toluenethiol (TolSH)	0.8 ± 0.1	1.9 ± 0.4
2-mercaptoethanol (2-ME)	6.6 ± 3.2	1.7 ± 0.08
$S_2O_3^{2-}$	5.9 ± 1.1	2.2 ± 0.6
SO_4^{2-}	0.8 ± 0.3	1.5 ± 0.3
NO_2^-	0.9 ± 0.2	3.2 ± 0.6
SNAP (NO)	0.05 ± 0.01	1.5 ± 0.5
$ONOO^-$	0.6 ± 0.2	4.0 ± 0.2
HNO	9.1 ± 0.2	3.3 ± 0.2

NMR Spectra

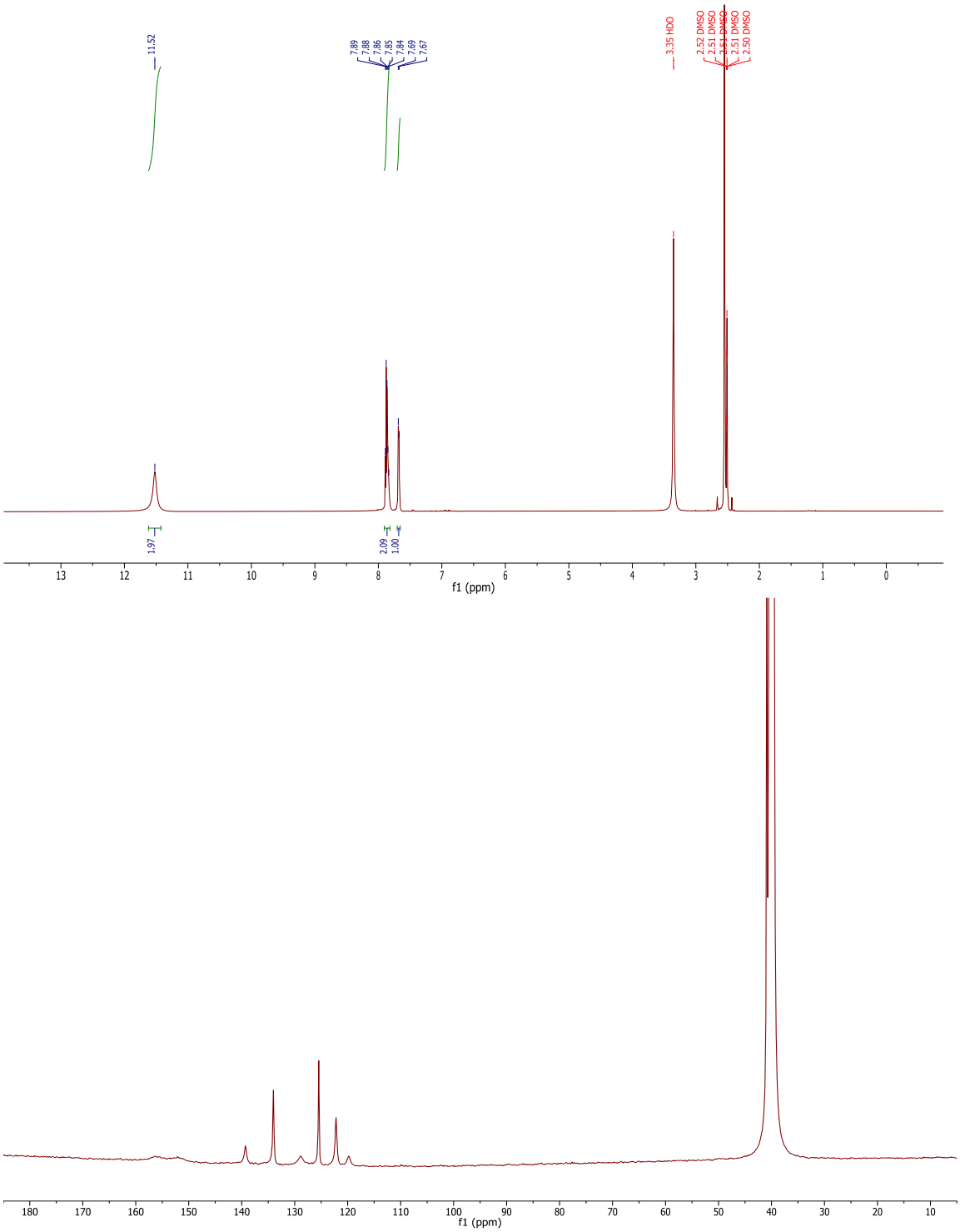

Figure B1. ^{1}H (600 MHz, DMSO) and $^{13}C\{^{1}H\}$ (150 MHz, DMSO) NMR spectra of CLSS-1.

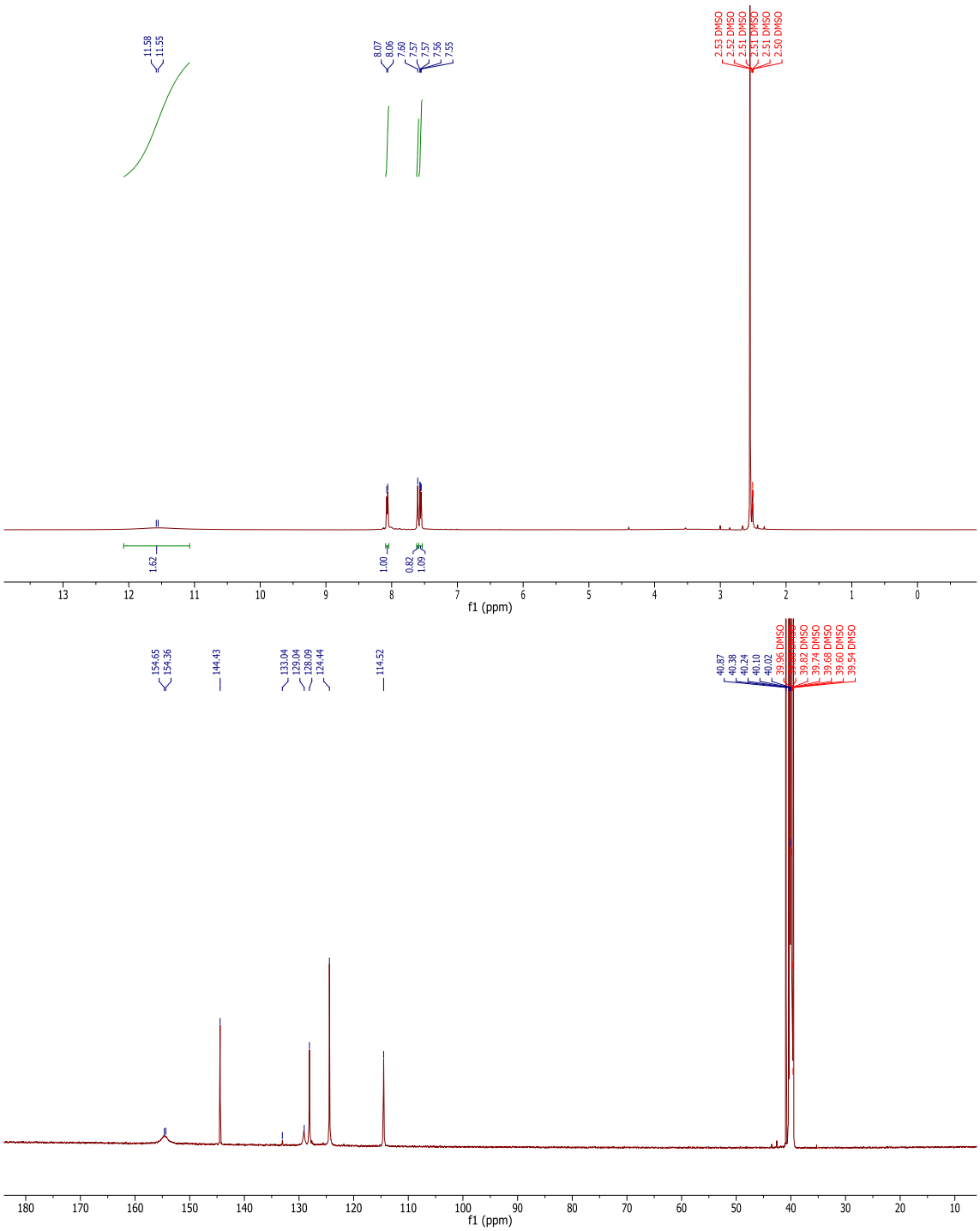

Figure B2. ^{1}H (600 MHz, DMSO) and $^{13}C\{^{1}H\}$ (150 MHz, DMSO) NMR spectra of CLSS-2.

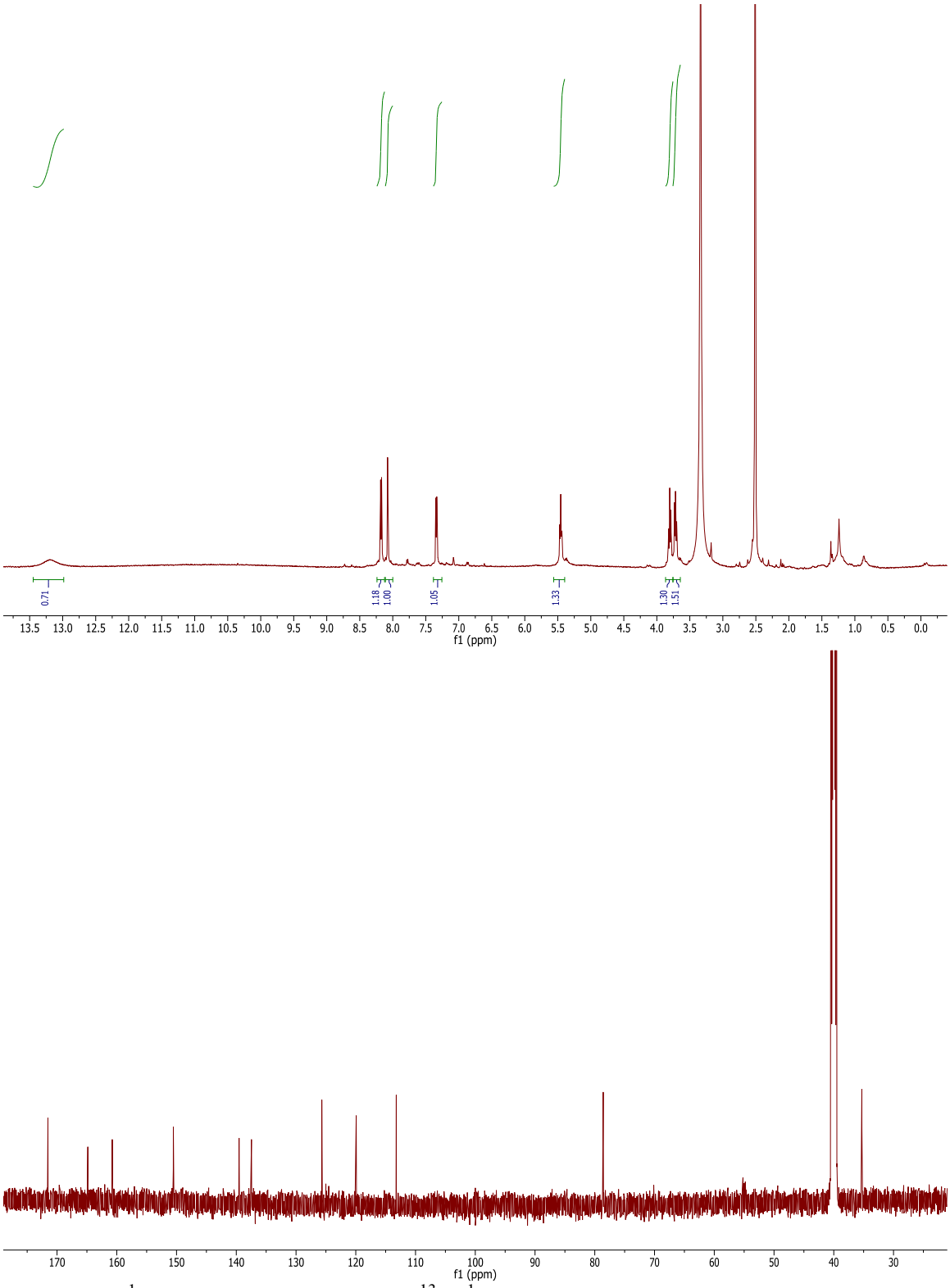

Figure B3. ^{1}H (600 MHz, DMSO) and $^{13}C\{^{1}H\}$ (150 MHz, DMSO) NMR spectra of CLSS-3.

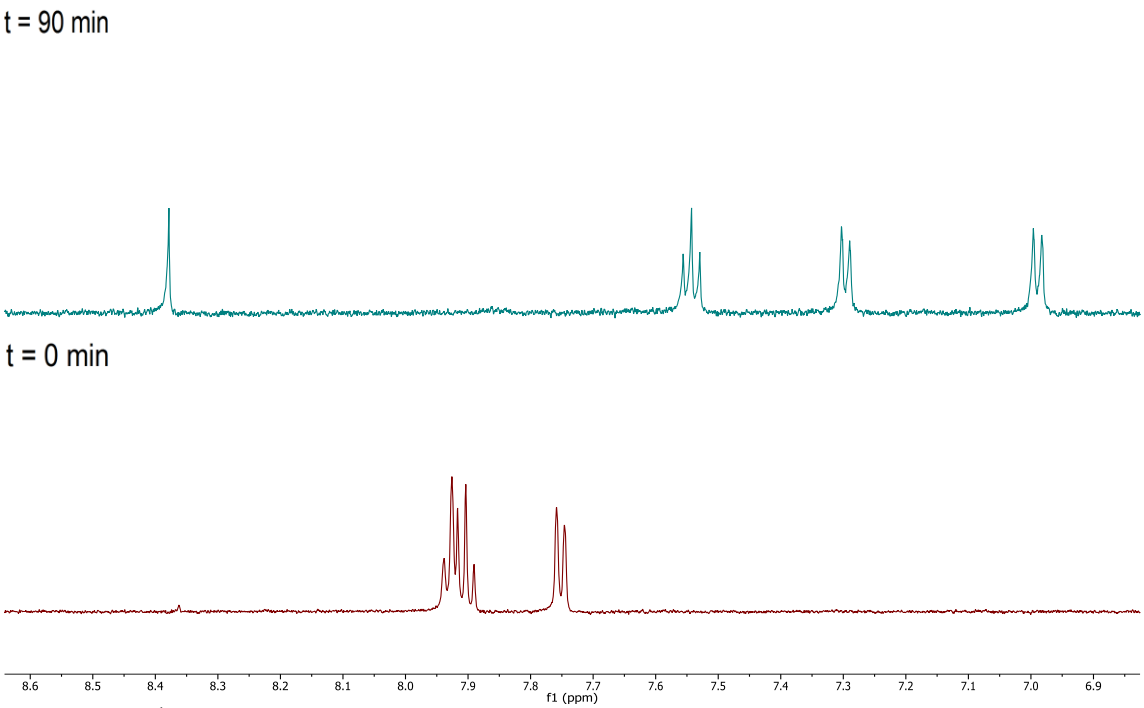

Figure B4. ^{1}H NMR spectra (600 MHz, 1% DMSO in D_2O) of CLSS-1 before (bottom) and 90 min after (top) reaction with H_2S showing clean conversion to the parent amine.

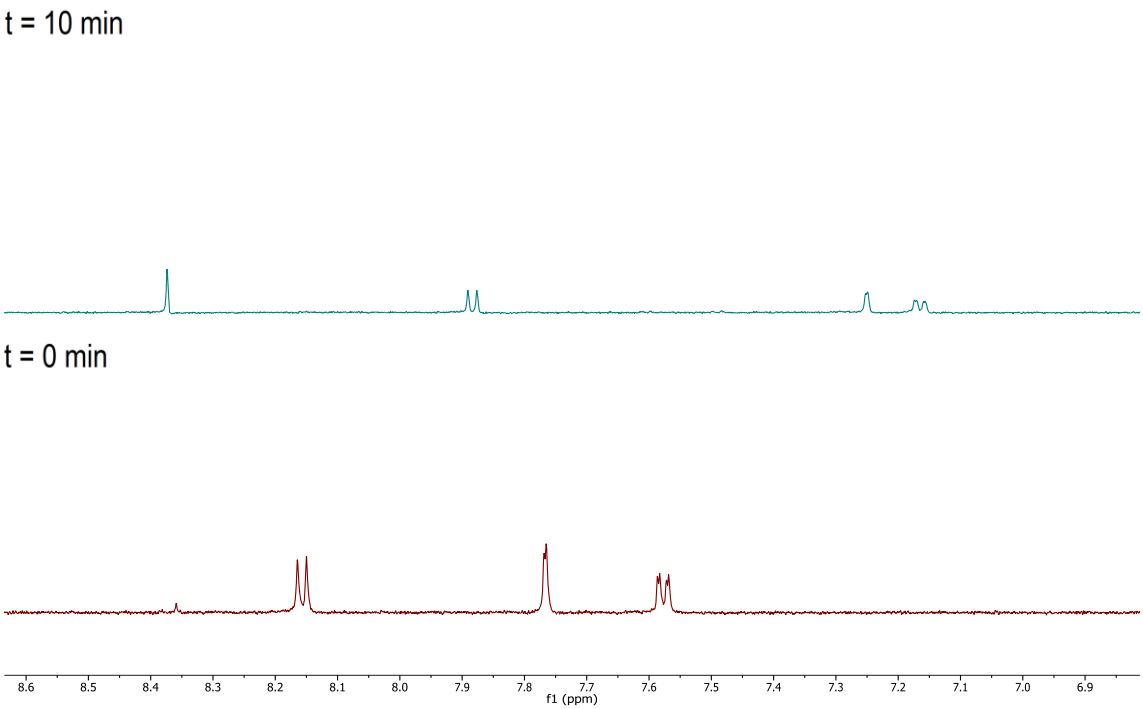

Figure B5. ^{1}H NMR spectra (600 MHz, 1% DMSO in D_2O) of CLSS-2 before (bottom) and 10 min after (top) reaction with H_2S showing clean conversion to the parent amine.

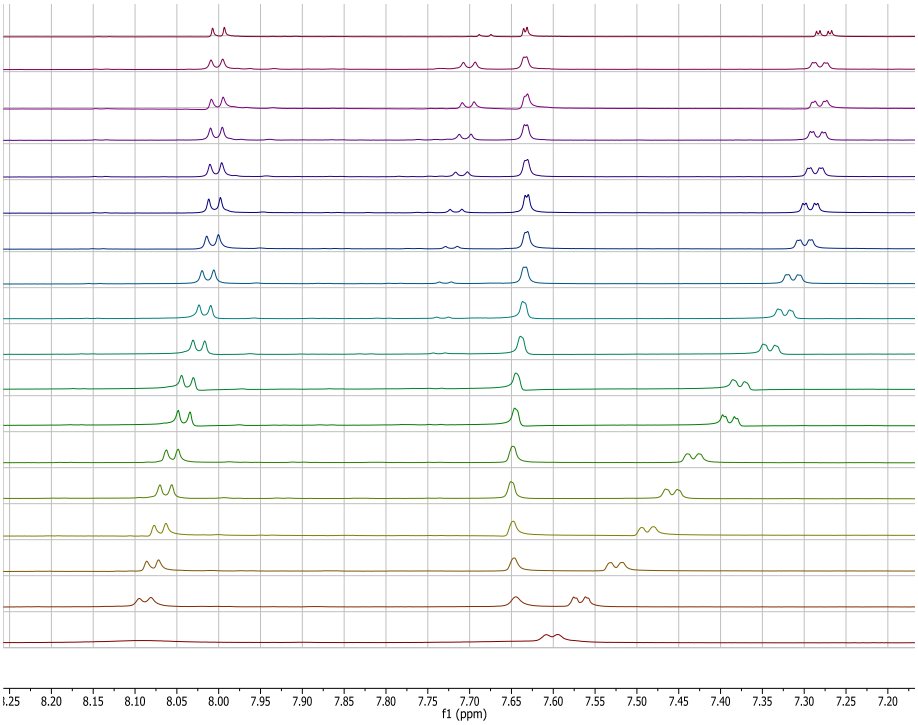

Figure B6. Representative titration of 10 mM CLSS-2 with 0-200 mM TBA-Ser.

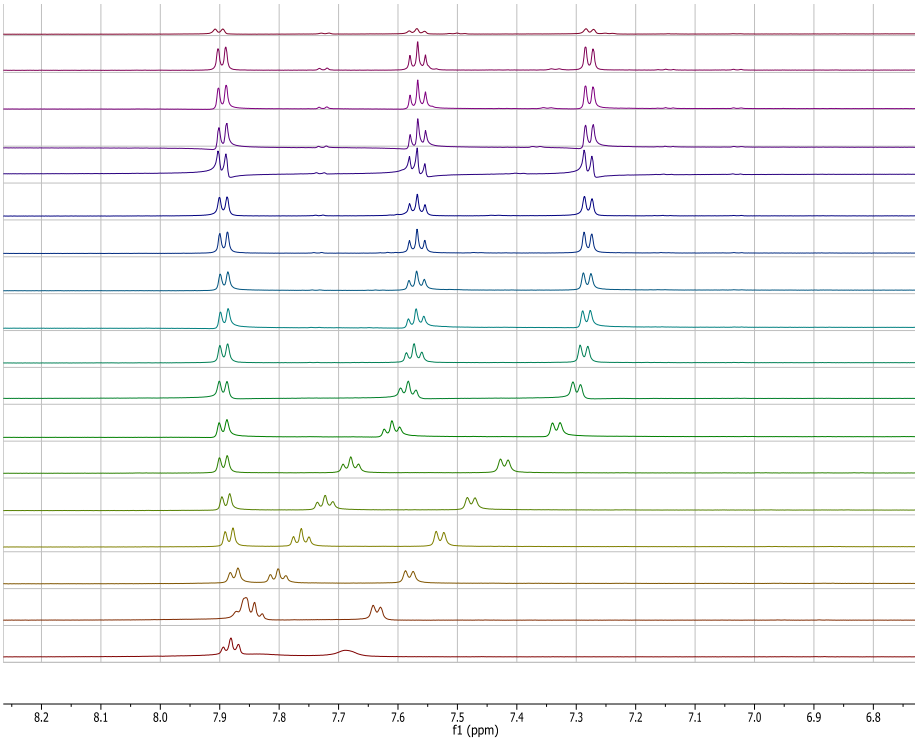

Figure B7. Representative titration of 10 mM CLSS-1 with 0-200 mM TBA-Val

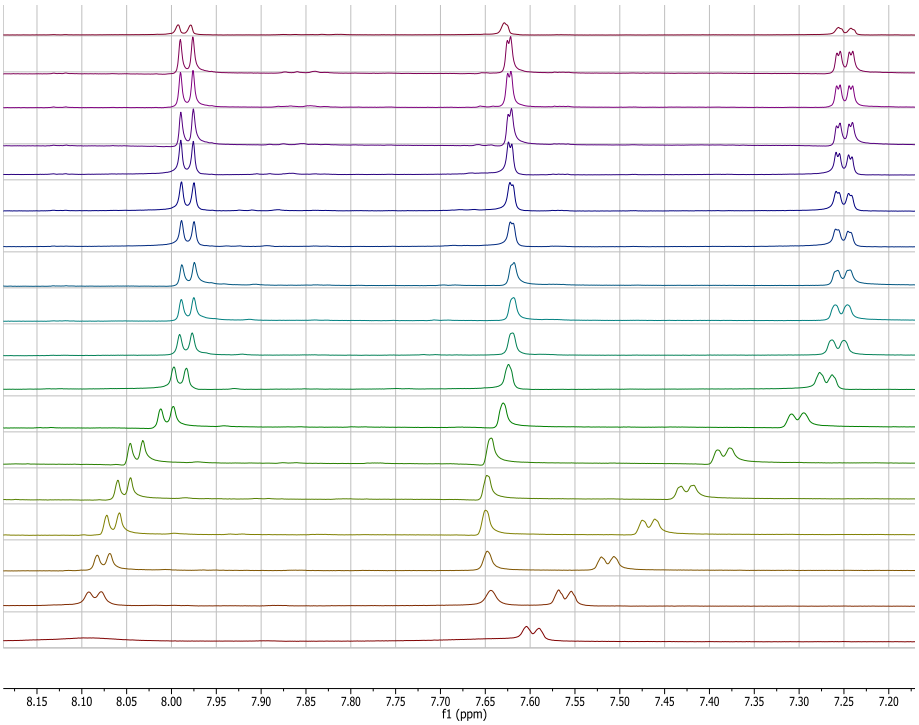

Figure B8. Representative titration of 10 mM CLSS-2 with 0-200 mM TBA-Val

Tabulated NMR Titration Data

Table B2. Tabulated titration data for CLSS-1 with TBA-Ser.

		Run 1		Run 2		Run 3	
[CLSS-1] (M)	[TBA-Ser] (M)	Proton 1 (ppm)	Proton 2 (ppm)	Proton 1 (ppm)	Proton 2 (ppm)	Proton 1 (ppm)	Proton 2 (ppm)
0.010091	0	7.883	7.687	7.881	7.685	7.898	7.694
0.010091	0.001353	7.847	7.643	7.841	7.636	7.84	7.634
0.010091	0.002688	7.818	7.602	7.805	7.587	7.803	7.583
0.010091	0.004006	7.789	7.563	7.775	7.548	7.772	7.542
0.010091	0.005307	7.766	7.533	7.751	7.514	7.748	7.51
0.010091	0.006591	7.746	7.507	7.731	7.485	7.727	7.482
0.010091	0.00973	7.707	7.457	7.691	7.437	7.69	7.434
0.010091	0.01277	7.681	7.423	7.667	7.405	7.665	7.403
0.010091	0.018575	7.649	7.383	7.636	7.367	7.636	7.366
0.010091	0.024038	7.633	7.361	7.621	7.348	7.62	7.346
0.010091	0.029189	7.622	7.348	7.612	7.335	7.611	7.335
0.010091	0.040865	7.607	7.329	7.602	7.318	7.598	7.319
0.010091	0.051081	7.6	7.32	7.591	7.31	7.591	7.31
0.010091	0.068108	7.593	7.311	7.586	7.303	7.585	7.302
0.010091	0.08173	7.589	7.307	7.584	7.299	7.583	7.298
0.010091	0.092874	7.587	7.303	7.582	7.297	7.581	7.296
0.010091	0.102162	7.587	7.302	7.58	7.296	7.579	7.294
0.010091	0.204324	7.579	7.287	7.576	7.288	7.577	7.287

Table B3. Tabulated titration data for CLSS-2 with TBA-Ser.

		Run 1		Run 2		Run 3	
[CLSS-2] (M)	[TBA-Ser] (M)	Proton 1 (ppm)	Proton 2 (ppm)	Proton 1 (ppm)	Proton 2 (ppm)	Proton 1 (ppm)	Proton 2 (ppm)
0.010091	0	7.598	8.094	7.599	8.109	7.601	8.093
0.010091	0.001339	7.577	8.088	7.568	8.087	7.567	8.088
0.010091	0.00266	7.542	8.082	7.515	8.074	7.525	8.077
0.010091	0.003964	7.509	8.075	7.47	8.063	7.487	8.07
0.010091	0.005252	7.482	8.069	7.438	8.054	7.458	8.063
0.010091	0.006522	7.455	8.061	7.416	8.048	7.432	8.056
0.010091	0.009628					7.389	8.042
0.010091	0.012636	7.383	8.039	7.354	8.026	7.377	8.036
0.010091	0.01838	7.35	8.027	7.326	8.016	7.341	8.024
0.010091	0.023786	7.33	8.021	7.313	8.011	7.323	8.018
0.010091	0.028883	7.321	8.016	7.304	8.006	7.313	8.014
0.010091	0.040437	7.304	8.009	7.294	8.004	7.299	8.007
0.010091	0.050546	7.297	8.008	7.288	8.003	7.292	8.005
0.010091	0.067395	7.291	8.004	7.283	7.999	7.286	8.004
0.010091	0.080874	7.287	8.003	7.28	7.999	7.2835	8.003
0.010091	0.091902			7.278	7.999	7.2815	8.002
0.010091	0.101092			7.277	7.998	7.28	8.002
0.010091	0.202184	7.275	7.999	7.276	7.998	7.275	8.001

Table B4. Tabulated titration data for CLSS-1 with TBA-Val

		Run 1		Run 2		Run 3	
[CLSS-1] (M)	[TBA-Val] (M)	Proton 1 (ppm)	Proton 2 (ppm)	Proton 1 (ppm)	Proton 2 (ppm)	Proton 1 (ppm)	Proton 2 (ppm)
0.010091	0	7.881	7.685	7.884	7.686	7.883	7.684
0.010091	0.001427	7.841	7.635	7.843	7.638	7.838	7.629
0.010091	0.002835	7.801	7.581	7.802	7.582	7.796	7.573
0.010091	0.004225	7.762	7.528	7.765	7.532	7.755	7.518
0.010091	0.005597	7.722	7.475	7.728	7.483	7.716	7.468
0.010091	0.006951	7.679	7.422	7.686	7.43	7.675	7.414
0.010091	0.01026	7.609	7.332	7.61	7.333	7.606	7.329
0.010091	0.013467	7.581	7.298	7.582	7.3	7.583	7.299
0.010091	0.019588	7.571	7.285	7.573	7.288	7.575	7.289
0.010091	0.025349	7.569	7.282	7.57	7.283	7.573	7.287
0.010091	0.030781	7.569	7.282	7.569	7.282	7.571	7.284
0.010091	0.043093	7.568	7.281	7.567	7.28	7.571	7.283
0.010091	0.053867	7.567	7.279	7.567	7.28	7.571	7.282
0.010091	0.071822	7.567	7.279	7.567	7.279	7.571	7.282
0.010091	0.086187	7.566	7.277	7.567	7.279	7.571	7.282
0.010091	0.097939	7.566	7.277	7.567	7.279	7.571	7.282
0.010091	0.107733	7.566	7.277	7.567	7.279		
0.010091	0.215466	7.566	7.277	7.567	7.279	7.568	7.277

Table B5. Tabulated titration data for CLSS-2 with TBA-Val.

		Run 1		Run 2		Run 3	
[CLSS-2] (M)	[TBA-Val] (M)	Proton 1 (ppm)	Proton 2 (ppm)	Proton 1 (ppm)	Proton 2 (ppm)	Proton 1 (ppm)	Proton 2 (ppm)
0.010152	0	8.101	7.598	8.103	7.6	8.092	7.597
0.010152	0.001367	8.088	7.563	8.088	7.564	8.084	7.559
0.010152	0.002715	8.079	7.519	8.082	7.521	8.075	7.513
0.010152	0.004046	8.067	7.476	8.067	7.476	8.066	7.467
0.010152	0.00536	8.058	7.433	8.056	7.433	8.053	7.424
0.010152	0.006657	8.04	7.382	8.04	7.386	8.039	7.382
0.010152	0.009827	8.005	7.298	8.005	7.304	8.003	7.3
0.010152	0.012897	7.993	7.271	7.991	7.269	7.99	7.268
0.010152	0.01876	7.986	7.258	7.983	7.256	7.984	7.256
0.010152	0.024277	7.986	7.257	7.982	7.254	7.981	7.252
0.010152	0.02948			7.982	7.252	7.981	7.252
0.010152	0.041271	7.985	7.253	7.982	7.252	7.981	7.251
0.010152	0.051589	7.985	7.253	7.982	7.252	7.981	7.251
0.010152	0.068786	7.985	7.253	7.982	7.252	7.981	7.25
0.010152	0.082543	7.985	7.252	7.982	7.25	7.981	7.249
0.010152	0.093799	7.984	7.252	7.982	7.25	7.981	7.249
0.010152	0.103178	7.984	7.252	7.982	7.25	7.981	7.248
0.010152	0.206357	7.984	7.252	7.982	7.25	7.981	7.248

MS Data

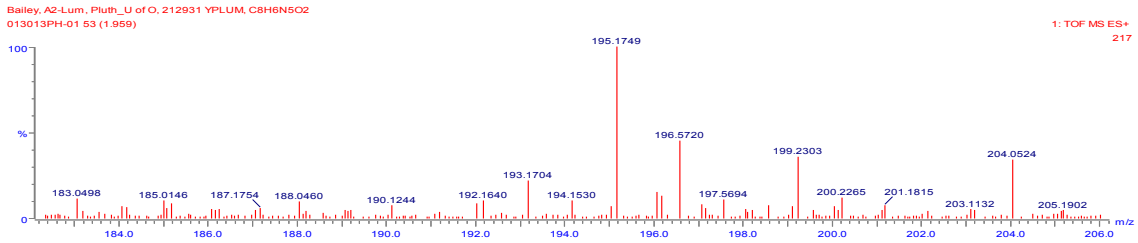

Figure B9. High resolution ESI mass spectrum of CLSS-1.

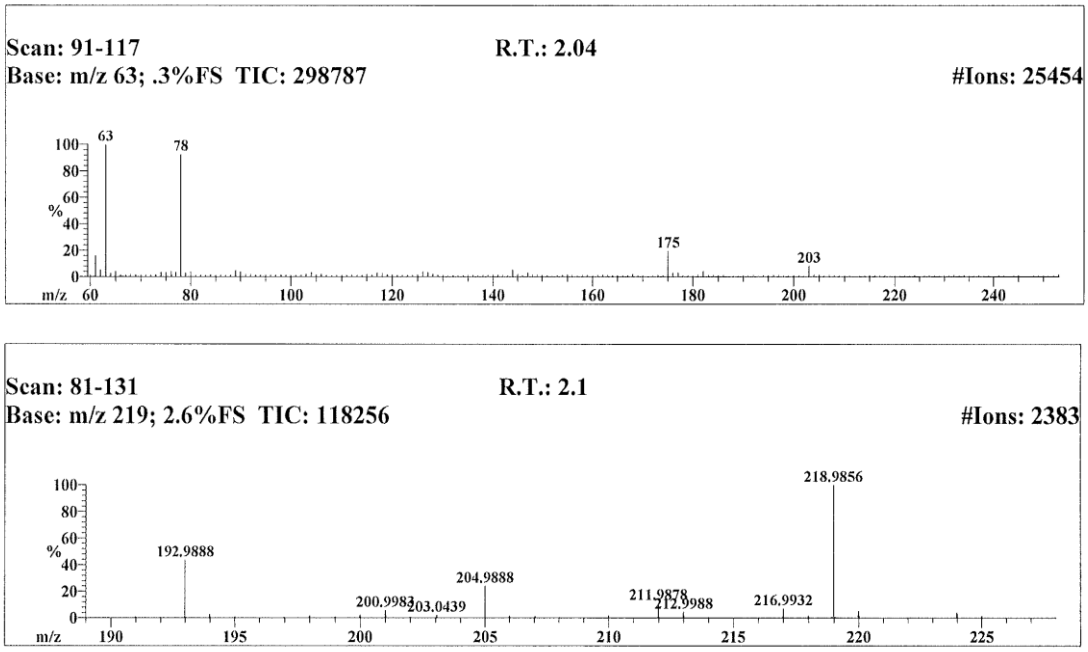

Figure B10. Low resolution (top) and high resolution (bottom) EI mass spectra of CLSS-2.

UV-Vis Data

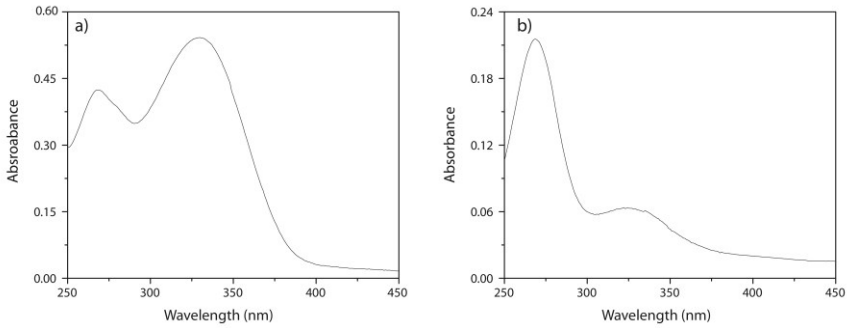

Figure B11. UV-Vis spectra of a) CLSS-1 and b) CLSS-2, measured at 33 μM in pH 7.4 PIPES buffer, 37 ^{o}C.

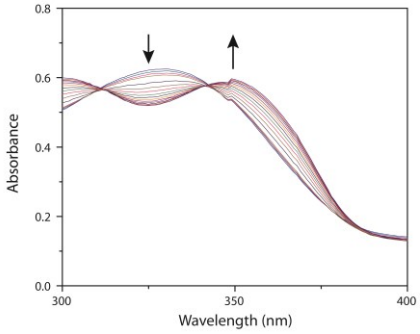

Figure B12. UV-Vis spectrum of CLSS-1 during the H_2S mediated reduction. pH 7.4 PIPES buffer, 37 ^{o}C, 1 hr.

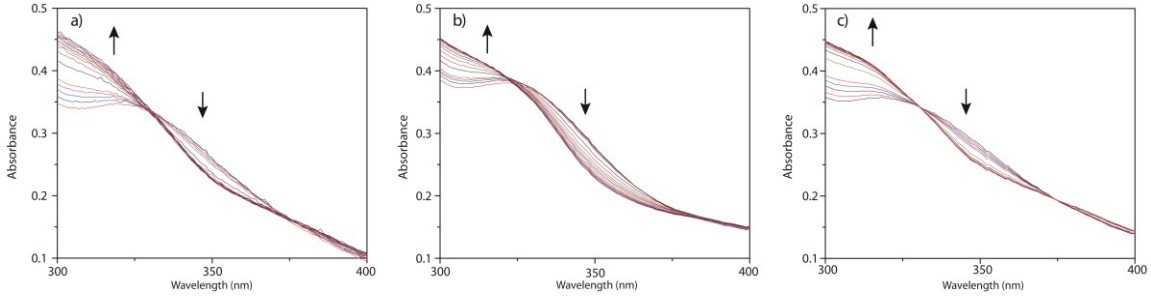

Figure B13. pH dependent H_2S reduction of CLSS-2. The spectra show 50 μM CLSS-2 being reduced by 33 equiv. H_2S in a) pH 7.0 PIPES buffer, b) pH 7.4 PIPES buffer, and c) pH 8.0 tris buffer at 37 ^{o}C over the course of 1 hr.

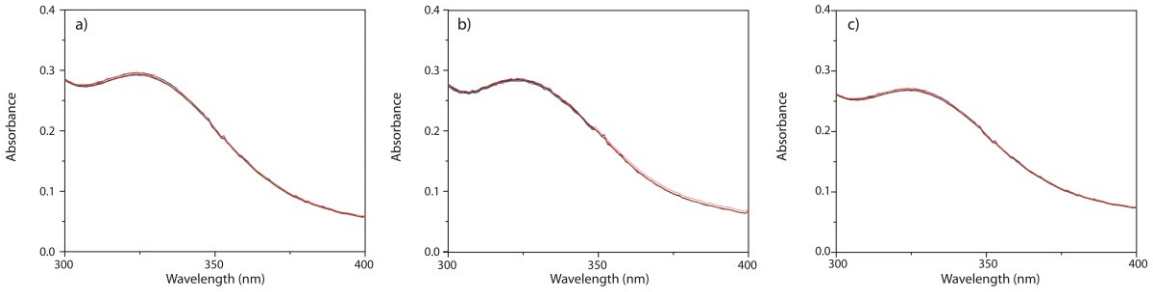

Figure B14. pH dependent reaction of CLSS-2 with cysteine. The spectra show 33 equiv. L-cysteine does not react with 50 μM CLSS-2 in a) pH 7.0 PIPES buffer, b) pH 7.4 PIPES buffer, or c) pH 8.0 tris buffer at 37 ^{o}C over the course of 1 hr.

DFT Calculations

Optimized Geometries

Cysteine
Calculated Enthalpy: -721.974543 Hartree
Zero Point Energy: 0.10770 Hartree
Lowest Frequency: 56.7 cm^{-1}
Coordinates:

Atom	x	y	z
N	-1.40186600	1.66348600	-0.05516900
H	-1.26669800	2.45430400	-0.67462700
H	-1.36440400	2.00878100	0.90013700
C	-0.40155600	0.61171400	-0.29509000
H	-0.17542600	0.61187900	-1.36607500
C	0.90929300	0.80374700	0.48509000
C	-1.07049000	-0.75149100	-0.02307600
H	1.20901600	1.84843300	0.39725000
H	0.76905600	0.58167500	1.54419900
S	2.36112600	-0.13352500	-0.14831200
O	-0.47125500	-1.79236500	0.13524000
H	1.84767900	-1.36334600	0.04928500
O	-2.40307200	-0.69553100	-0.00901300
H	-2.61303000	0.26961600	-0.10235800

Luminol Azide (CLSS-1)
Calculated Enthalpy: -732.08227 Hartree
Zero Point Energy: 0.13547 Hartree
Lowest Frequency: 46.9 cm^{-1}
Coordinates:

Atom	x	y	z
C	0.35420000	2.59415900	0.00000600
C	-0.94958100	2.12718700	0.00001000
C	-1.19372700	0.75023900	0.00001100
C	-0.13097600	-0.18091400	0.00001400
C	1.19421200	0.32610000	0.00000900
C	1.42412800	1.69793200	0.00000500
H	0.55441400	3.65852000	0.00000000
H	-1.79170500	2.80620000	0.00001000
C	-2.58692400	0.26986500	0.00000500
C	-0.48581700	-1.59696100	0.00001200
H	2.43954400	2.07592900	-0.00000300
N	-1.70674900	-2.02071800	-0.00002600
N	-2.70089900	-1.09157600	-0.00005600
O	0.44541300	-2.57594800	0.00005700
O	-3.58294300	0.99863700	0.00000900
N	2.24150100	-0.62726600	-0.00000200

N	3.41812500	-0.25101900	-0.00002900
N	4.52536000	-0.03613600	-0.00002200
H	-3.63363200	-1.48335400	-0.00006300
H	1.33715100	-2.17744700	0.00004400

Luminol Azide – Cysteine (CLSS-1/Cys; N_3-H bond)
Calculated Enthalpy: -1454.066548 Hartree
Zero Point Energy: 0.245206 Hartree
Lowest Frequency: 13.8 cm^{-1}
Coordinates:

Atom	x	y	z
C	-4.82580600	-1.01615500	-0.06144100
C	-4.46905700	0.31492900	-0.22493500
C	-3.12841600	0.68652200	-0.13186900
C	-2.11563200	-0.27016600	0.11832500
C	-2.49338200	-1.63274600	0.21334300
C	-3.84511300	-1.97873500	0.15276200
H	-5.86568900	-1.31430200	-0.11650700
H	-5.20975500	1.07887300	-0.41919800
C	-2.79734600	2.12191200	-0.31637500
C	-0.73649200	0.19832500	0.35807800
H	-4.10976500	-3.02349100	0.25587800
N	-0.50854100	1.51134000	0.18530100
H	0.44565700	1.89768200	0.35655700
N	-1.48252100	2.42213800	-0.16799500
H	-1.16477900	3.37506500	-0.28682400
O	0.19099500	-0.55070400	0.73566200
O	-3.62229300	2.99198400	-0.59906300
N	-1.62709800	-2.73515200	0.43264400
N	-0.57001900	-2.86411200	-0.18251700
N	0.40221800	-3.15526700	-0.67915400
O	2.00989700	2.42809800	0.61518400
C	3.07782800	2.06164000	0.04191800
C	3.59045600	0.63223600	0.39280500
O	3.77578200	2.69544000	-0.76240700
N	2.76301400	0.04554000	1.50053200
H	4.60862900	0.71764400	0.77393300
C	3.57125100	-0.27764400	-0.83616300
H	1.77059800	-0.13585500	1.19655300
H	2.57047800	-0.35285200	-1.26094900
H	4.22439900	0.16394600	-1.58540700
S	4.19957000	-1.98815900	-0.52702300
H	3.00104000	-2.58534500	-0.36769000
H	3.17105300	-0.83541200	1.82322800
H	2.72084600	0.69394200	2.28742200

Luminol Azide – Cysteine (CLSS-1/Cys; No N_3-H bond)
Calculated Enthalpy: -1454.063897 Hartree
Zero Point Energy: 0.245530 Hartree
Lowest Frequency: 12.1 cm^{-1}

Coordinates:

Atom	x	y	z
C	-5.07376700	0.63752700	0.13156500
C	-4.55917800	-0.64086400	0.29597300
C	-3.18394000	-0.84896000	0.19978800
C	-2.29330300	0.22250600	-0.05183000
C	-2.83238800	1.52994300	-0.14281400
C	-4.21599700	1.71095800	-0.08202400
H	-6.14195200	0.80820200	0.18671800
H	-5.20235100	-1.48818800	0.49201900
C	-2.68186400	-2.23365300	0.38533900
C	-0.87043100	-0.07764800	-0.30991800
H	-4.60361400	2.71678300	-0.18304000
N	-0.48652300	-1.35509000	-0.13818000
H	0.48669700	-1.64095300	-0.37472700
N	-1.34411800	-2.37716300	0.21339300
H	-0.90984700	-3.27961400	0.35558200
O	-0.04478600	0.77357700	-0.70589400
O	-3.39275100	-3.19365300	0.68629000
N	-2.10396400	2.72856300	-0.35491800
N	-1.06908800	2.97203900	0.26552800
N	-0.13819400	3.36548400	0.76971900
O	2.07572100	-2.03303600	-0.77541600
C	3.13406300	-1.52156300	-0.30650400
C	3.50964600	-0.11306000	-0.85852300
O	3.91355300	-2.01204700	0.52609900
N	2.43834500	0.32383500	-1.82700100
H	4.43157000	-0.20062700	-1.43556400
C	3.67570900	0.95511500	0.23059700
H	1.51890800	0.50866700	-1.34852400
H	3.66188300	1.95068600	-0.21608200
H	2.86261600	0.90049800	0.95526500
S	5.28746500	0.86520300	1.10619600
H	5.18099100	-0.44677400	1.41013200
H	2.71587600	1.15665800	-2.34896800
H	2.25938100	-0.43279400	-2.49025500

Luminol Azide Trimer [$(CLSS\text{-}1)_3$]
Calculated Enthalpy: -2196.276923 Hartree
Zero Point Energy: 0.409041 Hartree
Lowest Frequency: 13.0 cm^{-1}

Coordinates:

Atom	x	y	z
C	-4.77132500	5.00404100	-0.00159300
C	-4.55234100	3.63728300	-0.00073800
C	-3.24240000	3.15077600	0.00003700
C	-2.12368300	4.02287700	-0.00014000
C	-2.37605800	5.42230500	-0.00093100
C	-3.69282800	5.88611900	-0.00164700
H	-5.78016800	5.39827100	-0.00217600
H	-5.37187400	2.93168700	-0.00061200
C	-3.03206400	1.69801700	0.00117100
C	-0.80346500	3.39969500	0.00051700
H	-3.88267800	6.95287100	-0.00222200
N	-0.64085600	2.10985200	0.00176800
N	-1.74170300	1.30876500	0.00229900
O	0.28435400	4.17025800	-0.00025400
O	-3.95382600	0.85257500	0.00128300
N	-1.28169500	6.31096000	-0.00087500
N	-1.49523800	7.52391500	-0.00175000
N	-1.52826500	8.65512700	-0.00244400
H	1.12498800	3.63170800	0.00005200
H	-1.55452800	0.29716000	0.00277500
N	-1.50828400	-1.60987100	0.00232200
C	-2.54371600	-2.39587600	0.00069500
N	-0.26396000	-2.16219800	0.00313700
C	-2.42297000	-3.85056700	-0.00028800
O	-3.75514700	-1.83964000	-0.00015600
C	0.04449100	-3.47434100	0.00210800
H	0.51783600	-1.49354800	0.00353800
C	-1.10827800	-4.38311700	0.00039200
C	-3.50879600	-4.76854500	-0.00186200
H	-3.70918300	-0.84229100	0.00048300
O	1.23757800	-3.84974600	0.00272200
C	-0.87472700	-5.76082700	-0.00054500
C	-3.25220500	-6.14085100	-0.00276800
N	-4.82545100	-4.26437200	-0.00246100
C	-1.94897200	-6.63373000	-0.00213000
H	0.14604100	-6.11798300	0.00002300
H	-4.08076500	-6.83901700	-0.00396900
N	-5.76967800	-5.05522300	-0.00359200
H	-1.78596900	-7.70453600	-0.00286300

N	-6.73314600	-5.64887200	-0.00462000
N	2.14887000	-0.49979000	0.00243100
C	3.34716900	-1.00402100	0.00155100
N	2.00581100	0.85409800	0.00238200
C	4.54712700	-0.17255100	0.00064000
O	3.47012500	-2.33133100	0.00125000
C	2.98819800	1.77679600	0.00087900
H	1.03625100	1.19787500	0.00274700
C	4.35145500	1.23245200	-0.00016000
C	5.88515800	-0.65401900	0.00027200
H	2.58321700	-2.78961800	0.00175200
O	2.71657500	2.99770800	0.00060500
C	5.42791800	2.12337400	-0.00173600
C	6.94542700	0.25426900	-0.00143600
N	6.10689100	-2.04628500	0.00174900
C	6.72096000	1.62936000	-0.00250200
H	5.22696300	3.18599000	-0.00226800
H	7.96442000	-0.11422800	-0.00181400
N	7.26376400	-2.46872100	0.00162400
H	7.56693200	2.30577000	-0.00386200
N	8.25962400	-3.00627500	0.00175900

Isoluminol Azide (CLSS-2)
Calculated Enthalpy: -732.088312 Hartree
Zero Point Energy: 0.134688 Hartree
Lowest Frequency: 53.4 cm^{-1}

Coordinates:

Atom	x	y	z
C	1.57997700	-1.14733000	0.01396300
C	0.28900100	-1.64579800	0.02037300
C	-0.80958100	-0.77889300	0.01245400
C	-0.58917300	0.61055100	-0.00850200
C	0.70805900	1.11720100	-0.01408100
C	1.79314800	0.24252500	-0.00404900
H	2.41953900	-1.83217100	0.02249200
H	0.11419200	-2.71385400	0.03262200
C	-2.17792700	-1.33478700	0.00413200
C	-1.72990800	1.55877500	-0.00482900
N	-2.95568900	0.96964200	-0.04195100
H	-3.77769900	1.54299200	0.09549900
N	-3.17126800	-0.40192600	0.04364700
H	-4.12650300	-0.69653400	-0.11191400
O	-1.61623700	2.78450000	0.02155100
O	-2.44451200	-2.53746100	-0.02656900

H	0.86782400	2.18712900	-0.02686600
N	3.07179100	0.84223700	-0.01260500
N	4.07229400	0.11824000	-0.00380800
N	5.06959300	-0.41352600	0.00207900

Isoluminol Azide – Cysteine (CLSS-2 /Cys)
Calculated Enthalpy: -1454.075989 Hartree
Zero Point Energy: 0.245238 Hartree
Lowest Frequency: 21.8 cm^{-1}

Coordinates:

Atom	x	y	z
C	-4.42835800	0.60307700	-0.30380400
C	-3.64173800	1.73866800	-0.33998100
C	-2.25921100	1.65031900	-0.13073600
C	-1.68010100	0.39310500	0.11626400
C	-2.47027500	-0.75648500	0.15369200
C	-3.84378100	-0.65150200	-0.05650800
H	-5.49762300	0.66256900	-0.46377600
H	-4.08292800	2.70860700	-0.52962900
C	-1.42999200	2.87014500	-0.17306300
C	-0.22660900	0.27602300	0.34696900
N	0.47208300	1.41995700	0.28725700
H	1.50376300	1.41831900	0.44577600
N	-0.10264100	2.65394200	0.04607400
H	0.54208200	3.43282300	0.02602600
O	0.33711500	-0.81536600	0.58571300
O	-1.86051600	4.00579100	-0.38471600
O	3.14288500	1.36518800	0.75404300
C	4.09748300	0.64538900	0.33720000
C	4.06106900	-0.85328200	0.75506900
O	5.08012300	0.98702600	-0.33541600
N	2.86427500	-1.11141900	1.63323400
H	4.93526300	-1.03729100	1.38449500
C	4.12843900	-1.82980200	-0.41757300
H	1.94030800	-0.98466500	1.14195900
H	5.10349400	-1.70493800	-0.88529700
H	4.05762100	-2.86178600	-0.07174000
S	2.93162000	-1.56305200	-1.79257700
H	1.80725900	-1.93088200	-1.14521200
H	2.88912700	-2.04948900	2.03701400
H	2.86257600	-0.43719500	2.40050700
N	-4.73157200	-1.75024200	-0.03911000
N	-4.27613300	-2.87729400	0.17976900
N	-3.99922600	-3.95687700	0.36588300

H	-1.99278200	-1.70876300	0.34718400

Isoluminol Azide Trimer [$(CLSS\text{-}2)_3$]
Calculated Enthalpy: -2196.305164 Hartree
Zero Point Energy: 0.409167 Hartree
Lowest Frequency: 10.2 cm^{-1}

Coordinates:

Atom	x	y	z
C	5.19845400	-4.53825300	-0.10318600
C	3.82601600	-4.41709500	-0.03570600
C	3.23091800	-3.14851500	0.03279900
C	4.04797500	-1.99765300	0.03312100
C	5.44106400	-2.11957500	-0.03509900
C	6.01127900	-3.38723800	-0.10494000
H	5.66939900	-5.51170900	-0.15743900
H	3.19372000	-5.29543500	-0.03613000
C	1.77860200	-2.99503600	0.09525300
C	3.39293500	-0.70193800	0.09833800
N	2.10424300	-0.57884500	0.15667300
N	1.34686600	-1.71307400	0.16074000
O	4.16663200	0.38683100	0.09241900
O	0.95793400	-3.94039600	0.09026700
H	3.63390300	1.23139100	0.11854400
H	0.33020600	-1.55766100	0.18207800
N	-1.55367500	-1.53194700	0.13829100
C	-2.30437000	-2.58698300	0.08686500
N	-2.15784900	-0.30935800	0.14299500
C	-3.75449800	-2.50726100	0.03237100
O	-1.74773100	-3.80107800	0.07915200
C	-3.48437900	-0.04289900	0.08515700
H	-1.51465600	0.49326500	0.16379500
C	-4.34339500	-1.22446500	0.03339600
C	-4.55671900	-3.65328300	-0.02551900
H	-0.74953200	-3.76152600	0.09538000
O	-3.89288800	1.14046200	0.07860500
C	-5.74017600	-1.10651400	-0.02263700
C	-5.94020400	-3.51419000	-0.08351800
C	-6.53137900	-2.23512800	-0.07943600
H	-6.18531100	-0.12002100	-0.02146700
H	-7.61039500	-2.15695200	-0.12375900
N	-0.54903100	2.11107600	0.13372000
C	-1.08731200	3.28828600	0.07238700
N	0.81170500	2.02394600	0.16236900
C	-0.29319800	4.50462200	0.02734500

O	-2.41678700	3.41279000	0.04520100
C	1.70585600	3.04018500	0.11699700
H	1.18600600	1.06608100	0.18778300
C	1.11187200	4.37438400	0.05295700
C	-0.88457200	5.77168000	-0.04428600
H	-2.88238100	2.52912900	0.06813400
O	2.93505300	2.80322600	0.13021900
C	1.91226200	5.52570500	0.00883400
C	-0.07253100	6.90095200	-0.09092600
C	1.33050500	6.77459500	-0.06107800
H	2.98905300	5.41895600	0.02919600
H	1.93770900	7.67036700	-0.09660000
N	7.40127400	-3.62617500	-0.18225200
N	8.17177800	-2.66082400	-0.20022800
N	8.98742800	-1.87940300	-0.22545200
N	-6.84152900	-4.59970200	-0.15097700
N	-6.38827900	-5.74866300	-0.17097000
N	-6.11661000	-6.84506100	-0.19644200
H	6.05012000	-1.22507800	-0.03436400
H	-4.08617300	-4.62781900	-0.02769300
N	-0.56147100	8.22378800	-0.17063900
N	-1.78239800	8.40574200	-0.21765100
N	-2.86669800	8.71937100	-0.26744700
H	-1.96372900	5.85025100	-0.06400800

APPENDIX C

SUPPLEMENTAL INFORMATION: REACTIONS OF ISOLATED PERSULFIDES PROVIDE INSIGHTS INTO THE INTERPLAY OF H_2S AND PERSULFIDE REACTIVITY

NMR Spectra

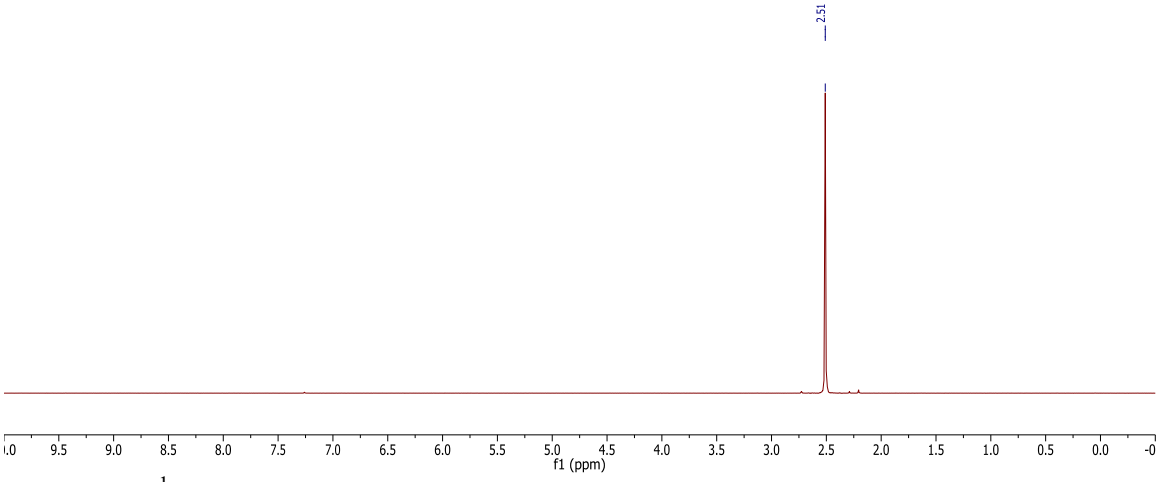

Figure C1: ^{1}H (600 MHz, $CDCl_3$) NMR spectrum of diacetylsulfide (**2**).

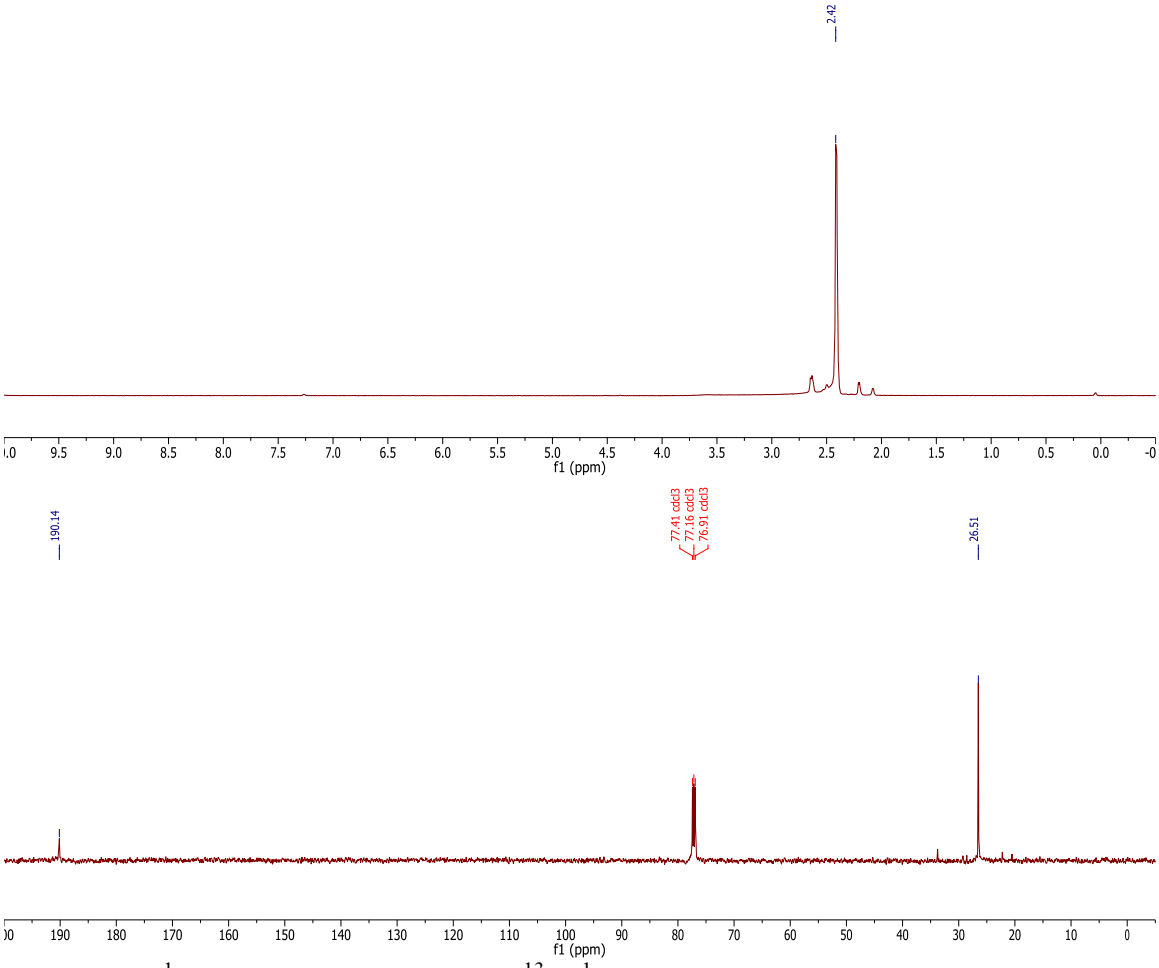

Figure C2: ^{1}H (600 MHz, $CDCl_3$) and $^{13}C\{^{1}H\}$ NMR spectra of acetyl sulfenylchloride (**3**).

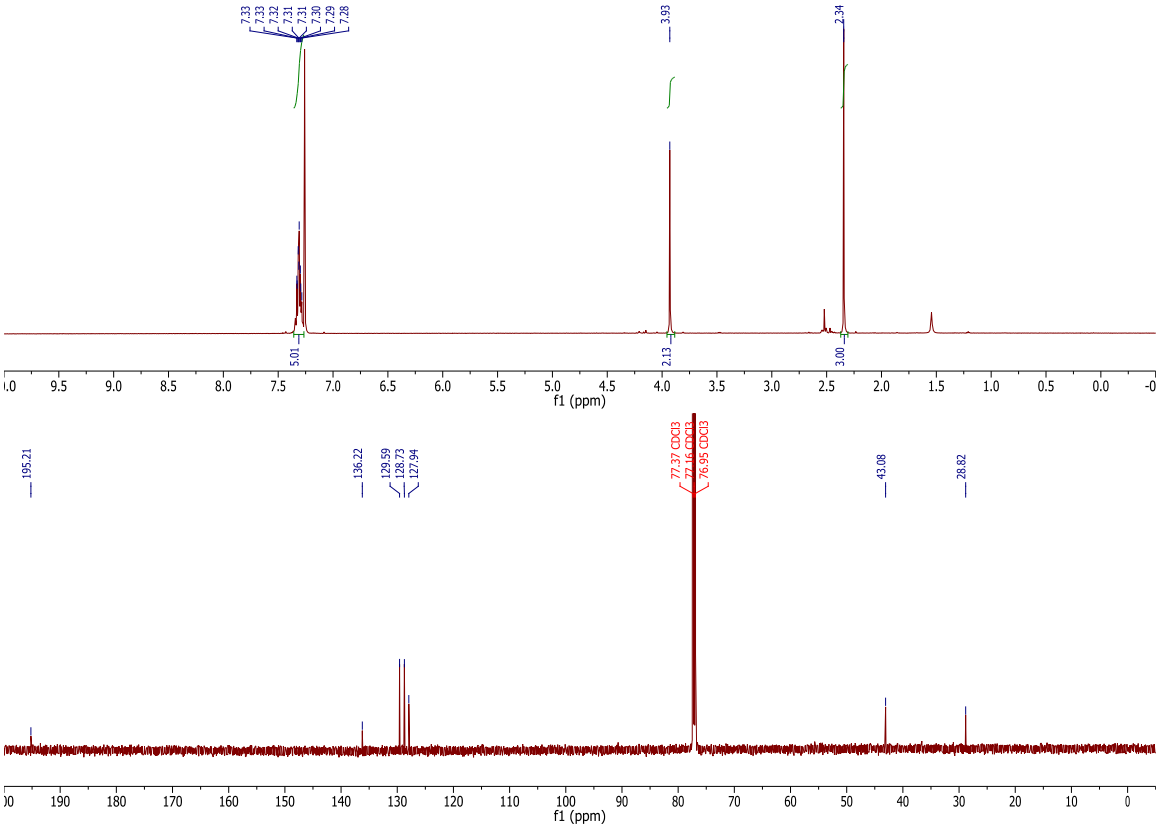

Figure C3. ^{1}H (600 MHz, $CDCl_3$) and $^{13}C\{^{1}H\}$ (150 MHz, $CDCl_3$) NMR spectra of benzylacetyldisulfide (**4a**).

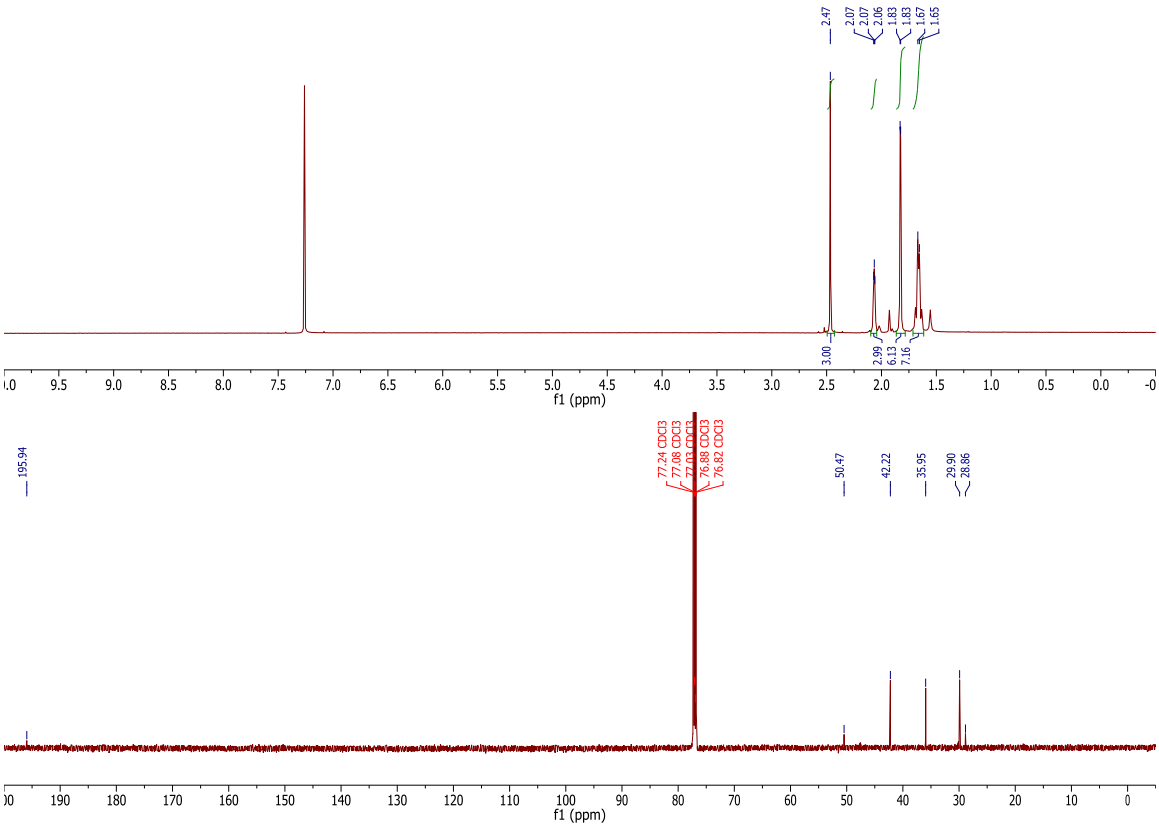

Figure C4. ^{1}H (600 MHz, $CDCl_3$) and $^{13}C\{^{1}H\}$ (150 MHz, $CDCl_3$) NMR spectra of adamantylacetyldisulfide (**4b**).

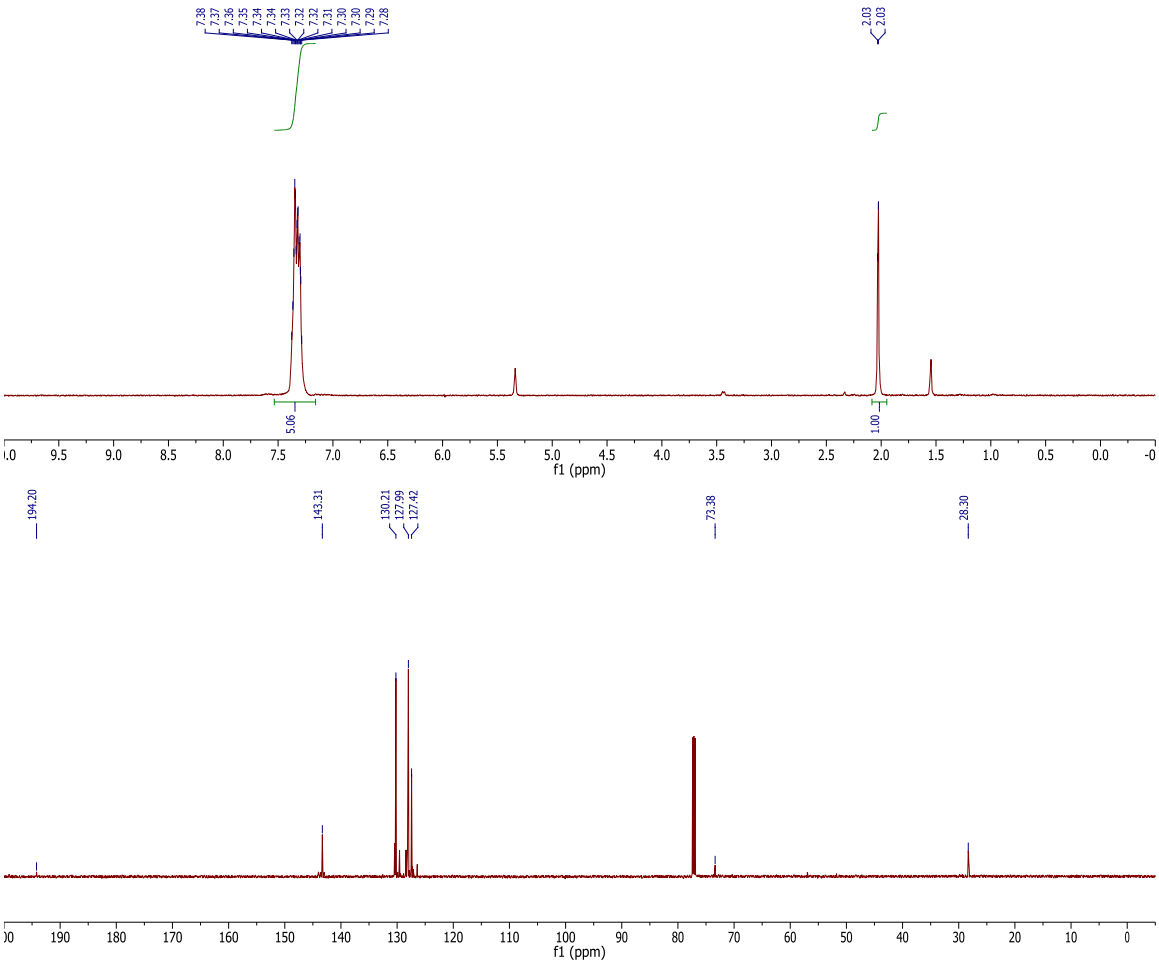

Figure C5: ^{1}H (600 MHz, CD_2Cl_2) and $^{13}C\{^{1}H\}$ (150 MHz, $CDCl_3$) NMR spectra of tritylacetyldisulfide (**4c**).

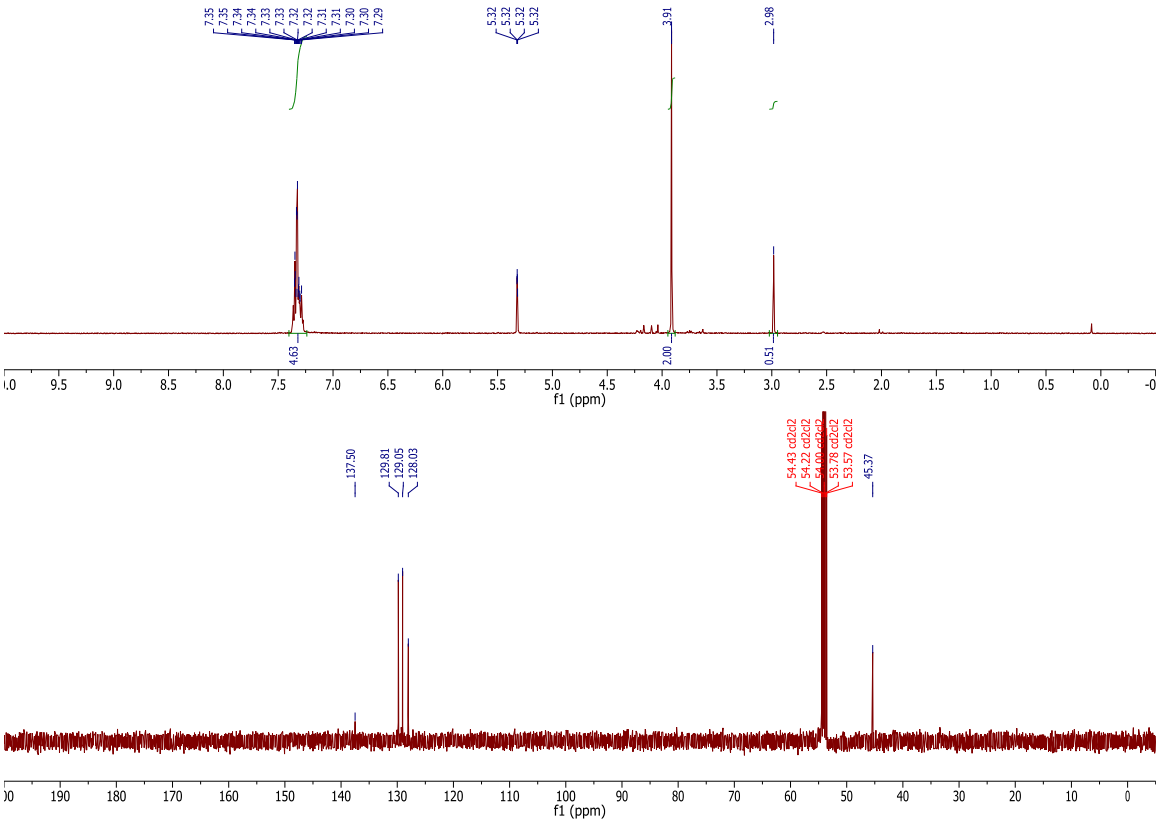

Figure C6. ^{1}H (600 MHz, CD_2Cl_2) and $^{13}C\{^{1}H\}$ (150 MHz CD_2Cl_2) NMR spectra of benzylhydrodisulfide (**BnSSH**). δ (SS-H): 2.96 ppm.

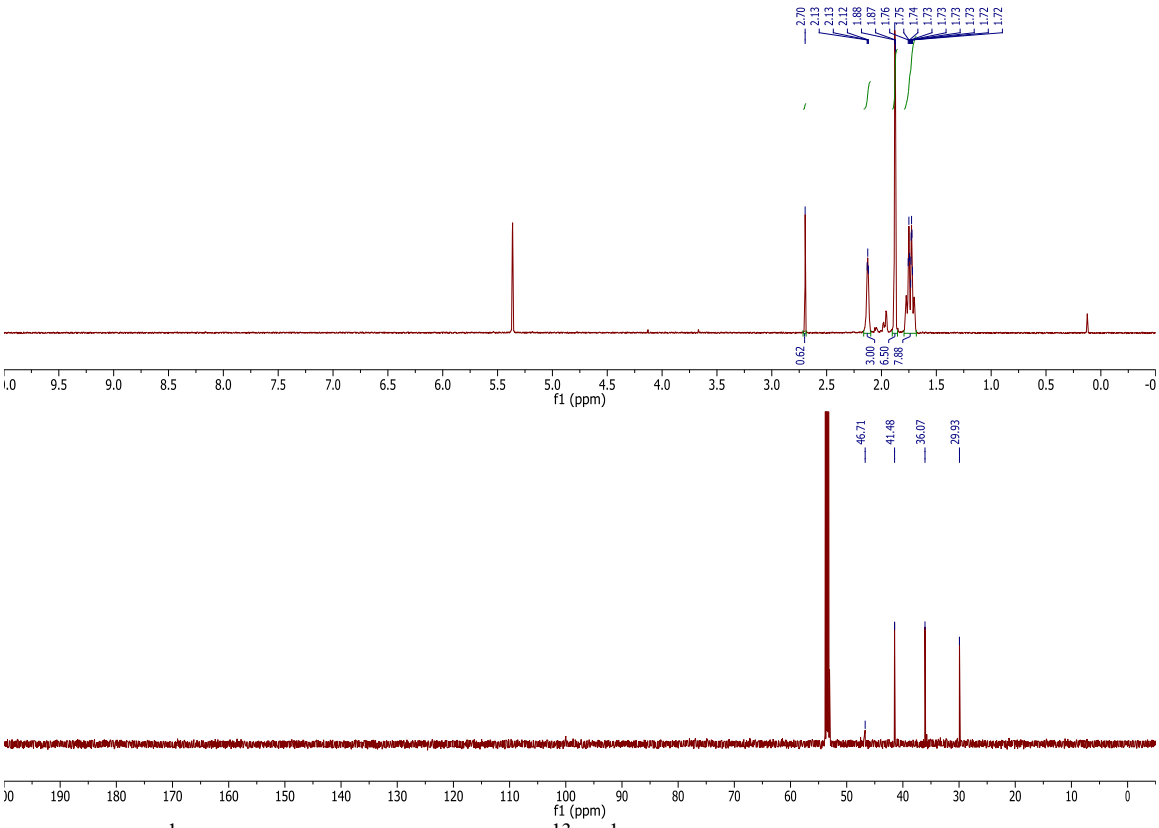

Figure C7. ^{1}H (600 MHz, CD_2Cl_2) and $^{13}C\{^{1}H\}$ (150 MHz CD_2Cl_2) NMR spectra of adamantylhydrodisulfide (**AdSSH**). δ (SS-H): 2.70 ppm.

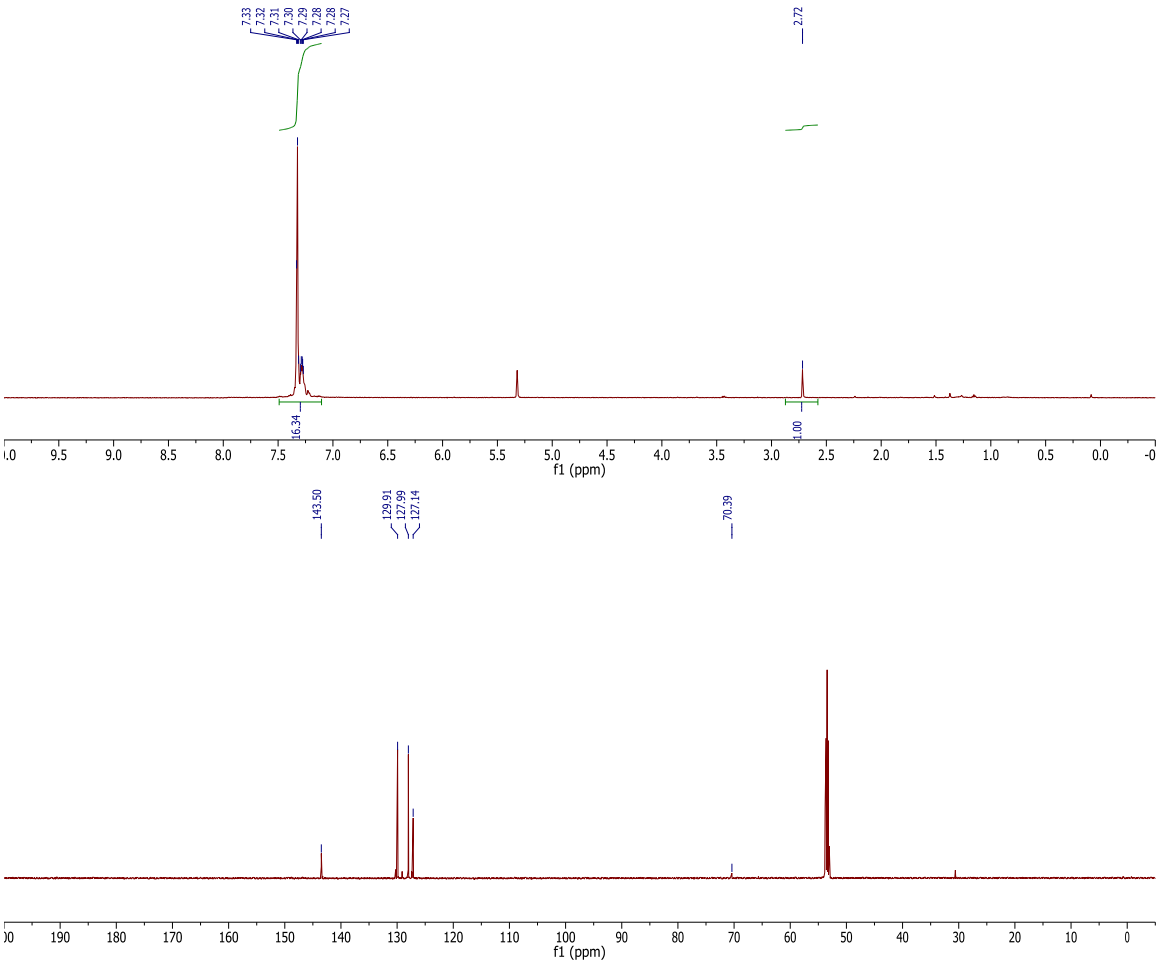

Figure C8: ^{1}H (600 MHz, CD_2Cl_2) and $^{13}C\{^{1}H\}$ NMR spectra of tritylhydrodisulfide (**TrtSSH**). δ (SS-H): 2.72 ppm.

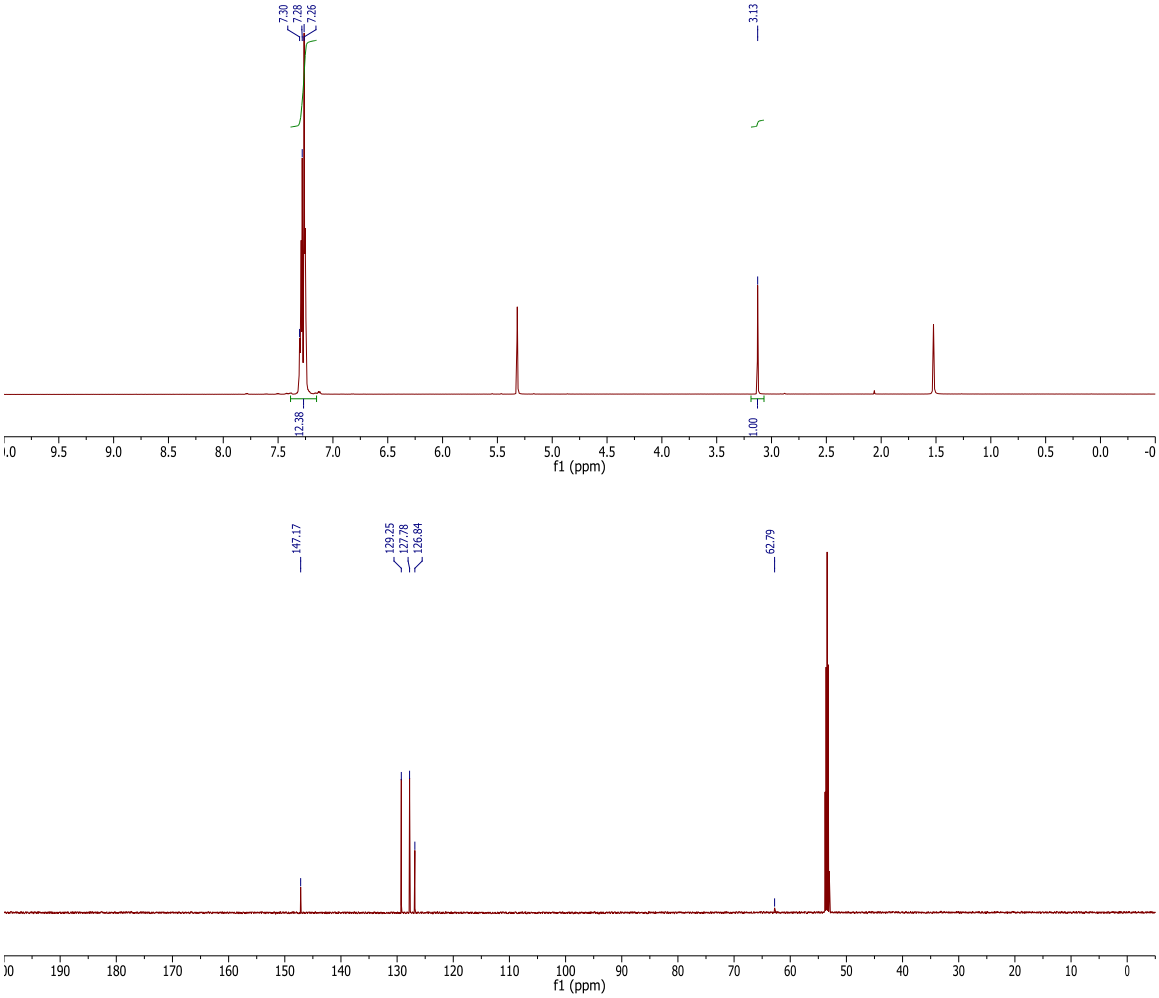

Figure C9: ^{1}H (600 MHz, CD_2Cl_2) and $^{13}C\{^{1}H\}$ NMR spectra of tritylthiol (**TrtSH**). δ (S-H): 3.13 ppm.

NMR Spectra of TrtSSH Reactivity Experiments

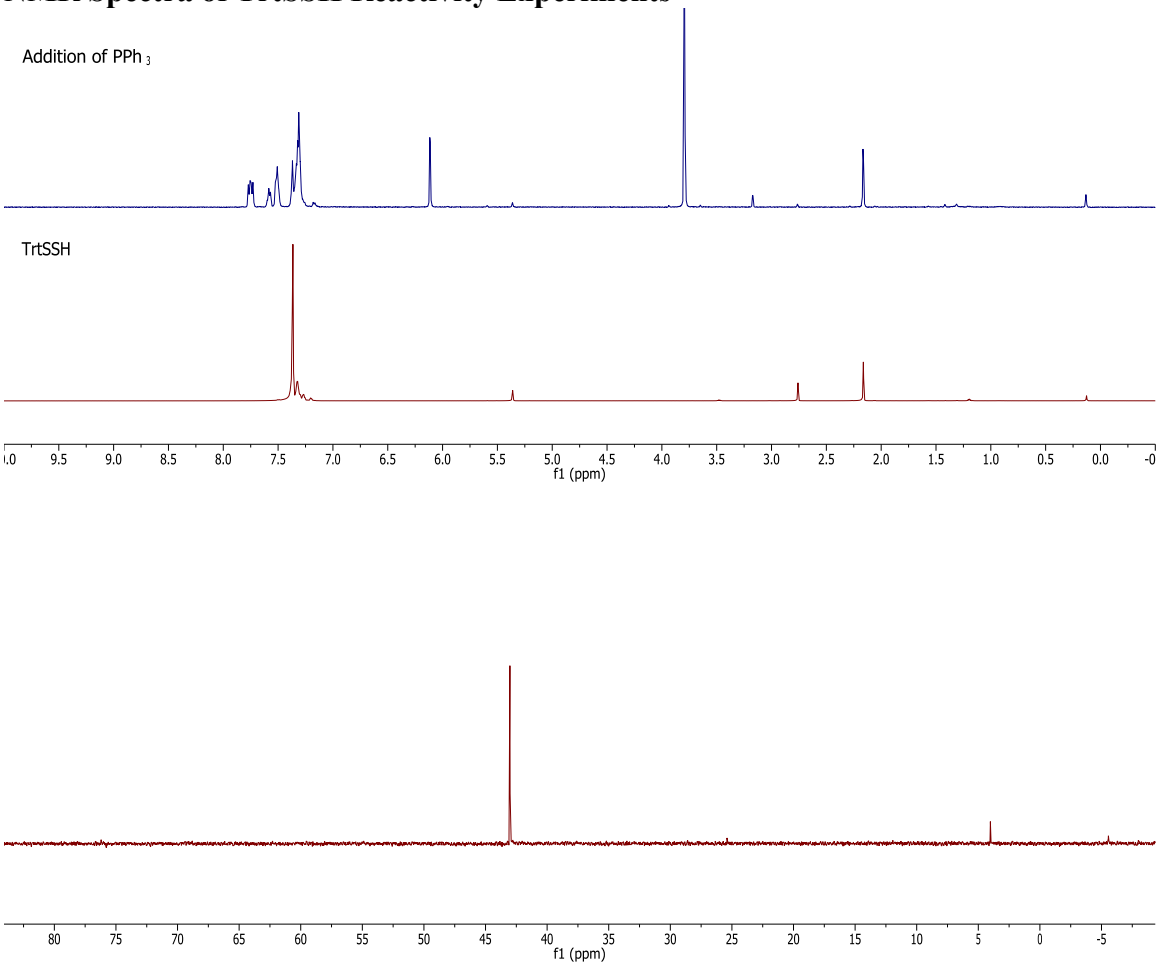

Figure C10: ^{1}H (500 MHz, CD_2Cl_2, top) and $^{31}P\{^{1}H\}$ (202 MHz, CD_2Cl_2, bottom) NMR spectra of TrtSSH upon addition of PPh_3. The ^{1}H NMR spectrum contains 1,3,5-trimethoxybenzene as an internal standard, which was used to quantify H_2S liberated. A minor acetone impurity is present at 2.1 ppm. Ph_3PO was added as an internal standard prior to acquisition of the $^{31}P\{^{1}H\}$ NMR spectrum. Ph_3PS is observed at 43 ppm in the $^{31}P\{^{1}H\}$ NMR spectrum.

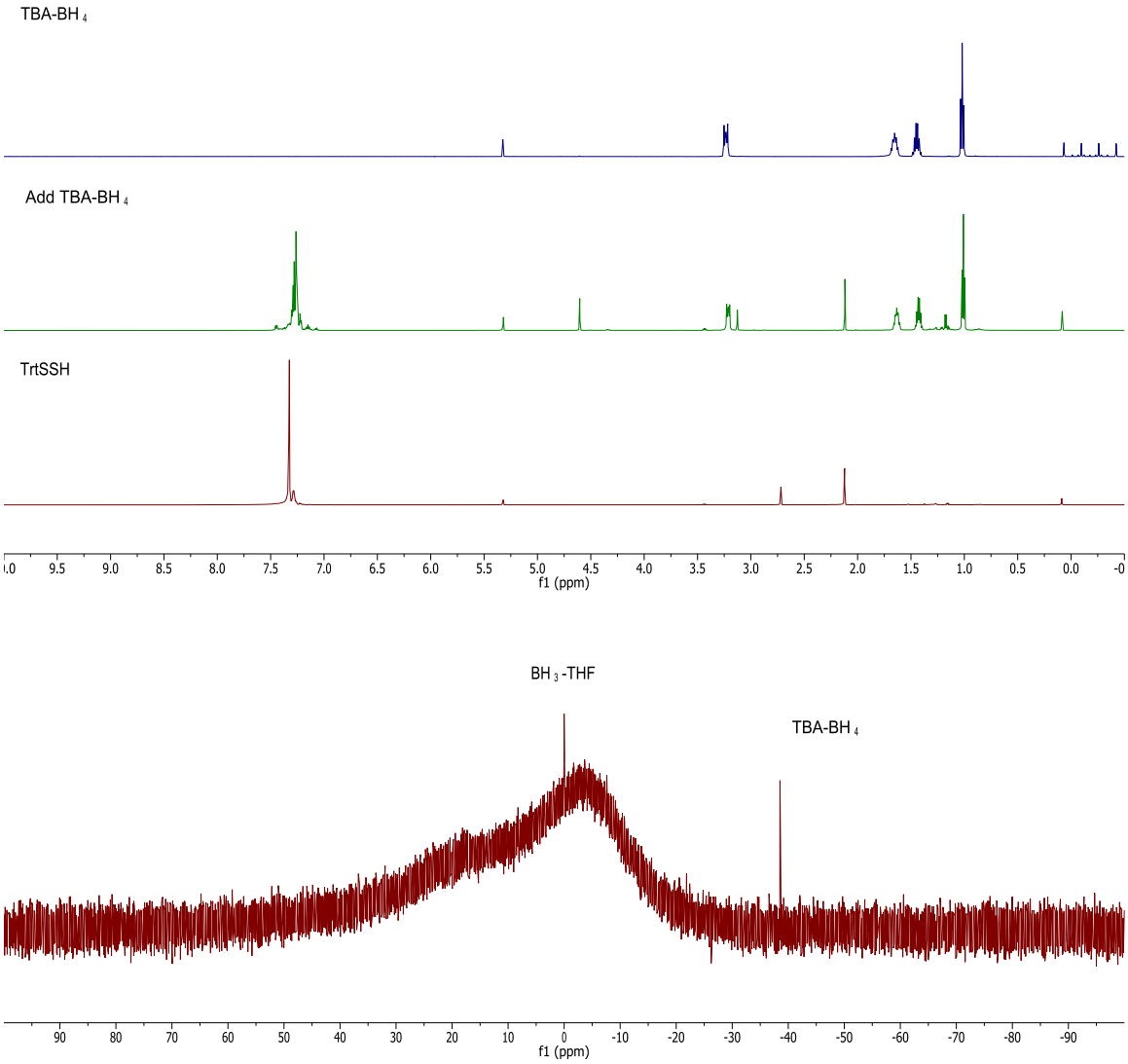

Figure C11: ^{1}H (500 MHz, CD_2Cl_2, top) and $^{11}B\{^{1}H\}$ (160 MHz, CD_2Cl_2, bottom) NMR spectra of TrtSSH upon addition of $[NBu_4^+][BH_4^-]$. The ^{1}H NMR spectrum contains a minor acetone impurity at 2.1 ppm. THF was added to the NMR sample prior to acquisition of the $^{11}B\{^{1}H\}$ NMR spectrum to complex any reduced BH_3 as BH_3THF. The ^{1}H NMR resonance at 4.53 ppm corresponding to liberated HS^- matched the resonance of HS^- generated from $[NBu_4][BH_4]$ reduction of S_8 in CD_2Cl_2 under anaerobic conditions.

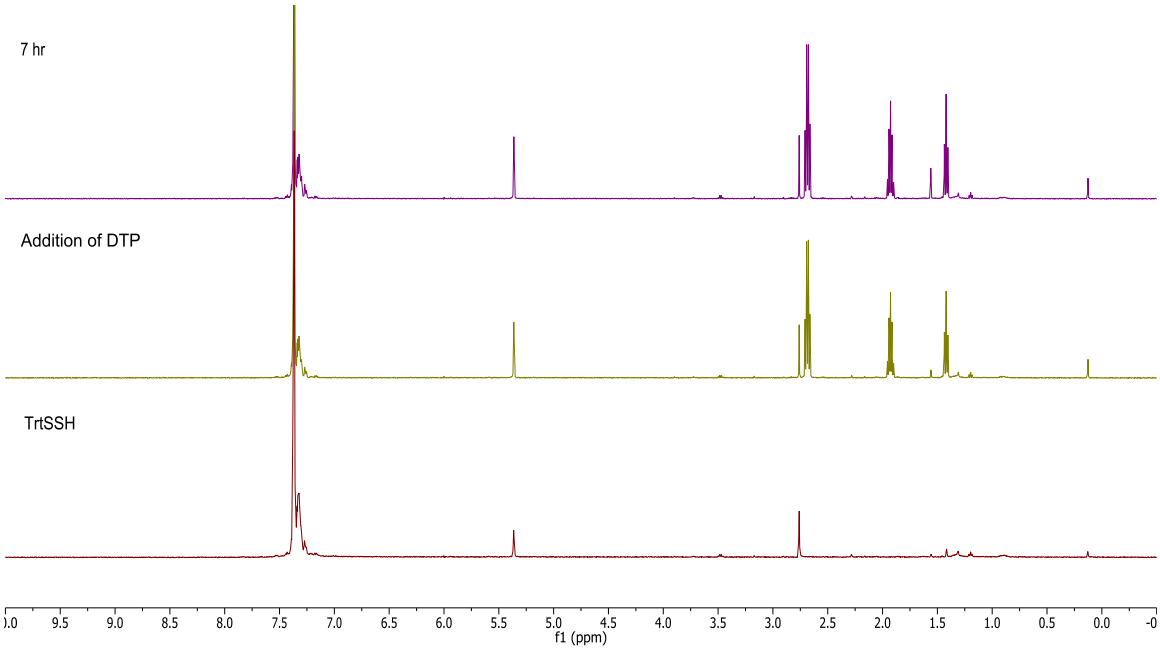

Figure C12: ^{1}H (500 MHz, CD_2Cl_2) NMR spectra of TrtSSH upon addition of DTP. No change to the TrtSSH ^{1}H NMR signal at 2.72 ppm was observed during the course of the reaction.

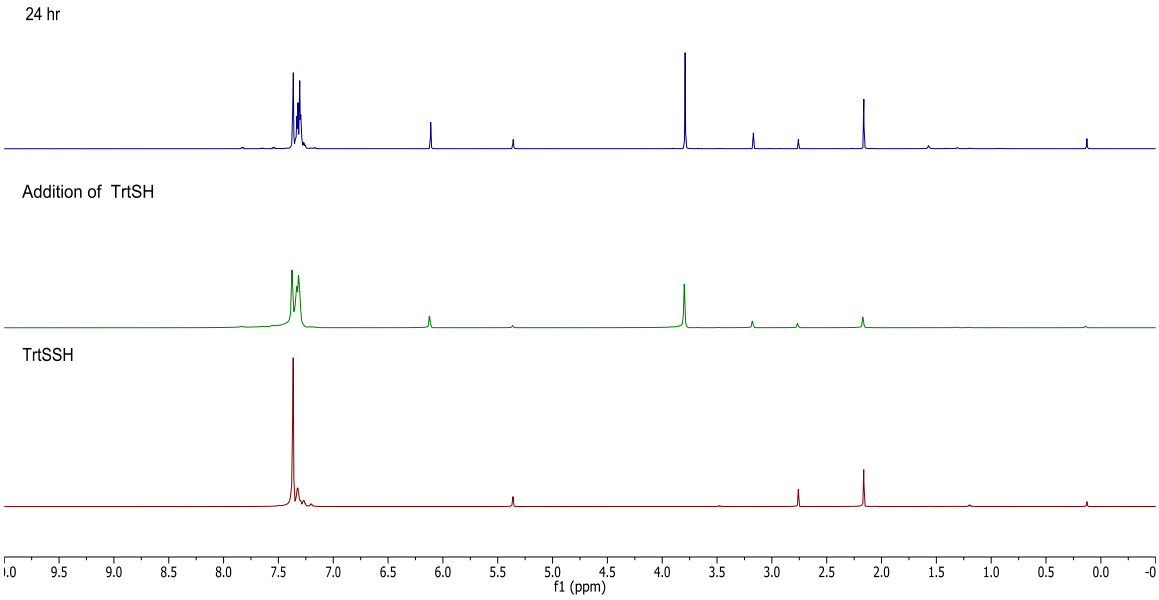

Figure C13: ^{1}H (500 MHz, CD_2Cl_2) NMR spectra of TrtSSH upon addition of TrtSH. The ^{1}H NMR spectra also show 1,3,5-trimethoxybenzene, which was used as an internal standard to quantify H_2S liberated. The ^{1}H NMR spectra also contain a minor acetone impurity at 2.1 ppm. No change to the TrtSSH ^{1}H NMR signal at 2.72 ppm was observed during the course of the reaction.

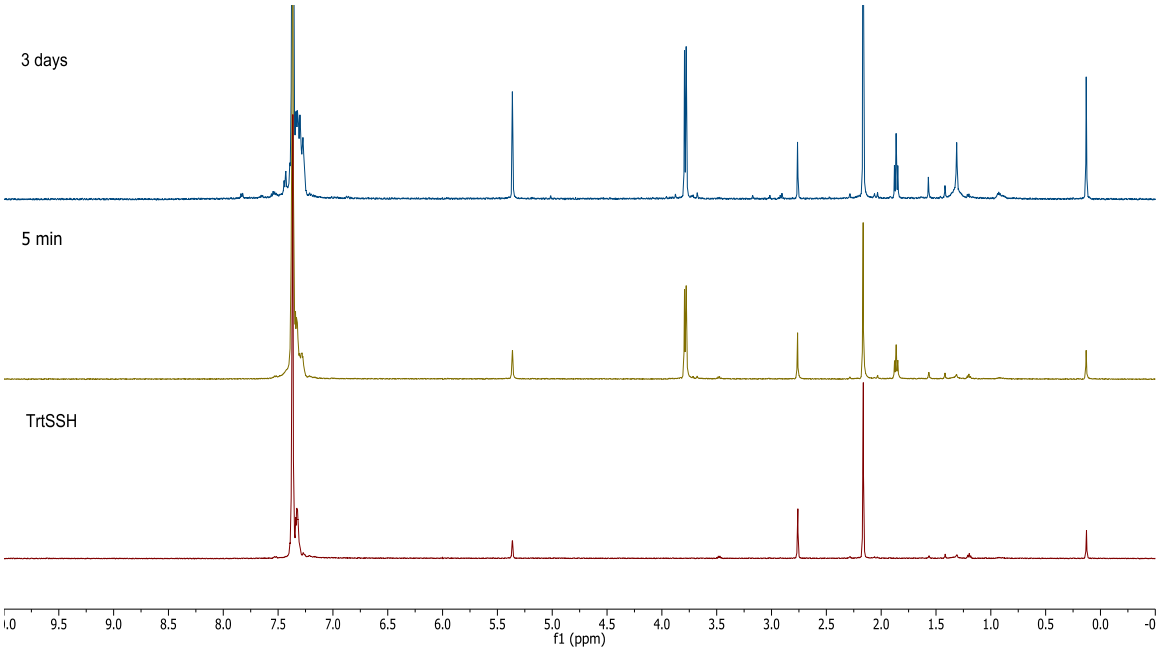

Figure C14: ^{1}H (500 MHz, CD_2Cl_2) NMR spectra of TrtSSH upon addition of BnSH. The ^{1}H NMR spectra contain a minor acetone impurity at 2.1 ppm. No change to the TrtSSH ^{1}H NMR signal at 2.72 ppm was observed during the course of the reaction.

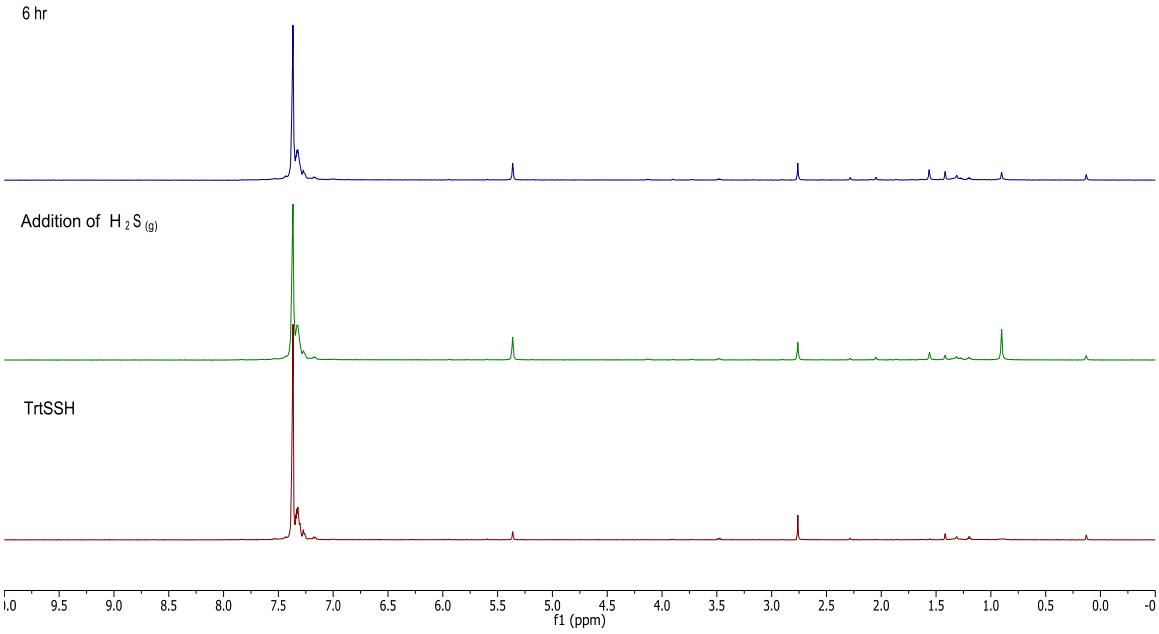

Figure C15: ^{1}H (500 MHz, CD_2Cl_2) NMR spectra of TrtSSH upon addition of $H_2S_{(g)}$. No change to the TrtSSH ^{1}H NMR signal at 2.72 ppm was observed during the course of the reaction.

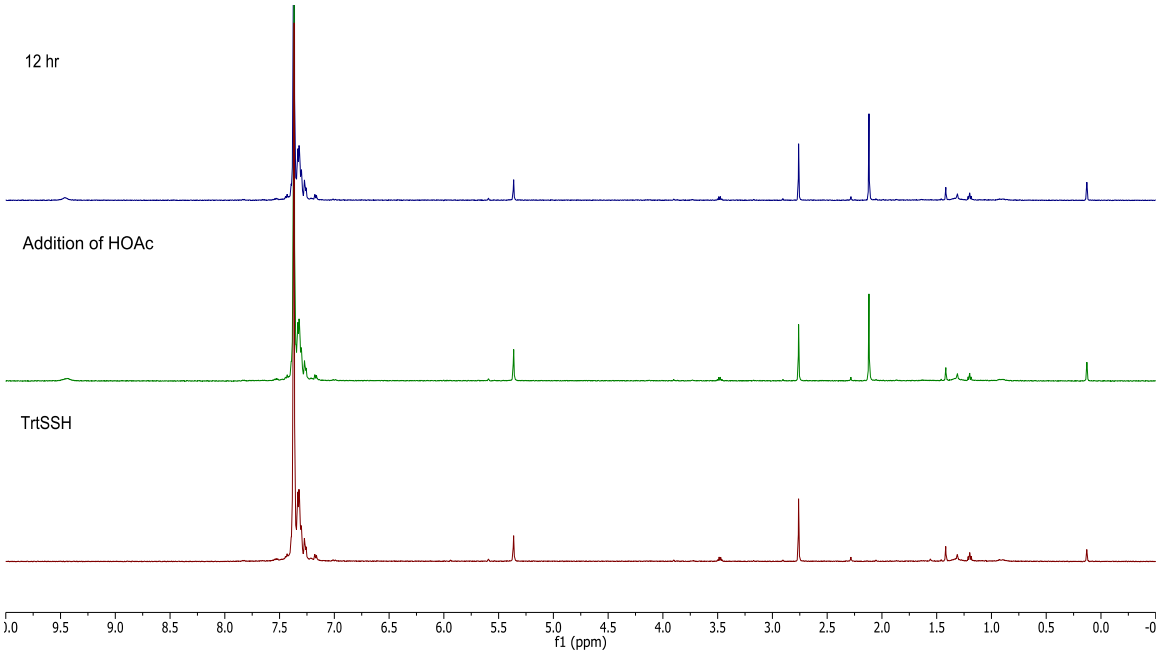

Figure C16: ^{1}H (500 MHz, CD_2Cl_2) spectra of TrtSSH upon addition of HOAc. No change to the TrtSSH ^{1}H NMR signal at 2.72 ppm was observed during the course of the reaction.

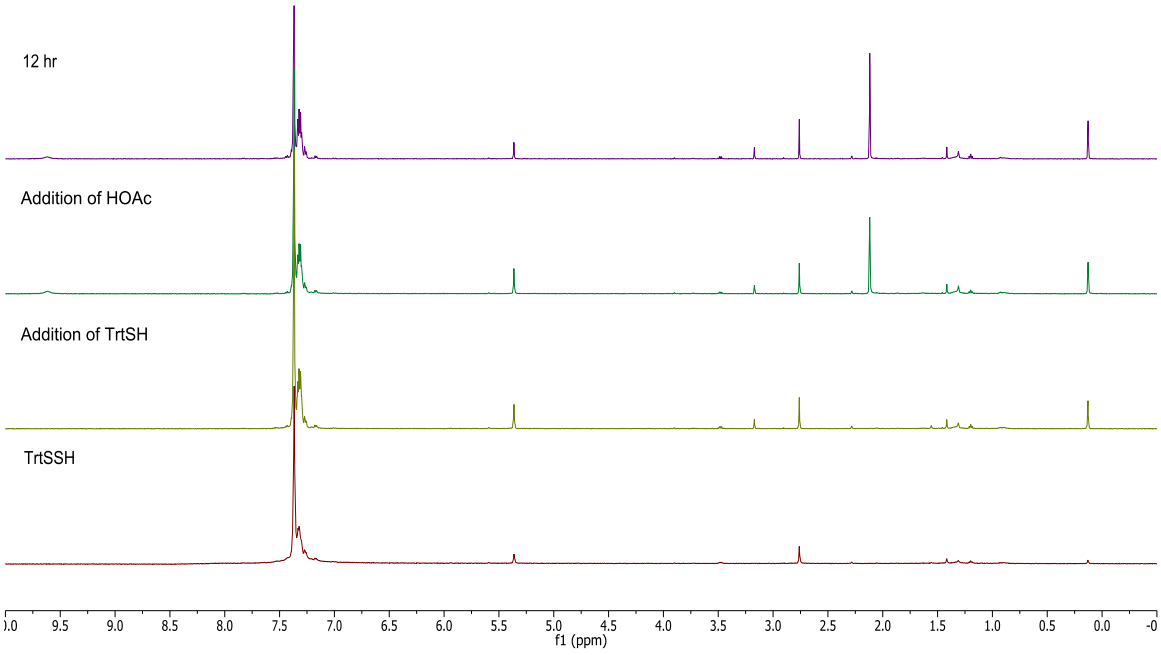

Figure C17: ^{1}H (500 MHz, CD_2Cl_2) NMR spectra of TrtSSH upon addition of HOAc and TrtSH. No change to the TrtSSH ^{1}H NMR signal at 2.72 ppm was observed during the course of the reaction.

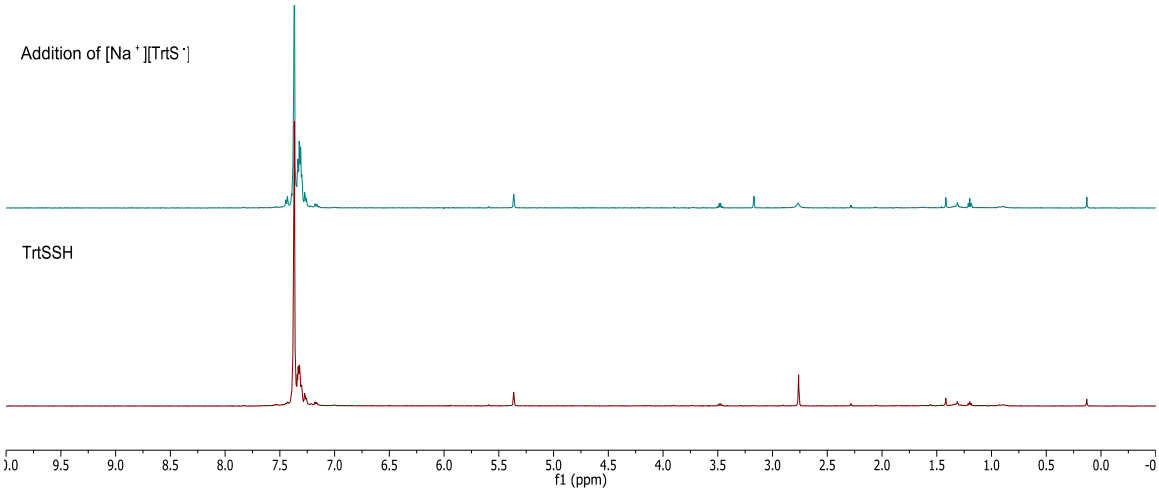

Figure C18: ^{1}H (500 MHz, CD_2Cl_2) NMR spectra of TrtSSH upon addition of $[Na^+][TrtS^-]$. A new peak at 3.1 ppm, corresponding to TrtSH, is observed during the course of the reaction.

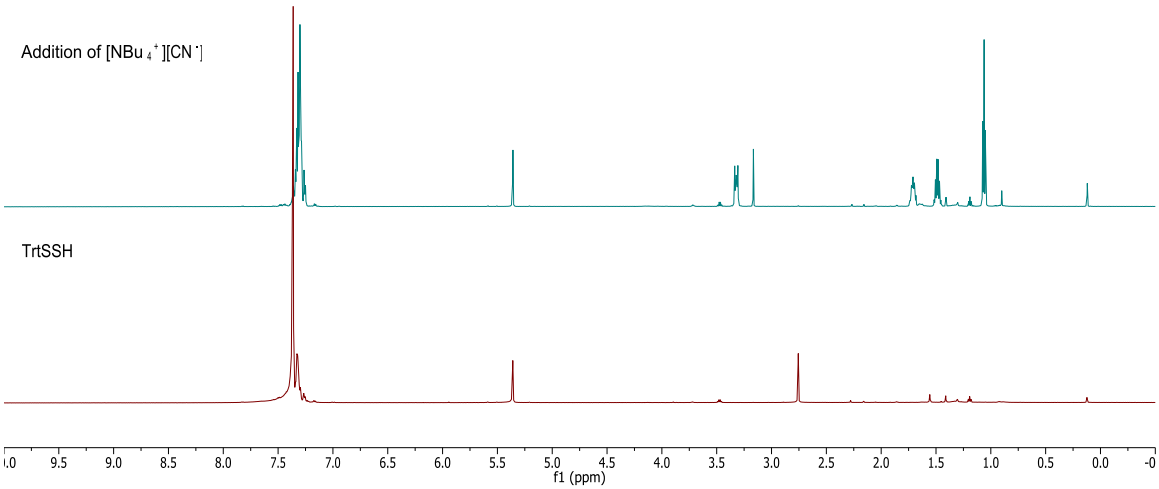

Figure C19: ^{1}H (500 MHz, CD_2Cl_2) NMR spectra of TrtSSH upon addition of $[NBu_4^+][CN^-]$. A new peak at 3.1 ppm, corresponding to TrtSH, is observed during the course of the reaction.

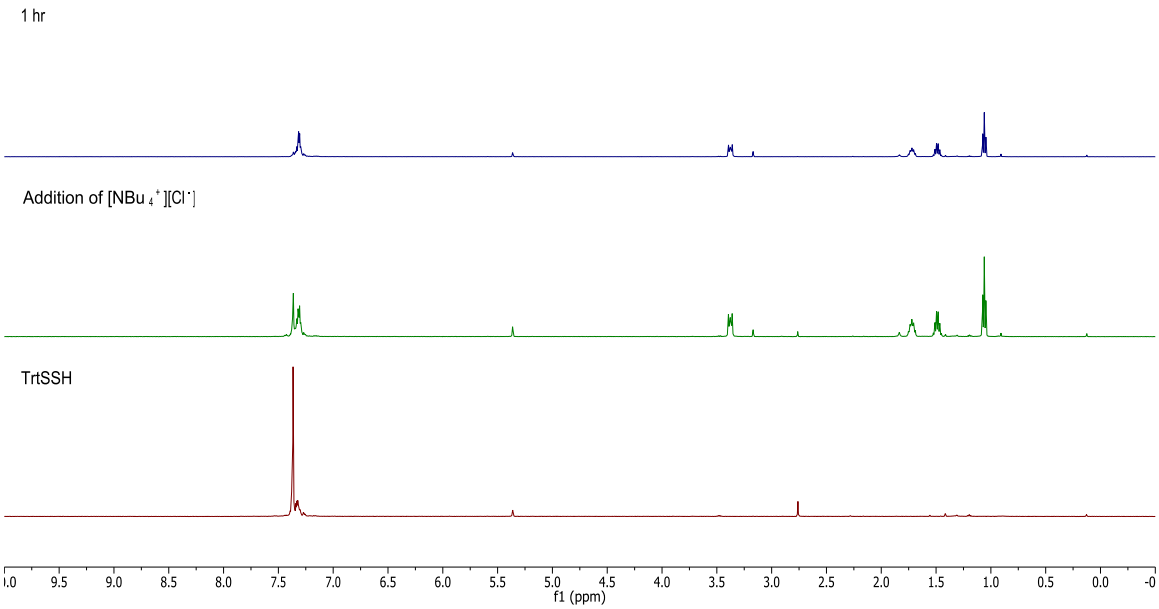

Figure C20: ^{1}H (500 MHz, CD_2Cl_2) NMR spectra of TrtSSH upon addition of $[NBu_4^+][Cl^-]$. A new peak at 3.1 ppm, corresponding to TrtSH, is observed during the course of the reaction.

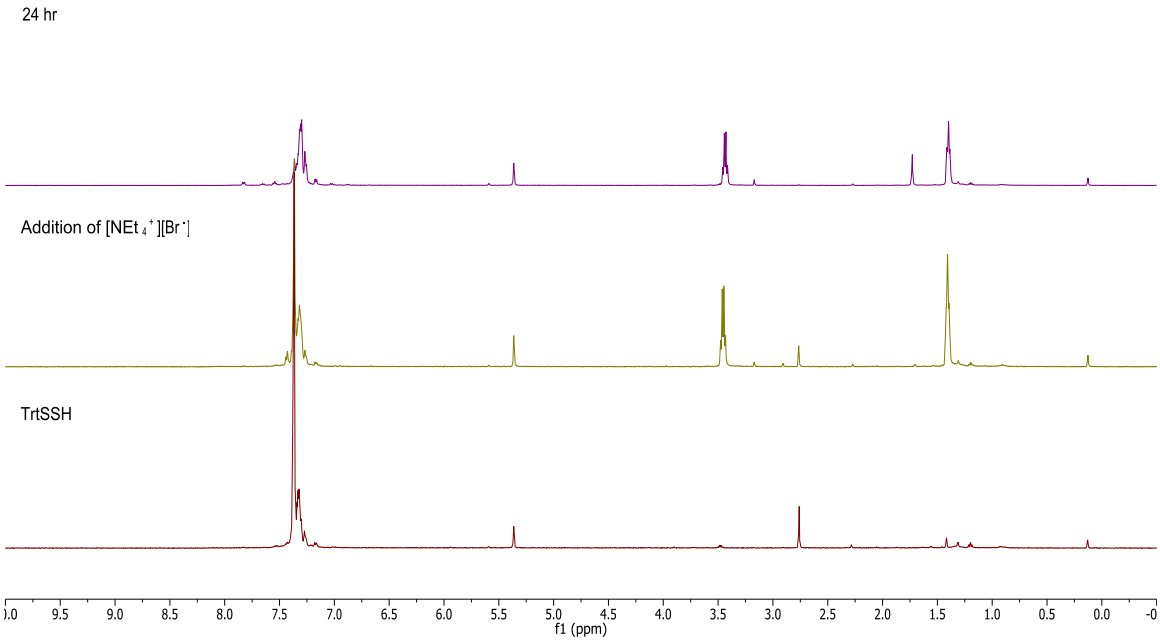

Figure C21: ^{1}H (500 MHz, CD_2Cl_2) NMR spectra of TrtSSH upon addition of $[NEt_4^+][Br^-]$. A new peak at 3.1 ppm, corresponding to TrtSH, is observed during the course of the reaction.

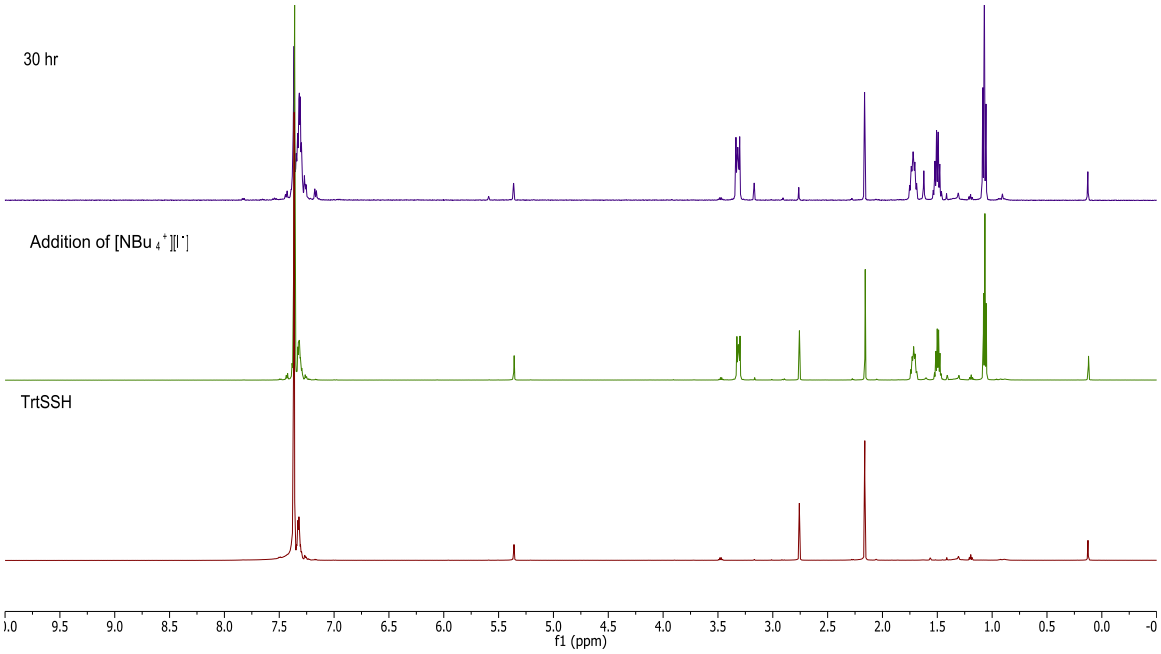

Figure C22: ^{1}H (500 MHz, CD_2Cl_2) NMR spectra of TrtSSH upon addition of $[NBu_4^+][I^-]$. The ^{1}H NMR spectra contain a minor acetone impurity at 2.1 ppm. A new peak at 3.1 ppm, corresponding to TrtSH, is observed during the course of the reaction.

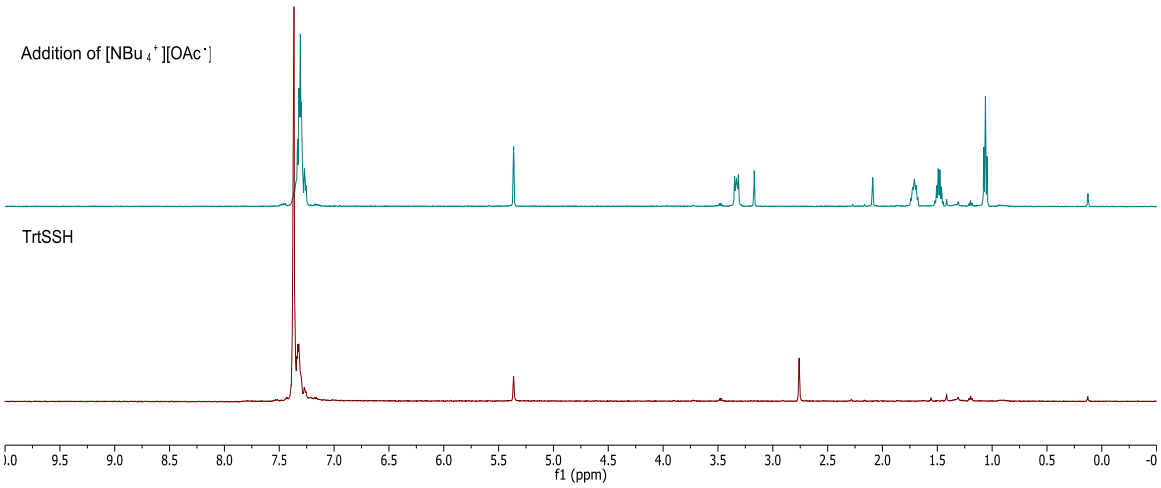

Figure C23: ^{1}H (500 MHz, CD_2Cl_2) spectra of TrtSSH upon addition of $[NBu_4^+][OAc^-]$. A new peak at 3.1 ppm, corresponding to TrtSH, is observed during the course of the reaction.

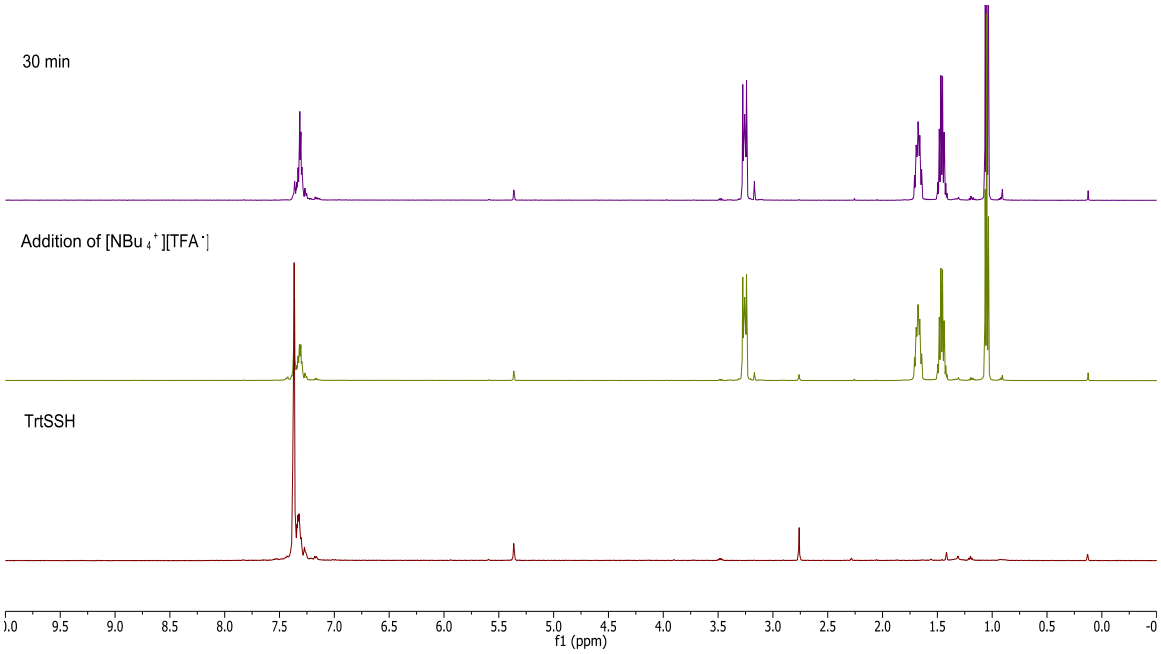

Figure C24: ^{1}H (500 MHz, CD_2Cl_2) NMR spectra of TrtSSH upon addition of $[NBu_4^+][TFA^-]$. A new peak at 3.1 ppm, corresponding to TrtSH, is observed during the course of the reaction.

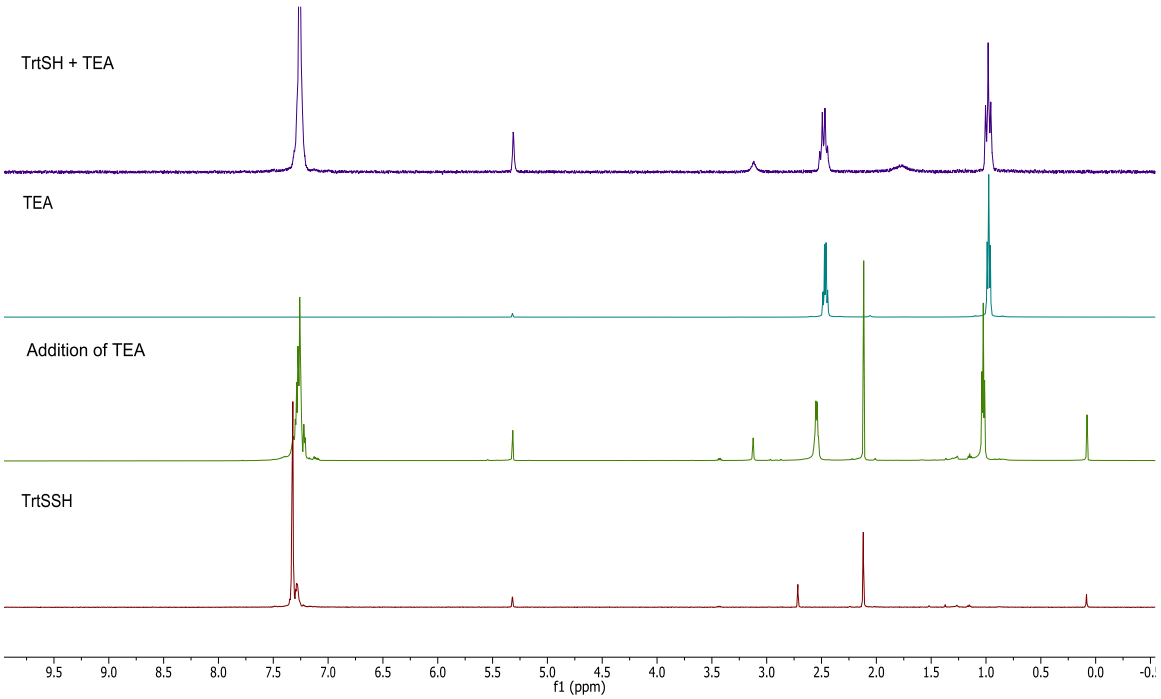

Figure C25: ^{1}H (500 MHz, CD_2Cl_2) NMR spectra of TrtSSH upon addition of NEt_3. The ^{1}H NMR spectra contain a minor acetone impurity at 2.1 ppm. A new peak at 3.1 ppm, corresponding to TrtSH, is observed during the course of the reaction.

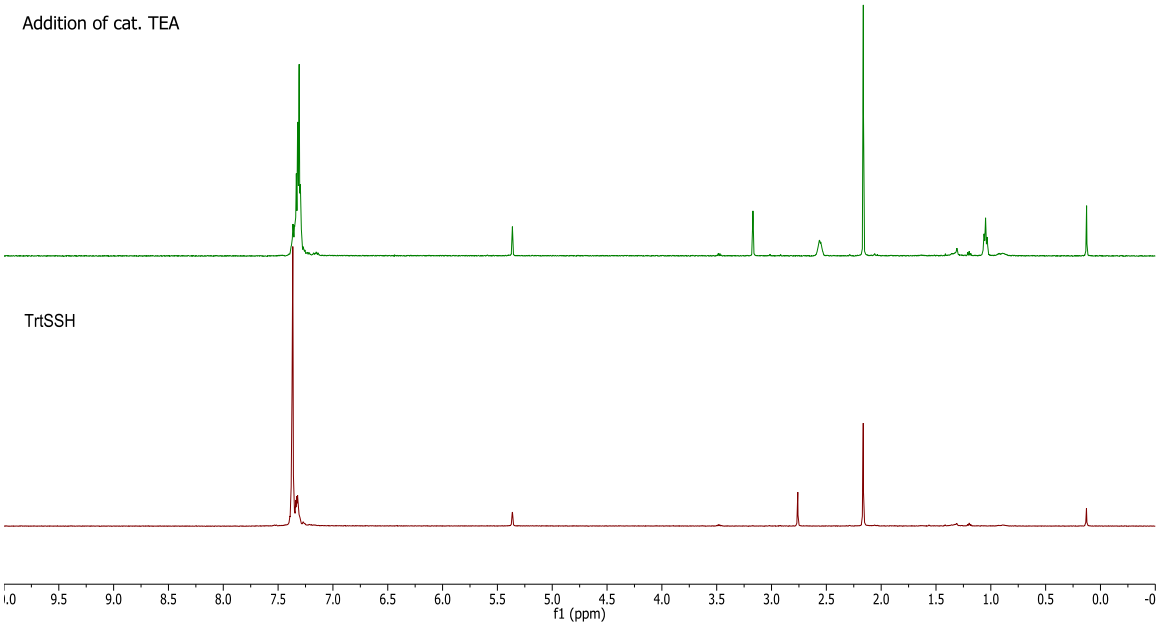

Figure C26: ^{1}H (500 MHz, CD_2Cl_2) NMR spectra of TrtSSH upon addition of 0.1 equiv. of NEt_3. The ^{1}H NMR spectra contains a minor acetone impurity at 2.1 ppm. A new peak at 3.1 ppm, corresponding to TrtSH, is observed during the course of the reaction.

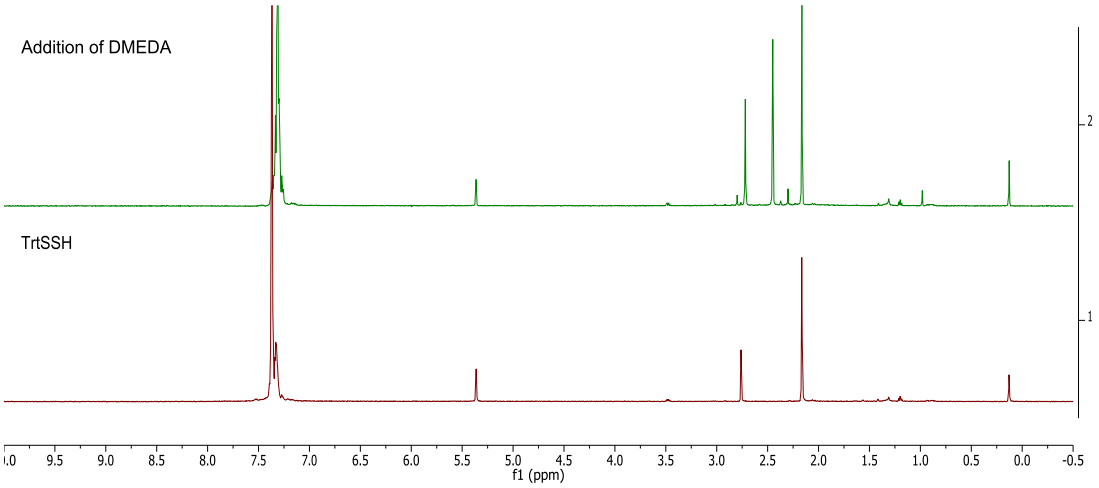

Figure C27: ^{1}H (500 MHz, CD_2Cl_2) NMR spectra of TrtSSH upon addition of DMEDA. The ^{1}H NMR spectra contain a minor acetone impurity at 2.1 ppm. The TrtSSH proton resonance disappears during the course of the reaction.

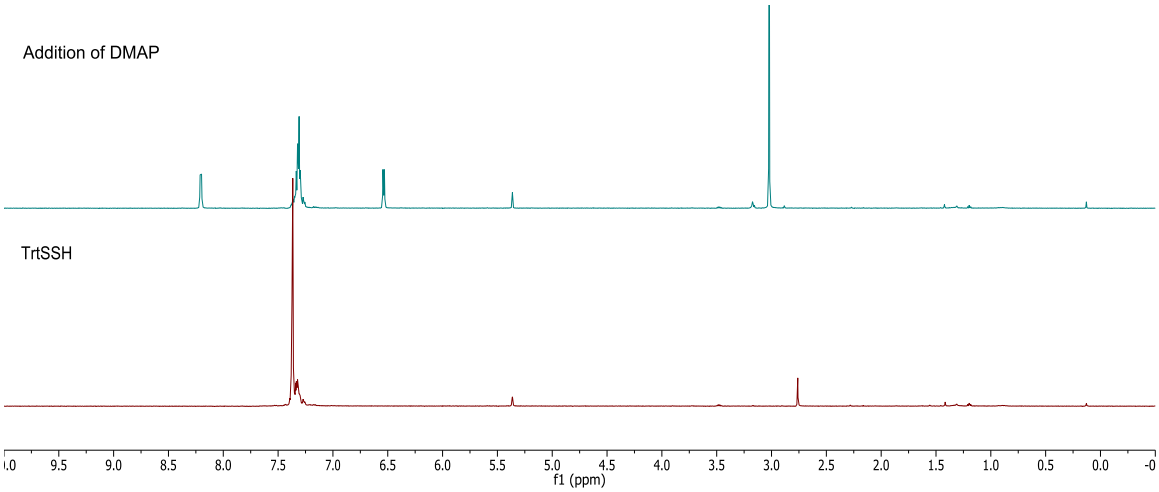

Figure C28: ^{1}H (500 MHz, CD_2Cl_2) NMR spectra of TrtSSH upon addition of DMAP. A new peak at 3.1 ppm, corresponding to TrtSH, is observed during the course of the reaction.

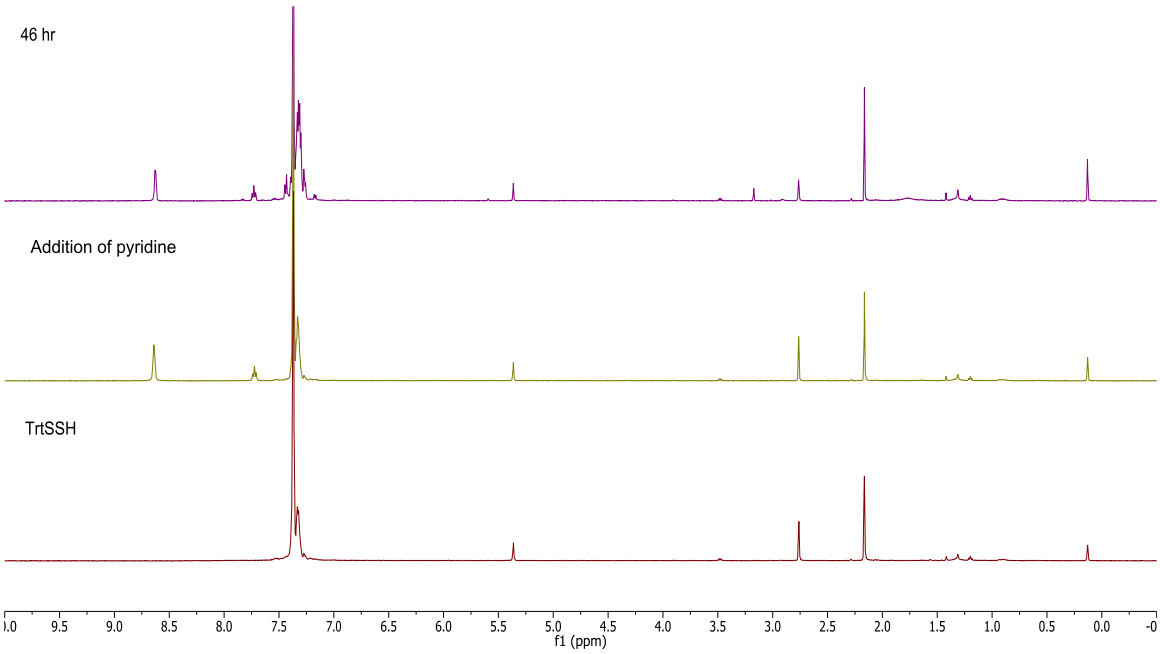

Figure C29: ^{1}H (500 MHz, CD_2Cl_2) NMR spectra of TrtSSH upon addition of pyridine. A new peak at 3.1 ppm, corresponding to TrtSH, is observed during the course of the reaction.

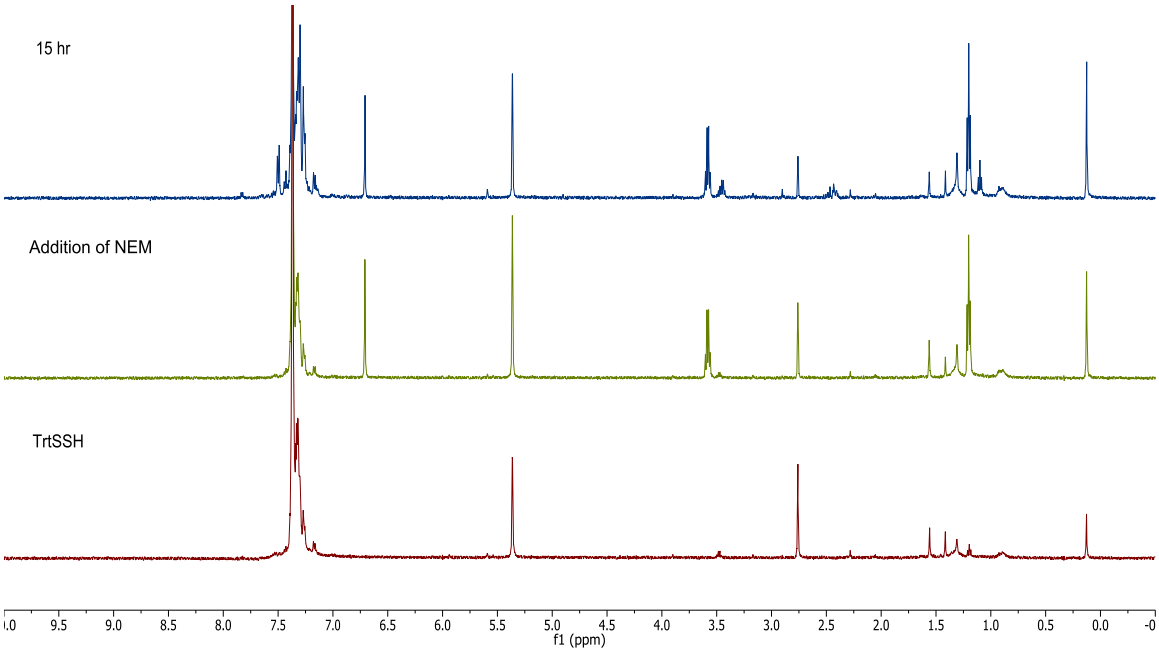

Figure C30: ^{1}H (500 MHz, CD_2Cl_2) NMR spectra of TrtSSH upon addition of *N*-ethyl-maleimide (NEM). The SSH peak at 2.7 ppm and the NEM alkene peak at 6.7 ppm decrease while muliplets at 3.1 ppm and 2.45 ppm begin to appear. The rate of reaction is slow because of proton transfer limitations in organic solvent.

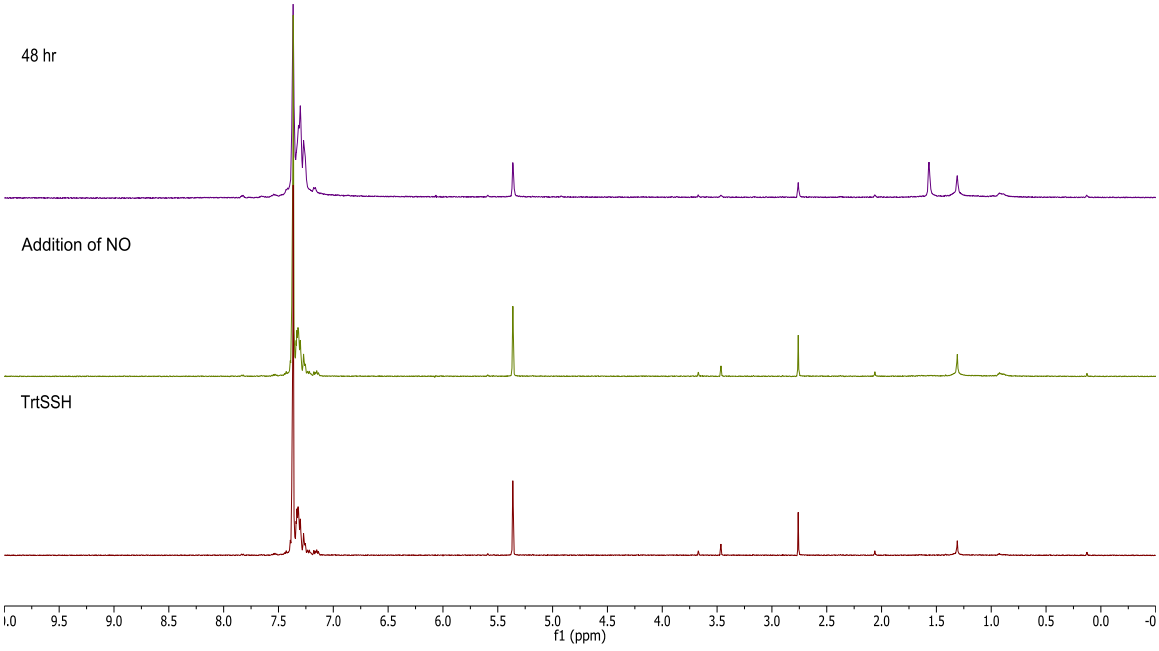

Figure C31. ^{1}H (500 MHz, CD_2Cl_2) spectra of TrtSSH upon addition of $NO_{(g)}$. No change to the TrtSSH ^{1}H NMR signal at 2.72 ppm was observed during the course of the reaction.

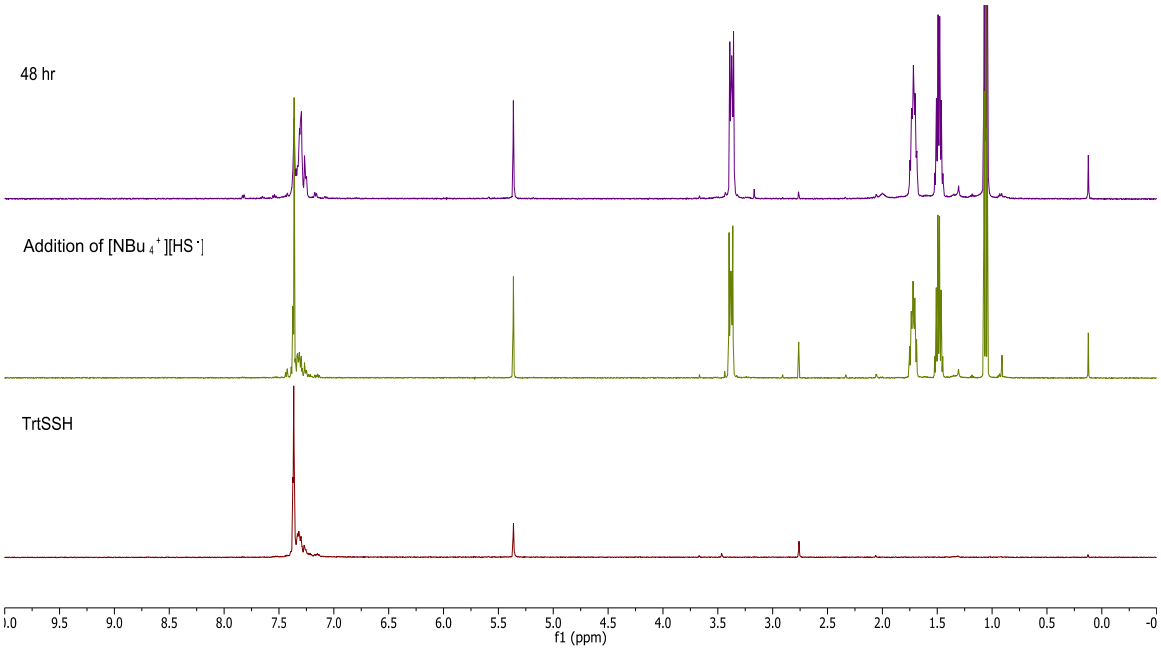

Figure C32. ^{1}H (500 MHz, CD_2Cl_2) NMR spectra of TrtSSH upon addition of $[NBu_4^+][HS^-]$. New peaks at 3.1 ppm, corresponding to TrtSH, and 0.9 ppm, corresponding to $H_2S_{(g)}$, are observed during the course of the reaction. Because $H_2S_{(g)}$ slowly diffuses out of solution, the total amount of S-H protons in solution decreases during the course of reaction.

NMR Spectra of BnSSH Reactivity Experiments

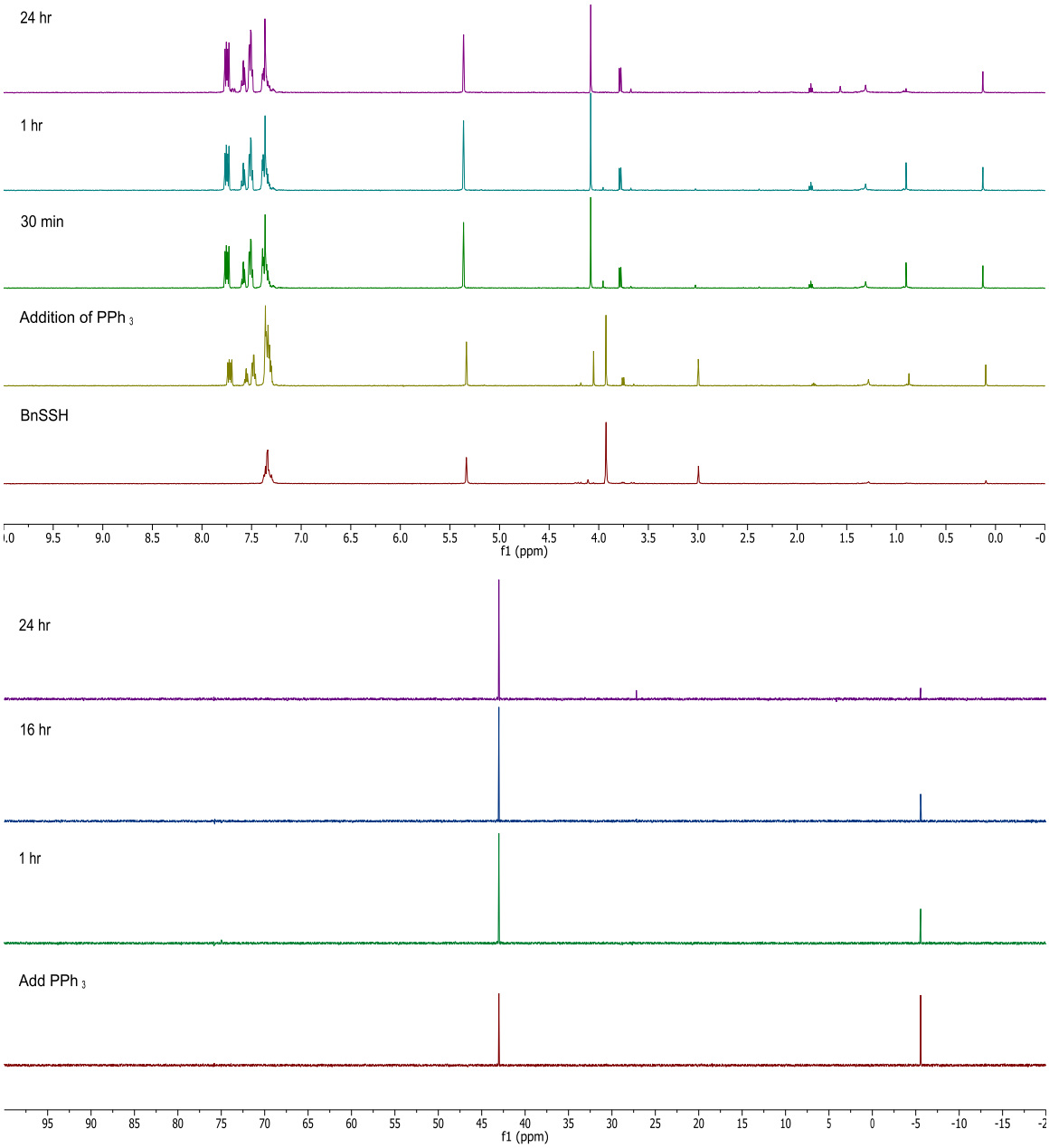

Figure C33. ^{1}H (500 MHz, CD_2Cl_2, top) and ^{31}P $\{^{1}H\}$ NMR (202 MHz, CD_2Cl_2, bottom) spectra of BnSSH upon addition of PPh_3. New peaks in the ^{1}H spectrum at 4.08 ppm, corresponding to BnSSSBn, 3.68 ppm, corresponding to BnSSBn, 3.79 and 1.86, corresponding to BnSH, and 0.9 ppm, corresponding to $H_2S_{(g)}$, are observed during the course of the reaction. The $^{31}P\{^{1}H\}$ peak at -6 ppm, corresponding to PPh_3, disappears and is replaced by a peak at 43 ppm, corresponding to $SPPh_3$.

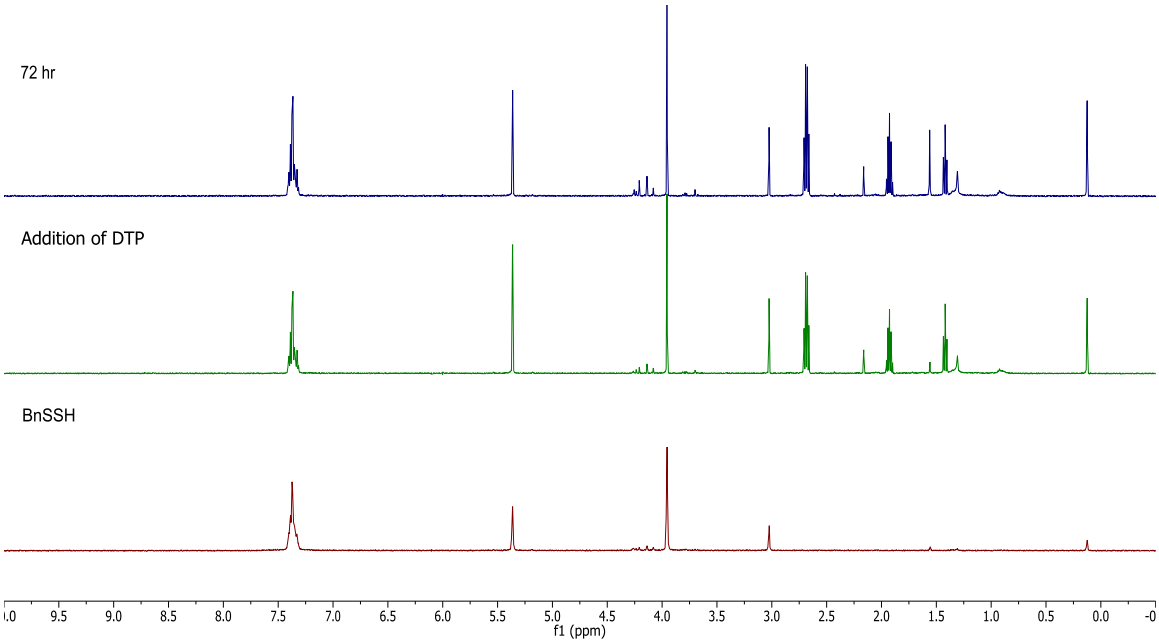

Figure C34. ^{1}H (500 MHz, CD_2Cl_2) and spectra of BnSSH upon addition of DTP. No reaction with DTP is observed after 72 hr.

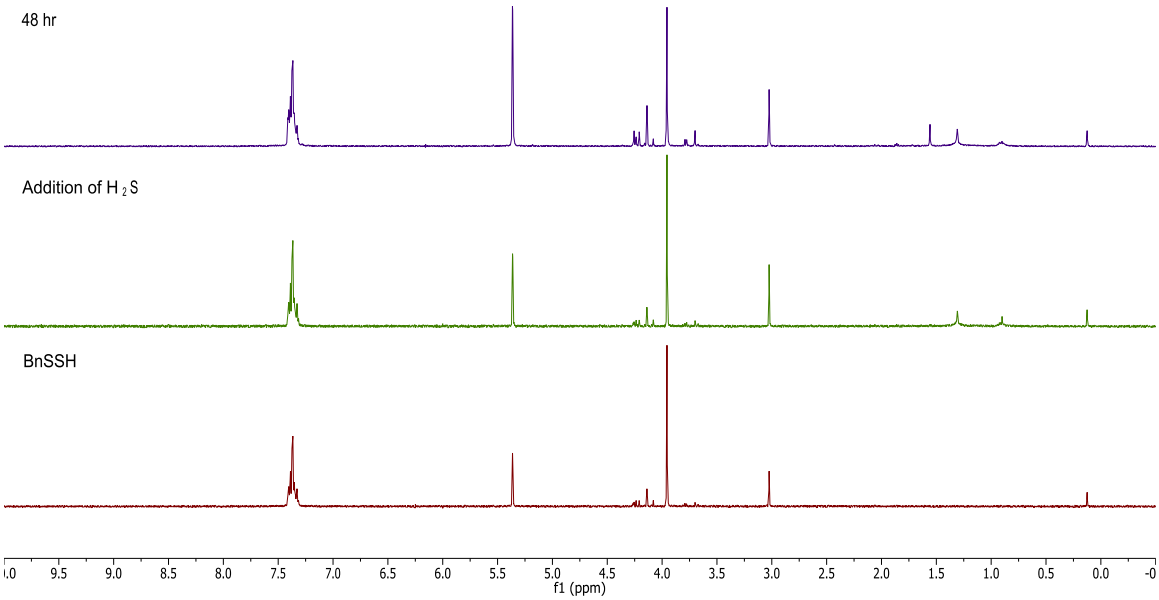

Figure C35. ^{1}H (500 MHz, CD_2Cl_2) and spectra of BnSSH upon addition of $H_2S_{(g)}$. No reaction with $H_2S_{(g)}$ is observed after 48 hr.

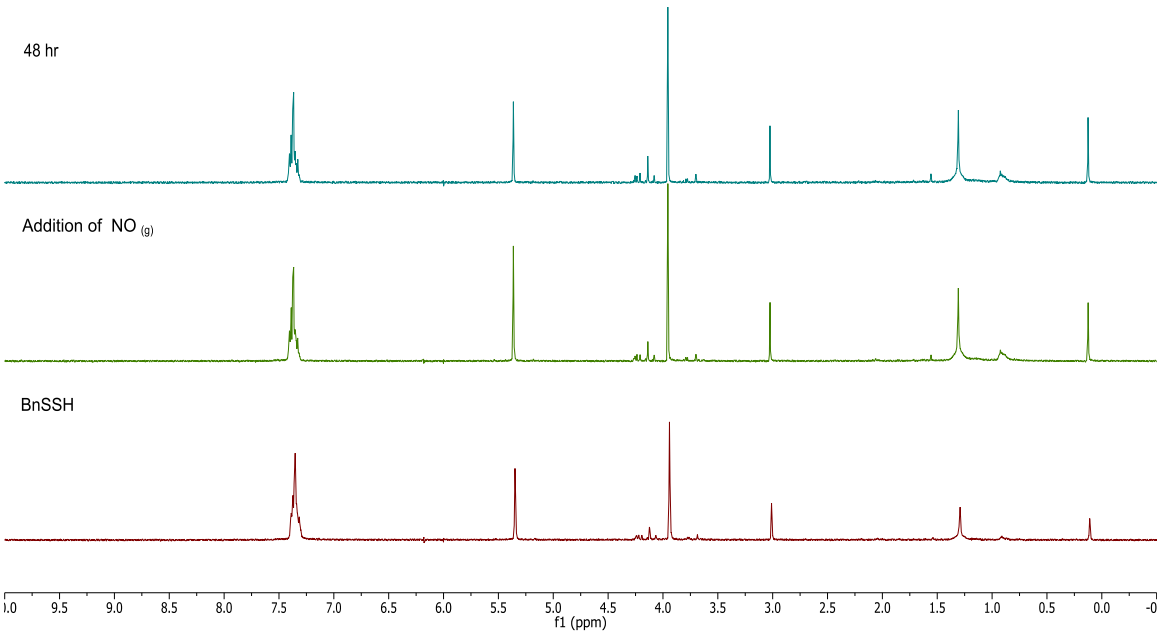

Figure C36. ^{1}H (500 MHz, CD_2Cl_2) and spectra of BnSSH upon addition of $NO_{(g)}$. No reaction with $NO_{(g)}$ is observed after 48 hr.

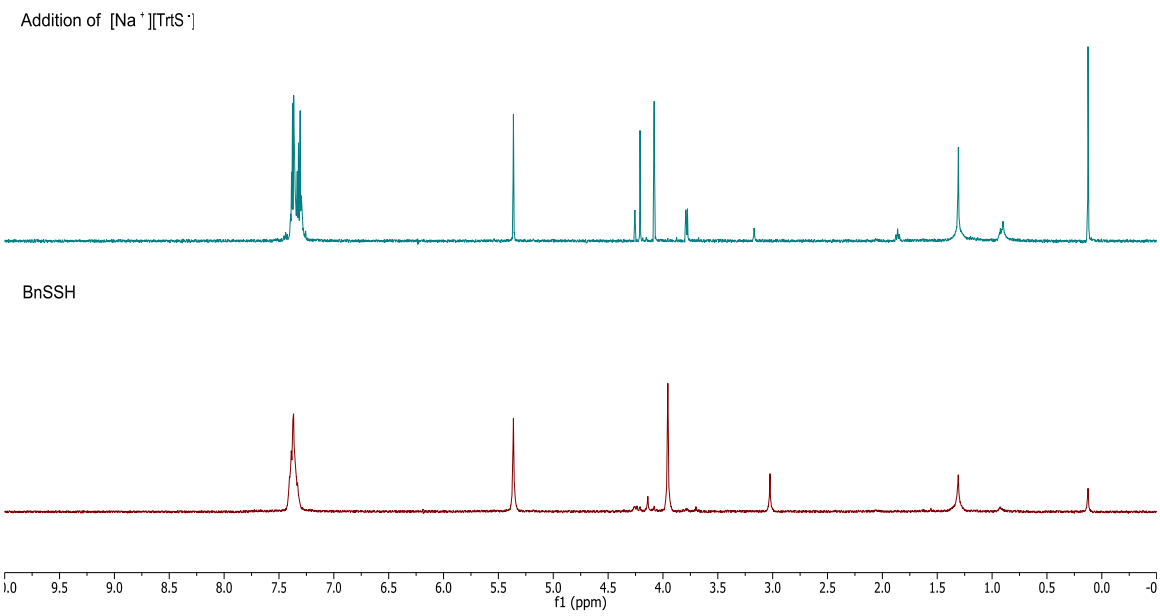

Figure C37. ^{1}H (500 MHz, CD_2Cl_2) and spectra of BnSSH upon addition of $[Na^{+}][TrtS^{-}]$. New peaks in the ^{1}H spectrum at 4.26 ppm, corresponding to BnSSSSSBn, 4.21 ppm, corresponding to BnSSSSBn, 4.08 ppm, corresponding to BnSSSBn, 3.79 and 1.86, corresponding to BnSH, and 0.9 ppm, corresponding to $H_2S_{(g)}$, are observed during the course of the reaction

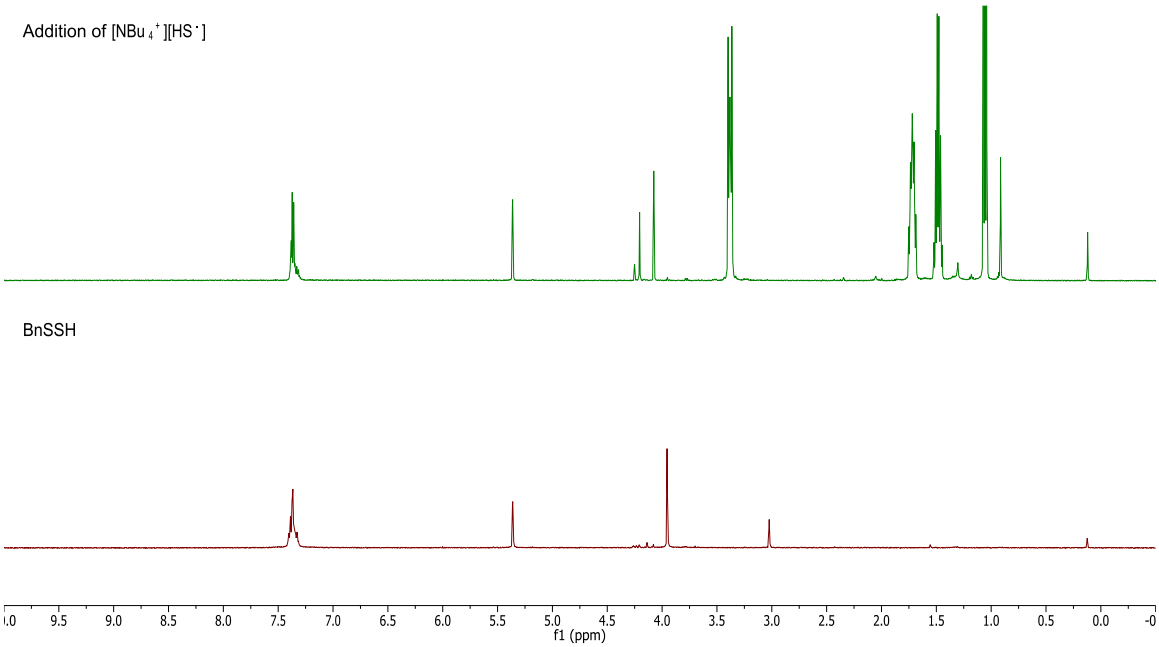

Figure C38. ^{1}H (500 MHz, CD_2Cl_2) NMR spectra of BnSSH upon addition of $[NBu_4^+][HS^-]$. New peaks in the ^{1}H spectrum at 4.26 ppm, corresponding to BnSSSSSBn, 4.21 ppm, corresponding to BnSSSSBn, and 4.08 ppm, corresponding to BnSSSBn, are observed during the course of the reaction.

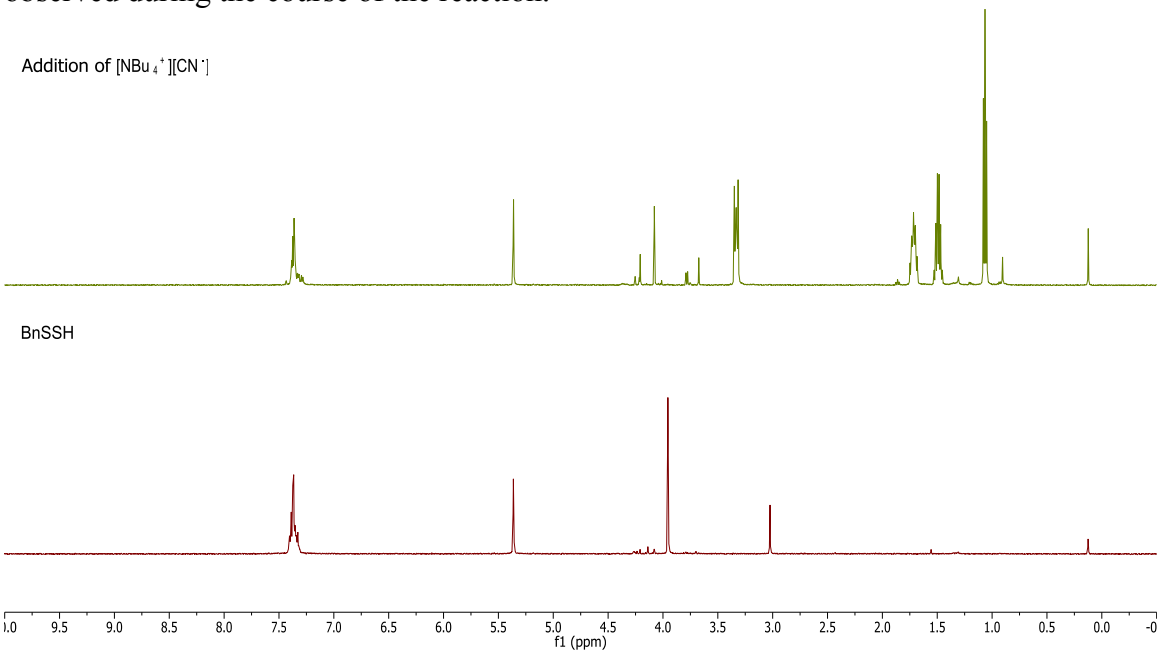

Figure C39. ^{1}H (500 MHz, CD_2Cl_2) NMR spectra of BnSSH upon addition of $[NBu_4^+][CN^-]$. New peaks in the ^{1}H spectrum at 4.26 ppm, corresponding to BnSSSSSBn, 4.21 ppm, corresponding to BnSSSSBn, 4.08 ppm, corresponding to BnSSSBn, 3.79 ppm, corresponding to BnSH, 3.63 ppm, corresponding to BnSSBn, and 0.9 ppm, corresponding to $H_2S_{(g)}$ are observed during the course of the reaction.

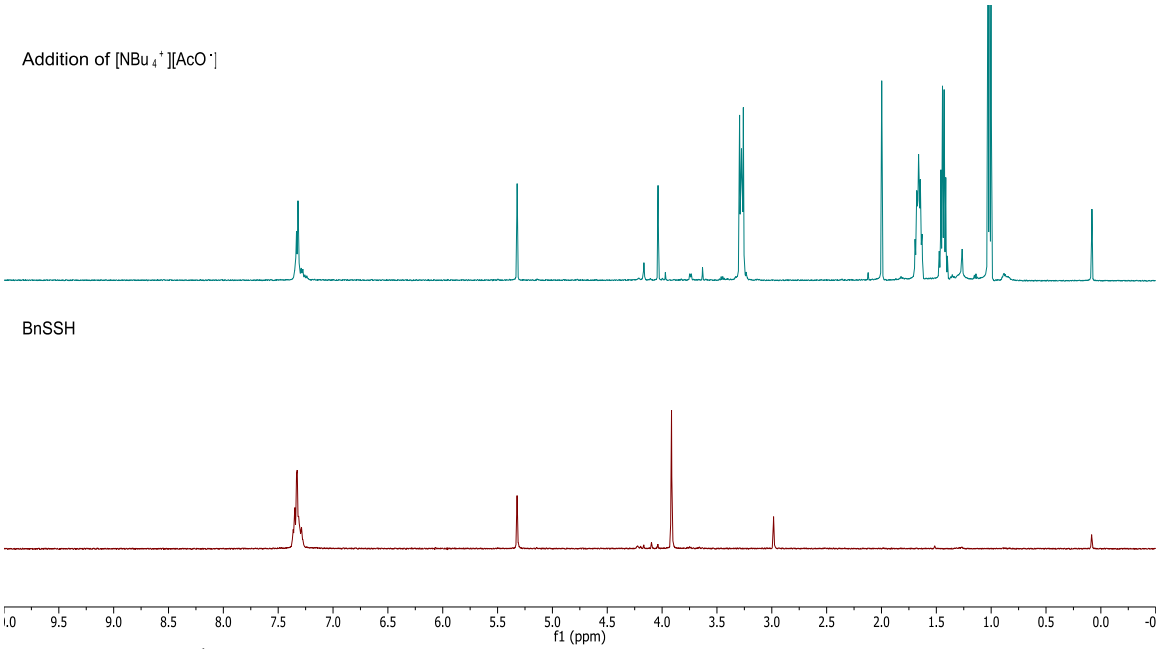

Figure C40. ^{1}H (500 MHz, CD_2Cl_2) NMR spectra of BnSSH upon addition of $[NBu_4^+][AcO^-]$. New peaks in the ^{1}H spectrum at 4.26 ppm, corresponding to BnSSSSSSBn, 4.21 ppm, corresponding to BnSSSSSBn, 4.08 ppm, corresponding to BnSSSBn, 3.79 ppm, corresponding to BnSH, and 3.62 ppm, corresponding to BnSSBn, are observed during the reaction.

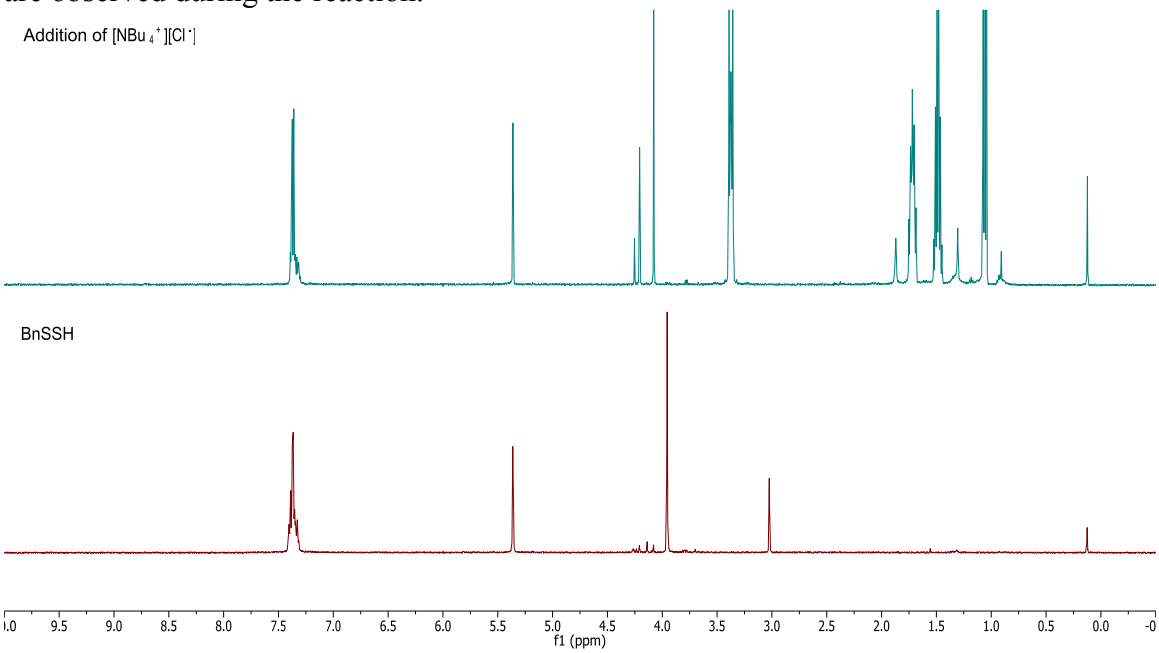

Figure C41: ^{1}H (500 MHz, CD_2Cl_2) NMR spectra of BnSSH upon addition of $[NBu_4^+][Cl^-]$. New peaks in the ^{1}H spectrum at 4.26 ppm, corresponding to BnSSSSSBn, 4.21 ppm, corresponding to BnSSSSBn, and 4.08 ppm, corresponding to BnSSSBn, are observed during the course of the reaction.

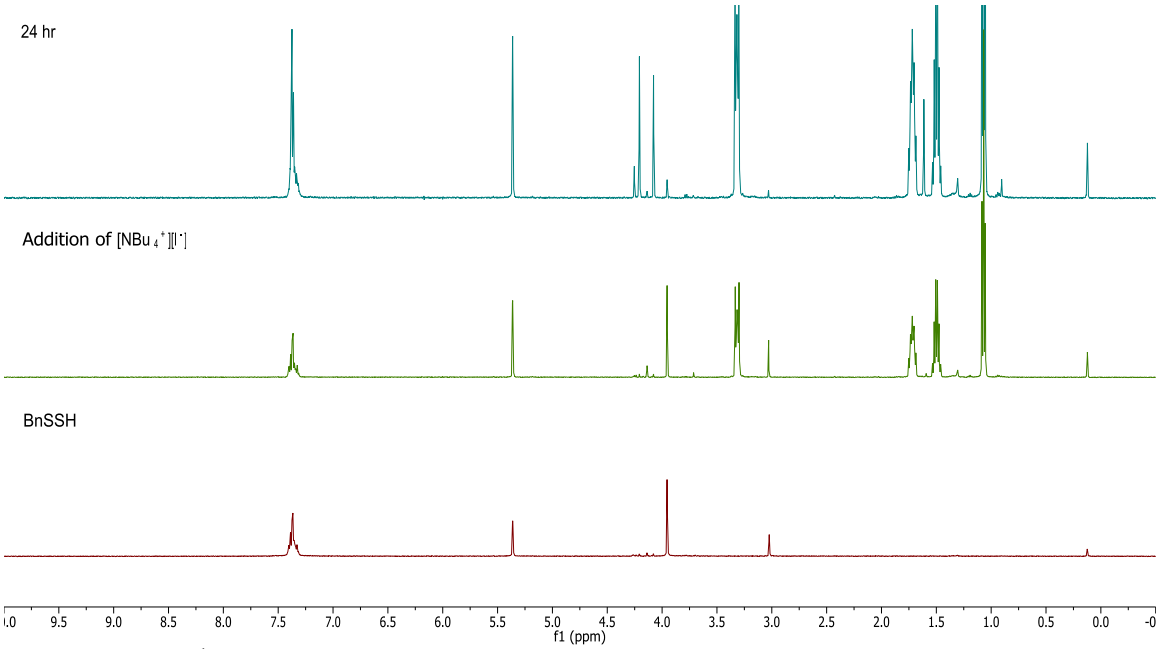

Figure C42. ^{1}H (500 MHz, CD_2Cl_2) NMR spectra of BnSSH upon addition of $[NBu_4^+][I^-]$. New peaks in the ^{1}H spectrum at 4.26 ppm, corresponding to BnSSSSSBn, 4.21 ppm, corresponding to BnSSSSBn, and 4.08 ppm, corresponding to BnSSSBn, are observed during the course of the reaction.

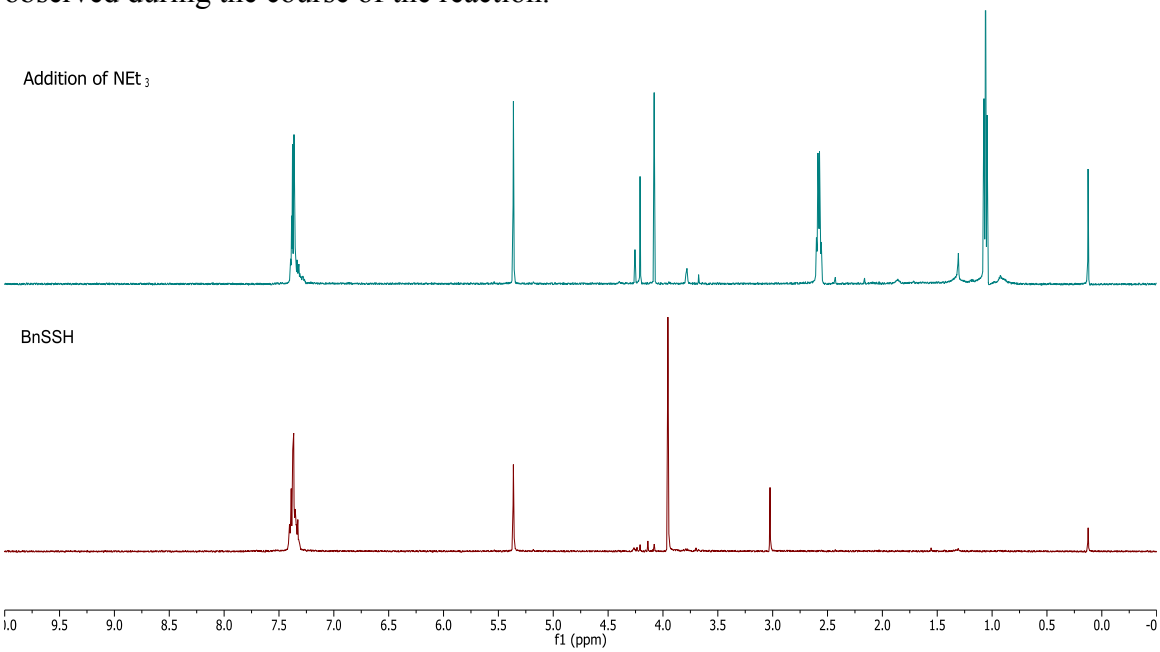

Figure C43. ^{1}H (500 MHz, CD_2Cl_2) NMR spectra of BnSSH upon addition of NEt_3. New peaks in the ^{1}H spectrum at 4.26 ppm, corresponding to BnSSSSSBn, 4.21 ppm, corresponding to BnSSSSBn, 4.08 ppm, corresponding to BnSSSBn, 3.79 ppm, corresponding to BnSH, and 3.63 ppm, corresponding to BnSSBn, are observed during the course of the reaction.

NMR Spectra of AdSSH Reactivity Experiments

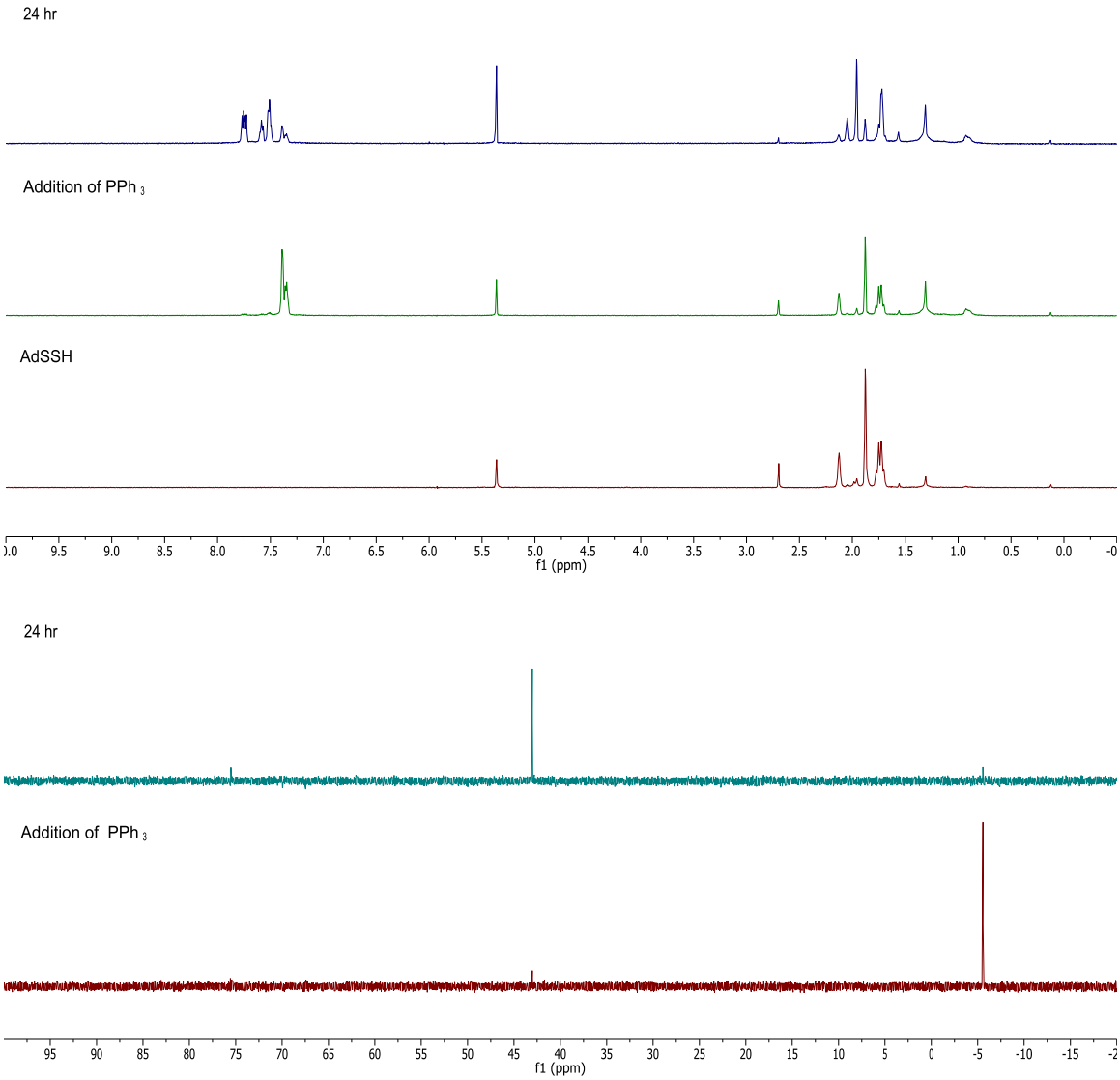

Figure C44. ^{1}H (500 MHz, CD_2Cl_2, top) and $^{31}P\{^{1}H\}$ NMR (202 MHz, CD_2Cl_2, bottom) spectra of AdSSH upon addition of PPh_3. New peaks in the ^{1}H spectrum at 2.06 ppm and 1.96 ppm, corresponding to AdSH are observed during the reaction. The $^{31}P\{^{1}H\}$ peak at -6 ppm, corresponding to PPh_3, disappears and is replaced by a peak at 43 ppm, corresponding to $SPPh_3$.

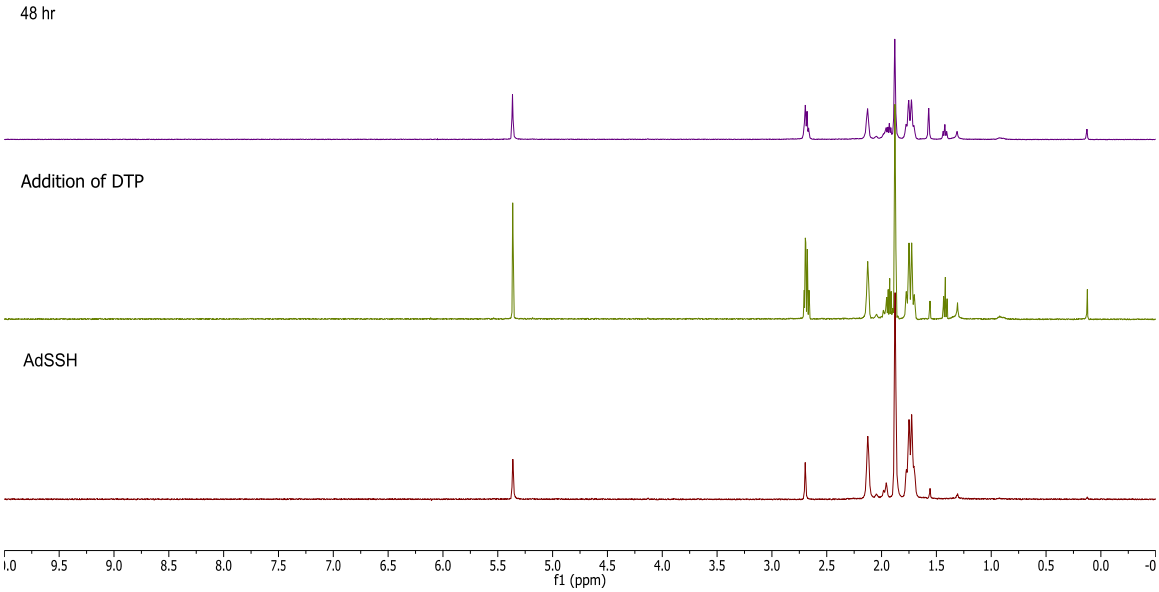

Figure C45. ^{1}H (500 MHz, CD_2Cl_2) and spectra of AdSSH upon addition of DTP. No reaction with DTP is observed after 48 hr.

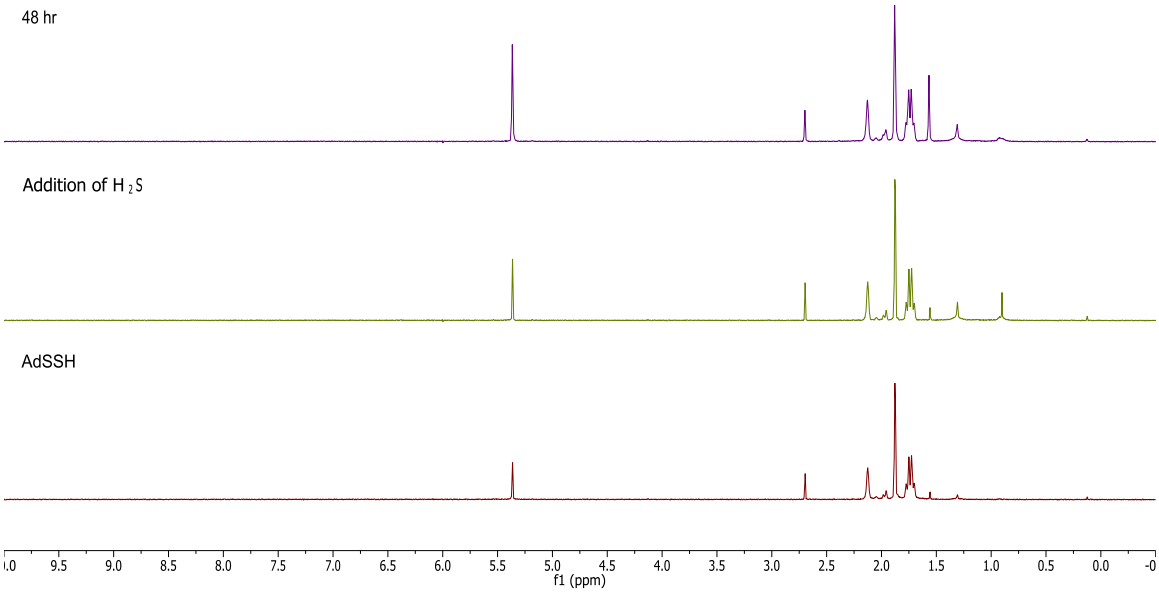

Figure C46. ^{1}H (500 MHz, CD_2Cl_2) and spectra of AdSSH upon addition of $H_2S_{(g)}$. No reaction with $H_2S_{(g)}$ is observed after 48 hr.

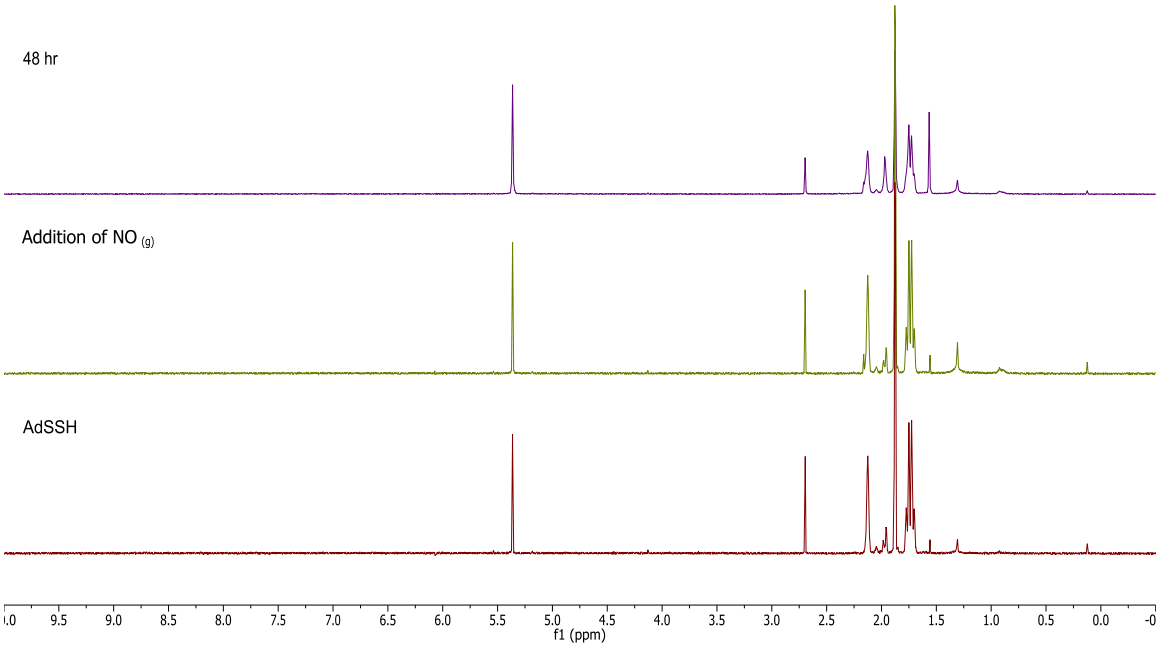

Figure C47. ^{1}H (500 MHz, CD_2Cl_2) and spectra of AdSSH upon addition of $NO_{(g)}$. No reaction with $NO_{(g)}$ is observed after 48 hr.

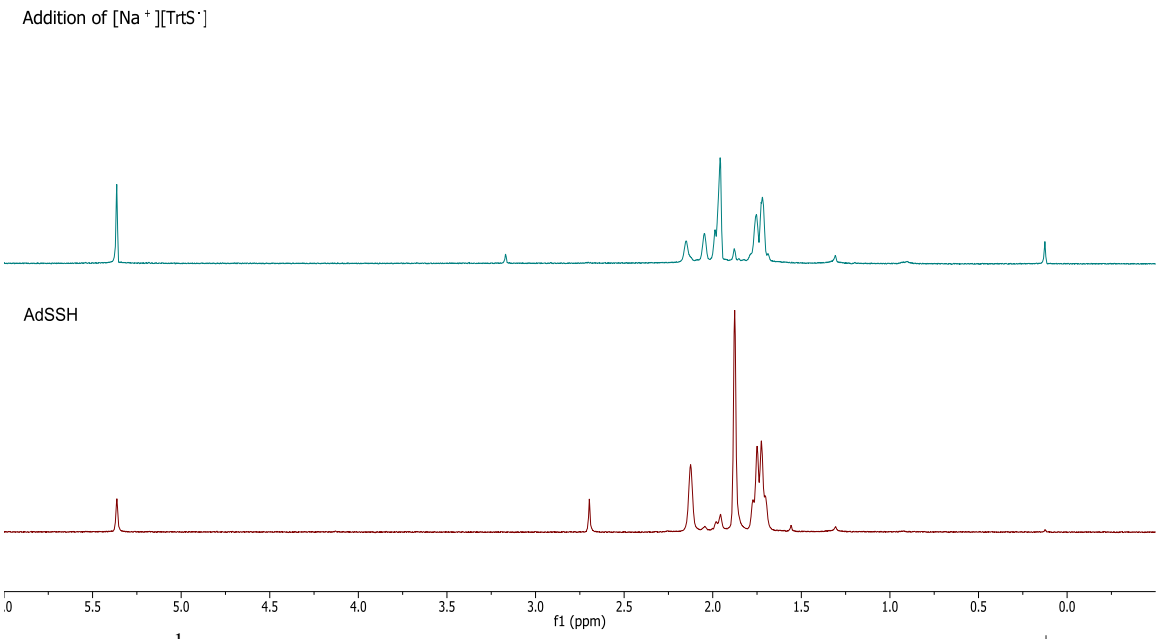

Figure C48. ^{1}H (500 MHz, CD_2Cl_2) and spectra of AdSSH upon addition of $[Na^{+}][TrtS^{-}]$. New peaks in the ^{1}H spectrum at 2.06 ppm and 1.96 ppm, corresponding to AdSH are observed during the reaction

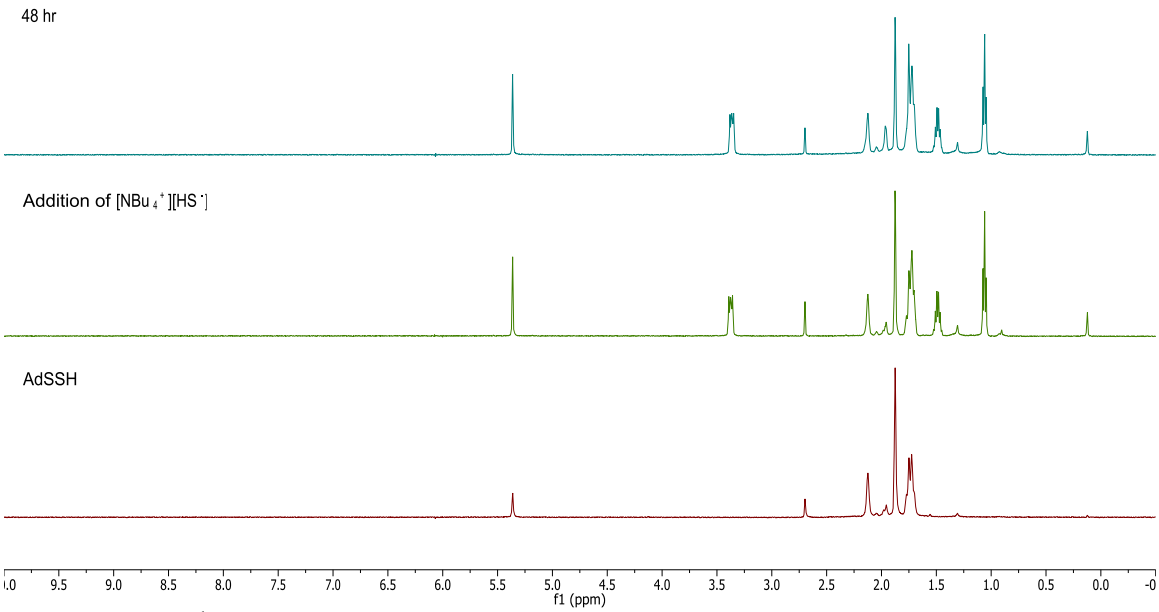

Figure C49. ^{1}H (500 MHz, CD_2Cl_2) NMR spectra of AdSSH upon addition of $[NBu_4^+][HS^-]$. No reaction with $[NBu_4^+][HS^-]$is observed after 48 hr.

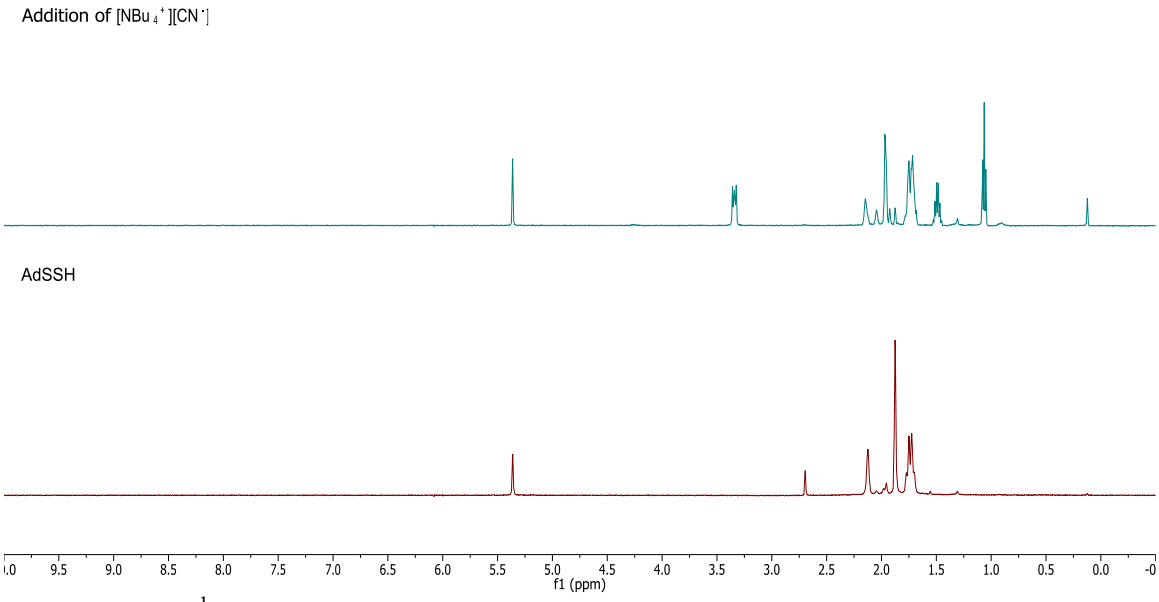

Figure C50: ^{1}H (500 MHz, CD_2Cl_2) NMR spectra of AdSSH upon addition of $[NBu_4^+][CN^-]$. New peaks in the ^{1}H spectrum at 2.06 ppm and 1.96 ppm, corresponding to AdSH are observed during the reaction

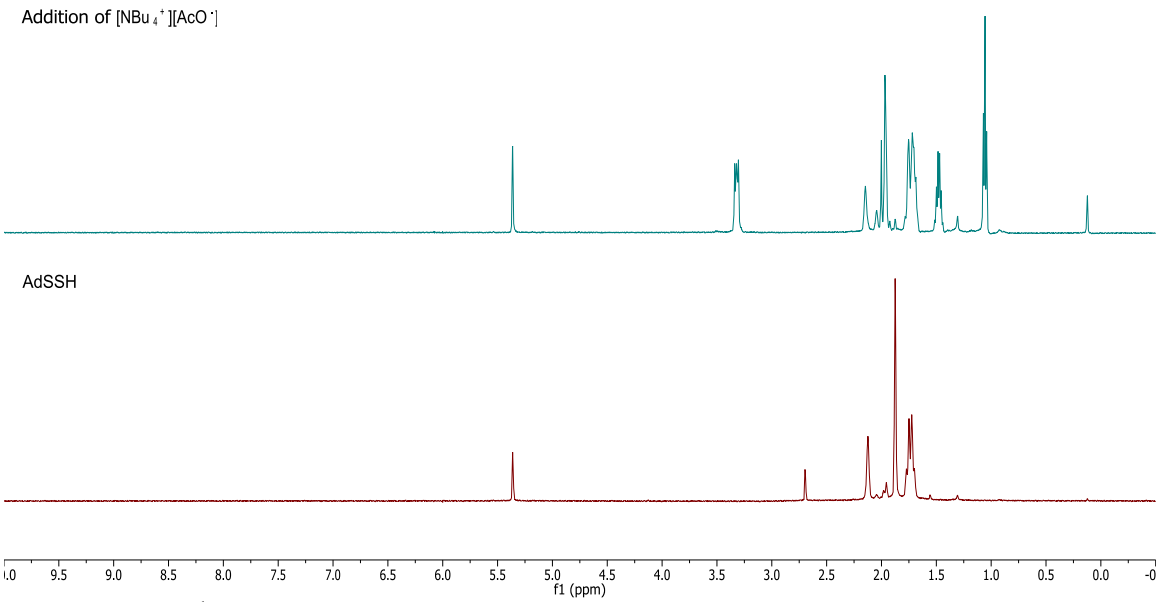

Figure C51. ^{1}H (500 MHz, CD_2Cl_2) NMR spectra of AdSSH upon addition of $[NBu_4^+][AcO^-]$. New peaks in the ^{1}H spectrum at 2.06 ppm and 1.96 ppm, corresponding to AdSH are observed during the reaction

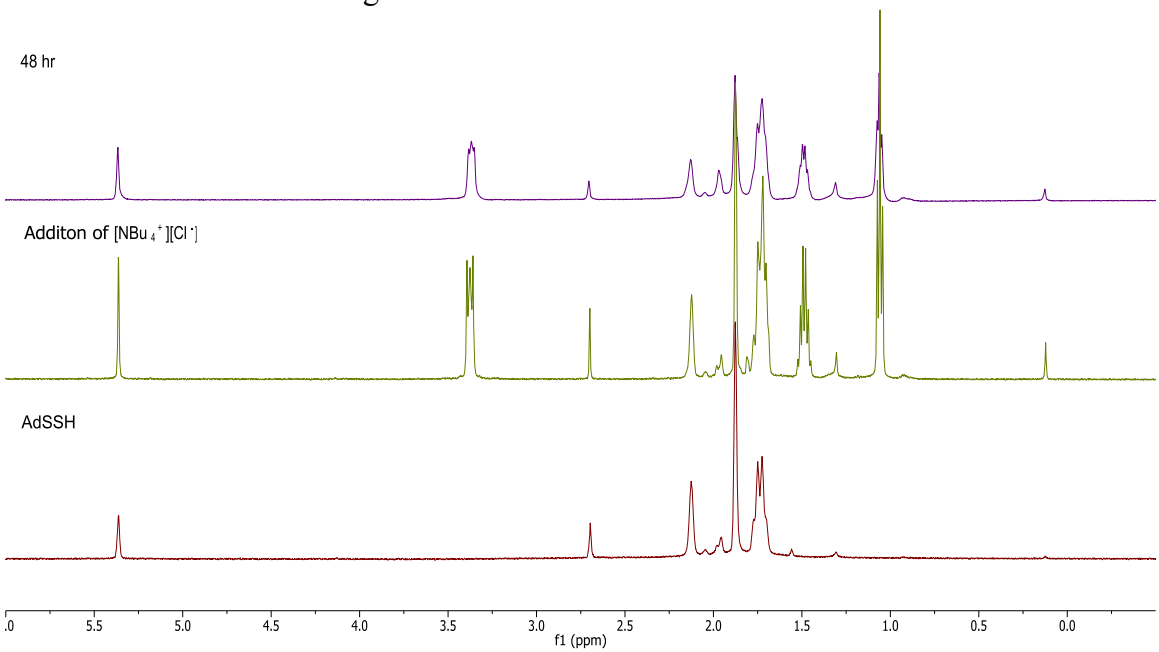

Figure C52. ^{1}H (500 MHz, CD_2Cl_2) NMR spectra of AdSSH upon addition of $[NBu_4^+][Cl^-]$. No reaction with $[NBu_4^+][Cl^-]$is observed after 48 hr.

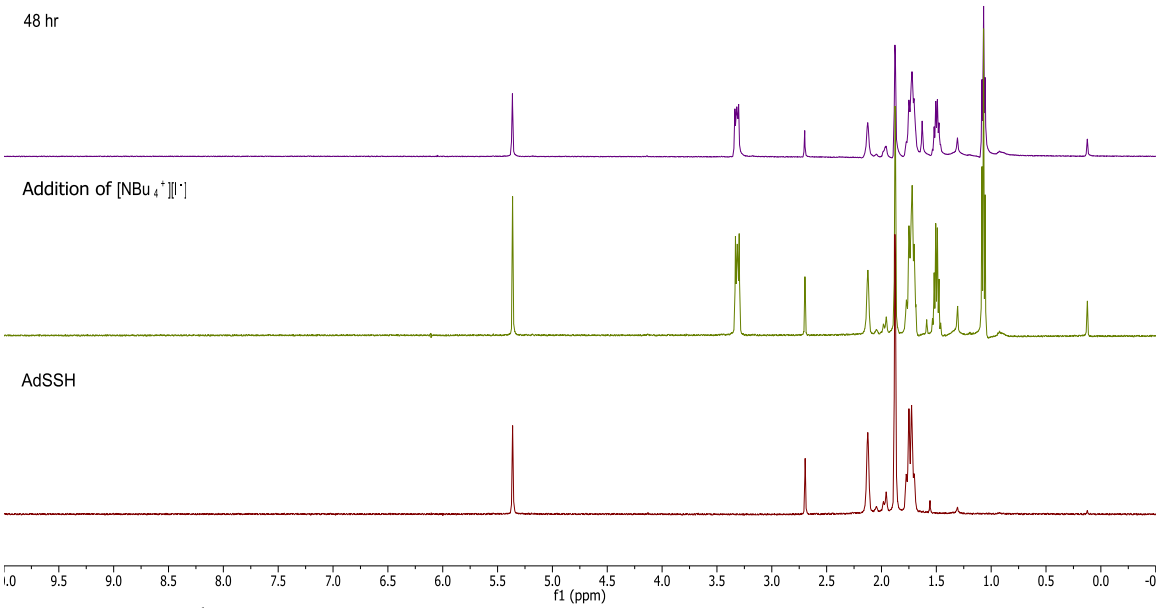

Figure C53. ^{1}H (500 MHz, CD_2Cl_2) NMR spectra of AdSSH upon addition of $[NBu_4^+][I^-]$. No reaction with $[NBu_4^+][I^-]$is observed after 48 hr.

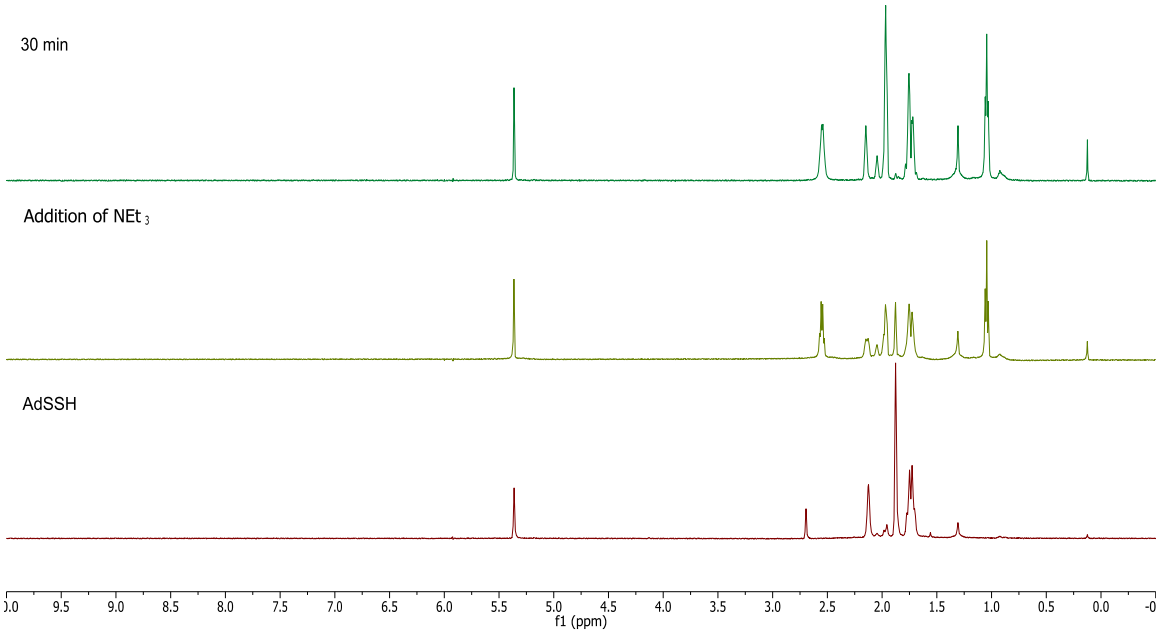

Figure C54. ^{1}H (500 MHz, CD_2Cl_2) NMR spectra of AdSSH upon addition of NEt_3. New peaks in the ^{1}H spectrum at 2.06 ppm and 1.96 ppm, corresponding to AdSH are observed during the reaction.

UV-Vis Spectroscopic Data

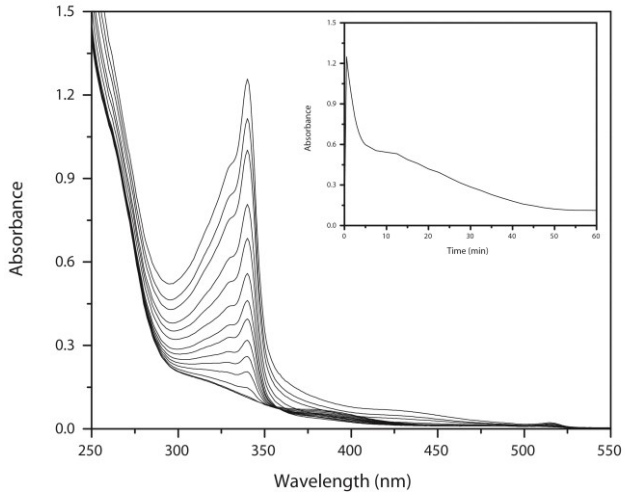

Figure C55: Reaction of TrtSSH with $[NBu_4^+][CN^-]$ monitored by UV-Vis spectroscopy. Condition: 1 mM TrtSSH, 1 mM $[NBu_4^+][CN^-]$, 25 °C in DCM under anaerobic conditions.

X-Ray crystallographic data

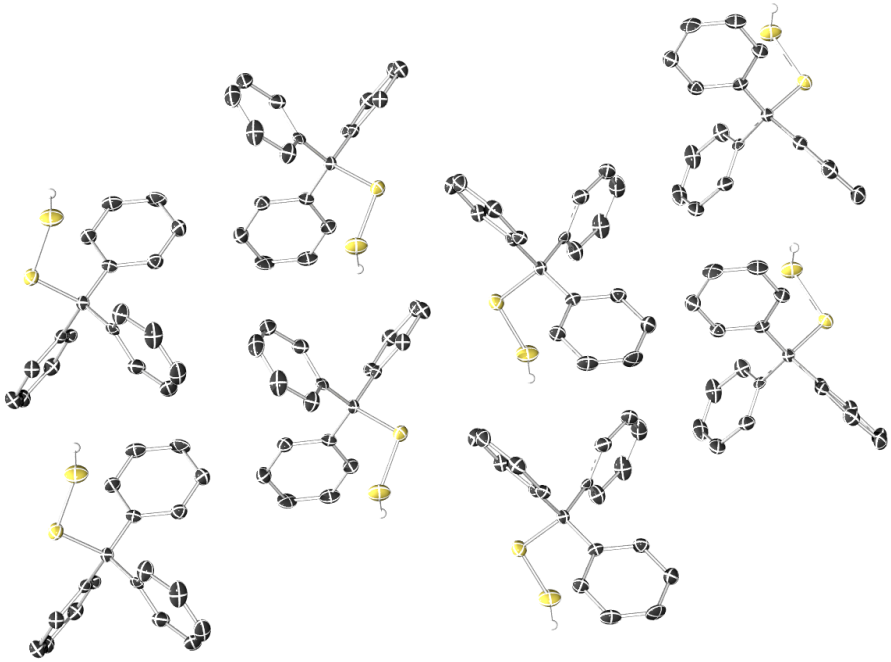

Figure C56: Packing diagram of the x-ray structure of TrtSSH.

Table C1. Crystal data and structure refinement for TrtSSH.

	TrtSSH
Empirical formula	$C_{19}H_{16}S_2$
Formula weight	308.44
Temperature (K)	150(2)
Wavelength (Å)	0.71073
Crystal system, space group	Orthorhombic, $P2_12_12_1$
Unit cell dimensions	a = 7.5037(16) Å; α= 90°
	b = 7.5470(16) Å; β= 90°
	c = 27.3474(6) Å; γ = 90°
Volume (Å^3)	1555.9(6)
Z	4
Calculated density (Mg/m^3)	1.317
Absorption coefficient (mm^{-1})	0.332
F(000)	648
Crystal size (mm)	0.19 x 0.13 x 0.04
Theta range for data collection	2.80 to 26.36°.
Index ranges	$-8 \le h \le 9$, $-9 \le k \le 9$, $-26 \le l \le 34$
Reflections collected	8185
Independent reflections	3154 [R_{int} = 0.0359]
Completeness to θ = 25.00° (%)	99.6
Absorption correction	Semi-empirical from equivalents
Max. and min. transmission	0.9868 and 0.9396
Refinement method	Full-matrix least-squares on F^2
Data / restraints / parameters	3154 / 56 / 259
Goodness-of-fit on F^2	1.025
Final R indices [I>2σ(I)]	R1 = 0.0446, wR2 = 0.1138
R indices (all data)	R1 = 0.0521, wR2 = 0.1179
Absolute structure parameter	0.14(10)
Largest diff. peak and hole (e/Å^{-3})	0.330 and -0.258

APPENDIX D

SUPPORTING INFORMATION: THE INTERSECTION OF NO AND H_2S: PERSULFIDES REACT WITH NITRITE TO PRODUCE NO

UV-Vis Data

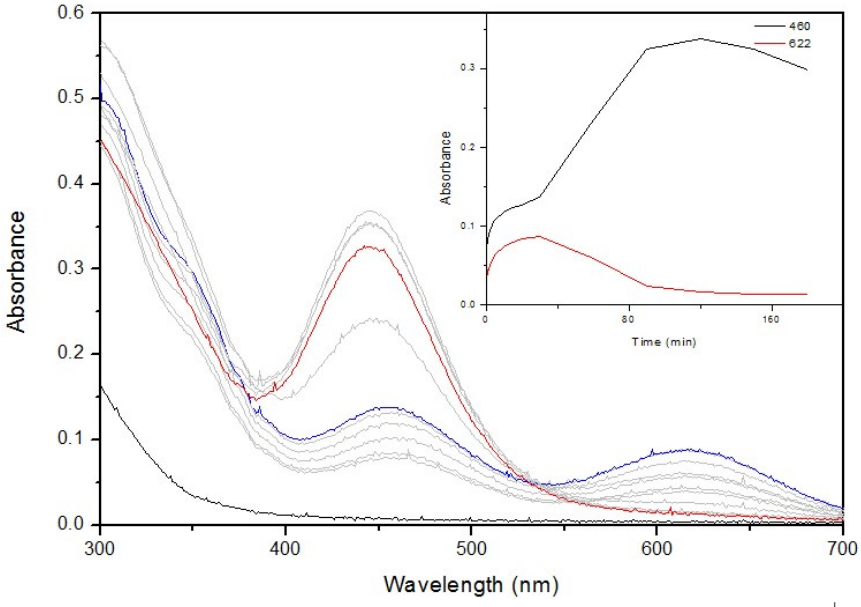

Figure D1. Reaction of 500 μM BnSSH (black trace) with 500 μM $[NBu_4^+][NO_2^-]$. The 617 nm species reaches its maximum intensity after 25 min (blue trace), at which time the band begins to decrease in intensity, with concurrent increase in the band at 446 nm. The reaction was monitored for 180 min (red trace) Inset: The intensity of the 620 nm (red) and the 446 nm (black band with respect to time

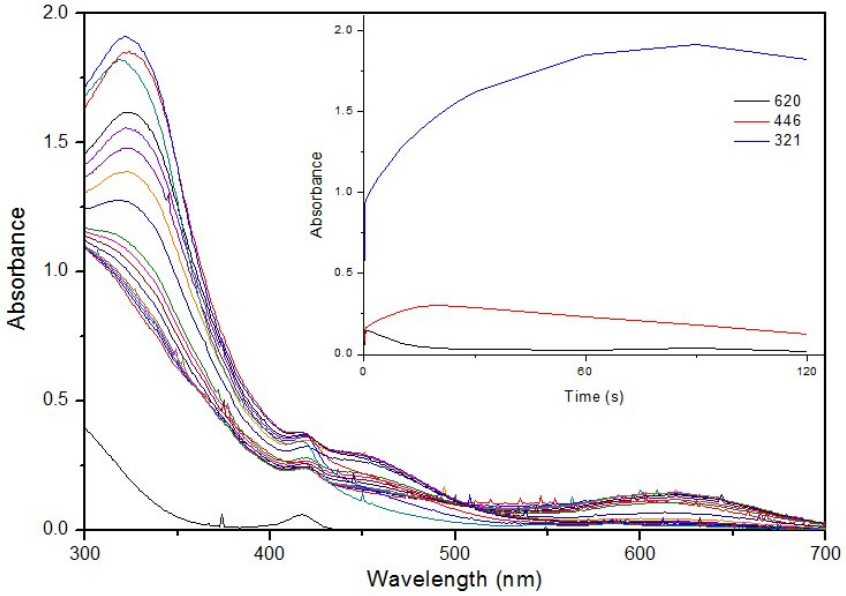

Figure D2. Reaction of 500 μM TrtSSH (black trace) with 500 μM $[PNP^+][NO_2^-]$. The 617 nm species reaches its maximum intensity after 1 min, at which time the band begins to decrease in intensity, with concurrent increase in the band at 446 nm. The reaction was monitored for 120 min. Inset: The intensity of the 620 nm (black) and the 446 nm (red) band with respect to time

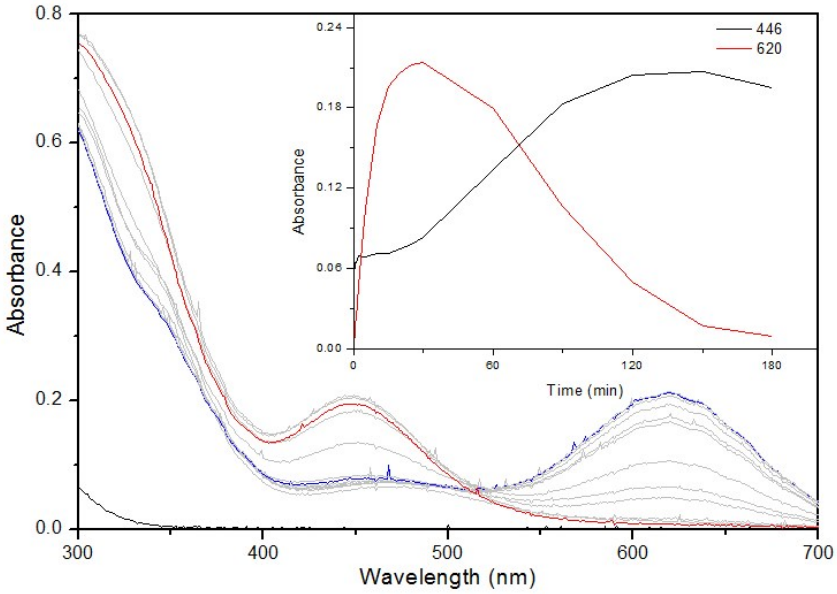

Figure D3. Reaction of 500 μM AdSSH (black trace) with 500 μM [PNP^+][NO_2^-]. The 617 nm species reaches its maximum intensity after 25 min (blue trace), at which time the band begins to decrease in intensity, with concurrent increase in the band at 446 nm. The reaction was monitored for 180 min (red trace) Inset: The intensity of the 620 nm (red) and the 446 nm (black band with respect to time

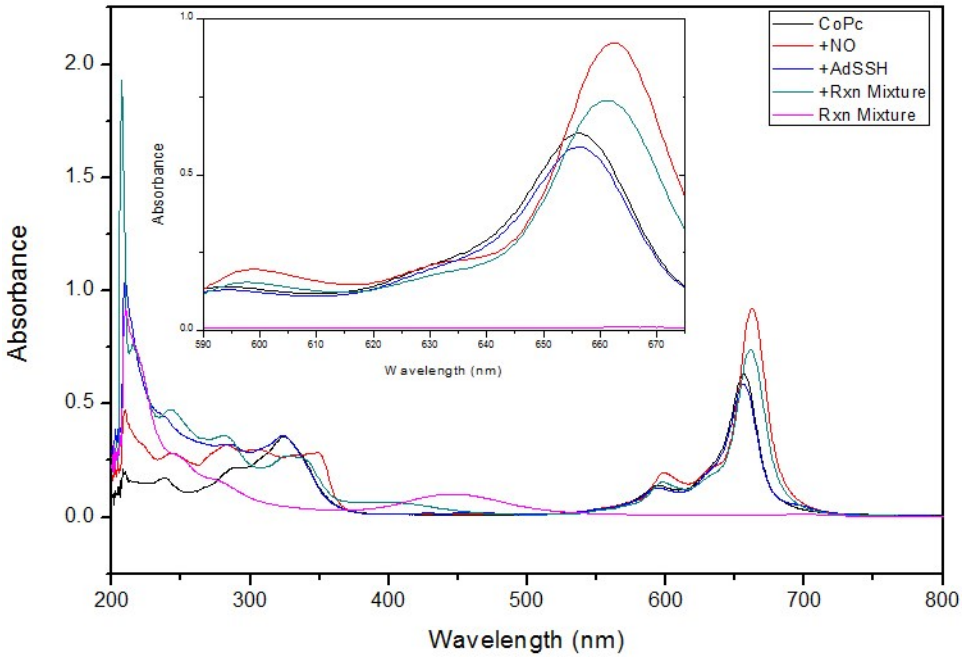

Figure D4. Measurement of $NO_{(g)}$ formation using CoPc (purple trace). 50 μL of a reaction mixture between 500 μM AdSSH with 500 μM [NBu_4^+][NO_2^-] (pink) was added to a 10 μM solution of CoPc (green) resulting in a 7 nm bathochomic shift of the soret band from 656 nm to 663 nm. This is consistent with addition of authentic $NO_{(g)}$ to CoPc (red) and not of addition of persulfides alone (blue).

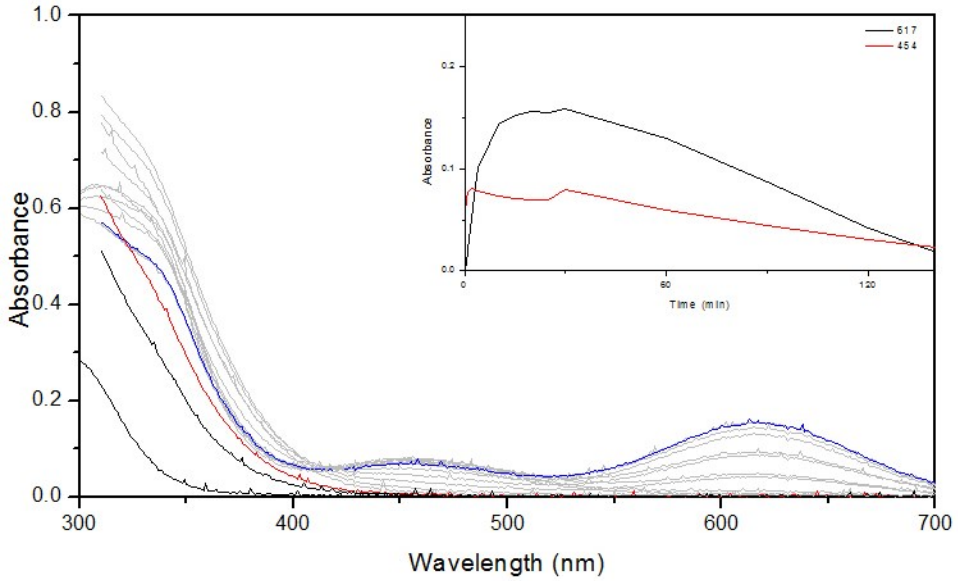

Figure D5. Production of $[S_3^{\bullet}]^-$ from AdSSH using $[NBu_4^+][AcO^-]$. The reaction between 500 μM AdSSH (black trace) and 500 mM $[NBu_4^+][AcO^-]$ was followed for 150 min. After 20 min the band at 617 nm reaches its maximum intensity (blue trace), before returning to baseline levels (red trace).

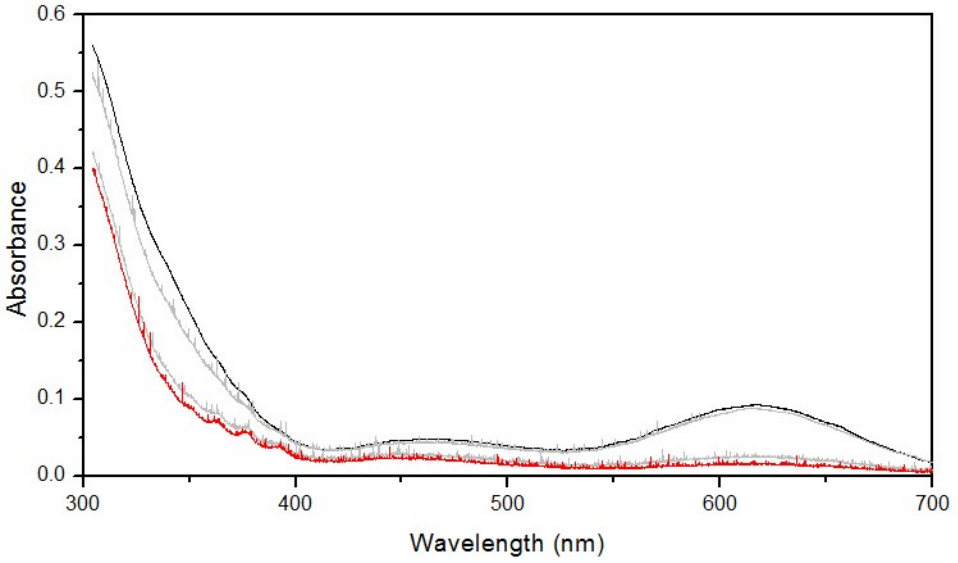

Figure D6. Quenching of $[S_3^{\bullet}]^-$ intermediate by BnCl. 500 μM AdSSH and 500 mM $[NBu_4^+][NO_2^-]$ were allowed to react for 20 min (blue trace). 5 equiv. of BnCl were added to the reaction mixture and the reaction was observed for 10 min, after which the absorbance at 617 nm has completely disappeared (red trace)

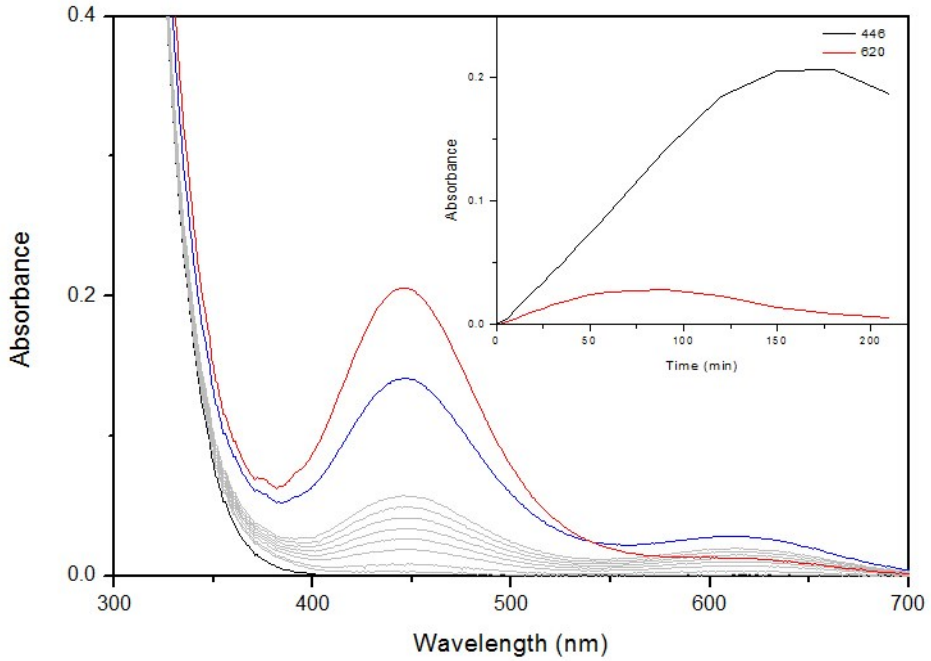

Figure D7. Reaction of 500 μM S_8 (black trace) with 500 μM $[NBu_4^+][NO_2^-]$. The 617 nm species reaches its maximum intensity after 100 min (blue trace), while the 446 nm species grows consistently throughout, reaching a maximum intensity after 200 min. The reaction was monitored for 210 min. Inset: The intensity of the 620 nm (red) and the 446 nm (black) band with respect to time.

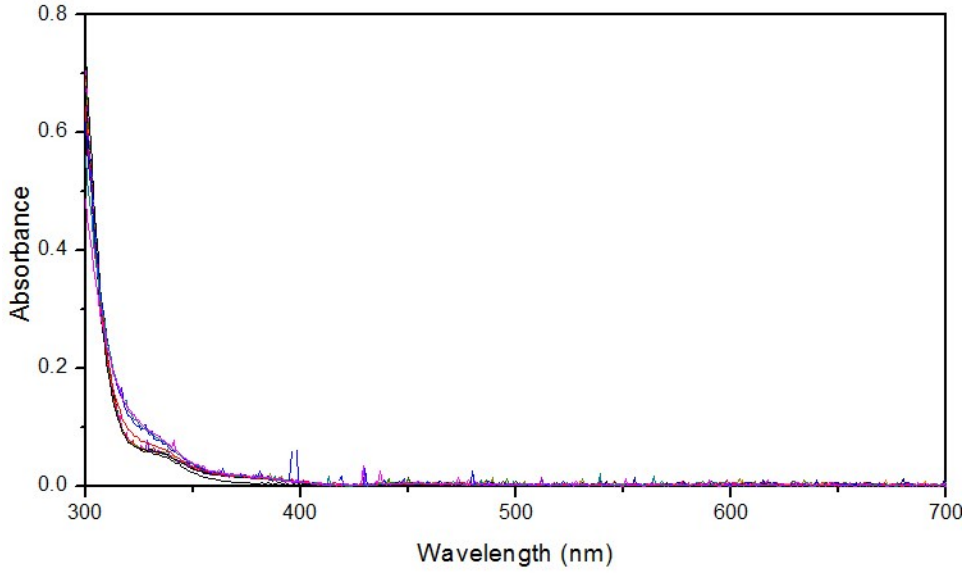

Figure D8. Reaction of 500 μM $[NBu_4^+][HS^-]$ with 500 μM $[NBu_4^+][NO_2^-]$. After 60 min no reaction is observed

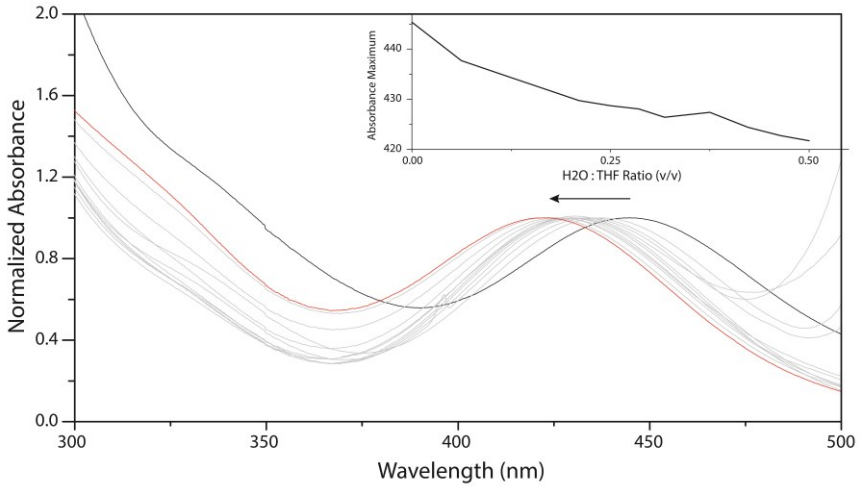

Figure D9. Solvatochromism of $ONSS^-$ in increasingly aqueous solution. $[NBu_4^+][ONSS^-]$ was prepared by addition of NO_g to a solution of $[S_3^{\bullet}]^-$. The UV-Vis spectrum was acquired in solvents ranging from 100% THF (balck trace) to 1:1 THF:H_2O (red trace). The acquired spectra are normalized to 1 at the λ_{max} for the $ONSS^-$ absorbance. Inset: The λ_{max} for the $ONSS^-$ absorbance. with respect to H_2O:THF ratio.

NMR Spectra

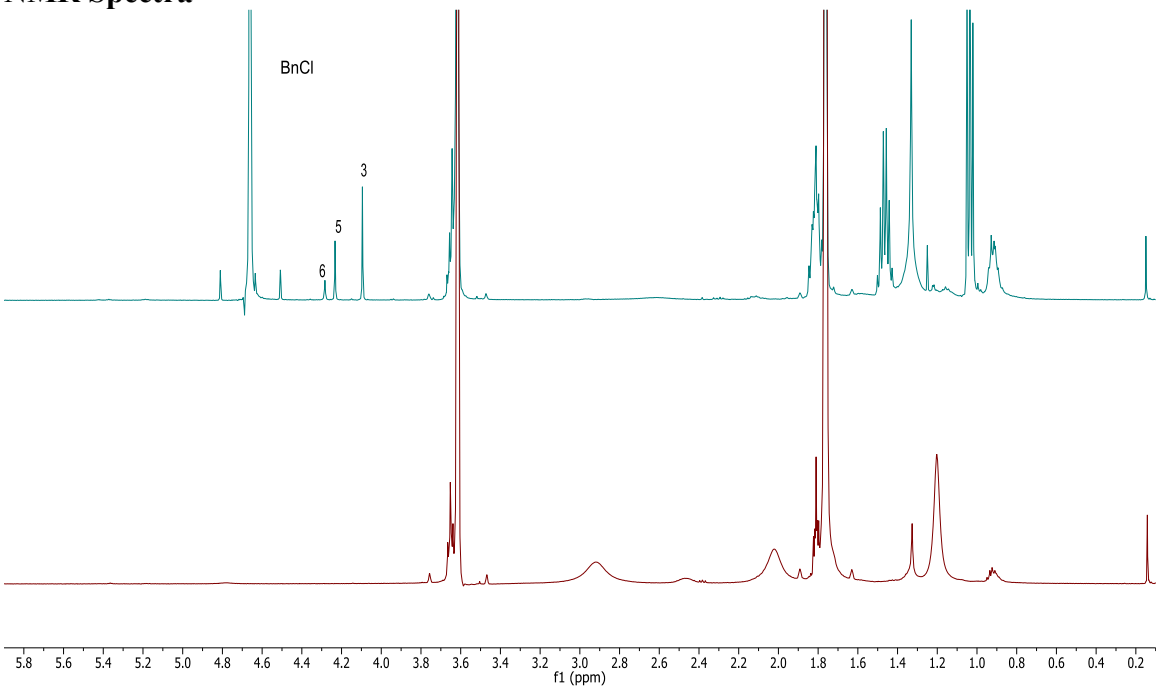

Figure D10. Quenching of $[S_3^{\bullet}]^-$ with BnCl in d_8-THF. Red: 30 mM S_8 treated with 6 mM $[NBu_4^+][HS^-]$. The broadened peaks for $[NBu_4^+]$ are the result of paramagnetic $[S_3^{\bullet}]^-$ in solution. Blue: Addition of Excess BnCl reveals 3 trappable polsulfide species in solution: S_3, S_5, and S_6.

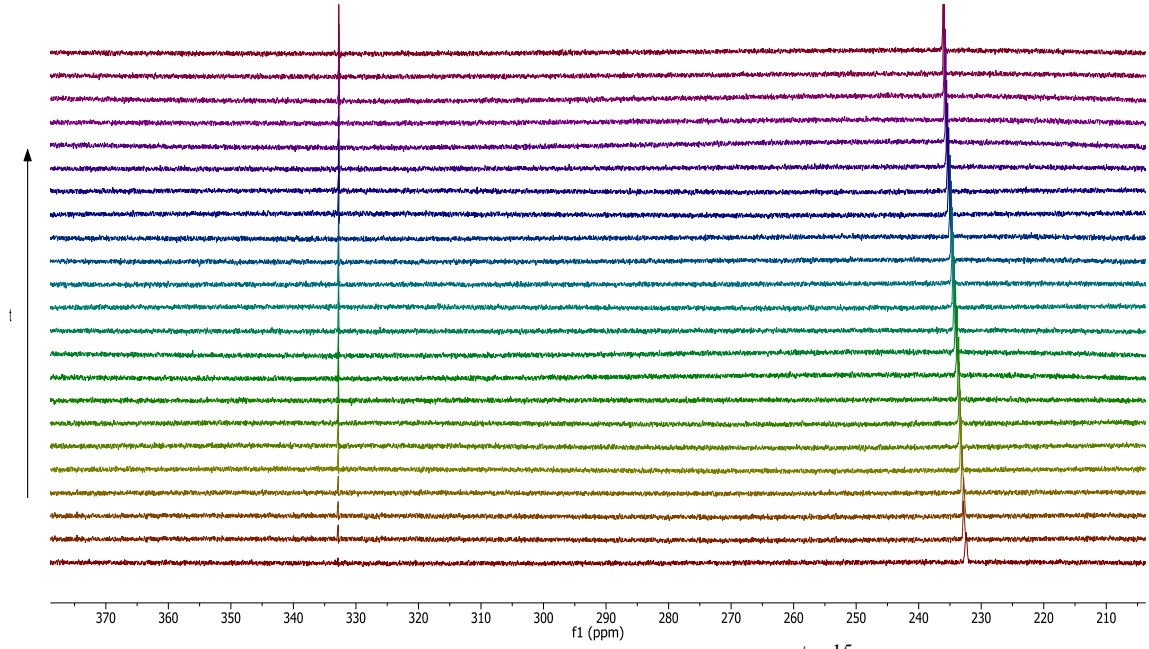

Figure D11. Reaction of 50 mM AdSSH with 50 mM $[NBu_4^+][^{15}NO_2^-]$ in d_8-THF. The reaction was monitored for 13 hr, with each spectrum being the average of 50 scans with a relaxation delay of 5s. The only observed species during the treaction time course are $[NBu_4^+][^{15}NO_2^-]$ and $[NBu_4^+][^{15}ONSS^-]$.

REFERENCES CITED

1) Wignall, P. B.; Twitchett, R. J. *Science* **1996**, *272*, 1155.

2) Kump, L. R.; Pavlov, A.; Arthur, M. A. *Geology* **2005**, *33*, 397.

3) Beauchamp, R. O.; Bus, J. S.; Popp, J. A.; Boreiko, C. J.; Andjelkovich, D. A.; Leber, P. *CRC Critical Reviews in Toxicology* **1984**, *13*, 25.

4) Wang, R. *Physiol Rev* **2012**, *92*, 791.

5) Kamoun, P. *Amino acids* **2004**, *26*, 243.

6) Shibuya, N.; Koike, S.; Tanaka, M.; Ishigami-Yuasa, M.; Kimura, Y.; Ogasawara, Y.; Fukui, K.; Nagahara, N.; Kimura, H. *Nature communications* **2013**, *4*, 1366.

7) Levitt, M. D.; Abdel-Rehim, M. S.; Furne, J. *Antioxidants & redox signaling* **2011**, *15*, 373.

8) Furne, J.; Saeed, A.; Levitt, M. D. *American journal of physiology. Regulatory, integrative and comparative physiology* **2008**, *295*, R1479.

9) Jiang, B.; Tang, G. H.; Cao, K.; Wu, L. Y.; Wang, R. *Antioxidants & redox signaling* **2010**, *12*, 1167.

10) Pietri, R.; Roman-Morales, E.; Lopez-Garriga, J. *Antioxid. Redox Signaling* **2011**, *15*, 393.

11) Li, Q.; Lancaster Jr, J. R. *Nitric Oxide* **2013**, *35*, 21.

12) Ubuka, T. *Journal of Chromatography B* **2002**, *781*, 227.

13) Whiteman, M.; Moore, P. K. *Journal of cellular and molecular medicine* **2009**, *13*, 488.

14) Shen, X.; Pattillo, C. B.; Pardue, S.; Bir, S. C.; Wang, R.; Kevil, C. G. *Free Radical Biology and Medicine* **2011**, *50*, 1021.

15) Shen, X.; Peter, E. A.; Bir, S.; Wang, R.; Kevil, C. G. *Free radical biology & medicine* **2012**, *52*, 2276.

16) Lin, V. S.; Chen, W.; Xian, M.; Chang, C. J. *Chemical Society Reviews* **2015**, *44*, 4596.

17) Lippert, A. R. *Journal of Inorganic Biochemistry* **2014**, *133*, 136.

18) Jung, H. S.; Chen, X.; Kim, J. S.; Yoon, J. *Chemical Society Reviews* **2013**, *42*, 6019.

19) Li, W.; Sun, W.; Yu, X.; Du, L.; Li, M. *J Fluoresc* **2013**, *23*, 181.

20) Sawa, M.; Hsu, T.-L.; Itoh, T.; Sugiyama, M.; Hanson, S. R.; Vogt, P. K.; Wong, C.-H. *Proceedings of the National Academy of Sciences of the United States of America* **2006**, *103*, 12371.

21) Song, Z. J.; Ng, M. Y.; Lee, Z.-W.; Dai, W.; Hagen, T.; Moore, P. K.; Huang, D.; Deng, L.-W.; Tan, C.-H. *MedChemComm* **2014**, *5*, 557.

22) Mok, Y.-Y. P.; Mohammed Atan, M. S. B.; Ping, C. Y.; Jing, W. Z.; Bhatia, M.; Moochhala, S.; Moore, P. K. *British Journal of Pharmacology* **2004**, *143*, 881.

23) Du, J.; Huang, Y.; Yan, H.; Zhang, Q.; Zhao, M.; Zhu, M.; Liu, J.; Chen, S. X.; Bu, D.; Tang, C.; Jin, H. *Journal of Biological Chemistry* **2014**, *289*, 9741.

24) Ida, T.; Sawa, T.; Ihara, H.; Tsuchiya, Y.; Watanabe, Y.; Kumagai, Y.; Suematsu, M.; Motohashi, H.; Fujii, S.; Matsunaga, T.; Yamamoto, M.; Ono, K.; Devarie-Baez, N. O.; Xian, M.; Fukuto, J. M.; Akaike, T. *Proceedings of the National Academy of Sciences of the United States of America* **2014**, *111*, 7606.

25) Ono, K.; Akaike, T.; Sawa, T.; Kumagai, Y.; Wink, D. A.; Tantillo, D. J.; Hobbs, A. J.; Nagy, P.; Xian, M.; Lin, J.; Fukuto, J. M. *Free Radical Biology and Medicine* **2014**, *77*, 82.

26) Pan, J.; Carroll, K. S. *ACS Chem. Biol.* **2013**, *8*, 1110.

27) Mustafa, A. K.; Gadalla, M. M.; Sen, N.; Kim, S.; Mu, W.; Gazi, S. K.; Barrow, R. K.; Yang, G.; Wang, R.; Snyder, S. H. *Science signaling* **2009**, *2*, ra72.

28) Park, C.-M.; Weerasinghe, L.; Day, J. J.; Fukuto, J. M.; Xian, M. *Mol. Biosys.* **2015**, *11*, 1775.

29) Francoleon, N. E.; Carrington, S. J.; Fukuto, J. M. *Arch. Biochem. Biophys.* **2011**, *516*, 146.

30) Wang, R. *Physiol. Rev.* **2012**, *92*, 791.

31) Vandiver, M. S.; Paul, B. D.; Xu, R.; Karuppagounder, S.; Rao, F.; Snowman, A. M.; Seok Ko, H.; Il Lee, Y.; Dawson, V. L.; Dawson, T. M.; Sen, N.; Snyder, S. H. *Nat Commun* **2013**, *4*, 1626.

32) Kimura, Y.; Mikami, Y.; Osumi, K.; Tsugane, M.; Oka, J.-I.; Kimura, H. *The FASEB Journal* **2013**, *27*, 2451.

33) Koike, S.; Ogasawara, Y.; Shibuya, N.; Kimura, H.; Ishii, K. *FEBS Letters* **2013**, *587*, 3548.

34) Mustafa, A. K.; Gadalla, M. M.; Sen, N.; Kim, S.; Mu, W.; Gazi, S. K.; Barrow, R. K.; Yang, G.; Wang, R.; Snyder, S. H. *Sci. Signal.* **2009**, *2*, ra72.

35) Bailey, T. S.; Zakharov, L. N.; Pluth, M. D. *J. Am. Chem. Soc.* **2014**, *136*, 10573.

36) Ida, T.; Sawa, T.; Ihara, H.; Tsuchiya, Y.; Watanabe, Y.; Kumagai, Y.; Suematsu, M.; Motohashi, H.; Fujii, S.; Matsunaga, T.; Yamamoto, M.; Ono, K.; Devarie-Baez, N. O.; Xian, M.; Fukuto, J. M.; Akaike, T. *Proc. Natl. Acad. Sci. USA* **2014**, *111*, 7606.

37) Ishigami, M.; Hiraki, K.; Umemura, K.; Ogasawara, Y.; Ishii, K.; Kimura, H. *Antioxidants & Redox Signaling* **2009**, *11*, 205.

38) Pollegioni, L.; Piubelli, L.; Sacchi, S.; Pilone, M. S.; Molla, G. *Cell. Mol. Life Sci.* **2007**, *64*, 1373.

39) Tedeschi, G.; Pollegioni, L.; Negri, A. In *Unnatural Amino Acids*; Pollegioni, L., Servi, S., Eds.; Humana Press: 2012; Vol. 794, p 381.

40) Wu, W.; Li, J.; Chen, L.; Ma, Z.; Zhang, W.; Liu, Z.; Cheng, Y.; Du, L.; Li, M. *Analytical Chemistry* **2014**.

41) Van de Bittner, G. C.; Dubikovskaya, E. A.; Bertozzi, C. R.; Chang, C. J. *Proceedings of the National Academy of Sciences* **2010**, *107*, 21316.

42) Yao, Z.; Bai, H.; Li, C.; Shi, G. *Chemical Communications* **2011**, *47*, 7431.

43) Van de Bittner, G. C.; Bertozzi, C. R.; Chang, C. J. *Journal of the American Chemical Society* **2013**, *135*, 1783.

44) Ren, H.; Xiao, F.; Zhan, K.; Kim, Y.-P.; Xie, H.; Xia, Z.; Rao, J. *Angewandte Chemie* **2009**, *121*, 9838.

45) Nguyen, D. P.; Elliott, T.; Holt, M.; Muir, T. W.; Chin, J. W. *Journal of the American Chemical Society* **2011**, *133*, 11418.

46) Baskin, J. M.; Prescher, J. A.; Laughlin, S. T.; Agard, N. J.; Chang, P. V.; Miller, I. A.; Lo, A.; Codelli, J. A.; Bertozzi, C. R. *Proceedings of the National Academy of Sciences* **2007**, *104*, 16793.

47) Abe, K.; Kimura, H. *Journal of Neuroscience* **1996**, *16*, 1066.

48) Whiteman, M.; Moore, P. K. *Journal of cellular and molecular medicine* **2009**, *13*, 488.

49) Wallace, J. L.; Dicay, M.; McKnight, W.; Martin, G. R. *The FASEB Journal* **2007**, *21*, 4070.

50) Wang, R. *Kidney international* **2009**, *76*, 700.

51) Yang, G. D.; Wu, L. Y.; Jiang, B.; Yang, W.; Qi, J. S.; Cao, K.; Meng, Q. H.; Mustafa, A. K.; Mu, W. T.; Zhang, S. M.; Snyder, S. H.; Wang, R. *Science* **2008**, *322*, 587.

52) Wu, L. Y.; Yang, W.; Jia, X. M.; Yang, G. D.; Duridanova, D.; Cao, K.; Wang, R. *Laboratory Investigation* **2009**, *89*, 59.

53) Chen, C.-Q.; Xin, H.; Zhu, Y.-Z. *Acta Pharmacol Sin* **2007**, *28*, 1709.

54) Qu, K.; Lee, S. W.; Bian, J. S.; Low, C. M.; Wong, P. T. H. *Neurochemistry International* **2008**, *52*, 155.

55) Filipovic, M. R.; Miljkovic, J. L.; Nauser, T.; Royzen, M.; Klos, K.; Shubina, T.; Koppenol, W. H.; Lippard, S. J.; Ivanovic-Burmazovic, I. *Journal of the American Chemical Society* **2012**, *134*, 12016.

56) DeLeon, E. R.; Stoy, G. F.; Olson, K. R. *Analytical Biochemistry* **2012**, *421*, 203.

57) J. K. Fogo; Popowsky, M. *Anal. Chem.* **1947**, *21*, 732.

58) Lawrence, N. S.; Davis, J.; Compton, R. G. *Talanta* **2000**, *52*, 771.

59) Qian, Y.; Karpus, J.; Kabil, O.; Zhang, S. Y.; Zhu, H. L.; Banerjee, R.; Zhao, J.; He, C. *Nat. Commun.* **2011**, *2*.

60) Liu, C. R.; Pan, J.; Li, S.; Zhao, Y.; Wu, L. Y.; Berkman, C. E.; Whorton, A. R.; Xian, M. *Angewandte Chemie-International Edition* **2011**, *50*, 10327.

61) Chen, Y.; Zhu, C.; Yang, Z.; Chen, J.; He, Y.; Jiao, Y.; He, W.; Qiu, L.; Cen, J.; Guo, Z. *Angewandte Chemie International Edition* **2013**, *52*, 1688.

62) Montoya, L. A.; Pearce, T. F.; Hansen, R. J.; Zakharov, L. N.; Pluth, M. D. *Journal of Organic Chemistry* **2013**, *78*, 6550.

63) Sasakura, K.; Hanaoka, K.; Shibuya, N.; Mikami, Y.; Kimura, Y.; Komatsu, T.; Ueno, T.; Terai, T.; Kimura, H.; Nagano, T. *Journal of the American Chemical Society* **2011**, *133*, 18003.

64) Lippert, A. R.; New, E. J.; Chang, C. J. *Journal of the American Chemical Society* **2011**, *133*, 10078.

65) Montoya, L. A.; Pluth, M. D. *Chemical Communications* **2012**, *48*, 4767.

66) Peng, H.; Cheng, Y.; Dai, C.; King, A. L.; Predmore, B. L.; Lefer, D. J.; Wang, B. *Angewandte Chemie International Edition* **2011**, *50*, 9672.

67) Thorson, M. K.; Majtan, T.; Kraus, J. P.; Barrios, A. M. *Angewandte Chemie-International Edition* **2013**, *52*, 4641.

68) Liu, T.; Xu, Z.; Spring, D. R.; Cui, J. *Organic Letters* **2013**, *15*, 2310.

69) Bae, S. K.; Heo, C. H.; Choi, D. J.; Sen, D.; Joe, E.-H.; Cho, B. R.; Kim, H. M. *Journal of the American Chemical Society* **2013**, *135*, 9915.

70) Chen, S.; Chen, Z.-J.; Ren, W.; Ai, H.-W. *Journal of the American Chemical Society* **2012**, *134*, 9589.

71) Lin, V. S.; Lippert, A. R.; Chang, C. J. *Proceedings of the National Academy of Sciences* **2013**, *110*, 7131.

72) Lin, V. S.; Chang, C. J. *Current Opinion in Chemical Biology* **2012**, *16*, 595.

73) Chen, B.; Li, W.; Lv, C.; Zhao, M.; Jin, H.; Jin, H.; Du, J.; Zhang, L.; Tang, X. *Analyst* **2013**, *138*, 946.

74) Williams, E. J.; Campbell, A. K. *Analytical Biochemistry* **1986**, *155*, 249.

75) Yuan, H.; Chong, H.; Wang, B.; Zhu, C.; Liu, L.; Yang, Q.; Lv, F.; Wang, S. *Journal of the American Chemical Society* **2012**, *134*, 13184.

76) Yan, X. *Journal of Separation Science* **2006**, *29*, 1931.

77) Thurbide, K. B.; Aue, W. A. *Spectrochimica Acta Part B: Atomic Spectroscopy* **2002**, *57*, 843.

78) Garcia, I. L.; Vinas, P.; Gil, J. A. M. *Fresenius J. Anal. Chem.* **1993**, *345*, 723.

79) McCutcheon, D. C.; Paley, M. A.; Steinhardt, R. C.; Prescher, J. A. *Journal of the American Chemical Society* **2012**, *134*, 7604.

80) Sun, Y. Q.; Liu, J.; Wang, P.; Zhang, J.; Guo, W. *Angewandte Chemie-International Edition* **2012**, *51*, 8428.

81) Van de Bittner, G. C.; Dubikovskaya, E. A.; Bertozzi, C. R.; Chang, C. J. *Proceedings of the National Academy of Sciences* **2010**, *107*, 21316.

82) Yamaguchi, S.; Kishikawa, N.; Ohyama, K.; Ohba, Y.; Kohno, M.; Masuda, T.; Takadate, A.; Nakashima, K.; Kuroda, N. *Analytica Chimica Acta* **2010**, *665*, 74.

83) Lee, D. W.; Erigala, V. R.; Dasari, M.; Yu, J. H.; Dickson, R. M.; Murthy, N. *Int. J. Nanomed.* **2008**, *3*, 471.

84) Zhang, X.; Zhou, H.; Ding, C.; Zhang, S. *Chem. Commun.* **2009**, *0*, 5624.

85) Díaz, A. N.; Sánchez, F. G.; González Garcia, J. A. *Journal of Bioluminescence and Chemiluminescence* **1998**, *13*, 75.

86) Dodeigne, C.; Thunus, L.; Lejeune, R. *Talanta* **2000**, *51*, 415.

87) White, E. H.; Roswell, D. F. *Accounts of Chemical Research* **1970**, *3*, 54.

88) Drew, H. D. K.; Garwood, R. F. *J. Chem. Soc.* **1939**, *0*, 836.

89) Chen, G. N.; Lin, R. E.; Zhuang, H. S.; Zhao, Z. F.; Xu, X. Q.; Zhang, F. *Analytica Chimica Acta* **1998**, *375*, 269.

90) Omote, Y.; Miyake, T.; Ohmori, S.; Sugiyama, N. *Bulletin of the Chemical Society of Japan* **1966**, *39*, 932.

91) Chen, Y.-H.; Yao, W.-Z.; Geng, B.; Ding, Y.-L.; Lu, M.; Zhao, M.-W.; Tang, C.-S. *CHEST Journal* **2005**, *128*, 3205.

92) Hyšpler, R. r.; Tichá, A.; Indrová, M.; Zadák, Z.; Hyšplerová, L.; Gasparič, J.; Churáček, J. *J. Chromatogr. B* **2002**, *770*, 255.

93) Savage, J. C.; Gould, D. H. *Journal of Chromatography B: Biomedical Sciences and Applications* **1990**, *526*, 540.

94) Wang, R. *The FASEB Journal* **2002**, *16*, 1792.

95) Cartwright, I. L.; Hutchinson, D. W.; Armstrong, V. W. *Nucleic Acids Research* **1976**, *3*, 2331.

96) Aitken, C. E.; Marshall, R. A.; Puglisi, J. D. *Biophysical Journal* **2008**, *94*, 1826.

97) Jocelyn, P. C. *European Journal of Biochemistry* **1967**, *2*, 327.

98) CLSS-1 and CLSS-2, like other azides, are incompatible with dithiols such as DTT (see reference 54) and phosphine-based reducing agents such as TCEP. For additional examples of this incompatibility, see the Staundinger reaction, .

99) Abushqara, E.; Blum, J. *Journal of Heterocyclic Chemistry* **1990**, *27*, 1197.

100) Baird, P. D.; Dho, J. C.; Fleet, G. W. J.; Peach, J. M.; Prout, K.; Smith, P. W. *Journal of the Chemical Society-Perkin Transactions 1* **1987**, 1785.

101) Darbon, N.; Oddon, Y.; Guy, E.; Ferrari, B.; Pavia, A. A.; Pepe, G.; Reboul, J. P. *Acta Crystallographica Section C-Crystal Structure Communications* **1985**, *41*, 1100.

102) Tchertanov, L. *Acta Crystallographica Section B-Structural Science* **1999**, *55*, 807.

103) Paradies, H. H. *Berichte der Bunsengesellschaft für Physikalische Chemie* **1992**, *96*, 1027.

104) Thordarson, P. *Chemical Society Reviews* **2011**, *40*, 1305.

105) CSE produces H2S 5-times faster using Hcy as a substrate compared to Cys.

106) Pfeffer, M.; Ressler, C. *Biochemical Pharmacology* **1967**, *16*, 2299.

107) Faccenda, A.; Wang, J.; Mutus, B. *Analytical Chemistry* **2012**, *84*, 5243.

108) Kandil, S.; Brennan, L.; McBean, G. J. *Neurochemistry International* **2010**, *56*, 611.

109) Tian, X.; Li, Z.; Lau, C.; Lu, J. *Analytical Chemistry* **2015**, *87*, 11325.

110) Ke, B.; Wu, W.; Liu, W.; Liang, H.; Gong, D.; Hu, X.; Li, M. *Analytical Chemistry* **2016**, *88*, 592.

111) Allen, C. R.; Richard, P. L.; Ward, A. J.; van de Water, L. G. A.; Masters, A. F.; Maschmeyer, T. *Tetrahedron Letters* **2006**, *47*, 7367.

112) Gaussian 09, Revision C.01, Frisch, M. J.; Trucks, G. W.; Schlegel, H. B.; Scuseria, G. E.; Robb, M. A.; Cheeseman, J. R.; Scalmani, G.; Barone, V.; Mennucci, B.; Petersson, G. A.; Nakatsuji, H.; Caricato, M.; Li, X.; Hratchian, H. P.; Izmaylov, A. F.; Bloino, J.; Zheng, G.; Sonnenberg, J. L.; Hada, M.; Ehara, M.; Toyota, K.; Fukuda, R.; Hasegawa, J.; Ishida, M.; Nakajima, T.; Honda, Y.; Kitao, O.; Nakai, H.; Vreven, T.; Montgomery, Jr., J. A.; Peralta, J. E.; Ogliaro, F.; Bearpark, M.; Heyd, J. J.; Brothers, E.; Kudin, K. N.; Staroverov, V. N.; Kobayashi, R.; Normand, J.; Raghavachari, K.; Rendell, A.; Burant, J. C.; Iyengar, S. S.; Tomasi, J.; Cossi, M.; Rega, N.; Millam, J. M.; Klene, M.; Knox, J. E.; Cross, J. B.; Bakken, V.; Adamo, C.; Jaramillo, J.; Gomperts, R.; Stratmann, R. E.; Yazyev, O.; Austin, A. J.; Cammi, R.; Pomelli, C.; Ochterski, J. W.;

Martin, R. L.; Morokuma, K.; Zakrzewski, V. G.; Voth, G. A.; Salvador, P.; Dannenberg, J. J.; Dapprich, S.; Daniels, A. D.; Farkas, Ö.; Foresman, J. B.; Ortiz, J. V.; Cioslowski, J.; Fox, D. J. ; Gaussian, Inc., Wallingford CT: 2009.

113) GaussView, Version 5, Dennington, R.; Keith, T.; Millam, J. ; Semichem Inc., Shawnee Mission KS: 2009.

114) Humphrey, W.; Dalke, A.; Schulten, K. *Journal of Molecular Graphics & Modelling* **1996**, *14*, 33.

115) Ahmad, N.; Maitra, S.; Dutta, B. K.; Ahmad, F. *Journal of Environmental Sciences* **2009**, *21*, 1735.

116) White, E. H.; Wörther, H.; Seliger, H. H.; McElroy, W. D. *Journal of the American Chemical Society* **1966**, *88*, 2015.

117) Chen, W.; Liu, C.; Peng, B.; Zhao, Y.; Pacheco, A.; Xian, M. *Chemical Science* **2013**, *4*, 2892.

118) Maclean, K.; Kraus, J. In *Signal Transduction and the Gasotransmitters*; Wang, R., Ed.; Humana Press: 2004, p 275.

119) Furne, J.; Saeed, A.; Levitt, M. D. *Am. J. Physiol. Regul. Integr. Comp. Physiol.* **2008**, *295*, R1479.

120) Zhao, W.; Ndisang, J. F.; Wang, R. *Canadian Journal of Physiology & Pharmacology* **2003**, *81*, 848.

121) Hosoki, R.; Matsuki, N.; Kimura, H. *Biochemical and Biophysical Research Communications* **1997**, *237*, 527.

122) Ishigami, M.; Hiraki, K.; Umemura, K.; Ogasawara, Y.; Ishii, K.; Kimura, H. *Antioxidants & redox signaling* **2009**, *11*, 205.

123) Clausen, T.; Kaiser, J. T.; Steegborn, C.; Huber, R.; Kessler, D. *Proceedings of the National Academy of Sciences* **2000**, *97*, 3856.

124) Johnson, D. C.; Dean, D. R.; Smith, A. D.; Johnson, M. K. *Annual Review of Biochemistry* **2005**, *74*, 247.

125) Shen, X.; Peter, E. A.; Bir, S.; Wang, R.; Kevil, C. G. *Free Radical Biology and Medicine* **2012**, *52*, 2276.

126) Mishanina, T. V.; Libiad, M.; Banerjee, R. *Nat Chem Biol* **2015**, *11*, 457.

127) Mueller, E. G. *Nat Chem Biol* **2006**, *2*, 185.

128) Greiner, R.; Pálinkás, Z.; Bäsell, K.; Becher, D.; Antelmann, H.; Nagy, P.; Dick, T. P. *Antioxidants & Redox Signaling* **2013**, *19*, 1749.

129) Shen, X. G.; Peter, E. A.; Bir, S.; Wang, R.; Kevil, C. G. *Free Radic. Biol. Med.* **2012**, *52*, 2276.

130) Levitt, M. D.; Abdel-Rehim, M. S.; Furne, J. *Antioxid. Redox Signal.* **2011**, *15*, 373.

131) Ishigami, M.; Hiraki, K.; Umemura, K.; Ogasawara, Y.; Ishii, K.; Kimura, H. *Antiox. Redox. Signal.* **2009**, *11*, 205.

132) Wróbel, M.; Sura, P.; Srebro, Z. *Comparative Biochemistry and Physiology Part B: Biochemistry and Molecular Biology* **2000**, *125*, 211.

133) Kessler, D. *FEMS Microbiology Reviews* **2006**, *30*, 825.

134) Mustafa, A. K.; Gadalla, M. M.; Sen, N.; Kim, S.; Mu, W.; Gazi, S. K.; Barrow, R. K.; Yang, G.; Wang, R.; Snyder, S. H. *Sci. Signal.* **2009**, *2*, ra72.

135) Kabil, O.; Banerjee, R. *Journal of Biological Chemistry* **2012**, *287*, 44561.

136) Paul, B. D.; Snyder, S. H. *Nat Rev Mol Cell Biol* **2012**, *13*, 499.

137) Everett, S. A.; Schoeneich, C.; Stewart, J. H.; Asmus, K. D. *The Journal of Physical Chemistry* **1992**, *96*, 306.

138) Ono, K.; Akaike, T.; Sawa, T.; Kumagai, Y.; Wink, D. A.; Tantillo, D. J.; Hobbs, A. J.; Nagy, P.; Xian, M.; Lin, J.; Fukuto, J. M. *Free Radic. Biol. Med.* **2014**, *77*, 82.

139) Zhao, Y.; Bhushan, S.; Yang, C.; Otsuka, H.; Stein, J. D.; Pacheco, A.; Peng, B.; Devarie-Baez, N. O.; Aguilar, H. C.; Lefer, D. J.; Xian, M. *ACS Chem. Biol.* **2013**, *8*, 1283.

140) Artaud, I.; Galardon, E. *ChemBioChem* **2014**, *15*, 2361.

141) Zhang, D.; Macinkovic, I.; Devarie-Baez, N. O.; Pan, J.; Park, C.-M.; Carroll, K. S.; Filipovic, M. R.; Xian, M. *Angewandte Chemie International Edition* **2014**, *53*, 575.

142) Galardon, E.; Padovani, D. *Bioconjugate Chemistry* **2015**, *26*, 1013.

143) Nakabayashi, T.; Tsurugi, J.; Yabuta, T. *J. Org. Chem.* **1964**, *29*, 1236.

144) Tsurugi, J.; Nakabaya.T; Ishihara, T. *J. Org. Chem.* **1965**, *30*, 2707.

145) Kawamura, S.; Kitao, T.; Nakabaya.T; Horii, T.; Tsurugi, J. *J. Org. Chem.* **1968**, *33*, 1179.

146) Tsurugi, J.; Abe, Y.; Nakabaya.T; Kawamura, S.; Kitao, T.; Niwa, M. *J. Org. Chem.* **1970**, *35*, 3263.

147) Kawamura, S.; Horii, T.; Tsurugi, J. *Bull. Chem. Soc. Jap.* **1971**, *44*, 2878.

148) Franzi, R.; Geoffroy, M.; Bernardinelli, G. *Mol. Phys.* **1984**, *52*, 947.

149) Liu, D. K.; Chang, S. G. *Can. J. Chem.* **1987**, *65*, 770.

150) Derbesy, G.; Harpp, D. N.; Rather, B.; Carroll, G. *Sulfur Lett.* **1992**, *14*, 199.

151) Chatterji, T.; Keerthi, K.; Gates, K. S. *Bioorg. Med. Chem. Lett.* **2005**, *15*, 3921.

152) PPh3 reduces S0 to S2– which is trapped as SPPh3. This sulfide can be liberated by hydrolysis. Direct reduction of the hydrodisulfide by PPh3 is more likely than deprotonation followed by reaction with S8 because compounds of similar or higher basicity react with the hydrodisulfide at a much slower rate

153) Libiad, M.; Yadav, P. K.; Vitvitsky, V.; Martinov, M.; Banerjee, R. *Journal of Biological Chemistry* **2014**, *289*, 30901.

154) Hall, C. D.; Tweedy, B. R.; Kayhanian, R.; Lloyd, J. R. *J. Chem. Soc. Perkin Trans. 2* **1992**, 775.

155) Ahrika, A.; Robert, J.; Anouti, M.; Paris, J. *Acta Chem. Scand.* **1999**, *53*, 513.

156) Liu, D. K.; Chang, S. G. *Canadian Journal of Chemistry* **1987**, *65*, 770.

157) Tsurugi, J.; Nakabayashi, T. *The Journal of Organic Chemistry* **1959**, *24*, 807.

158) Heimer, N. E.; Field, L.; Waites, J. A. *The Journal of Organic Chemistry* **1985**, *50*, 4164.

159) Nakabayashi, T.; Tsurugi, J.; Yabuta, T. *The Journal of Organic Chemistry* **1964**, *29*, 1236.

160) Sheldrick, G. *Acta Crystallographica Section A* **2008**, *64*, 112.

161) Sheldrick, G. M.; University of Göttingen: Göttingen, Germany: 2000.

162) Sheldrick, G. M.; University of Göttingen: Göttingen, Germany: 2008.

163) Eberhardt, M.; Dux, M.; Namer, B.; Miljkovic, J.; Cordasic, N.; Will, C.; Kichko, T. I.; de la Roche, J.; Fischer, M.; Suárez, S. A.; Bikiel, D.; Dorsch, K.; Leffler, A.; Babes, A.; Lampert, A.; Lennerz, J. K.; Jacobi, J.; Martí, M. A.; Doctorovich, F.; Högestätt, E. D.; Zygmunt, P. M.; Ivanovic-Burmazovic, I.; Messlinger, K.; Reeh, P.; Filipovic, M. R. *Nat Commun* **2014**, *5*.

164) Coletta, C.; Papapetropoulos, A.; Erdelyi, K.; Olah, G.; Modis, K.; Panopoulos, P.; Asimakopoulou, A.; Gero, D.; Sharina, I.; Martin, E.; Szabo, C. *Proceedings of the National Academy of Sciences of the United States of America* **2012**, *109*, 9161.

165) Wang, R. *Kidney international* **2009**, *76*, 700.

166) Jiang, B.; Tang, G.; Cao, K.; Wu, L.; Wang, R. *Antioxidants & redox signaling* **2010**, *12*, 1167.

167) Zhao, W.; Zhang, J.; Lu, Y.; Wang, R. *The EMBO Journal* **2001**, *20*, 6008.

168) Testai, L.; D'Antongiovanni, V.; Piano, I.; Martelli, A.; Citi, V.; Duranti, E.; Virdis, A.; Blandizzi, C.; Gargini, C.; Breschi, M. C.; Calderone, V. *Nitric Oxide* **2015**, *47*, 25.

169) Heine, C. L.; Schmidt, R.; Geckl, K.; Schrammel, A.; Gesslbauer, B.; Schmidt, K.; Mayer, B.; Gorren, A. C. *The Journal of biological chemistry* **2015**, *290*, 24932.

170) Carballal, S.; Cuevasanta, E.; Yadav, P. K.; Gherasim, C.; Ballou, D. P.; Alvarez, B.; Banerjee, R. *The Journal of biological chemistry* **2016**, *291*, 8004.

171) Bucci, M.; Papapetropoulos, A.; Vellecco, V.; Zhou, Z.; Pyriochou, A.; Roussos, C.; Roviezzo, F.; Brancaleone, V.; Cirino, G. *Arteriosclerosis, thrombosis, and vascular biology* **2010**, *30*, 1998.

172) Bianco, C. L.; Fukuto, J. M. *Proceedings of the National Academy of Sciences of the United States of America* **2015**, *112*, 10573.

173) Cortese-Krott, M. M.; Fernandez, B. O.; Kelm, M.; Butler, A. R.; Feelisch, M. *Nitric Oxide* **2015**, *46*, 14.

174) Whiteman, M.; Li, L.; Kostetski, I.; Chu, S. H.; Siau, J. L.; Bhatia, M.; Moore, P. K. *Biochemical and Biophysical Research Communications* **2006**, *343*, 303.

175) Cortese-Krott, M. M.; Fernandez, B. O.; Santos, J. L.; Mergia, E.; Grman, M.; Nagy, P.; Kelm, M.; Butler, A.; Feelisch, M. *Redox biology* **2014**, *2*, 234.

176) Filipovic, M. R.; Miljkovic, J. L.; Nauser, T.; Royzen, M.; Klos, K.; Shubina, T.; Koppenol, W. H.; Lippard, S. J.; Ivanović-Burmazović, I. *Journal of the American Chemical Society* **2012**, *134*, 12016.

177) Quiroga, S. L.; Almaraz, A. E.; Amorebieta, V. T.; Perissinotti, L. L.; Olabe, J. A. *Chemistry (Weinheim an der Bergstrasse, Germany)* **2011**, *17*, 4145.

178) Miljkovic, J. L.; Kenkel, I.; Ivanović-Burmazović, I.; Filipovic, M. R. *Angewandte Chemie International Edition* **2013**, *52*, 12061.

179) Wedmann, R.; Zahl, A.; Shubina, T. E.; Dürr, M.; Heinemann, F. W.; Bugenhagen, B. E. C.; Burger, P.; Ivanovic-Burmazovic, I.; Filipovic, M. R. *Inorganic Chemistry* **2015**, *54*, 9367.

180) Martinsen, A.; Songstad, J. *Acta Chemica Scandinavica A* **1977**, *31*, 645.